

**Mitigation of Alkali-Silica Reaction in the Bibb Graves Bridge**

by

Robert Leslie Warnock

A thesis submitted to the Graduate Faculty of  
Auburn University  
in partial fulfillment of the  
requirements for the Degree of  
Master of Science

Auburn, Alabama  
August 4, 2012

Keywords: Alkali-silica reaction, silane, mitigation,  
concrete, moisture diffusion, finite-element analysis

Copyright 2012 by Robert Leslie Warnock

Approved by

Anton K. Schindler, Chair, Associate Professor of Civil Engineering  
Robert W. Barnes, James J. Mallett Associate Professor of Civil Engineering  
James S. Davidson, Associate Professor of Civil Engineering

## **Abstract**

The Bibb Graves Bridge in Wetumpka, AL has severe damage due to alkali-silica reaction (ASR) in two of its reinforced concrete arches. A mitigation procedure developed in the summer of 2010 by the FHWA, ALDOT, and Auburn University was implemented during the fall of 2010. The mitigation procedure included the application of a silane sealant, flexible sealant in the large cracks, and an epoxy flood coat to fill the small cracks on the tops of the arches.

For this research, the internal relative humidity and external concrete strains in the arches of span 4 and 5 were monitored and analyzed to determine the effectiveness of the ASR mitigation procedure. Additionally, time frames in which results from the ASR mitigation procedure may be seen were determined through analytical methods.

It was found that over the 18-month data collection period, the ASR mitigation procedure was not effective at lowering the relative humidity to a level such that ASR expansion slowed.



## **Acknowledgments**

First and foremost, I would like to thank Dr. Schindler for his direction and guidance throughout my time at Auburn University. Secondly I would like to thank my parents, Bill and Becky Warnock, for their constant love, support, and encouragement. Thank you to my girlfriend, Chelsi Rodriguez, who was always patiently there to provide love and encouragement.

Thank you to the research assistants, Adam Wilkinson and Patrick Kimmons, for your help during the summer of 2011, basting like turkeys in the Alabama red clay, and for visiting the bridge with me countless times. Your help is more appreciated than you know.

Thanks to Billy Wilson, the concrete lab manager, for helping me with numerous things over the last few years. Thanks to my committee members, Dr. Barnes and Dr. Davidson, for your instruction during my time here at Auburn University, and for reading and editing this thesis.

Finally, thanks to the members of the Federal Highway Administration (FHWA) and the Alabama Department of Transportation (ALDOT) that provided me with the opportunity and funding to study such a fascinating and beautiful bridge.

## Table of Contents

|  |     |
|--|-----|
| Abstract.....  | ii  |
| Acknowledgements.....                                      | iii |
| List of Tables .....                                       | x   |
| List of Figures .....                                      | xiv |
| Chapter 1: Introduction.....                               | 1   |
| 1.1 Background.....  | 1   |
| 1.2 Statement of Objectives.....                           | 5   |
| 1.3 Research Methodology.....                              | 6   |
| 1.4 Thesis Organization .....                              | 7   |
| Chapter 2: Literature Review.....                          | 10  |
| 2.1 Introduction.....                                      | 10  |
| 2.2 Alkali-Silica Reaction: Mechanisms and Mitigation..... | 10  |
| 2.2.1 Occurrence of ASR .....                              | 14  |
| 2.2.2 The mechanisms behind the reaction.....              | 15  |
| 2.2.3 Damage caused by ASR.....                            | 17  |
| 2.2.3.1 Microcracking.....                                 | 19  |
| 2.2.3.2 Surface Cracking.....                              | 21  |
| 2.2.3.3 Surface Discoloration .....                        | 23  |
| 2.2.3.4 Pop-Outs .....                                     | 24  |

|            |   |    |
|------------|---|----|
| 2.2.3.5    | Surface Deposits .....  | 24 |
| 2.2.4      | Effects of exposure conditions on ASR damage .....                                      | 25 |
| 2.2.4.1    | Wetting and Drying .....  | 25 |
| 2.2.4.2    | Freezing and Thawing .....  | 26 |
| 2.2.5      | Evaluation of ASR through petrographic analysis .....                                   | 27 |
| 2.2.5.1    | ASTM C 856 Standard practice for petrographic<br>examination of hardened concrete ..... | 27 |
| 2.2.5.2    | Damage Rating Index .....   | 29 |
| 2.2.6      | Mitigation of ASR .....   | 31 |
| 2.2.6.1    | Silane's effectiveness in mitigating ASR .....  | 31 |
| 2.2.6.2    | Lithium-based mitigation methods .....  | 48 |
| 2.2.6.3    | Minimizing or managing symptoms of ASR ....   | 51 |
| 2.3        | Modeling moisture movement in hardened concretes .....                                  | 52 |
| 2.3.1      | Background theory .....   | 52 |
| 2.3.2      | The moisture diffusion / heat transfer analogy .....                                    | 54 |
| 2.4        | Summary.....  | 56 |
| Chapter 3: | Bibb Graves Bridge .....  | 58 |
| 3.1        | Background.....   | 58 |
| 3.2        | Construction, layout, and general information .....                                     | 61 |
| 3.3        | ASR in the Bibb Graves Bridge .....   | 64 |
| 3.3.1      | Petrography of concrete in span 4 and 5 .....   | 67 |
| 3.3.1.1    | Coring layout and details .....   | 67 |
| 3.3.1.2    | WJE's Petrographic study results .....  | 67 |

|            |   |     |
|------------|---|-----|
| 3.3.1.3    | The Transtec Group’s petrographic study |     |
| Results    | .....                                   | 71  |
| 3.3.2      | Crack mapping                           | 74  |
| 3.3.3      | Examples of distress                    | 82  |
| 3.4        | Summary                                 | 86  |
| Chapter 4: | ASR Mitigation Procedure                | 87  |
| 4.1        | Introduction                            | 87  |
| 4.2        | Selection of ASR Mitigation Method      | 87  |
| 4.2.1      | Protocol Option A                       | 88  |
| 4.2.2      | Protocol Option B                       | 88  |
| 4.2.3      | Protocol Option C                       | 89  |
| 4.2.4      | Protocol Option D                       | 90  |
| 4.3        | Final ASR mitigation procedure          | 91  |
| 4.4        | Installation of ASR mitigation method   | 94  |
| 4.5        | Summary                                 | 97  |
| Chapter 5: | Monitoring Instrumentation              | 99  |
| 5.1        | Introduction                            | 99  |
| 5.2        | RH Measurements                         | 99  |
| 5.3        | Concrete Strain Measurements            | 105 |
| 5.4        | Summary                                 | 113 |
| Chapter 6: | Experimental Results and Discussion     | 114 |
| 6.1        | Introduction                            | 114 |
| 6.2        | Internal RH                             | 115 |

|         |   |     |
|---------|---|-----|
| 6.2.1   | RH measurement identification system.....   | 117 |
| 6.2.2   | RH data for the average of all measurement depths.....                                  | 117 |
| 6.2.2.1 | Linear regression analysis of RH data for the<br>average of all measurement depths..... | 124 |
| 6.2.2.2 | RH difference analysis for the average of all<br>measurement depths.....                | 125 |
| 6.2.3   | RH data for the 3-inch measurement depth.....   | 129 |
| 6.2.3.1 | Linear regression analysis for the 3-inch<br>measurement depth.....                     | 135 |
| 6.2.3.2 | RH difference analysis for the 3-inch<br>measurement depth.....                         | 136 |
| 6.2.4   | RH data analysis summary.....   | 138 |
| 6.3     | Concrete strain measurements.....   | 139 |
| 6.3.1   | Concrete strain measurement identification system.....                                  | 140 |
| 6.3.2   | Concrete strain measurement data.....   | 140 |
| 6.3.2.1 | Linear regression analysis of prominent<br>trends.....                                  | 155 |
| 6.3.3   | Concrete strain difference analysis .....   | 157 |
| 6.3.3.1 | Concrete strain difference plots with<br>$R^2 < 0.5$ .....                              | 162 |
| 6.3.4   | Concrete strain measurement summary.....  | 165 |
| 6.4     | Correlation between RH and concrete strain trends.....                                  | 170 |

|            |   |     |
|------------|---|-----|
| Chapter 7: | Moisture Diffusion Modeling.....                                      | 170 |
| 7.1        | Purpose of moisture diffusion modeling.....                           | 170 |
| 7.2        | Finite-element methods.....   | 171 |
| 7.2.1      | Element selection.....  | 171 |
| 7.2.2      | Defining the material model.....                                      | 172 |
| 7.2.3      | Cross section model and loads applied.....                            | 174 |
| 7.3        | Results from finite-element analysis.....                             | 177 |
| 7.3.1      | Moisture diffusion time frames.....                                   | 182 |
| 7.3.2      | Steady state humidity analysis.....                                   | 183 |
| 7.4        | Experimental work to calibrate the finite-element model results...185 |     |
| 7.4.1      | Arch test section construction.....                                   | 186 |
| 7.4.2      | Arch test section sealing treatments.....                             | 190 |
| 7.4.3      | RH instrumentation for arch test sections.....                        | 191 |
| 7.5        | Summary.....  | 191 |
| Chapter 8: | Summary, Conclusions, Recommendations.....                            | 194 |
| 8.1        | Project summary.....  | 195 |
| 8.1.1      | Presence of ASR in the Bibb Graves Bridge.....                        | 194 |
| 8.1.2      | ASR mitigation procedure.....   | 195 |
| 8.1.3      | Monitoring the effectiveness of the ASR mitigation<br>procedure ..... | 196 |
| 8.1.4      | Moisture diffusion modeling.....                                      | 196 |
| 8.2        | Conclusions.....  | 198 |
| 8.2.1      | Effectiveness of the ASR mitigation procedure.....                    | 198 |

|       |  |     |
|-------|--|-----|
| 8.2.2 | Moisture Diffusion Modeling.....                                   | 198 |
| 8.3   | Recommendations .....  | 199 |
|       | References.....  | 201 |
|       | Appendix A: Coring Procedure .....                                 | 207 |
|       | Appendix B: RH Survey data .....                                   | 221 |
|       | Appendix C: Concrete Strain Measurement Survey Data and Plots..... | 242 |
| C.1   | Survey data.....   | 243 |
| C.2   | Concrete strain difference plots for $r^2 < 0.5$ .....             | 253 |

## List of Tables

|   |     |
|---|-----|
| Table 2.1: Deleteriously Reactive Rocks, Minerals, and Synthetic Substances<br>(Mehta et al. 2006).....                               | 12  |
| Table 2.2: Exposure cycles applied to laboratory cylinders<br>(Bérubé et al. 2002a).....  | 13  |
| Table 2.3: Petrographic features and weighing factors for the DRI<br>(Grattan-Bellew et al. 2006) .....                               | 30  |
| Table 2.1: Relationships between thermal and moisture diffusivity<br>(Madenci and Guven 2006) .....                                   | 57  |
| Table 3.1: Span lengths for various arches (Taylor 1930).....   | 63  |
| Table 3.2: Summary of the petrographic observations of the cores<br>(The Transtec Group 2010) .....                                   | 72  |
| Table 5.1: Summary of concrete strain measurement locations<br>on span 4 and 5.....   | 108 |
| Table 6.1: RH survey dates, with corresponding ages from the first reading....  | 116 |
| Table 6.2: 18-month RH (%) averages for the average of all<br>measurement depths.....   | 122 |
| Table 6.3: Coefficients of determination ( $r^2$ ) of the linear regression trends for the<br>average of all measurement depths ..... | 124 |
| Table 6.4: Coefficients of determination for RH difference analyses for the<br>average of all measurement depths.....                 | 126 |
| Table 6.5: 18-month averages for the 3-inch measurement depth .....   | 134 |



|   |     |
|---|-----|
| Table 6.6: Coefficients of determination ( $r^2$ ) of the linear regression trends for the 3-inch measurement depth .....             | 136 |
| Table 6.7: Coefficients of determination for “RH difference” analyses for the 3-inch measurement depth .....                          | 137 |
| Table 6.8: Concrete strain measurement survey dates.....  | 145 |
| Table 6.9: Prominent trends in Figures 6.16 through 6.25, with corresponding $r^2$ values, trend line slopes, and figure numbers..... | 156 |
| Table 6.10: Coefficients of determination for linear regression trend lines for the concrete strain difference analyses.....          | 158 |
| Table 6.11: Slopes of the trend lines for the concrete strain difference analyses .....   | 159 |
| Table 6.12: Slopes ( $10^{-6}$ in./in./month) of the prominent trends for all concrete strain data and analyses.....                  | 165 |
| Table 6.13: RH trends versus concrete strain trends at various locations.....   | 167 |
| Table 7.1: Conductivity information for 2000 psi concrete input into ANSYS.....   | 173 |
| Table 7.2: Conductivity information for 3250 psi concrete input into ANSYS.....   | 173 |
| Table 7.3: 30-year average for monthly ambient RH for Montgomery, AL, (Horstmeyer 2008).....  | 175 |
| Table 7.4: Years needed to reach 80 percent internal RH for various depths within the concrete.....                                   | 181 |
| Table 7.5: Years needed for entire cross section to reach 80 percent internal RH.....   | 182 |
| Table 7.6: Years needed for entire cross section to reach 80 % internal RH ...  | 184 |
| Table A.1: Information for 1A – South (ALDOT 2010).....   | 213 |
| Table A.2: Information for Core 2A – South (ALDOT 2010).....  | 214 |
| Table A.3: Information for Core 1B – South (ALDOT 2010).....  | 215 |

|   |     |
|---|-----|
| Table A.4: Information for Core 2B – South (ALDOT 2010).....        | 216 |
| Table A.5: Information for 1A – North (ALDOT 2010) .....            | 217 |
| Table A.6: Information for 2A – North (ALDOT 2010) .....            | 218 |
| Table A.7: Information for Core 1B – North (ALDOT 2010).....        | 219 |
| Table A.8: Information for Core 2B – North (ALDOT 2010) .....       | 220 |
| Table B.1: RH data, average of all measurement depths summary ..... | 222 |
| Table B.2: RH data, 3-inch measurement depth summary .....          | 223 |
| Table B.3: RH data, 2 inch measurement depth summary.....           | 224 |
| Table B.4: RH data, 1 inch measurement depth summary.....           | 224 |
| Table B.5: 4-S-WT raw RH data .....                                 | 226 |
| Table B.6: 4-S-WB raw RH data .....                                 | 227 |
| Table B.7: 4-S-ET raw RH data .....                                 | 228 |
| Table B.8: 4-S-EB raw RH data .....                                 | 229 |
| Table B.9: 4-N-WT raw RH data .....                                 | 230 |
| Table B.10: 4-N-WB raw RH data .....                                | 231 |
| Table B.11: 4-N-ET raw RH data .....                                | 232 |
| Table B.12: 4-N-EB raw RH data .....                                | 233 |
| Table B.13: 5-S-WT raw RH data .....                                | 234 |
| Table B.14: 5-S-WB raw RH data .....                                | 235 |
| Table B.15: 5-S-ET raw RH data .....                                | 236 |
| Table B.16: 5-S-EB raw RH data .....                                | 237 |
| Table B.17: 5-N-WT raw RH data .....                                | 238 |

|  |     |
|--|-----|
| Table B.18: 5-N-WB raw RH data .....   | 239 |
| Table B.19: 5-N-ET raw RH data .....   | 240 |
| Table B.20: 5-N-EB raw RH data .....   | 241 |
| Table C.1: Arch 4-S concrete strain data gauge readings.....   | 243 |
| Table C.2: Arch 4-N concrete strain data gauge readings.....   | 244 |
| Table C.3: Arch 5-S concrete strain data gauge readings.....   | 245 |
| Table C.4: Arch 5-N concrete strain data gauge readings.....   | 246 |
| Table C.5: Concrete strain gauge readings from 2005 with new concrete strain<br>gauge readings ..... | 247 |
| Table C.6: Changes in concrete strain ( $10^{-6}$ in./in.) for arch 4-S .....                        | 248 |
| Table C.7: Changes in concrete strain ( $10^{-6}$ in./in.) for arch 4-N.....                         | 249 |
| Table C.8: Changes in concrete strain ( $10^{-6}$ in./in.) for arch 5-S .....                        | 250 |
| Table C.9: Changes in concrete strain ( $10^{-6}$ in./in.) for arch 5-N .....                        | 251 |
| Table C.10: Changes in concrete strain ( $10^{-6}$ in./in.) for plots with data<br>from 2005.....    | 252 |

## List of Figures

|  |    |
|--|----|
| Figure 1.1: The Bibb Graves Bridge in Wetumpka, AL.....  | 1  |
| Figure 1.2: ASR Induced cracking on the Bibb Graves Bridge.....  | 2  |
| Figure 1.3: Concrete strain measurement being taken on the<br>Bibb Graves Bridge.....  | 3  |
| Figure 1.4: RH measurement being taken .....   | 4  |
| Figure 1.5: Arch test sections for finite-element analysis calibration.....  | 5  |
| Figure 2.1: Threshold RH for expansion to occur due to ASR (Stark 1991).....   | 13 |
| Figure 2.2: Occurrence of ASR in United States (FHWA 2002) .....   | 15 |
| Figure 2.3: ASR reaction rim (WJE 2010) .....  | 16 |
| Figure 2.4: Bridge deck core showing vertical and horizontal cracks due to ASR.<br>Top of core to right (Forster et al. 1998) .....  | 17 |
| Figure 2.5: Typical “map-cracking” due to ASR. (Forster et al. 1998).....  | 18 |
| Figure 2.6: Microcracking in aggregate particles at a) 0.065 % and b) 0.149 %<br>expansion (Fournier et al. 2004) .....  | 19 |
| Figure 2.7: Extensive microcracking at 0.25 % expansion in aggregate particles<br>and cement paste; also, a void filled with alkali-silica gel<br>(Fournier et al. 2004) ..... | 20 |
| Figure 2.8: Thin section of concrete showing a crack highlighted by alkali-silica<br>gel (Thomas et al. 2008) .....  | 20 |
| Figure 2.9: Sketch of a concrete slab subjected to ASR cracking with surface<br>map-cracking, and subparallel internal cracks (Forster et al. 1998) .....                      | 21 |

|   |    |
|---|----|
| Figure 2.10: ASR-cracking orienting itself to underlying steel reinforcement (Fournier et al. 2004) .....   | 22 |
| Figure 2.11: Examples of surface discoloration around cracks on a) a highway median barrier and b) a 25-year-old highway parapet wall (Fournier et al. 2004) .....                          | 23 |
| Figure 2.12: Example of a pop-out induced by ASR (Fournier et al. 2004) .....   | 24 |
| Figure 2.13: Example of efflorescence and alkali-silica gel exuding to the surface of a concrete foundation suffering from ASR (Fournier et al. 2004) .....                                 | 25 |
| Figure 2.14: Effect of silane sealant on concrete .....   | 31 |
| Figure 2.15: Silane being applied with a low-pressure garden sprayer .....  | 33 |
| Figure 2.16: Silane's basic chemical structure and chemistries (Selley 2010)....  | 36 |
| Figure 2.17: Siloxane Molecule (Selley 2010) .....  | 37 |
| Figure 2.18: Representation of silane repelling water (Selley 2010) .....   | 38 |
| Figure 2.19: (a) Expansion and (b) cumulative mass variation of unsealed and sealed air-entrained concrete cylinders subjected to exposure cycle C5 (Bérubé et al. 2002a) .....             | 41 |
| Figure 2.20: (a) Unsealed and (b) silane-sealed air-entrained concrete cylinders subjected to exposure cycle C4 after 1.5 years (Bérubé et al. 2002a) .....                                 | 42 |
| Figure 2.21: Examples of the unsealed and sealed highway median barriers 3 years after the application of silane sealants in (a) Montmorency and (b) Sainte-Foy (Bérubé et al. 2002b) ..... | 44 |
| Figure 2.22: RH measured from 1994 to 1997 in highway median barriers in (a) Montmorency and (b) Sainte-Foy (Bérubé et al. 2002b) .....   | 46 |
| Figure 2.23: Topical application of lithium compounds (Fournier et al. 2010) .....  | 49 |
| Figure 2.24: Diffusion coefficients for varying strength of concrete .....  | 54 |
| Figure 3.1: Map of Alabama with a star denoting Wetumpka (gkpedia, n.d.) .....  | 58 |

|   |    |
|---|----|
| Figure 3.2: Covered bridge built in 1844 (Blackburn 1997) .....   | 59 |
| Figure 3.3: Iron bridge constructed in 1887 (Blackburn 1997) .....  | 59 |
| Figure 3.4: 1887 Iron Bridge in the background with Lock 31, completed in 1896,<br>in the foreground (Blackburn 1997) .....   | 60 |
| Figure 3.5: Aerial view of the Bibb Graves Bridge (Bing 2012a) .....  | 61 |
| Figure 3.6: Elevation and plan view of Bibb Graves Bridge .....   | 62 |
| Figure 3.7: Bibb Graves Bridge under construction (Taylor 1930) .....   | 63 |
| Figure 3.8: Concrete placement schedule for various concrete strengths .....  | 64 |
| Figure 3.9: Examples of distress in the late 1990s on the a) top and b) bottom of<br>a span 5 arch.....   | 65 |
| Figure 3.10: Arches on the Bibb Graves Bridge. (a) Unaffected arch and (b) arch<br>affected by ASR .....  | 66 |
| Figure 3.11: Core Extraction Layout (ALDOT 2010).....   | 68 |
| Figure 3.12: Core 1A – South: Typical dark glassy rim on white friable quartzite<br>coarse aggregate particle. Arrows show ASR cracks in aggregate<br>periphery (WJE 2010) .....                        | 69 |
| Figure 3.13: Crack at periphery of quartzite aggregate particle (top right) and<br>multiple veinlets, indicated with arrows, filled with ASR gel<br>(WJE 2010) .....                                    | 70 |
| Figure 3.14: Core 1A – South: Microcracks filled with ettringite, shown with<br>arrows. Small amount of gel at outside edge of crack in aggregate is<br>circled. Field width is 1.2 mm (WJE 2010) ..... | 71 |
| Figure 3.15: Reaction rims (RR) surrounding chert (CH) coarse aggregates<br>(The Transtec Group 2010) .....   | 73 |
| Figure 3.16: Installation of grid lines for crack survey .....  | 75 |
| Figure 3.17: Crack mapping grid system after installation .....   | 75 |

|   |    |
|---|----|
| Figure 3.18: Crack width gauge in use .....   | 75 |
| Figure 3.19: Crack- mapping survey. November 5, 2010. Span 4 – South Arch –<br>Plan View .....  | 76 |
| Figure 3.20: Crack- mapping survey. November 5, 2010. Span 4 – South Arch –<br>Bottom View .....                                      | 77 |
| Figure 3.21: Crack- mapping survey. November 4, 2010. Span 5 – South Arch –<br>Plan View .....  | 78 |
| Figure 3.22: Crack- mapping survey. November 4, 2010. Span 5 – South Arch –<br>Bottom View .....                                      | 79 |
| Figure 3.23: Crack- mapping survey. November 4, 2010. Span 5 – North Arch –<br>Top View .....   | 80 |
| Figure 3.24: Crack- mapping survey. November 4, 2010. Span 5 – North Arch –<br>Bottom View .....                                      | 81 |
| Figure 3.25: Severe distress due to ASR on the eastern side of the southern arch<br>of span 5 on 3-11-2008 .....                      | 82 |
| Figure 3.26: A closer view of the severe distress due to ASR on the eastern side<br>of the southern arch of span 5 on 3-11-2008 ..... | 83 |
| Figure 3.27: An example of spalling on span 5 on 12-14-2009 .....   | 84 |
| Figure 3.28: Severe cracks greater than 0.1 inches on 3-11-2008 .....   | 84 |
| Figure 3.29: Severe cracks on the bottom of the arch on 3-11-2008 .....   | 85 |
| Figure 3.30: Map-cracking on the abutment of span 5 .....   | 85 |
| Figure 4.1: Span 4 and 5 of the Bibb Graves Bridge .....  | 92 |
| Figure 4.2: Schematic of the ASR mitigation procedure applied .....   | 93 |
| Figure 4.3: Timeline of the fall 2010 installation of the ASR mitigation<br>procedure .....   | 94 |
| Figure 4.4: Overview of ASR mitigation procedure implementation .....   | 94 |

|  |     |
|--|-----|
| Figure 4.5: Water-blasted arches prepared for ASR mitigation procedure .....               | 95  |
| Figure 4.6: (a) Water-based silane sealant and (b) application of silane .....             | 96  |
| Figure 4.7: (a) Application of flexible sealant and (b) smoothing sealant by<br>hand ..... | 96  |
| Figure 5.1: RH tube with plug installed and tube sealed with a silicone<br>sealant .....   | 100 |
| Figure 5.2: Plug being removed from tube .....   | 101 |
| Figure 5.3: RH probe being inserted into tube .....  | 101 |
| Figure 5.4: Plug being placed around probe wire .....                                      | 102 |
| Figure 5.5: Plastic cup being placed around probe assembly .....                           | 102 |
| Figure 5.6: RH measurement locations for all arches .....                                  | 103 |
| Figure 5.7: Vaisala’s Humidity Probe Calibrator, HMK15 .....                               | 104 |
| Figure 5.8: Example of installed DEMEC stud in the Bibb Graves Bridge.....                 | 105 |
| Figure 5.9: Mayes DEMEC Concrete strain Gauge a) field use<br>and b) dial gauge.....       | 105 |
| Figure 5.10: DEMEC Locations - Span 4 - South Arch. Not to Scale.....                      | 109 |
| Figure 5.11: DEMEC Locations - Span 4 - North Arch. Not to Scale.....                      | 110 |
| Figure 5.12: DEMEC Locations - Span 5 - South Arch. Not to Scale.....                      | 111 |
| Figure 5.13: DEMEC Locations - Span 5 - North Arch. Not to Scale.....                      | 112 |
| Figure 6.1: Maxwell Air Force Base near Montgomery, AL (Bing 2012b) .....                  | 116 |
| Figure 6.2: RH measurements, West Top, average of all measurement<br>depths .....          | 118 |
| Figure 6.3: RH measurements, West Bottom, average of all measurement<br>depths .....       | 119 |



|   |     |
|---|-----|
| Figure 6.4: RH measurements, East Top, average of all measurement depths .....    | 120 |
| Figure 6.5: RH measurements, East Bottom, average of all measurement depths ..... | 121 |
| Figure 6.6: Schematic of “RH difference” plot for various scenarios.....          | 126 |
| Figure 6.7: RH difference for 5-N-WB-AVG .....                                    | 127 |
| Figure 6.8: RH difference for 5-N-EB-AVG .....                                    | 128 |
| Figure 6.9: RH difference for 5-S-EB-AVG .....                                    | 128 |
| Figure 6.10: RH measurements, West Top, 3-inch depth .....                        | 130 |
| Figure 6.11: RH measurements, West Bottom, 3-inch depth .....                     | 131 |
| Figure 6.12: RH measurements, East Top, 3-inch depth .....                        | 132 |
| Figure 6.13: RH measurements, East Bottom, 3-inch depth .....                     | 133 |
| Figure 6.14: RH difference for 5-S-EB-3” .....                                    | 138 |
| Figure 6.15: Temperature effect error bar for a 70 °F day.....                    | 142 |
| Figure 6.16: Change in concrete strain for Side Perpendicular since 2005.....     | 143 |
| Figure 6.17: Change in concrete strain for Side Perpendicular since 11/2010..     | 144 |
| Figure 6.18: Change in concrete strain for Bottom Low since 2005.....             | 145 |
| Figure 6.19: Change in concrete strain for Bottom Low since 11/2010 .....         | 146 |
| Figure 6.20: Change in concrete strain for Top Low since 2005.....                | 147 |
| Figure 6.21: Change in concrete strain for Top Low since 11/2010.....             | 148 |
| Figure 6.22: Change in concrete strain for Side Horizontal since 11/2010.....     | 149 |
| Figure 6.23: Change in concrete strain for Bottom High since 11/2010.....         | 150 |
| Figure 6.24: Change in concrete strain for Top High since 11/2010.....            | 151 |

|   |     |
|---|-----|
| Figure 6.25: Change in concrete strain for Abutment since 11/2010 .....                 | 152 |
| Figure 6.26: Concrete strain difference plot for BL measurement location.....           | 159 |
| Figure 6.27: Concrete strain difference plot for TL measurement location.....           | 160 |
| Figure 6.28: Concrete strain difference plot for BH measurement location .....          | 160 |
| Figure 6.29: Concrete strain difference plot for TH measurement location .....          | 161 |
| Figure 6.30: Concrete strain difference plot for BL, with $r^2 < 0.5$ .....             | 163 |
| Figure 6.31: Concrete strain difference plot for TL, with $r^2 < 0.5$ .....             | 163 |
| Figure 6.32: Concrete strain difference plot for SH, with $r^2 < 0.5$ .....             | 164 |
| Figure 6.33: Concrete strain difference plot for BH, with $r^2 < 0.5$ .....             | 164 |
| Figure 6.34: Concrete strain difference for TH measurement locations.....               | 168 |
| Figure 6.35: Concrete strain difference for BH measurement locations .....              | 169 |
| Figure 7.1: Plane55 Geometry (SAS IP 2009) .....  | 171 |
| Figure 7.2: Multilinear approximation of the moisture diffusion coefficient .....       | 174 |
| Figure 7.3: Arch cross section modeled in ANSYS .....                                   | 176 |
| Figure 7.4: Moisture loss in concrete coated with silane only .....                     | 178 |
| Figure 7.5: Moisture flux for 2000 psi concrete and no epoxy flood coat.....            | 178 |
| Figure 7.6: Moisture flux for 3250 psi concrete and no epoxy flood coat.....            | 179 |
| Figure 7.7: Moisture loss in concrete coated with an epoxy flood coat.....              | 180 |
| Figure 7.8: Moisture flux for 2000 psi concrete with an epoxy flood coat .....          | 180 |
| Figure 7.9: Moisture flux for 3250 psi concrete with an epoxy flood coat .....          | 181 |
| Figure 7.10: Moisture diffusion with steady state ambient RH, with silane<br>only ..... | 184 |

|  |     |
|--|-----|
| Figure 7.11: Moisture loss with steady state ambient RH, with silane and an epoxy flood coat.....                | 185 |
| Figure 7.13: Construction of strip footings and slab on grade .....  | 187 |
| Figure 7.14: Finished strip footings and slab on grade .....   | 187 |
| Figure 7.15: 12 inch SonoTubes column formwork .....   | 188 |
| Figure 7.16: Finished columns .....  | 188 |
| Figure 7.17: Arch test section formwork and rebar .....  | 189 |
| Figure 7.18: Finished arch test sections with no treatment .....   | 189 |
| Figure 7.19: Silane application on arch models .....   | 190 |
| Figure 7.20: Epoxy flood coat application on arch model .....  | 190 |
| Figure A.1: Use of ground penetrating radar to locate rebar (ALDOT 2010).....                                    | 207 |
| Figure A.2: Close up of drilling interface (ALDOT 2010).....   | 208 |
| Figure A.3: Drilling for core specimen (ALDOT 2010).....   | 208 |
| Figure A.4: Close up of drilling process (ALDOT 2010) .....  | 209 |
| Figure A.5: Core holes left after drilling (ALDOT 2010) .....  | 209 |
| Figure A.6: Extraction of core samples (ALDOT 2010).....   | 210 |
| Figure A.7: Labeling of core samples (ALDOT 2010).....   | 210 |
| Figure A.8: Wrapping of core samples (ALDOT 2010) .....  | 211 |
| Figure A.9: Packing of core sample for a) W.J.E. in Illinois and b) Laval University in Canada (ALDOT 2010)..... | 211 |
| Figure A.10: Schematic of core shipping (ALDOT 2010) .....   | 212 |
| Figure A.11: Core 1A – South (ALDOT 2010) .....  | 213 |
| Figure A.12: Core 2A – South (ALDOT 2010) .....  | 214 |

|   |     |
|---|-----|
| Figure A.13: Core 1B – South (ALDOT 2010) .....                         | 215 |
| Figure A.14: Core 2B – South (ALDOT 2010) .....                         | 216 |
| Figure A.15: Core 1A – North (ALDOT 2010) .....                         | 217 |
| Figure A.16: Core 2A – North (ALDOT 2010) .....                         | 218 |
| Figure A.17: Core 1B – North (ALDOT 2010) .....                         | 219 |
| Figure A.18: Core 2B – North (ALDOT 2010) .....                         | 220 |
| Figure C.1: Concrete strain difference plot for BL, $r^2 < 0.5$ .....   | 253 |
| Figure C.2: Concrete strain difference plot for SH, $r^2 < 0.5$ .....   | 253 |
| Figure C.3: Concrete strain difference plot for E-TH, $r^2 < 0.5$ ..... | 254 |
| Figure C.4: Concrete strain difference plot for W-TH, $r^2 < 0.5$ ..... | 254 |
| Figure C.5: Concrete strain difference plot for AB, $r^2 < 0.5$ .....   | 255 |

## Chapter 1

### Introduction

#### 1.1 Background

The Bibb Graves Bridge crosses the Coosa River in Wetumpka, Alabama. Built in 1931, the reinforced concrete bridge consists of seven spans with arches supporting a suspended roadway, as seen in Figure 1.1. The majority of the bridge is in sound condition; however, span 5 has severe cracking due to alkali-silica reaction (ASR). An example of ASR-induced cracking in one of the affected arches can be seen in Figure 1.2.



**Figure 1.1:** The Bibb Graves Bridge in Wetumpka, Alabama





**Figure 1.2:** ASR-Induced cracking on the Bibb Graves Bridge

Since 2005, the Alabama Department of Transportation (ALDOT) and the Federal Highway Administration (FHWA) have monitored the effects of ASR in the Bibb Graves Bridge.

Stark (1991) and Bérubé et al. (2002a) have shown that an internal relative humidity (RH) of 80 % or greater is required for expansion due to ASR. During the summer of 2010, ALDOT, FHWA, and Auburn University developed an ASR mitigation procedure to slow or stop the expansion due to ASR in the arches of span 5 by lowering the internal RH to 80 % or less. The ASR mitigation procedure included the application of a water repelling silane sealer on all exposed concrete of the arches, a flexible silicone sealant in the wide cracks

of the ASR-affected arches, and an epoxy flood coat on the top surface of the arches to seal all intermediate to narrow cracks.

From October to November of 2010, Auburn University assisted in the implementation and documentation of the ASR mitigation procedure at the Bibb Graves Bridge. During this time, instrumentation was also added to monitor the effectiveness of the ASR mitigation procedure. The instrumentation was installed by personnel from the FHWA, Auburn University, and ALDOT's Materials and Test Bureau. Installed instrumentation allow for the collection of data pertaining to concrete strain and internal RH. Concrete strain measurements are taken monthly, as shown in Figure 1.3, to evaluate if the ASR mitigation procedure has decreased the rate of expansion.



**Figure 1.3:** Concrete strain measurement being taken on the Bibb Graves Bridge

Internal RH readings are taken monthly, as shown in Figure 1.4, to determine if the ASR mitigation procedure is effectively lowering the internal RH. Concrete strain and internal RH data have been collected since November 17, 2010.



**Figure 1.4:** RH measurement being taken

Due to the uncertainty of the time in which the ASR mitigation procedure should take effect, a moisture diffusion analysis of the arch cross section was performed. Using finite-element analysis, the moisture diffusion model was used to determine an upper and lower-bound time in which results should be seen if the ASR mitigation procedure is effective. To calibrate the finite-element model, three concrete arch test sections were constructed, as shown in Figure 1.5.





**Figure 1.5:** Arch test sections for finite-element analysis calibration

## **1.2 Statement of Objectives**

The primary objective of this project is to monitor the effectiveness of the ASR mitigation procedure in suppressing ASR-related expansions on the Bibb Graves Bridge. Secondary objectives include

1. Documenting the selection and installation of the ASR mitigation procedure implemented,
2. Monitoring and evaluation of internal RH of the instrumented arches over time,
3. Monitoring and evaluation of the changes in concrete strain of the instrumented arches over time, and
4. Determining a time frame in which results from the ASR mitigation procedure should be seen, if effective, through analytical methods.

### **1.3 Research Methodology**

To determine the effectiveness of the ASR mitigation procedure, a four-stage research plan was developed. First, the selection of the ASR mitigation procedure, the initial damage on the Bibb Graves Bridge, and the installation of the ASR mitigation procedure and monitoring instrumentation were documented. Documentation of the selection of the ASR mitigation procedure highlighted material selection and the order of installation. Documentation of the initial damage on the Bibb Graves Bridge was performed as a crack mapping survey that recorded all cracks and crack widths on the tops and bottoms of the arches damaged by ASR, and one control arch with little to no ASR-related damage. Documentation of installation of the ASR mitigation procedure and monitoring instrumentation highlighted the methods of installation, and monitoring equipment used.

Second, internal RH and concrete strain were monitored. Internal RH and concrete strain data surveys were conducted on the first Thursday of every month, weather permitting. RH data were collected at forty-eight total locations on four arches, two affected by ASR and two not affected by ASR. Concrete strain data were collected at forty-seven total locations on the same 4 arches. A password-protected website was developed where the data were summarized and presented for review by ALDOT and members of the FHWA's research team.

Third, "effectiveness time frames" were determined through analytical analysis. These were calculated to determine when the results, in the form of

lowered internal humidities, should be expected to be seen in the Bibb Graves Bridge. Moisture diffusion was modeled using the finite-element software ANSYS 12.0.

Finally, analyses of the RH and concrete strain data were conducted. Since two arches that showed little no ASR-related distress were instrumented to provide monitoring data, these arches were used for comparison to the severely cracked arches. The data were evaluated to determine if the ASR-mitigation procedure was effective in sealing the arch against liquid water penetration while allowing water vapor to leave the arch.

#### **1.4 Thesis organization**

A literature review that focuses on ASR mechanisms, damage caused by ASR, and ASR mitigation techniques is presented in Chapter 2. The chapter opens with an introduction that details the constituents needed for ASR. A brief overview of the occurrence of ASR across the United States is then shown. Following this, the mechanisms behind ASR are overviewed. Damage caused by ASR is the next section in Chapter 2. The effects of the wetting and drying cycles and freezing and thawing cycles on ASR damage are then shown. After the review of ASR damage, the evaluation of ASR through petrographic analysis is covered. This section includes two methods of analysis: ASTM C 856 and the Damage Rating Index. The mitigation of ASR is the next section in Chapter 2. In this section, the effectiveness of silane sealants and lithium-based compounds is reviewed. Since silane sealants were used in this project, their review is much

more detailed than the review for lithium compounds. After the mitigation sections, different ways to minimize or manage symptoms due to ASR are explored. These include crack filling, confinement of expansion, slot cutting, and concrete removal. The last section in Chapter 2 pertains to the modeling of moisture movement in concrete. The background theory is detailed, and then a moisture diffusion / heat transfer analogy is defined for use in finite-element software.

An overview of the Bibb Graves Bridge is found in Chapter 3. This overview contains background of the bridge location, background of its construction, bridge layout, and general information. Following this, the occurrence of ASR in the Bibb Graves Bridge is reviewed. Petrography results are shown next, followed by a crack mapping survey, and then examples of distress.

The ASR mitigation procedure is covered in Chapter 4. The selection process for the ASR mitigation procedure is detailed in the opening section. Following this, the final ASR mitigation procedure that was chosen to be installed on the Bibb Graves Bridge is presented. Finally, an installation summary for the ASR mitigation procedure is shown.

The instrumentation used to monitor the effectiveness of the ASR mitigation procedure is reviewed in Chapter 5. The RH measurements are covered first, followed by the concrete strain measurements.

An 18-month data collection period is reviewed in Chapter 6. The relative humidity data are analyzed first, followed by the concrete strain data. Finally, relationships between RH data and concrete strain data are explored.

To model moisture movement through concrete, a finite-element analysis was performed using ANSYS 12.0, and the results are presented in Chapter 7. The finite-element methods used during modeling, such as element selection, material model definition, and model creation are reviewed in the first section. Finally, the experiment built in the summer of 2011 to calibrate the finite-element model is reviewed.

A summary of important information, conclusions, and recommendations is presented in Chapter 8.

Appendix A contains information on the coring procedure that ALDOT performed to obtain core samples for petrographic analysis to determine if the Bibb Graves Bridge had ASR. Appendix B contains all data and plots pertaining to RH measurements that were not discussed in Chapter 6. Appendix C contains all data and plots pertaining to concrete strain measurements that were not discussed in Chapter 6.

## **Chapter 2**

### **Literature Review**

#### **2.1 Introduction**

This literature review focuses on ASR's fundamental ingredients, reaction mechanisms, resulting damage, response to various exposure conditions, and mitigation methods. Additionally, this literature review covers modeling of moisture movement in hardened concretes by finite-element analysis.

#### **2.2 Alkali-Silica Reaction: Mechanisms and Mitigation**

ASR is the process where, in an alkaline environment, the dissolution of silica ( $\text{SiO}_2$ ) in the aggregate forms expansive alkali-silica gel in the concrete (Diamond 1989). In the presence of moisture, alkali-silica gel causes deterioration with the development of differential volume change within the concrete (Forster et al. 1998). There are three fundamental conditions that must be present for ASR to occur in concrete (Forster et al. 1998):

1. Sufficient alkalinity in the cement
2. The presence of reactive silica
3. Sufficient moisture within the concrete

In terms of the first condition that must be met for ASR to occur, a limit of 0.40 percent on the  $\text{Na}_2\text{O}$  equivalent alkali content of portland cement has been

suggested by Tuthill (1980) to eliminate expansion due to ASR. Although a 0.60 percent limit on the equivalent alkali content (low-alkali cement) is used in specifications to minimize deterioration of concretes made with reactive aggregates, several studies have shown that significant deterioration due to ASR resulted despite the use of these low-alkali cements (Hadley 1968; Lerch 1959; Stark 1978, 1980; Tuthill 1980, 1982; Ozol and Dusenberry 1992).

In terms of the second condition, ASR can occur with a wide range of siliceous aggregates. The reactivity of the aggregate depends on the mechanics of its formation and its mineralogy (Forster et al. 1998). Table 2.1 has been adapted from Mehta et al. (2006) to provide a comprehensive list of siliceous rocks, minerals, and synthetic substances that are subject to ASR.

The last condition is the availability of sufficient moisture present within the concrete. Stark (1991) states that “the threshold level above which expansive ASR can be supported in concrete is 80 %.” Figure 2.1 is a plot of expansion of mortar bars that contain reactive aggregates due to ASR versus the RH. The mortar bars expanded when RH values were held above 80 %. Below 80 % RH, the contraction of the mortar bars was primarily due to the progressive shrinking of ASR gel reaction products and the hydrated cement paste in response to severe drying effects from an expanded condition (Stark 1991).

Bérubé et al. (2002a) presented a laboratory study on highly ASR prone concrete cylinders exposed to rigorous 14-day “exposure cycles”, as shown in Table 2.2.

**Table 2.1:** Deleteriously Reactive Rocks, Minerals, and Synthetic Substances  
(Mehta et al. 2006)

| Reactive substance   | Chemical composition   | Physical characteristics  |
|--|--|---|
| Opal   | SiO <sub>2</sub> nH <sub>2</sub> O   | Amorphous   |
| Chalcedony   | SiO <sub>2</sub>   | Microcrystalline to cryptocrystalline; commonly fibrous   |
| Certain forms of quartz  | SiO <sub>2</sub>   | Microcrystalline to cryptocrystalline; crystalline, but intensely fractured, concrete strained, and/or inclusion filled |
| Cristobalite   | SiO <sub>2</sub>   | Crystalline   |
| Tridymite  | SiO <sub>2</sub>   | Crystalline   |
| Rhyolitic, dacitic, latitic, or andesitic glass or cryptocrystalline devitrification products  | Siliceous, with lesser proportions of Al <sub>2</sub> O <sub>3</sub> , Fe <sub>2</sub> O <sub>3</sub> , alkaline earths, and alkalis | Glass or cryptocrystalline material as the matrix of volcanic rocks or fragments in tuffs                               |
| Synthetic siliceous glasses  | Siliceous, with less proportions of alkalis, alumina, and/or other substances  | Glass   |
| The most important deleterious alkali-reactive rocks (that is, rocks containing excessive amounts of one or more of the substances listed above) are as follows: |  |   |
| Opaline cherts   | Andesites and tuffs  |   |
| Chalcedonic cherts   | Siliceous shales   |   |
| Quartzose cherts   | Phyllites  |   |
| Siliceous limestones   | Opaline concretions  |   |
| Siliceous dolomites  |  |   |
| Rhyolites and tuffs  | Fractured, concrete strained, and inclusion-filled quartz and quartzites   |   |
| Dacites and tuffs  |  |   |



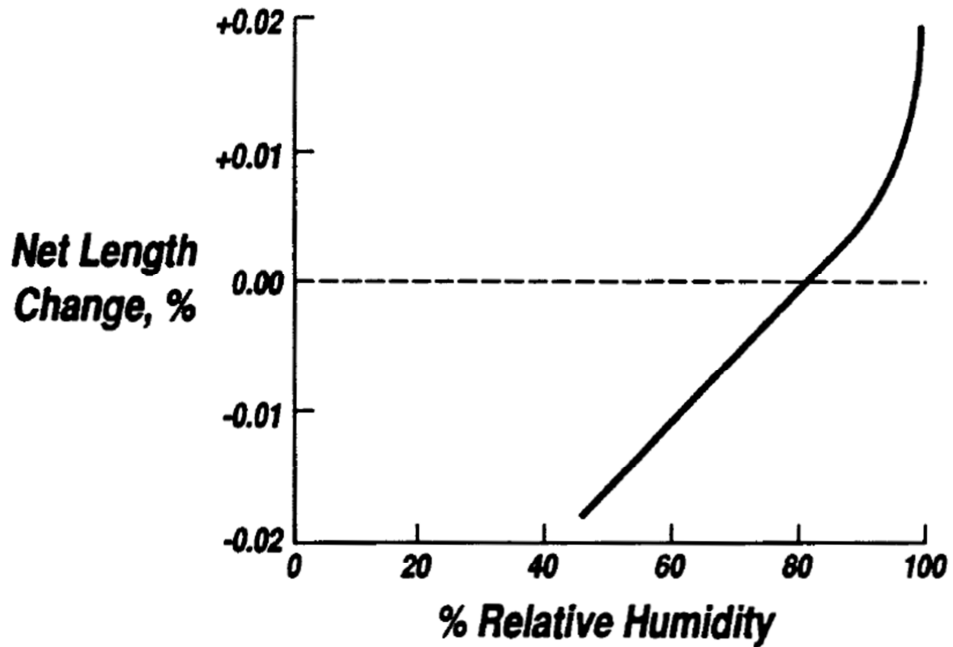


**Figure 2.1:** Threshold RH for expansion to occur due to ASR (Stark 1991)

**Table 2.2:** Exposure cycles applied to laboratory cylinders  
(Bérubé et al. 2002a)

| Type   | Conditioning of Cylinders                                    |
|--|--|
| Exposure cycle<br><b>C4</b><br>14 days Total | 7 days in 38 °C and > 95 % RH                                |
|  | 4 days of drying at 38 °C and 30 % RH                        |
|  | A 30-minute complete immersion in tap water                  |
|  | 3 days of freezing and thawing cycles                        |
| Exposure cycle<br><b>C5</b><br>14 days Total | 7 days in 38 °C and > 95 % RH                                |
|  | 4 days of drying at 38 °C and 30 % RH                        |
|  | 30-minute complete immersion in 3 % NaCl salt water solution |
|  | 3 days of freezing and thawing cycles                        |

Bérubé found a direct connection between internal RH and ASR related expansion. Bérubé et al. (2002a) state,

Measurements made immediately after a period of humid storage inside two 1-year-old cylinders exposed to cycle C4 indicated that the RH is significantly higher in the unsealed and expansive cylinder (95 % RH in center and 96 % near surface) than in the silane-sealed and non-expansive specimen (86 % RH in center and 81 % near surface), particularly near the surface. This suggests in turn that “internal” humidity conditions over 80–85 % are necessary for ASR expansion.

Ordinary concretes usually have internal relative humidities above this 80 % threshold, due to high ambient relative humidities or the presence of mixing water that has not yet been used in hydration. In ASR-prone concretes that have access to external sources of water, such as slabs on ground, pavements, etc., the reaction will occur until one of the reactive ingredients is used up (Forster et al. 1998).

### **2.2.1 Occurrence of ASR**

Adapted from a 1994 FHWA showcase workshop on ASR, Figure 2.2 is a map of the United States showing where ASR had been identified in structures up to 1994. Obviously, ASR is not a problem localized to a certain geographic area or climate type. Instead, it can be seen that ASR is a widespread problem that has been identified in almost every state.

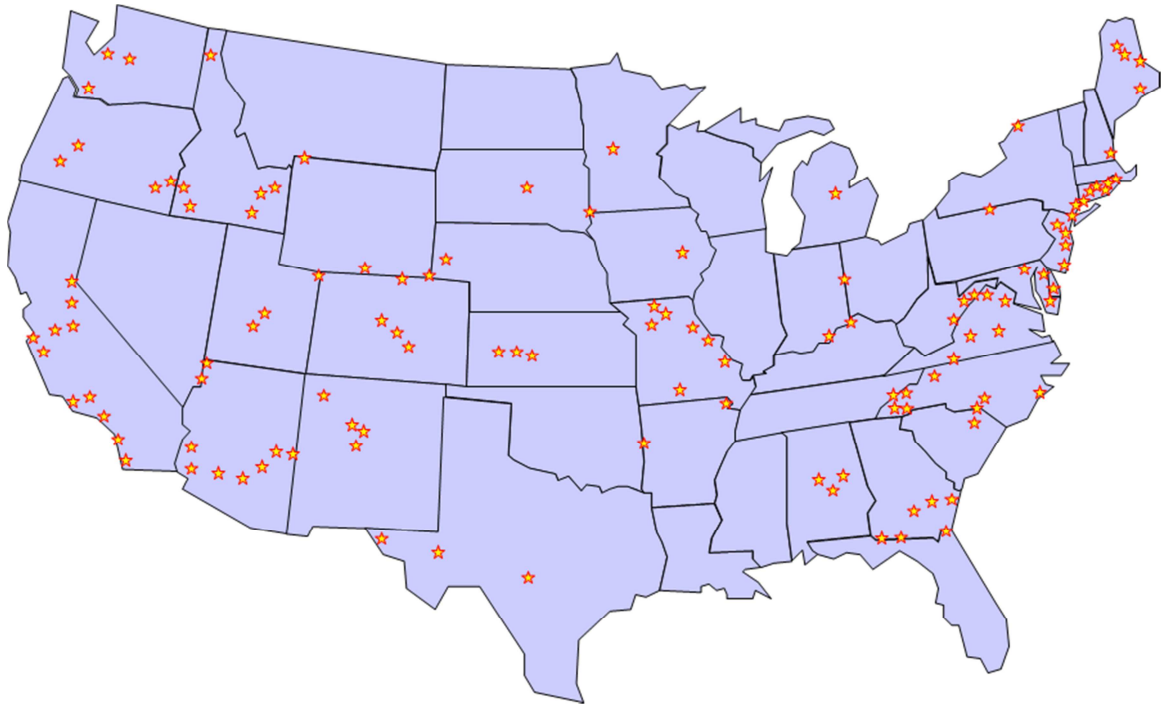


**Figure 2.2:** Occurrence of ASR in United States (FHWA 2002)

### 2.2.2 The mechanisms behind the reaction

The mechanisms of the reaction are described here by Forster et al. (1998):

The hydroxyl ions present in the pore fluid in concrete react chemically with various forms of silica present in many aggregates. The sodium and potassium alkalis play two roles in the reaction. First, higher percentages of these alkalis in the concrete result in higher concentrations of hydroxyl ions in the concrete pore fluid (higher pH). The more alkaline (higher pH) the pore fluid, the more readily it attacks (reacts with) the reactive silica. Once in solution, the silica reacts with the alkalis forming alkali-silica gel. This alkali-silica gel then imbibes water and swells so that its volume is greater than that of the individual reacted materials, and expansive stress is exerted on the concrete.

In concretes that contain all of the reactive ingredients, ASR begins occurring immediately after water contacts the cement. One of the first indications is a discolored “reaction rim” within and around the aggregate particle, shown in Figure 2.3.

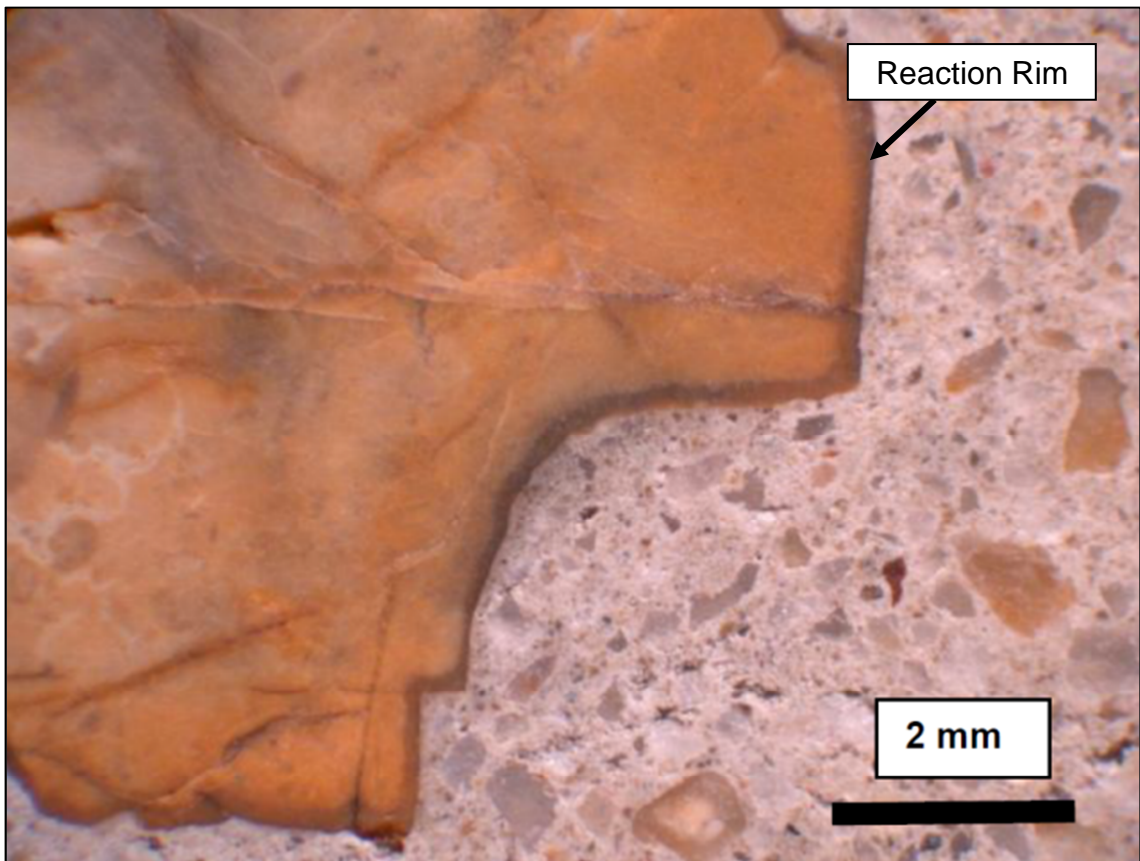


**Figure 2.3:** ASR reaction rim (WJE 2010)

Although the reaction begins immediately upon hydration, the rate of the reaction is often very slow, and external evidence of the reaction, such as ASR gel extrusions, cracking, spalling, etc., is often not seen for years (Forster et al. 1998).

### 2.2.3 Damage caused by ASR

Concrete deterioration caused by ASR is typically a result of excessive tensile stresses within the concrete due to differential volume change (Forster et al. 1998). The initial phase of deterioration is microcracking within the aggregate particles and cement paste matrix surrounding the aggregate particles. As the damage develops, microcracks propagate and surface cracks begin appearing. Unrestrained concrete cracking will be in all three dimensions within the structure, shown in Figure 2.4, and typical surface cracks appear in a polygonal pattern termed as “map-cracking” which is demonstrated in Figure 2.5 (Forster et al. 1998).

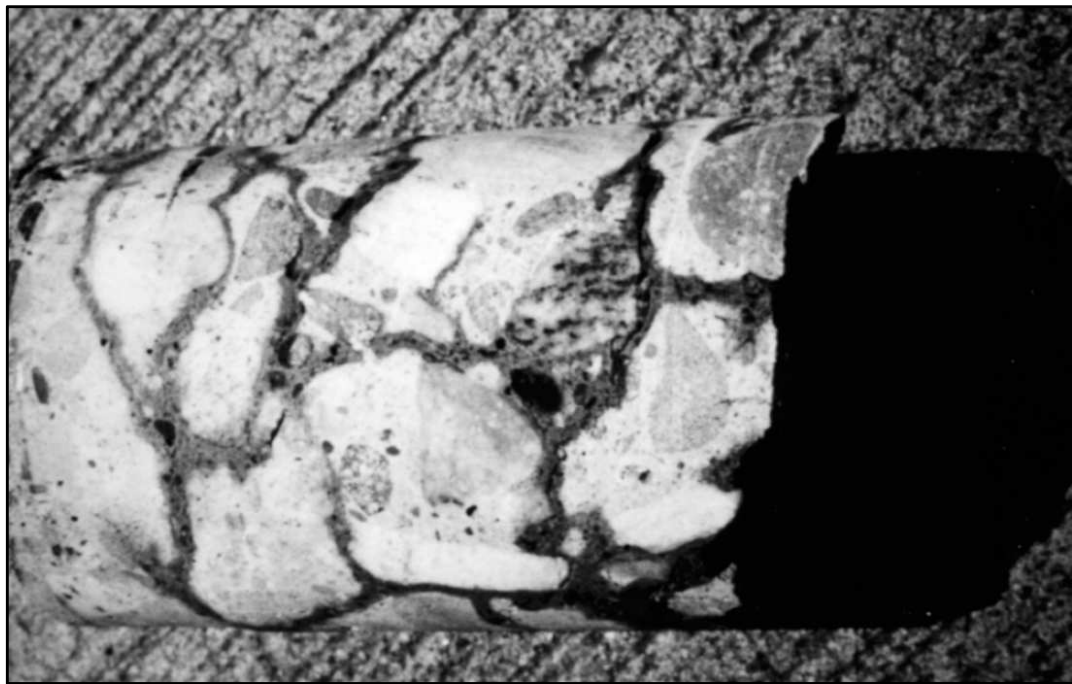


**Figure 2.4:** Bridge deck core showing vertical and horizontal cracks due to ASR.

Top of core to right (Forster et al. 1998)



**Figure 2.5:** Typical “map-cracking” due to ASR (Forster et al. 1998)

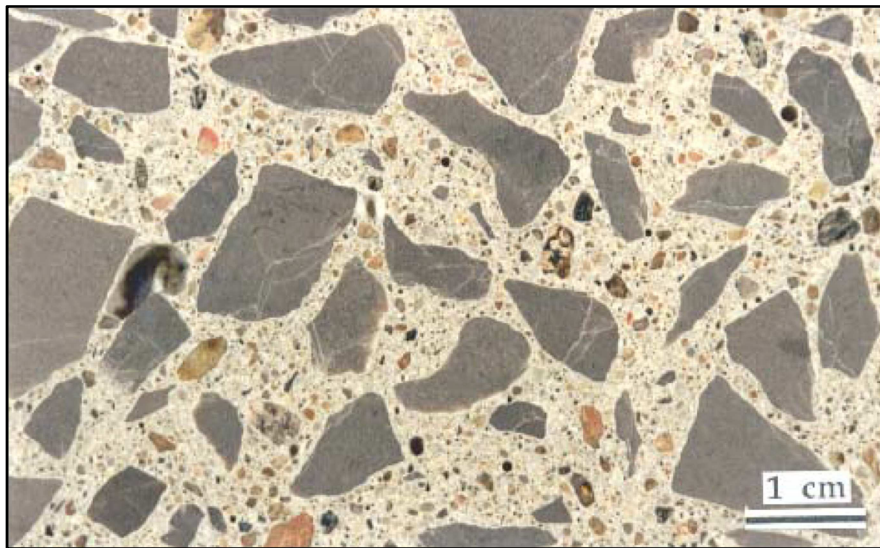
Fournier et al. (2004) states that the level of ASR-induced deterioration and the rate at which it occurs is dependent on the following five factors:

1. The inherent reactivity (nature and level of reactivity) of the aggregate material.
2. The pH of the concrete pore fluid, which is related to the total alkali content of the concrete mixture.
3. The availability of moisture.
4. The temperature and thermal gradients.
5. Configuration and structural restraint provided to the concrete structure or element.

### 2.2.3.1 Microcracking

Expansive forces that develop to form microcracking are generated through swelling of alkali-silica gel or by swelling aggregate particles. When the reaction is in its infant stages, ASR microcracking is typically limited to the aggregate particles and the cement paste-aggregate interface, as shown in Figure 2.6 (Fournier et al. 2004).

a)



b)

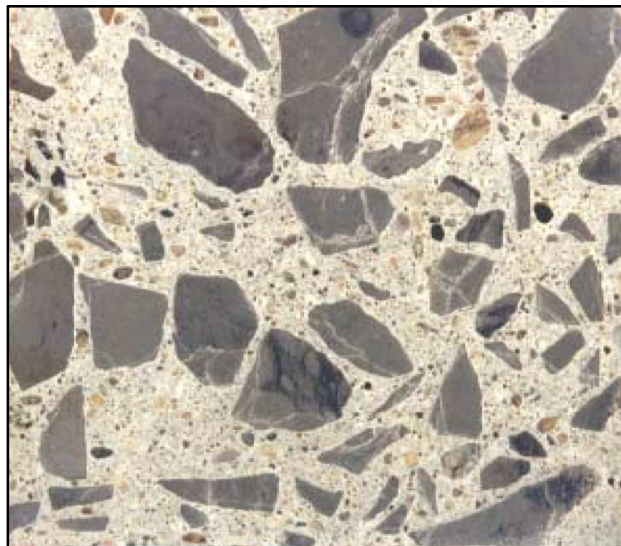


**Figure 2.6:** Microcracking in aggregate particles at a) 0.065 % and b) 0.149 % expansion (Fournier et al. 2004)



As expansion continues, microcracking extends through the cement paste matrix, and can sometimes fill voids with alkali silica gel as shown in Figure 2.7.

Figure 2.8 is a closer view of a microcrack highlighted by alkali-silica gel.



**Figure 2.7:** Extensive microcracking at 0.25 % expansion in aggregate particles and cement paste; also, a void filled with alkali-silica gel (Fournier et al. 2004)

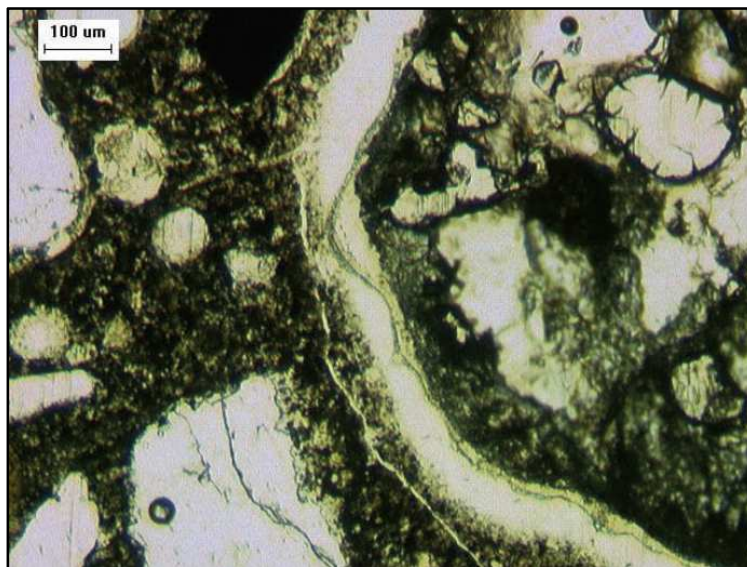


**Figure 2.8:** Thin section of concrete showing a crack highlighted by alkali-silica gel (Thomas et al. 2008)



### 2.2.3.2 Surface Cracking

As microcracks propagate, the small cracks in the aggregates and cement paste matrix fill with additional alkali-silica gel, and this gel continues to swell in the presence of moisture, causing additional larger-scale cracking. Figure 2.9 is a sketch of a concrete slab with surface cracking due to ASR.

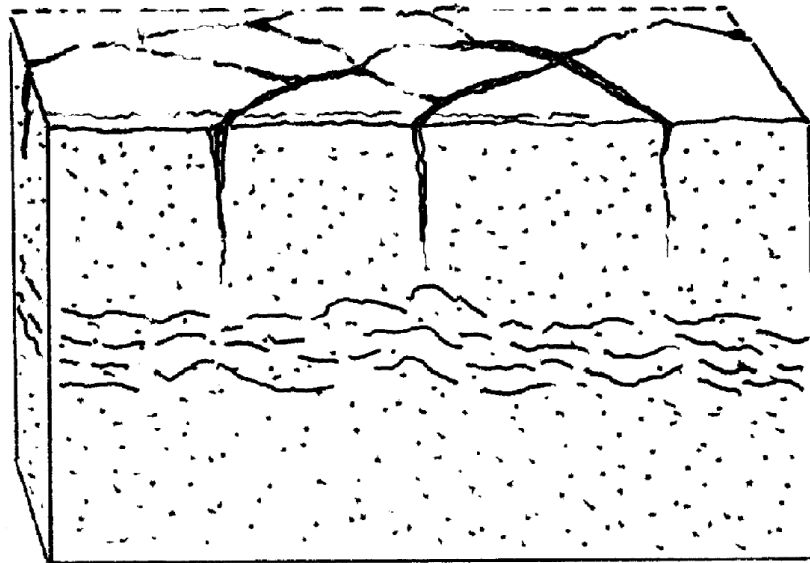


**Figure 2.9:** Sketch of a concrete slab subjected to ASR cracking with surface map-cracking, and subparallel internal cracks (Forster et al. 1998)

The mechanisms behind surface map-cracking, illustrated the concrete slab example are described here by Forster et al. (1998):

Swelling due to the uptake of water by alkali-silica reaction product generates tensile stresses that lead to the local formation of fine cracks in the concrete slab. Since the least restraint occurs in a direction perpendicular to the surface, the cracks tend to align themselves subparallel to the surface. The expansion occurring within the concrete causes tension to occur in the concrete near the surface of the slab,

where less expansion is taking place due to a lower rate of reaction. These tensile stresses are relieved by the formation of relatively wider cracks perpendicular to the surface. Viewed from above, these cracks tend to occur in a polygonal pattern that is the basis for the term “map-cracking”.

In reinforced concrete members the map-cracking pattern is less likely to appear; however, cracking will tend to orient itself to the underlying steel, or perpendicular to the direction of the confinement, as shown in Figure 2.10.



**Figure 2.10:** ASR-cracking orienting itself to underlying steel reinforcement

(Fournier et al. 2004)

### 2.2.3.3 Surface Discoloration

It is common for ASR-induced cracking to be highlighted by a broad brown area that gives the impression of permanent dampness, as shown in Figure 2.11 (Fournier et al. 2004).

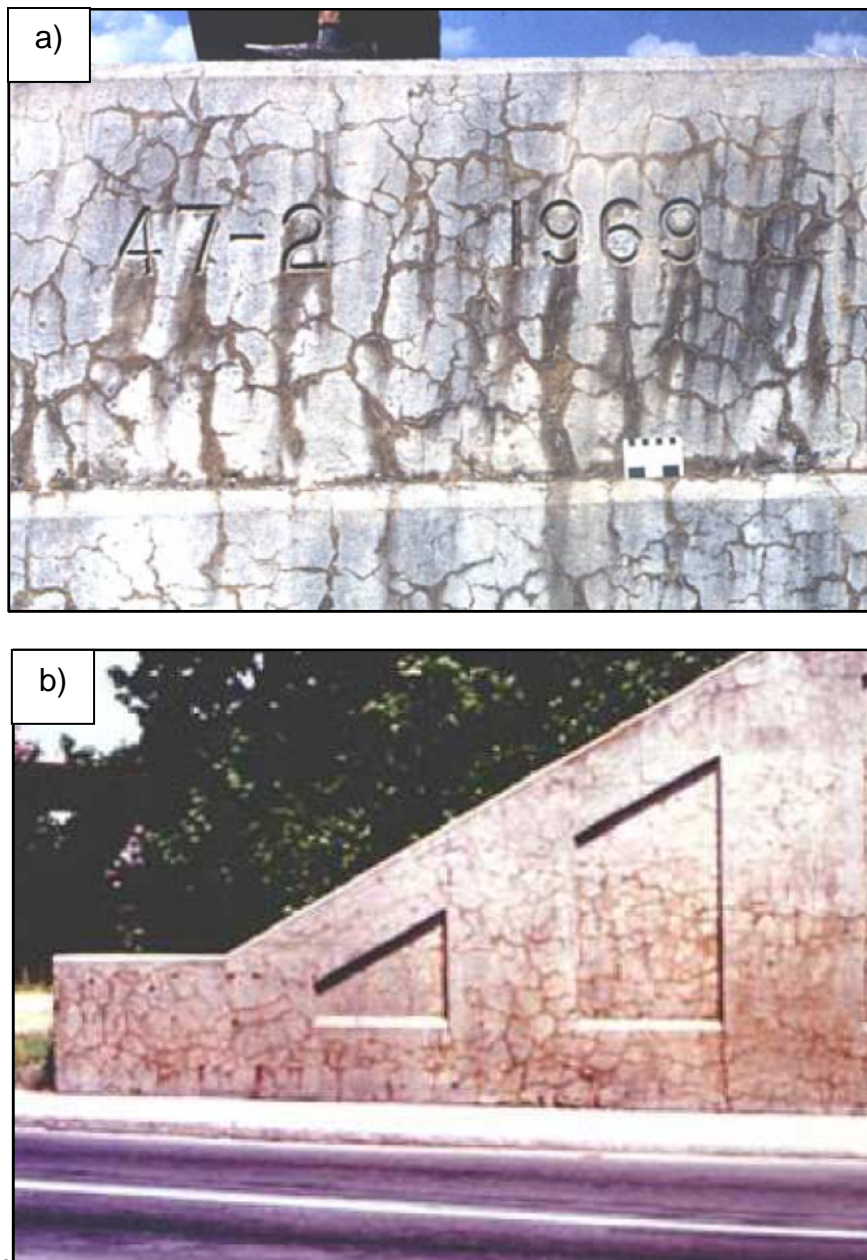


**Figure 2.11:** Examples of surface discoloration around cracks on a) a highway median barrier and b) a 25-year-old highway parapet wall (Fournier et al. 2004)

#### 2.2.3.4 Pop-Outs

Pop-outs are conical portions of the concrete surface that detach from the concrete mass, as shown in Figure 2.12. Pop-outs can be the result of expansion alkali-silica reactive aggregates at or near the concrete surface (Fournier et al. 2004). However, the presence of pop-outs does not necessarily entail the presence of ASR, as they can be produced by freezing and thawing cycles or other mechanisms.



**Figure 2.12:** Example of a pop-out induced by ASR (Fournier et al. 2004)

#### 2.2.3.5 Surface Deposits

Surface deposits of alkali-silica gel exudations, shown in Figure 2.13, are a common feature of ASR-affected concretes. However, the presence of surface deposits does not necessarily mean that the concrete is affected by ASR. Surface deposits can also include efflorescence, with or without the presence of ASR gel. “It is good investigative practice during a site survey to record the



extent and location of surface deposits along with their color, texture, dampness, and hardness” (Fournier et al. 2004).



**Figure 2.13:** Example of efflorescence and alkali-silica gel exuding to the surface of a concrete foundation suffering from ASR (Fournier et al. 2004)

#### **2.2.4 Effects of exposure conditions on ASR damage**

Exposure conditions of concrete with ASR are paramount. The availability of moisture, wetting and drying cycles, and freezing and thawing cycles all play an extremely important role in ASR-related deterioration, expansion, and the rate of the reaction itself (Bérubé et al. 2002a).

##### **2.2.4.1 Wetting and Drying**

Wetting and drying cycles tend to introduce higher levels of surface deterioration. In fact, these cycles can introduce such severe surface cracking that it may not equate to the level of internal deterioration, such as microcracking and expansion (Nishibayashi et al. 1989). Lower humidity in the drying cycles

creates an environment less conducive for ASR development in the outer layer of the concrete mass, approximately within an inch in depth. Since the interior of the concrete mass does not experience this drying cycle, the surface concrete experiences tension under the expansive pressures from the underlying concrete (Bérubé et al. 2002a). Therefore the following three phenomenon are explained:

1. Surface cracking of ASR-affected members typically only penetrates approximately an inch into the concrete mass (Bérubé et al. 2002a).
2. ASR-affected concrete masses typically deteriorate less when they have a constant source of moisture (immersed or underground) when compared to those subjected to wetting and drying cycles (Bérubé et al. 1989).
3. South-facing concrete surfaces that have more exposure to sun and drying typically demonstrate more map-cracking than northern-facing concrete surfaces (Ludwig 1989).

#### **2.2.4.2 Freezing and Thawing**

Freezing and thawing cycles can increase the rate of deterioration of ASR prone concrete by two different means. First, freezing and thawing cycles can increase the rate of deterioration of concrete already affected by cracking due to ASR. Once concrete is cracked due to ASR, moisture can more easily penetrate the concrete, and deterioration increases upon a freezing cycle (Bérubé et al. 2002a).

Additionally, the rate of ASR deterioration can be increased if the concrete is first cracked by freezing and thawing cycles. In this case, the concrete is first

cracked by freezing and thawing cycles, therefore moisture can more easily penetrate the concrete, which in turn increases the rate of ASR (Bérubé et al. 2002a).

In both cases the rate of deterioration is increased, because moisture can more easily penetrate the concrete, and because the damaged concrete is weaker and not as able to withstand the expansive forces generated by ASR (Bérubé et al. 2002a).

### **2.2.5 Evaluation of ASR through Petrographic Analysis**

Petrographic analysis of concrete samples can be used to determine if distress in existing concrete structures is due to ASR. Two methods will be discussed in this section: ASTM C 856 *Standard Practice for Petrographic Examination of Hardened Concrete*, and the Damage Rating Index (DRI).

#### **2.2.5.1 ASTM C 856 Standard Practice for Petrographic Examination of Hardened Concrete**

ASTM C 856 is an outline of procedures for the petrographic examination of samples of hardened concrete. The practice covers many different examination purposes, but the following pertain to ASR (ASTM 2011):

- Concrete from existing construction
  1. Determination in detail of the condition of concrete in existing construction.
  2. Determination of the causes of inferior quality, distress, or deterioration of concrete in a construction.

3. Determination of the probable future performance of the concrete.
4. Determination whether alkali - silica or alkali – carbonate reactions, or cement- aggregate reactions, or reactions between contaminants and the matrix have taken place, and their effects upon the concrete.
5. Determination of whether alkali - silica reaction has taken place, what aggregate constituents were affected, what evidence of the reaction exists, and what were the effects of the reaction on the concrete. The technique in Annex A1 is helpful for identifying locations where alkali-silica gel may be present.
6. Establishment of whether any other cement – aggregate reaction has taken place. In addition to alkali-silica and alkali-carbonate reactions, these include hydration of anhydrous sulfates, rehydration of zeolites, wetting of clays and reactions involving solubility, oxidation, sulfates, and sulfides.

ASTM C856 should only be performed by qualified petrographers with at least 5 years' experience in petrographic examinations of concrete and concrete-making materials (ASTM 2011). The preferred sample size is a 6 in. diameter core, 1-ft in length; however, it is noted that core samples this large are rare, as they are expensive and difficult to obtain. Most typically, samples are sawed longitudinally before visual examination, which provides an overview of the in-place concrete characteristics. The samples are also examined with the use of a stereomicroscope at 6x to 10x magnification. Stereomicroscope examination notes similar characteristics as the visual examination, but also includes more



specific cracking information pertaining to microcracking. Samples are also prepared into thin sections, 1/16-in thick, and examined under a microscope.

Finally, Annex A1 provides a technique for detecting alkali-silica gel by “treating the surface of conditioned concrete with a solution of uranyl-acetate and observing the treated surface exposed to short-wave ultraviolet light” (ASTM 2011). As the petrographer views the specimen under UV light, they look for alkali-silica gel, which will, “fluoresce bright greenish yellow, and usually occurs in and around aggregate particles, in voids, and in cracks (ASTM 2011).

Details on the specific examination procedures, specimen preparations, apparatus used, etc. can be found in ASTM C856 (2011).

#### **2.2.5.2 Damage Rating Index**

The damage rating index (DRI) is described by Grattan-Bellew (1992) and Dunbar et al. (1995) as a method to evaluate the condition of concrete by counting the number of typical ASR-related petrographic features on concrete sections that have been polished, and that are under 18x magnification. Table 2.3 summarizes the petrographic features and weighing factors for the DRI.

The procedure entails drawing a grid on a polished concrete section, with a minimum of 150 grid squares, 0.39 in. by 0.39 in. (1 cm by 1 cm), counting the presence of typical petrographic features over the surface, and then multiplying by their respective weighing factors to relate their relative importance in the overall deterioration process. The DRI represents the normalized value, to the 15.5 in.<sup>2</sup> (100 cm<sup>2</sup>), of the weighed petrographic features (The Transtec Group 2010). The higher the DRI, the more severe the deterioration due to ASR.

**Table 2.3:** Petrographic features and weighing factors for the DRI  
(Grattan-Bellew et al. 2006)

| <b>Petrographic feature</b>                        | <b>Abbreviation</b> | <b>Weighing factor</b> |
|--|---------------------|------------------------|
| Coarse aggregate with cracks                       | CrCa                | x 0.75                 |
| Open crack in coarse aggregate                     | OCrCA               | x 4.00                 |
| Coarse aggregate with cracks and reaction products | CR + RPCA           | x 2.00                 |
| Coarse aggregate debonded                          | CAD                 | x 3.00                 |
| Reaction rims around aggregate                     | RR                  | x 0.50                 |
| Cement paste with cracks                           | CrCP                | x 2.00                 |
| Cement paste with cracks and reaction products     | Cr+RPCP             | x 4.00                 |
| Air voids lined or filled with reaction products   | RPAV                | x 0.50                 |

The Transtec Group (2010) states,

There is currently no rating system for the DRI values that correspond to concrete affected to a low, moderate or severe degree by ASR. However, our experience is such that values below 200-250 are indicative of a low degree of reaction / deterioration, DRIs in excess of about 500-600 represent a high to very high (DRI > 1000) degree of ASR. It is important to mention, however, that since the DRI is not a standardized method, values can vary significantly from one petrographer to another.

## 2.2.6 Mitigation of ASR

In this section, the most effective mitigation methods of ASR in existing concrete structures will be reviewed. This includes the use of silane sealants, lithium compounds, confinement of expansion, and allowing expansion through slot cutting or concrete removal.

Since this project is only related to the mitigation of ASR in existing structures, the preventative mitigation measures pertaining to new construction will not be covered. However, a detailed review of these preventative measures can be found in chapter 5 of Forster et al. (1998).

### 2.2.6.1 Silane's effectiveness in mitigating ASR

Recalling from earlier, if the internal RH can be reduced to less than 80 percent, expansion due to ASR can be stopped (Fournier et al. 2010). For this to occur, a sealer must be applied that prevents external liquid water from penetrating into the concrete, but allows water vapor to move out of the concrete, thus creating an overall decrease in internal RH (Fournier et al. 2010). A behavioral schematic of this type of sealant on concrete is shown in Figure 2.14.

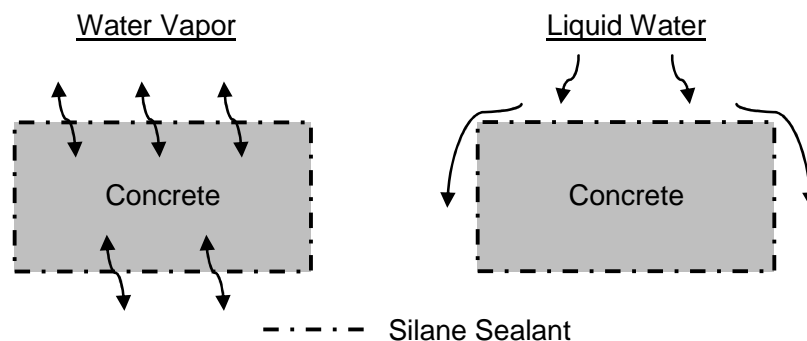


**Figure 2.14:** Effect of silane sealant on concrete

Silane water repelling sealants contain the properties needed to repel liquid water, while allowing water vapor to penetrate. However, having these properties alone does not ensure that the silane sealants will be effective. According to a report by the Canadian Standards Association (2002), in order for a sealer to reduce the internal RH in concrete, it must have the following five characteristics:

1. Resist water absorption.
2. Penetrate concrete to a measurable depth.
3. Resist deterioration from ultraviolet (UV) radiation.
4. Exhibit long-term stability in an alkaline environment.
5. Allow vapor transmission.

#### **2.2.6.1.1 General Silane Information**

Before delving into the specifics of chemical makeup and performance, it may be helpful to understand a few general characteristics of silane/siloxane water repelling sealants. There are a large variety of formulated silane/siloxane water repelling sealants on the market today. Typically, these sealants are sold as solvent-based or water-based solutions, with varying degrees of active ingredients. Alkoxysilane is a special type of silane that allows the compound to act as a bridge between the inorganic concrete and the organic alkyl tails that repel water. The amount of alkoxysilane in the solution, and the coverage rate at which it is applied, determines the sealer's effectiveness. Typical levels of alkoxysilane in effective sealants range from a minimum of 40 % to a maximum of close to 100 %, although solutions with as low as 20 % alkoxysilane are

available. Silane sealants are generally applied using a low-pressure garden sprayer as shown in Figure 2.15, but can also be painted on using a roller. Coverage rates can vary from 100-200 square feet per gallon for diluted silanes, and up to 200-300 square feet per gallon for pure silanes (Selley 2010).

Volatile organic compound (VOC) regulations play a very important role in both the type of solvent used and the level of alkoxy silane in the silane solutions. Tightening regulations have pushed manufacturers to start producing more water-based treatments and have limited the production and use of solvent-based treatments (Selley 2010).



**Figure 2.15:** Silane being applied with a low-pressure garden sprayer

#### **2.2.6.1.2 Application of Silane**

The following is an example of surface preparation and application instructions for a water-based 40 % silane penetrating sealer, called *Enviroseal 40* (BASF Construction Chemicals 2007):

1. Verify concrete has cured to a minimum of 80 % of the design strength.
2. Use water blasting, sand blasting, or shot blasting to obtain a clean concrete surface free of all sand, surface dust, dirt, oil, grease, chemical films, coating, and other contaminants.
3. Application of sealant should only be performed if all materials and surfaces involved are between 40 – 110 °F during application. In addition, sealant should not be applied if temperatures are expected to fall below 40 °F within 12 hours of application.
4. For maximum penetration of sealant, the concrete surface should be dry; however, it is permissible to have a slightly damp surface. If standing water is present, the silane sealant should not be applied.
5. Crack sealing by caulking, patchwork, or other sealants can be applied before or after silane application. However, if applied before silane application, a minimum curing time of 6-12 hours should be allowed.
6. The silane solution should be stirred thoroughly before and during application.
7. Apply silane solution by using a low-pressure, non-atomizing spray. Be sure to distribute silane solution evenly over the application area.
8. Typical drying time of silane after application is 4 hours at 70 °F and 50 % ambient RH. Cooler temperatures or higher RH may result in increased drying times.

### **2.2.6.1.3 Chemistry of Formulated Silane / Siloxane Sealants**

The word “silane” is often used as a generic term to refer to formulated silane/siloxane water repelling sealants. However, silane is by definition a monomeric silicon compound with four chemical bonds. Due to the confusion of terminology, the following definitions are provided to set the terminology that will be used in this study (adapted from Selley 2010).

- **Silicon (Si)** – An element, which is the second most abundant element in the earth’s crust.
- **Silica (SiO<sub>2</sub>)** – Naturally occurs as sand (quartz). Present in natural stone and concrete.
- **Silane** – A functional monomeric silicon compound with four chemical attachments.
- **Siloxane** – Linear Si-O-Si polymer or prepolymer, i.e., silicone.
- **Formulated Silane / Siloxane** – A product formulated from one or more of the above, to meet a variety of applications.

The following five sections will provide the chemistry of how silane / siloxane water repelling sealants satisfy each of the five CSA “effective sealer” characteristics. To review, these characteristics are

1. Resist water absorption.
2. Penetrate concrete to a measurable depth.
3. Resist deterioration from UV radiation.
4. Exhibit long-term stability in an alkaline environment.
5. Allow vapor transmission.

### 2.2.6.1.3.1 CSA Characteristic No. 1: Be able to resist water absorption

According to Selly (2010), silane has two unique characteristics that make it useful as a component in water repelling sealers. The first is silane's ability to repel water, and the second is its ability to act as a "coupling" monomer. A monomer is a basic molecule that is able to bond to other monomer molecules to form larger and more complex polymers. To repel water, a certain group of silanes called alkoxy silanes are used. Using this formulation of silane, the silicon compound has the ability to act as a connector between organic and inorganic compounds. This allows the silane compound to act as a bridge between the inorganic concrete and the organic alkyl tails that repel water. Alkoxy silanes are named for the structure of the monomer, which contains an alkyl attachment and one or more attachments containing oxygen. The basic chemical structures and chemistries of alkoxy silane are illustrated in Figure 2.16.

**R =**

- Amino
- Methacryl
- Epoxy / Glycidoxy
- Vinyl
- Sulfido
- Chloroalkyl
- Alkyl
- Phenyl

**OR' =**

- Methoxy
- Ethoxy
- Actoxy

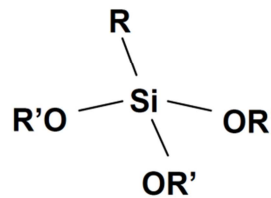


**Figure 2.16:** Silane's basic chemical structure and chemistries (Selly 2010)



Now that it is understood what a silane monomer is, there is the question of what constitutes a formulated silane/siloxane water repellent. According to Selly (2010), these water repellents consist of combinations of alkoxy-silanes, siloxane polymers, and “enabling additives”. Siloxane polymers are used due to their exceedingly hydrophobic nature. Siloxane molecules are silicone polymers, typically made up of siloxane units that are attached through oxygen as shown in Figure 2.17. The amount of each ingredient in the formulated silane/siloxane water repellent is dependent on the intended application. For example, a water-based silane treatment may need to satisfy penetration depth criteria; therefore, an enabling additive may be added to lower the surface tension and enhance penetration depths.

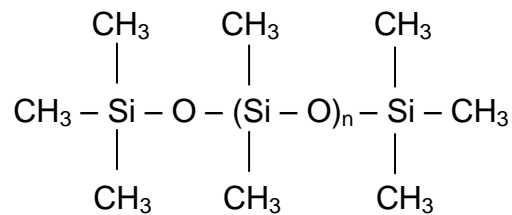


**Figure 2.17:** Siloxane Molecule (Selley 2010)

Formulated silane/siloxane sealants repel water due to the following phenomenon described by Selley (2010), which is also graphically shown in Figure 2.18:

When silanes have a longer hydrophobic alkyl tail – such as a butyl (4 carbon) or octyl (8 carbon) group – they tend to orient themselves such that this tail is pointed out towards the air. The effect is to impart a low surface energy to the substrate. Water, of course, has high surface

energy (surface tension). The difference between these energies causes water to be more attracted to itself than to the substrate, and so the water has a tendency to stay in a spherical droplet shape. This is why water “beads” on a hydrophobic surface. Water beading is not an absolute measure of the ability to keep out water, but because water does not “wet-out” on a surface, the tendency for water to find and flow into small cracks in the surface is substantially reduced.

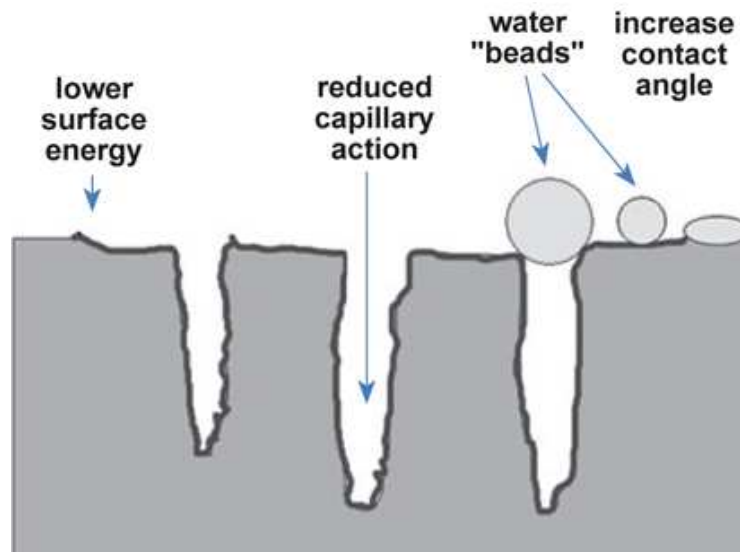


**Figure 2.18:** Representation of silane repelling water (Selley 2010)

#### **2.2.6.1.3.2 CSA Characteristic No. 2: Penetrate concrete to a measurable depth**

Liquid silane water repellents have three characteristics, which in turn allow measureable penetration into concrete surfaces. They have exceedingly low viscosity, low molecular weight, and low surface tension (Selley 2010). Although penetration depths of silane applied by hand-held pump sprayers are typically less than 0.20 to 0.24 inches (5 to 6 mm), these depths are adequate for silane

to serve as a water repelling sealant (Fournier et al. 2010). However, studies have shown that the re-application of silane to concrete that had a previous coating increased penetration depth and in turn *improved* the sealer performance (Carter 1994). The depth of penetration is due to a number of variables within the concrete itself, including the porosity, internal RH, silica content, and pH. Penetration depth is not only important for water-repelling performance, but also for resistance to wear and protection against UV radiation degradation (Engstrom 1994).

**2.2.6.1.3.3 CSA Characteristic No. 3: Resist deterioration from UV radiation**

Durability against UV radiation is achieved through the chemistry of the siloxane molecules in the formulated silanes. Because the silicon-oxygen bond energy is relatively high, the energy needed to break the bond is typically greater than that exhibited by normal UV radiation from sunlight (Selley 2010). Therefore, a single application of silane can generally remain effective for up to 5 years before a reapplication is needed (Fournier et al. 2010).

**2.2.6.1.3.4 CSA Characteristic No. 4: Exhibit long-term stability in an alkaline environment**

One of the prominent features of silicon-based products is their ability to resist degradation from pH extremes (Selley 2010). Silane must not deteriorate when subjected to the highly alkaline environments of ASR-prone concretes. This includes resisting alkalis from sources such as deicing salts or salt water. Although the mechanisms of the alkaline resistance is not discussed here,

several studies have shown silane and siloxane sealant's ability to resist extremely alkaline environment while remaining effective (Bérubé et al. 2002a; Bérubé et al. 2002b).

#### **2.2.6.1.3.5 CSA Characteristic No. 5: Allow vapor transmission**

Finally, one of silane's most important properties is its ability to be hydrophobic while being simultaneously water vapor permeable. Once again, this phenomenon is described by Selley (2010):

[This phenomenon is] due to the fact that the siloxane bond is quite long (on an atomic scale), so the spaces between the silicone and attached oxygen are actually larger than the size of the individual water molecules. This allows water vapor to pass through the polymer or network. At the same time, the methyl groups (most commonly) attached to the silicon are quite hydrophobic, so the liquid water is repelled.

#### **2.2.6.1.4 Preventative Silane Application to mitigate ASR**

Several studies have demonstrated silane's effectiveness when used as a preventative measure on concrete that is known to have ASR. Bérubé et al. (2002a) presented a laboratory study on highly ASR prone concrete cylinders exposed to rigorous 14-day "exposure cycles", as shown in Table 2.2. The expansion measurement for the cylinders exposed to cycle C5, which can be seen in Figure 2.19(a), showed that "all high-alkali cylinders sealed early with silane, which proved to be the best product among all tested, satisfied the [Canadian Standards Association suggested 0.04 % expansion limit after 1 year] regardless of the air content and the exposure conditions" (Bérubé et al. 2002a).

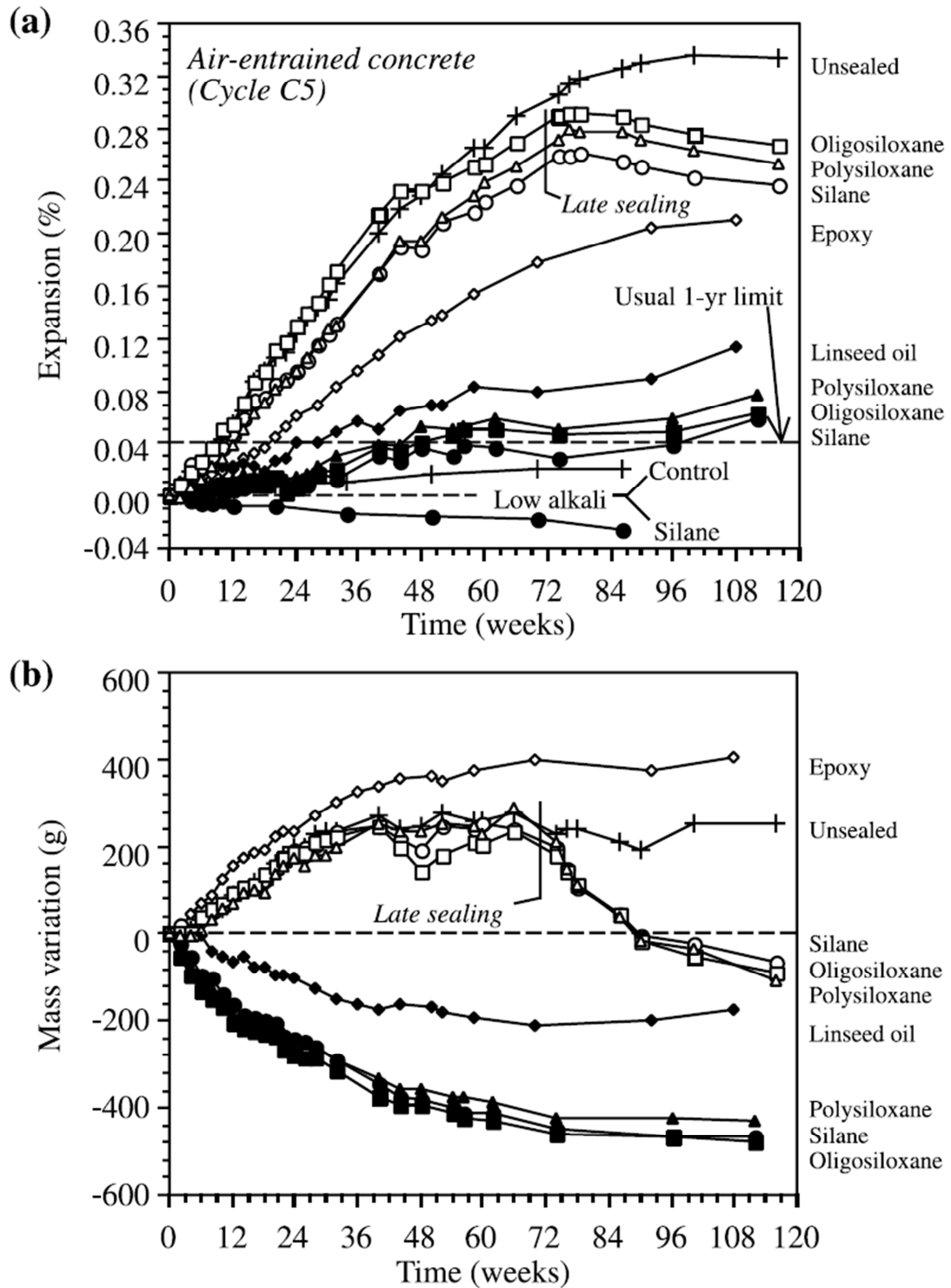


**Figure 2.19:** (a) Expansion and (b) cumulative mass variation of unsealed and sealed air-entrained concrete cylinders subjected to exposure cycle C5

(Bérubé et al. 2002a)

Although the expansion measurements are powerful evidence alone, the absence of map cracking on the surface of the cylinders is quite striking when compared to the control specimens. The comparison between 1.5-year-old unsealed and silane-sealed cylinders subjected to the rigorous 14-day exposure cycle C4 can be seen in Figure 2.20.

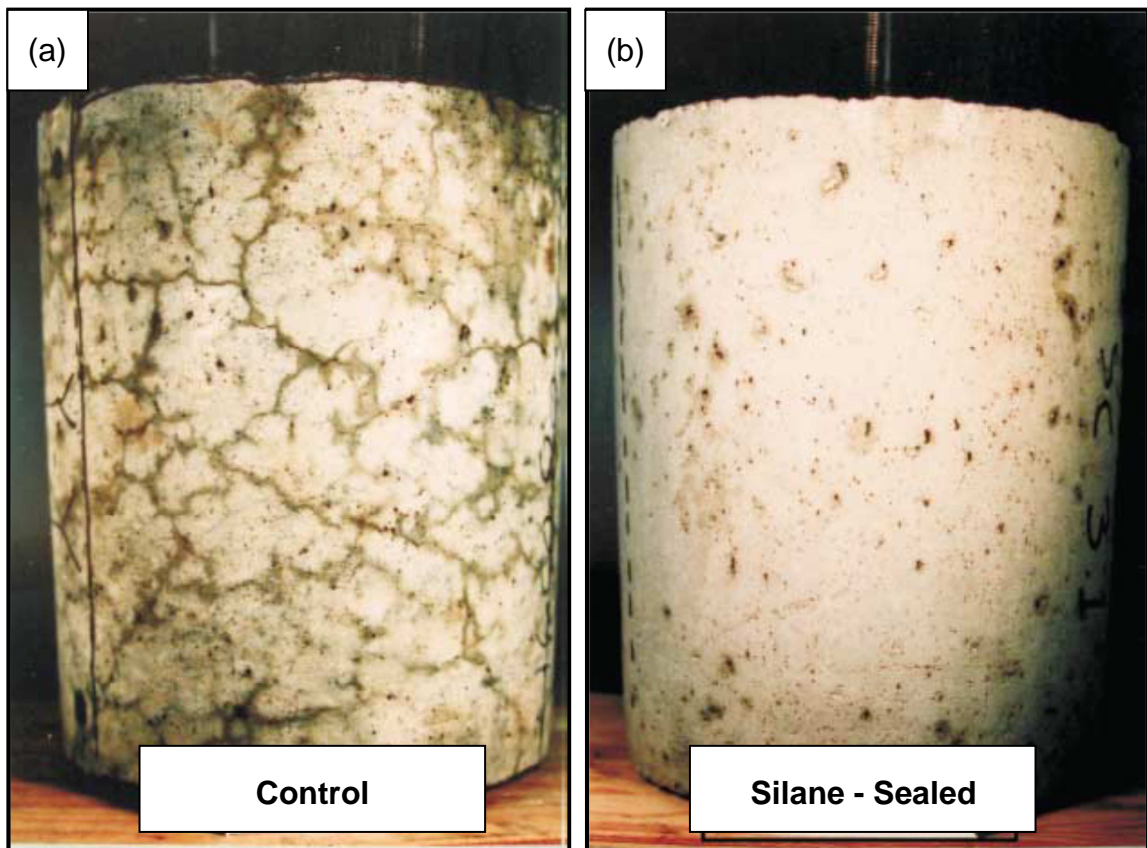


**Figure 2.20:** (a) Unsealed and (b) silane-sealed air-entrained concrete cylinders subjected to exposure cycle C4 after 1.5 years (Bérubé et al. 2002a)

### **2.2.6.1.5 Effectiveness of Silane Sealant on Concrete with ASR Cracking before Application**

Unfortunately, there is a lack of research pertaining to the effectiveness of silane sealants applied to structures that have distress due to ASR. However, there have been a small number of studies done on the subject, and thus far have shown promising results.

Bérubé et al. (2002a) performed laboratory studies where silane and siloxane were applied to ASR-affected cylinders after 1 or 1.5 years. The cylinders began to *lose mass and contract immediately* after the application of the silane or siloxane treatment as seen in Figure 8. Map cracking appearance also began to diminish as the concrete began to dry.

In an additional study by Bérubé et al. (2002b), the previously discussed laboratory findings were validated in the field by applying silane and siloxane based products to highway median barriers showing various degrees of deterioration due to ASR. The highway median barriers, located in Montmorency and Sainte-Foy in Canada, were already exhibiting ASR related map cracking to various degrees. Two examples of the highway median barriers can be seen in Figure 2.21. At the time of silane application, the deterioration of the Montmorency highway median barriers was more severe than that of the Sainte-Foy median barriers, which had more severe map cracking. Therefore, it can be assumed that the median barriers in Montmorency would have likely been more permeable due to the presence of additional internal microcracking (Bérubé et al. 2002b).



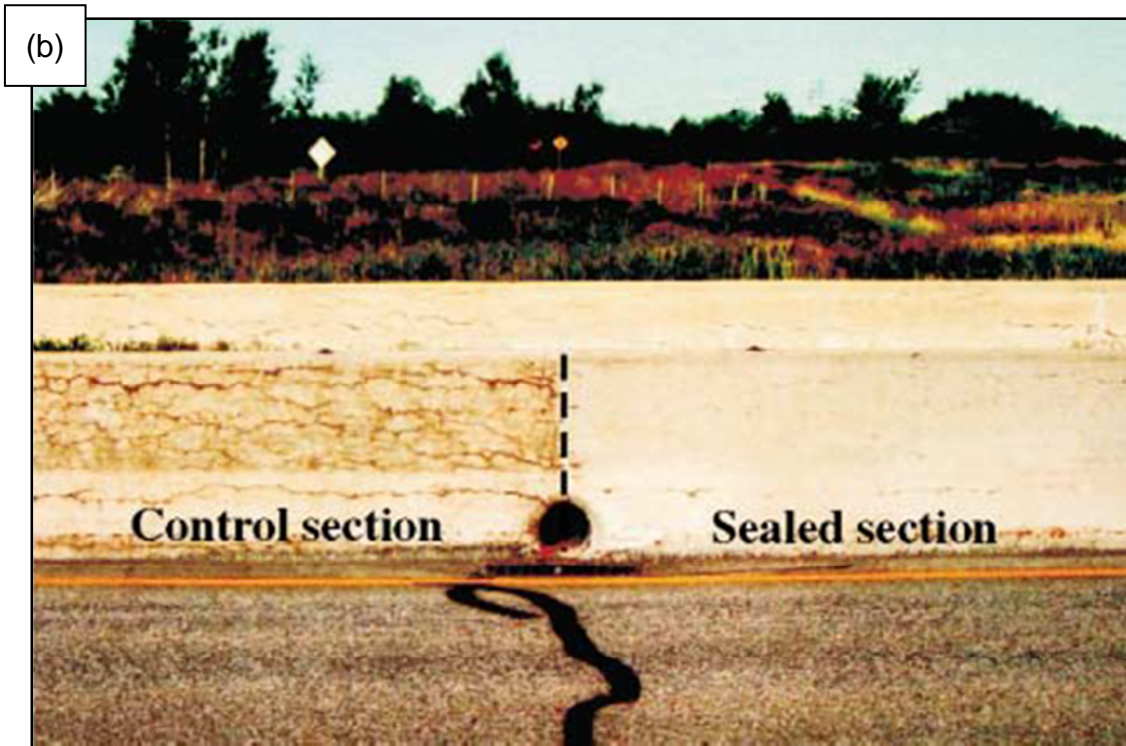
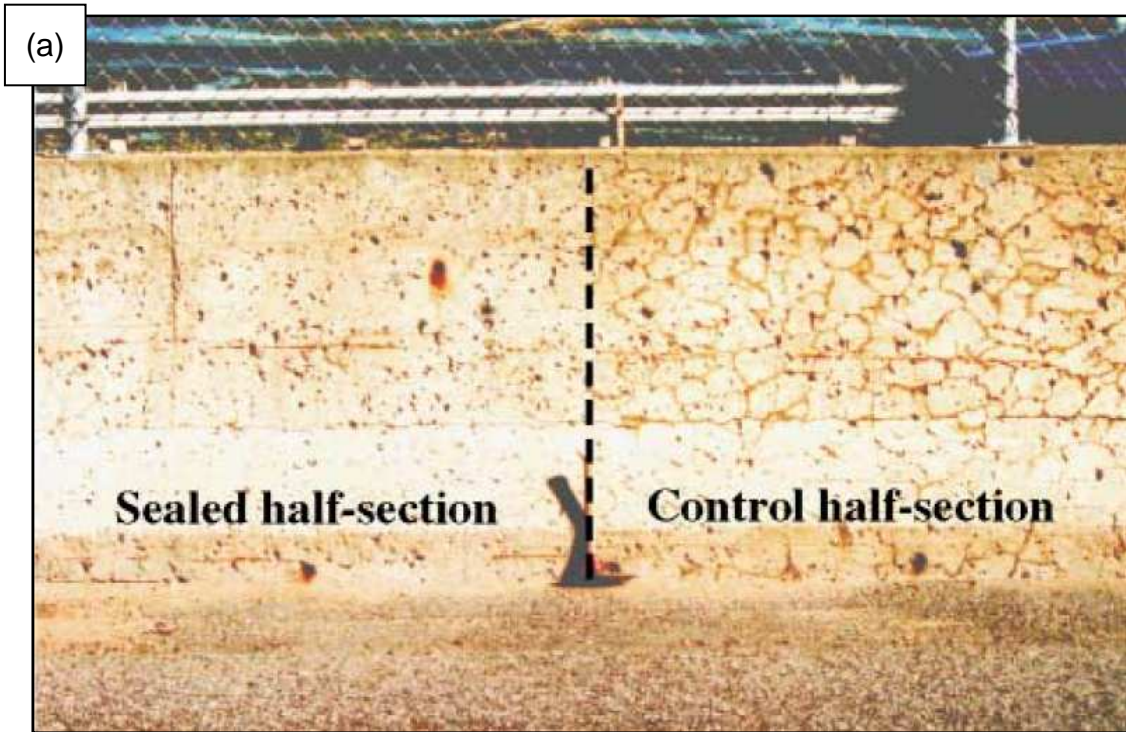


**Figure 2.21:** Examples of the unsealed and sealed highway median barriers 3 years after the application of silane sealants in (a) Montmorency and (b) Sainte-

Foy (Bérubé et al. 2002b)



At both locations the silane sealant was effective. Internal RH data were previously collected and are presented in Figure 2.22. There is a significant difference in RH between the unsealed and sealed highway median barriers at both locations. From 3- 6 years after the silane application, the average difference in between the RH of the unsealed and sealed sections of the median barriers was about 13 % and 12 % for Montmorency and Sainte-Foy, respectively (Bérubé et al. 2002b).

From trends shown in the RH at both locations, it can be seen that *the higher the degree of deterioration due to ASR, the shorter the amount of time that a good sealer such as silane remains maximally effective*. In Figure 2.22a, the converging trend of the RH in the highway median barriers in Montmorency suggests that the silane, while still effective, had passed its point of maximum effectiveness. In Figure 2.22b, the diverging trend of the RH in the highway median barriers in Sainte-Foy suggests that the silane had not yet reached a point of maximum effectiveness (Bérubé et al. 2002b).

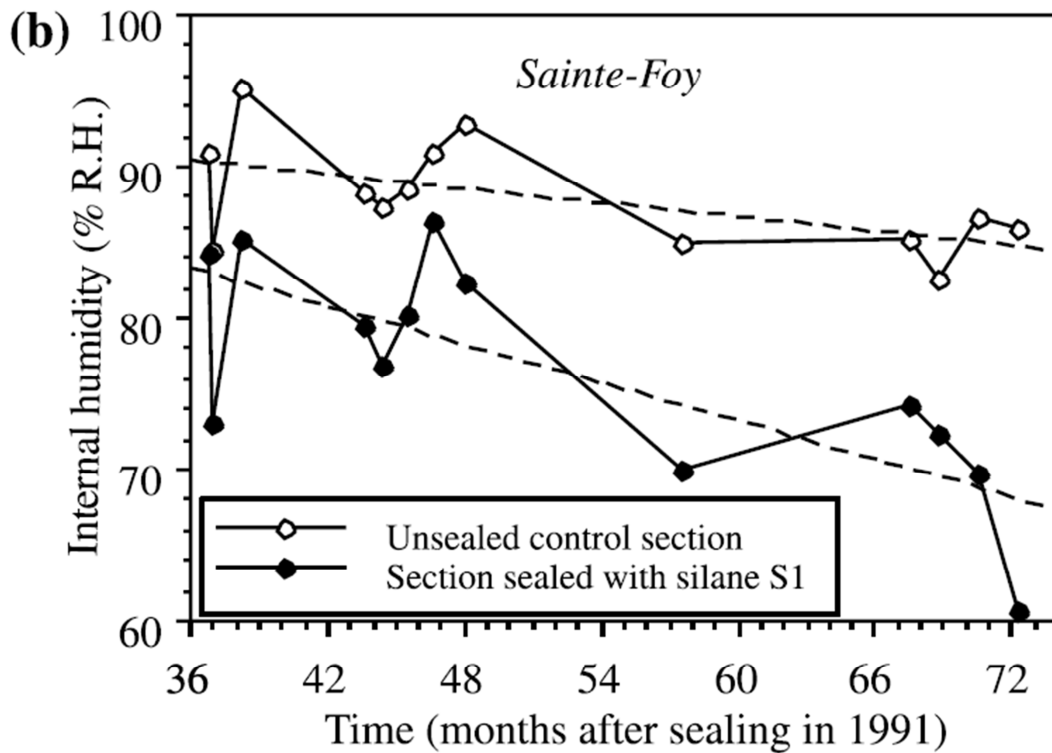
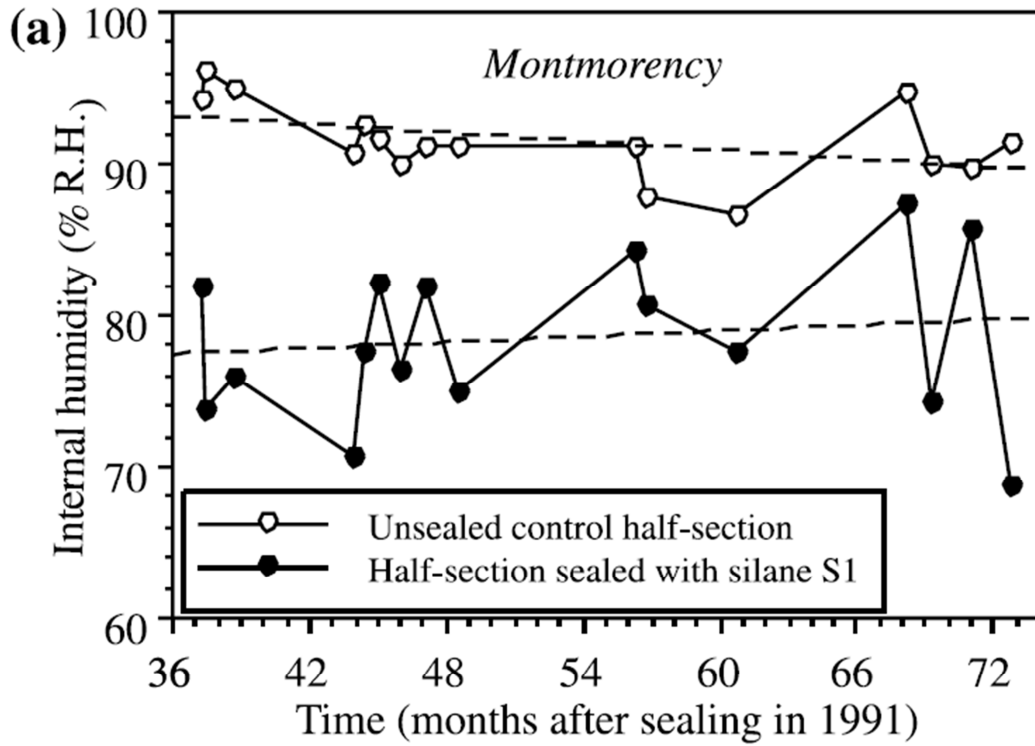


**Figure 2.22:** RH measured from 1994 to 1997 in highway median barriers in (a) Montmorency and (b) Sainte-Foy (Bérubé et al. 2002b)

#### **2.2.6.1.6 Limitations and Uncertainties of Silane**

Although silane and siloxane formulated water-repelling sealants have shown good results in preliminary field and laboratory studies in terms of slowing ASR-related expansion, there are still some uncertainties and limitations that have yet to be reviewed.

From a durability perspective, the main objective of a good sealer is to prevent expansion due to ASR over an extended period. The effectiveness of silane is dependent on the amount of deterioration of the concrete at the time of application, and the field trials of Bérubé et al. (2002b) have indicated that silane can remain effective for up to 6 years on concrete that has been subjected to map cracking. However, the amount of deterioration that is acceptable for silane to function effectively has not been quantified. Silane is not effective on concrete with “large crack widths” (Fournier et al. 2010). The larger the crack width, the easier the infiltration of water into the concrete, and the less effective the silane sealer becomes. “Large cracks” must be sealed with a flexible sealant, such as a silicone caulk or similar products, to eliminate the ingress of water into the concrete. Therefore, further research on silane’s effectiveness on concrete severely affected by ASR is needed.

Uncertainties surrounding silane’s performance include silane’s effectiveness on concrete elements with relatively large cross sections already severely affected by ASR. The studies examined previously in this literature review on the effectiveness of silane sealants on concrete with ASR cracking before application were done with specimens with dimensions of approximately

10 inches in diameter and 12 inches in thickness. These are relatively small dimensions in the terms of some in-place concrete structures; therefore, research pertaining to concrete structures of larger cross sections is needed.

Finally, there are certain situations where silane application will never be effective. In any application where moisture is available from below / beneath the silane treated surface such as slabs on grade, pavements, retaining walls, etc., silane cannot be effective as moisture ingress will always be possible from another face. Additionally, if the concrete is to be continuously wet or fully submerged, silane's effectiveness is negated due to the need of an ambient RH of less than 80 % as previously discussed (Fournier et al. 2010).

#### **2.2.6.2 Lithium-Based Mitigation Methods**

The exact mechanism of how lithium compounds reduce ASR expansion is not exactly known; however, Fournier et al. (2010) states that, "it is generally believed that lithium compounds enter into the existing gel and change the nature and behavior of the gel from expansive to essentially non-expansive." Stark et al. (1993), Stokes et al. (2000), and Barborak et al. (2004) have shown that the use of lithium compounds on ASR-affected concrete can reduce future expansions of small concrete specimens in accelerated laboratory tests.

This being said, there is, "very little, if any, documentation that lithium is effective in reducing ASR-induced expansion in actual structures in the field" (Fournier et al. 2010). The most common application method for lithium compounds is topical application, as shown in Figure 2.23. Topical application has shown limited effectiveness due to lack of penetration, "with dosages of

lithium necessary to suppress expansion measured only down to the first 2 to 3 mm, even after three treatments in heavily cracked pavements” (Fournier et al. 2010).



**Figure 2.23:** Topical application of lithium compounds (Fournier et al. 2010)

Due to the lack of penetration in topical application, recent studies have focused on increasing penetration depth with the use of vacuum impregnation and electrochemical methods. Vacuum impregnation has shown limited results in the terms of surface penetration. Fournier et al. (2010) states,

For ASR-affected bridge columns in which lithium nitrate was applied via vacuum, the depths of lithium penetration were found only to be in the present in the outer 9 to 12 mm, drawing into question whether such an elaborative and expensive vacuuming technique is justified.

Electrochemical methods of driving lithium compounds have shown better, but still limited results. Referring to the same study, Fournier et al. (2010) states, Substantially higher depths of penetration were observed in the same study when lithium nitrate was electrochemically driven into bridge columns, with dosages sufficient to reduce ASR measured all the way down to the reinforcing steel (50 mm from outer surface). However, one “side effect” of the latter process must be addressed. Lithium ions were clearly driven to the reinforcing steel, as was the intention, but because the steel serves as a cathode in the electrochemical process, hydroxyl ions are produced at the surface of the reinforcing steel. To maintain charge neutrality and to offset the production of hydroxyl ions at the reinforcing steel surface, sodium and potassium ions from within the concrete migrated towards the steel surface. This creates an increase in the hydroxyl ion concentration and a subsequent increase in alkali (sodium and potassium) concentration near the surface of the reinforcing steel may exacerbate ASR-induced expansion and cracking in this region. Future monitoring of these columns (expansion, cracking, microstructural evaluations aimed at regions near the concrete/steel interface) should help to determine if the potentially detrimental side effects of electrochemical impregnation outweigh the benefits of the significant lithium penetration.

Details on the processes of the electrochemical method are found in East (2007).

### **2.2.6.3 Minimizing or managing symptoms of ASR**

Instead of slowing the reaction, or minimizing expansion of the reaction product, one can allow ASR to occur but attempt to lessen the impact on the performance or service life of the structure (Fournier et al. 2010). This section covers three methods in which this can be achieved:

1. crack filling to limit the ingress of water, chloride, or other harmful ions,
2. confinement of expansion, or
3. permitting expansion through the use of slot cutting or concrete removal.

#### **2.2.6.3.1 Crack filling**

Filling cracks initially caused by ASR limits the ingress of water, chloride ions, external alkalis, and sulfates that can exacerbate ASR, cause corrosion of reinforcing steel, and sulfate attack (Fournier et al. 2010). Fournier et al. (2010) recommend that cracks be filled with a flexible grout or caulk if the cracks become wider than 0.006 in. (0.15 mm) for reinforced members of bridges, and 0.012 in. (0.30 mm) for pavements and non-reinforced members of bridges.

#### **2.2.6.3.2 Confinement of expansion**

Physical confinement or restraint of concrete by means of encapsulation with non-reactive concrete, or an applied stress through post-tensioning or reinforcing has been shown to considerably reduce the expansions due to ASR in the direction of restraint (Fournier et al. 2004).

### **2.2.6.3.3 Slot cutting or concrete removal**

Slot cutting or removing concrete in pavements and dam structures has been shown to extend their service life (Fournier et al. 2010). The removed sections can be replaced with new, non-reactive concrete, and the slot cuts allow room for future expansions. Slot cutting and concrete removal only addresses the stresses acquired from ASR expansion, but does nothing to slow future expansions (Fournier et al. 2010).

## **2.3 Modeling moisture movement in hardened concretes**

To determine how the internal RH decreases after silane application, one must first understand the movement of moisture through concrete. This section reviews the background theories governing moisture diffusion, and provides a moisture diffusion/ heat transfer analogy for use in finite-element analysis.

### **2.3.1 Background theory**

Fick's second law states that the rate of moisture change in a given direction is governed by the following differential equation (Bažant and Najjar 1971):

$$\frac{\partial C}{\partial t} = \nabla(D \times \nabla C) \quad \text{(Equation 1)}$$

Where C is the moisture concentration in the concrete (mass per unit volume), t is time, and D is the diffusion coefficient of the concrete. Equation 1 is only applicable in situations where the temperature is a constant, and where change in the concrete properties due to hydration is negligible. Moisture diffusion, spread to three dimensions, is governed by the following equation (Bažant and Najjar 1971):



$$\frac{\partial C}{\partial t} = D \left( \frac{\partial^2 C}{\partial x^2} + \frac{\partial^2 C}{\partial y^2} + \frac{\partial^2 C}{\partial z^2} \right) \quad (\text{Equation 2})$$

The diffusion coefficient (D) describes the moisture movement through the concrete as it relates to the internal RH. Bažant and Najjar (1971) proposed a model for the diffusion coefficient in relation to RH and concrete strength, shown as equation 3. The CEB-FIB Model Code (2010) adopted Bažant and Najjar's work and produced a standardization of the coefficients within the equation.

$$D(H) = D_1 \left[ \delta + \frac{1-\delta}{1+[(1-H)/(1-H_c)^n]} \right] \quad (\text{Equation 3})$$

Where:

H = Internal Relative Humidity

$D_1$  = maximum of D(H) for H = 1 (m<sup>2</sup>/s),

$D_0$  = minimum of D(H) for H = 0 (m<sup>2</sup>/s),

$\delta = D_0 / D_1$  (Can be assumed to be 0.05),

$H_c$  = Relative Pore Humidity (Can be assumed to be 0.80),

n = 15,

$D_1 = D_{1,0} / (f_{ck}/f_{ck0})$  ,

$D_{1,0} = 1 \times 10^{-9}$  (m<sup>2</sup>/s), and

$f_{ck0} = 10$  MPa.

This nonlinear diffusion coefficient produces an S-shaped curve that is shown in Figure 2.24. As the strength of the concrete decreases, the diffusivity of the concrete increases. Therefore, it should be expected that concrete with lower strength should allow moisture to mitigate through it faster than concrete with higher strength.

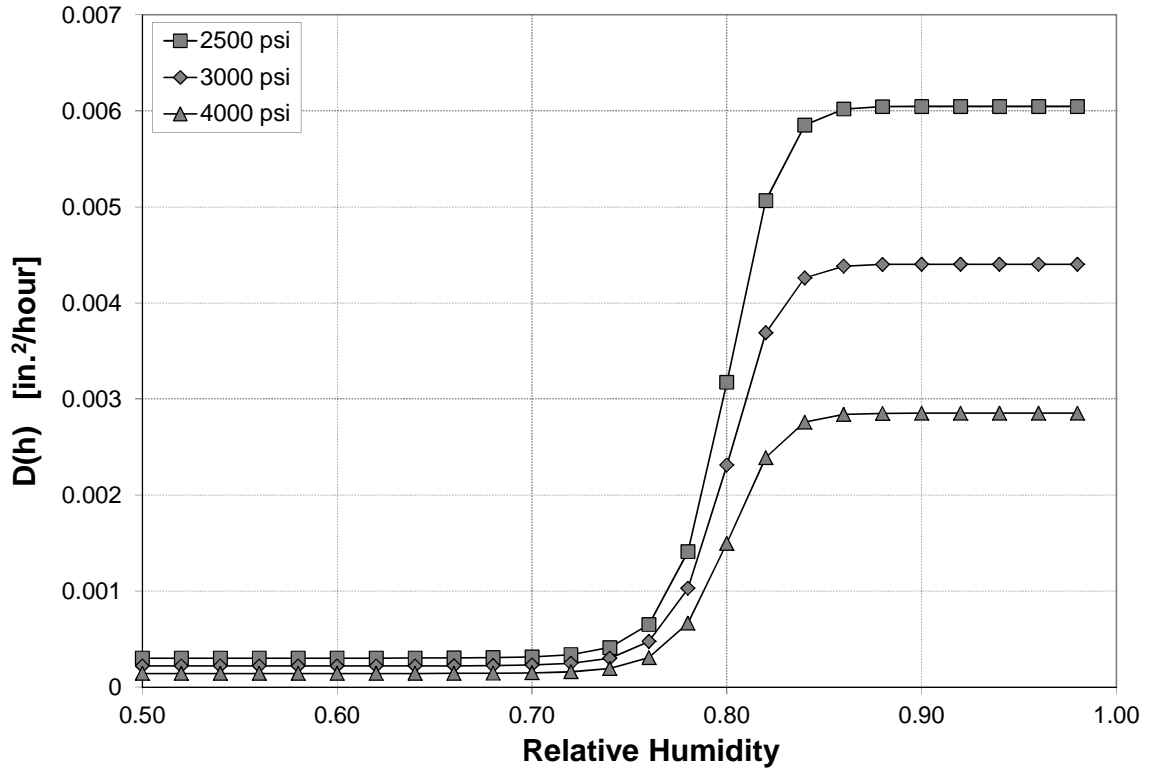


**Figure 2.24:** Diffusion coefficients for varying strength of concrete

### 2.3.2 The Moisture Diffusion / Heat Transfer Analogy

The software ANSYS 12.0 was used in this project to model the moisture movement in concrete. ANSYS 12.0 does not contain a moisture diffusion modeling capabilities. However, it does contain thermal analysis capabilities. Therefore, a moisture diffusion / heat transfer analogy was needed to model moisture diffusion in terms of heat transfer.

Equation 2 describes moisture diffusion in three dimensions relative to the diffusion coefficient and the moisture concentration. Equation 4 is an analogous equation that governs heat diffusion in terms of temperature and the thermal diffusivity (Madenci and Guven 2006).

$$\frac{\partial T}{\partial t} = \alpha \left( \frac{\partial^2 T}{\partial x^2} + \frac{\partial^2 T}{\partial y^2} + \frac{\partial^2 T}{\partial z^2} \right) \quad \text{(Equation 4)}$$

Where  $T$  is temperature, and  $\alpha$  is thermal diffusivity. Thermal diffusivity is written in terms of thermal conductivity ( $\kappa$ ), density ( $\rho$ ), and specific heat ( $c$ ), as shown in equation 5.

$$\alpha = \frac{\kappa}{\rho c} \quad (\text{Equation 5})$$

Unlike temperature, moisture concentration does not have to be continuous across material boundaries (Madenci and Guven 2006). Therefore, the moisture diffusion equation 2 cannot be used interchangeably with the heat diffusion equation 4. However, if moisture concentration is normalized with the saturated moisture concentration,  $C_{\text{sat}}$ , the thermal diffusion equation can be used for finite-element formulation of moisture diffusion problems (Madenci and Guven 2006). The wetness parameter,  $w$ , normalizes moisture concentration and is the last relation needed to be able to use heat transfer for moisture diffusion finite-element analysis.

$$w = \frac{C}{C_{\text{sat}}} \quad (\text{Equation 6})$$

Finally, the correspondence between the two diffusion conditions is summarized in Table 2.1.

**Table 2.1:** Relationships between thermal and moisture diffusivity  
(Madenci and Guven 2006)

| <b>Property</b>         | <b>Thermal</b>              | <b>Moisture</b>                       |
|-------------------------|-----------------------------|---------------------------------------|
| <i>Primary Variable</i> | <i>Temperature, T</i>       | <i>Wetness, w</i>                     |
| Density                 | $\rho$ (kg/m <sup>3</sup> ) | 1                                     |
| Conductivity            | $\kappa$ (W/m·°C)           | $D \cdot C_{\text{sat}}$ (kg/s·m)     |
| Specific heat           | $c$ (J/kg·°C)               | $C_{\text{sat}}$ (kg/m <sup>3</sup> ) |

## 2.4 Summary

To review, ASR is a deleterious reaction that occurs in concrete with the following three conditions (Forster et al. 1998):

1. Sufficient alkalinity in the cement
2. The presence of reactive silica
3. Sufficient moisture within the concrete

When these three ingredients are present, the reaction produces ASR gel. ASR gel swells in the presence of moisture, and can create significant distress leading to major deterioration. Map cracking is typically seen on the surface of structures with ASR, as shown in Figure 2.5. In reinforced concrete structures, cracking patterns typically run parallel to underlying reinforcement, as shown in Figure 2.10. The effects of exposure conditions on ASR are paramount. Wetting and drying cycles can lead to cracking that is more pronounced than in concrete subjected to constant moisture. Likewise, freezing and thawing can expedite cracking due to ASR.

To determine if an in-place concrete structure has ASR, two evaluation methods can be used: ASTM C 856 - Standard Practice for Petrographic Examination of Hardened Concrete, and the Damage Rating Index. Both methods require skilled petrographers to determine the presence of ASR in hardened concretes.

To mitigate ASR in existing concrete structures, there are only a few different options, with varying levels of effectiveness. If the internal RH can be lowered to less than 80 % internal RH, it has been shown that ASR expansion

can be slowed or stopped (Bérubé et al. 2002a; Stark 1991). Previous studies have shown that silane sealants have been effective in lowering internal RH to less than 80 % in laboratory cylinders and thin field structures (Bérubé et al. 2002a, 2002b).

Another mitigation option is the use of lithium compounds, which has shown the reduction of future expansions of small concrete specimens in accelerated laboratory tests (Stark et al. 1993; Stokes et al. 2000; Barborak et al. 2004). There is “very little, if any, documentation that lithium is effective in reducing ASR-induced expansion in actual structures in the field” (Fournier et al. 2010).

Instead of mitigating ASR in field structures, one can minimize or manage the symptoms caused by ASR. This can be achieved by crack filling, confinement of expansion, slot cutting, or by concrete removal.

Finally, to determine how the internal RH decreases after silane application, one must first understand the movement of moisture through concrete. Fick’s second law is the fundamental principle that governs moisture movement through concrete. Using Fick’s second law, Bažant and Najjar (1971) derived a model for the diffusion coefficient in relation to RH and concrete strength. The CEB-FIP Model Code (2010) adopted Bažant and Najjar’s work and produced a standardization of the coefficients within the equation. Using the CEB-FIP Model Code’s diffusion coefficient, a moisture diffusion/ heat transfer analogy can be made to be used in modern finite-element analysis.

## Chapter 3

### Bibb Graves Bridge

#### 3.1 Background

Wetumpka, Alabama is located approximately 20 miles north-north-east of Montgomery, as shown in Figure 3.1. The Bibb Graves Bridge is the fifth bridge built to span the Coosa River in Wetumpka, AL (Blackburn 1997).

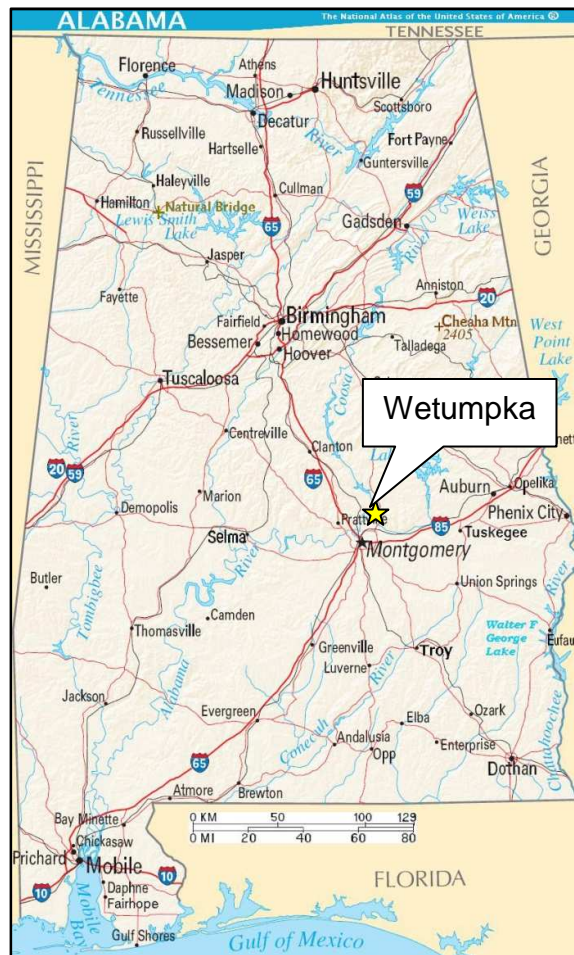


Figure 3.1: Map of Alabama with a star denoting Wetumpka (gkpedia, n.d.)

All of the information in this section, unless otherwise noted, is adapted from Blackburn (1997). The first recorded bridge that spanned the Coosa River in Wetumpka was erected in 1830. How this bridge was destroyed is unknown, but it is known that the next bridge was built in 1834. This toll bridge survived for ten years until it was washed away in a flood in 1844. The same year, a wooden covered bridge was built under the supervision of Horace King, a slave. A photograph of the covered bridge is shown in Figure 3.2.



**Figure 3.2:** Covered bridge built in 1844 (Blackburn 1997)

This bridge fared better, surviving 22 years before the “Great Flood of 1866” washed it away. It was not until 1887 that another bridge was constructed. Built in 1887 by the Southern Bridge Company of Birmingham, the structure was the first iron bridge at this location. Photographs of the iron bridge are shown in Figure 3.3 and 3.4.



**Figure 3.3:** Iron bridge constructed in 1887 (Blackburn 1997)



**Figure 3.4:** 1887 Iron Bridge in the background with Lock 31, completed in 1896, in the foreground (Blackburn 1997)

The iron bridge served the county well for 40 years. However, due to the need of extensive and expensive maintenance, the commissioners thought it more cost effective to build a new bridge rather than spending money to maintain the old one.

Governor Bibb Graves wanted the new bridge to be constructed out of steel, but the commissioners were adamant that the new bridge be made of reinforced concrete. Ultimately the decision was made to use reinforced concrete, and to split the estimated cost of \$177,400 between the state and county equally. Designed by Edward Houk, the Bibb Graves Memorial Bridge was constructed in 1931. The Bibb Graves Bridge is the most recognizable landmark of Wetumpka, and has become the emblem of choice for most local organizations and events. An interesting fact is that several scenes of the 2003 movie *Big Fish* were filmed on the bridge.



### 3.2 Construction, Layout, and General Information

The Bibb Graves Bridge, which carries AL 111, is the main thoroughfare across the Coosa River connecting the two sides of Wetumpka, Alabama. Today, the bridge carries pedestrian and motorized traffic, at a rate of approximately 9,370 vehicles a day (Holth 2010). An aerial view of the Bibb Graves Bridge, as it is seen today, is shown in Figure 3.5.

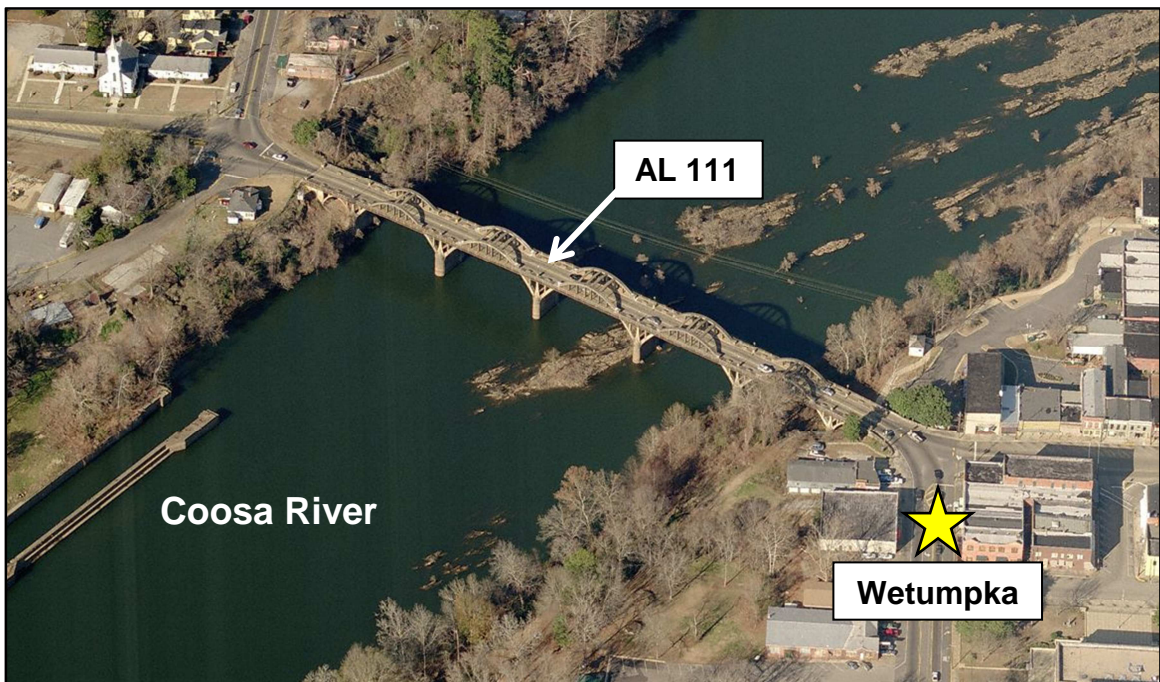


**Figure 3.5:** Aerial view of the Bibb Graves Bridge (Bing 2012a)

The reinforced concrete bridge is 700 ft long and has a 24 ft wide roadway. The bridge consists of seven arches that support the bridge deck, as shown in Figure 3.6. Other than span 1 and 7, the bridge deck is suspended from the arches at half-height. The arch lengths for the various spans are summarized in Table 3.1. The massive concrete piers for the arches average 10 feet in width and 40 feet in length, and are imbedded into 8 to 10 feet of solid rock (Taylor 1930).

Figure 3.6: Elevation and plan view of Bibb Graves Bridge

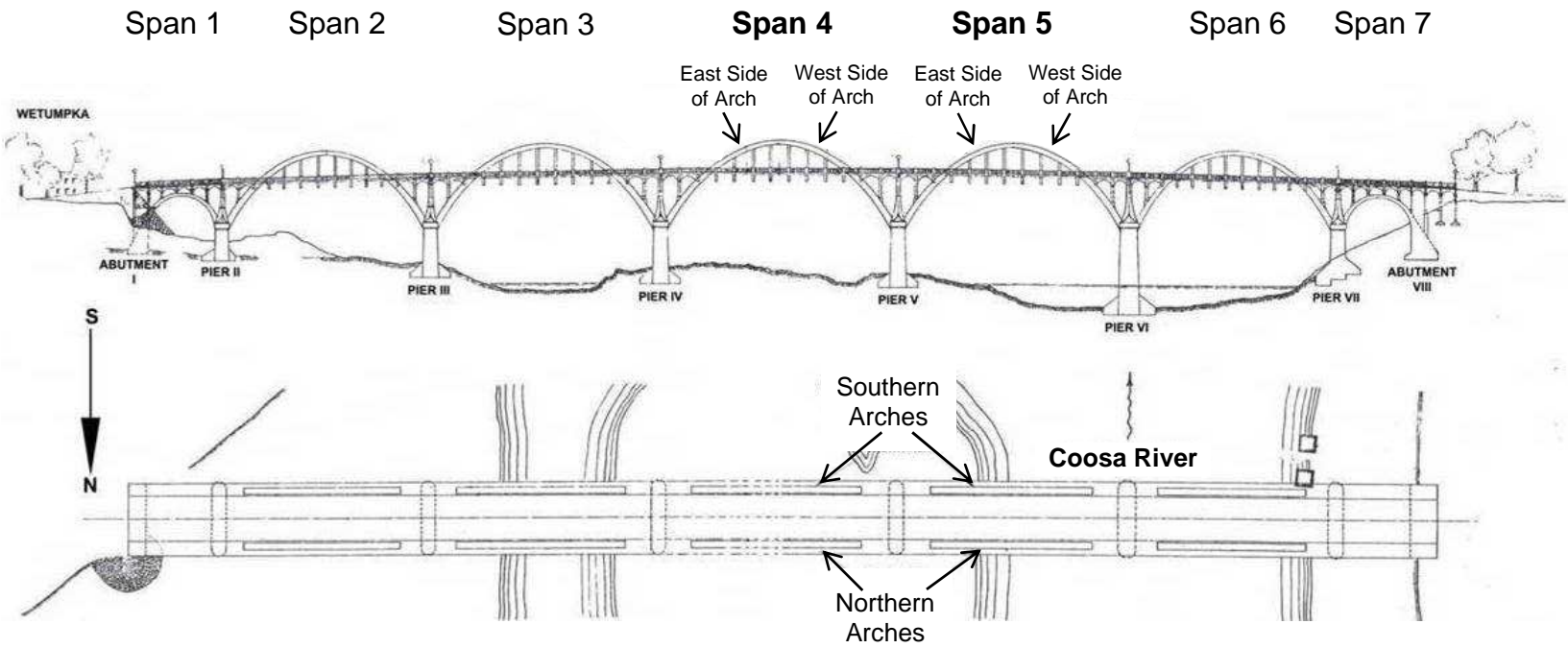


**Table 3.1:** Span lengths for various arches (Taylor 1930)

|             | Span   |        |        |        |        |        |        |
|-------------|--------|--------|--------|--------|--------|--------|--------|
|             | Span 1 | Span 2 | Span 3 | Span 4 | Span 5 | Span 6 | Span 7 |
| Length (ft) | 40     | 117    | 128    | 132    | 128    | 117    | 40     |

The arches that support the roadway are 4 ft wide and 2 ft thick. During arch construction, shown in Figure 3.7, four different specified strengths of concrete were used. The strengths vary from 2,000 psi to 4,000 psi. The concrete placement schedule for these various concrete strengths is shown in Figure 3.8. The reason behind the different strengths was to expedite placement operations. Taylor (1930) states, “High early strength is desirable in section 4 since it will have less time to set than the other before the forms are removed. The increased cost of the rich mixture used in sections 3 and 4 will be balanced by the time saved in being able to remove the form earlier.”

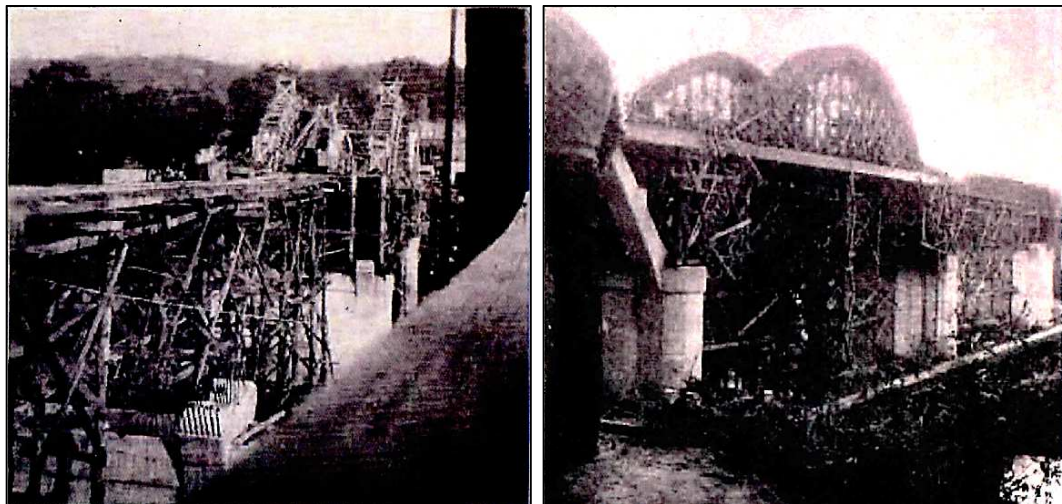


**Figure 3.7:** Bibb Graves Bridge under construction (Taylor 1930)

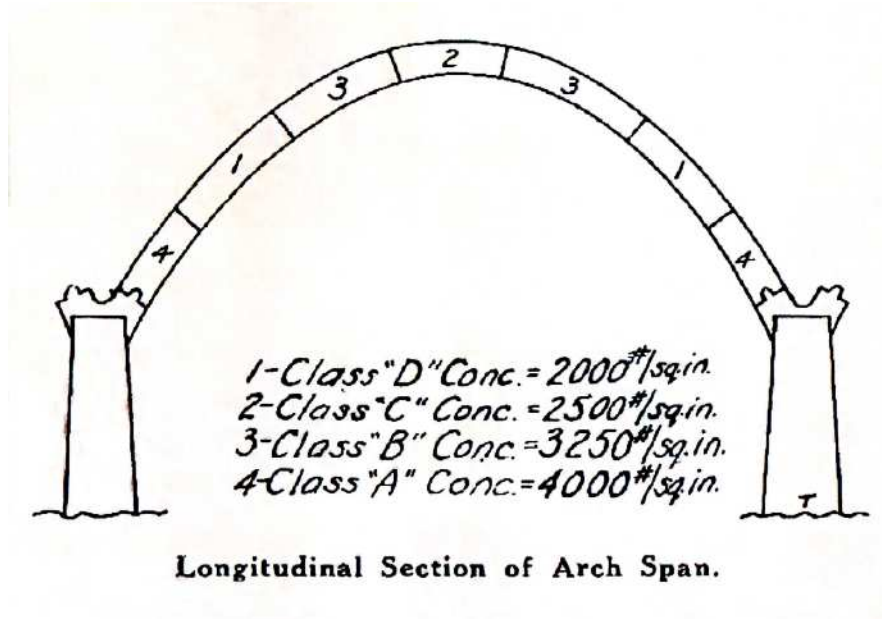


**Figure 3.8:** Concrete placement schedule for various concrete strengths  
(Taylor 1930)

### 3.3 ASR in the Bibb Graves Bridge

The majority of the Bibb Graves Bridge is in sound condition; however, the two arches supporting the fifth span are severely cracked due to expansion caused by ASR. The presence of ASR in the Bibb Graves Bridge was first noted in the 1956 ALDOT report by Hester and Smith. Significant distress was first noticed in 1993 by Sergio Rodriguez, who was ALDOT's Concrete Engineer at the time. Two photographs of ASR distress, taken by Sergio Rodriguez, are shown in Figure 3.9. Figure 3.10a provides an example of an arch unaffected by ASR, and Figure 3.10b provides a view of a similar section of concrete on span 5 that is damaged by ASR.



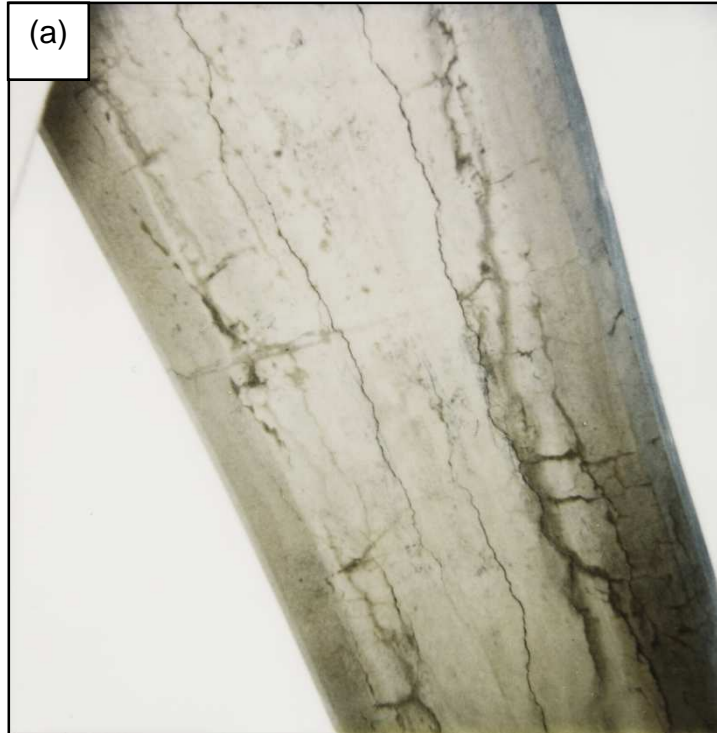


**Figure 3.9:** Examples of distress in the late 1990s on the  
a) top and b) bottom of a span 5 arch



**Figure 3.10:** Arches on the Bibb Graves Bridge in 2010

(a) Unaffected arch and (b) arch affected by ASR

### **3.3.1 Petrography of Concrete in Span 4 and 5**

In January of 2010, cores were extracted from the Bibb Graves Bridge by ALDOT for evaluation by The Transtec Group through Dr. Benoit Fournier in Canada, and Wiss, Janney, Elstner Associates, Inc. (WJE), Illinois, to determine the cause of distress.

#### **3.3.1.1 Coring Layout and Details**

All of the information in this section, unless otherwise noted, was adapted from ALDOT (2010). Three-inch diameter cores were extracted from four locations, as shown in Figure 3.11. Two cores were taken from each location, for a total of eight cores. The coring process involved locating rebar, drilling, extracting, labeling, wrapping, packing, and shipping to Illinois and Canada. This is shown in Appendix A, Figures A.1, A.2-A.5, A.6, A.7, A.8, A.9, and A.10, respectively. Pictures of the cores are shown in Appendix A, Figures A.11-A.18. Core details are also available in Appendix A, Tables A.1-A.8.

#### **3.3.1.2 WJE's Petrographic Study Results**

All of the information in this section was adapted from WJE (2010). WJE was sent four concrete cores: 1A-South, 1A-North, 1B-South, and 1B-North. Petrographic studies were conducted with the methods of ASTM C 856 *Standard Practice for Petrographic Examination of Hardened Concrete*.

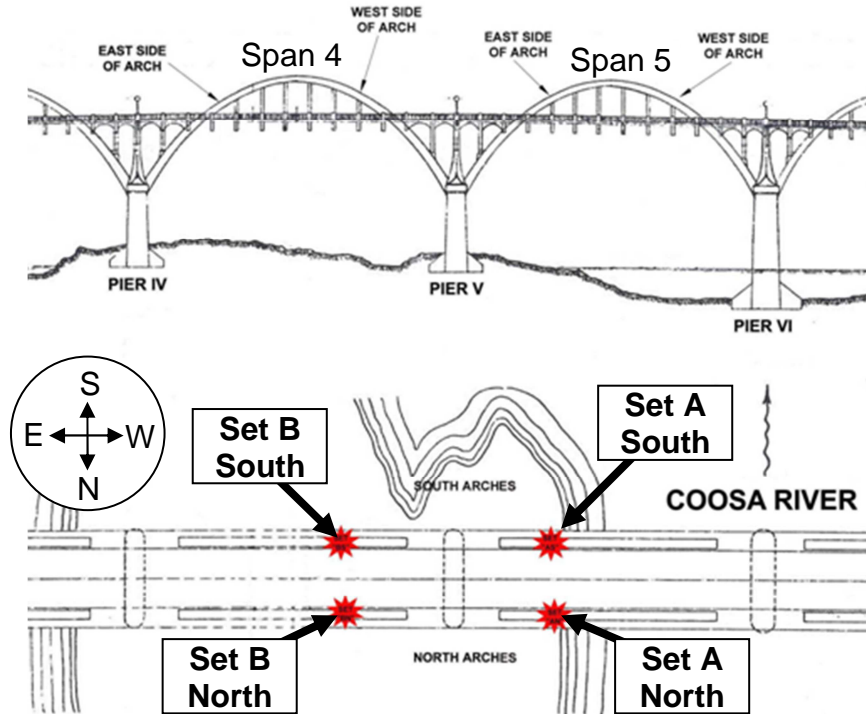


**Figure 3.11: Core Extraction Layout (ALDOT 2010)**

### **3.3.1.2.1 Concrete Composition**

The concrete in all four samples was considered well consolidated. Coarse aggregate particles consist of siliceous gravel that is composed of quartzite and chert. Coarse aggregate particles were found to be rounded to sub-angular, mostly oblong in shape, and typically poorly graded, with the exception of core 1B-South. Dark rims were commonly observed around coarse aggregate particles, as shown in Figure 3.12. The fine aggregate consists of natural siliceous sand that is mainly composed of quartz, quartzite, chert, iron oxides, mica, and small amounts of limestone and a slag-like material. Paste properties were good except in the locations where the concrete was in distress.



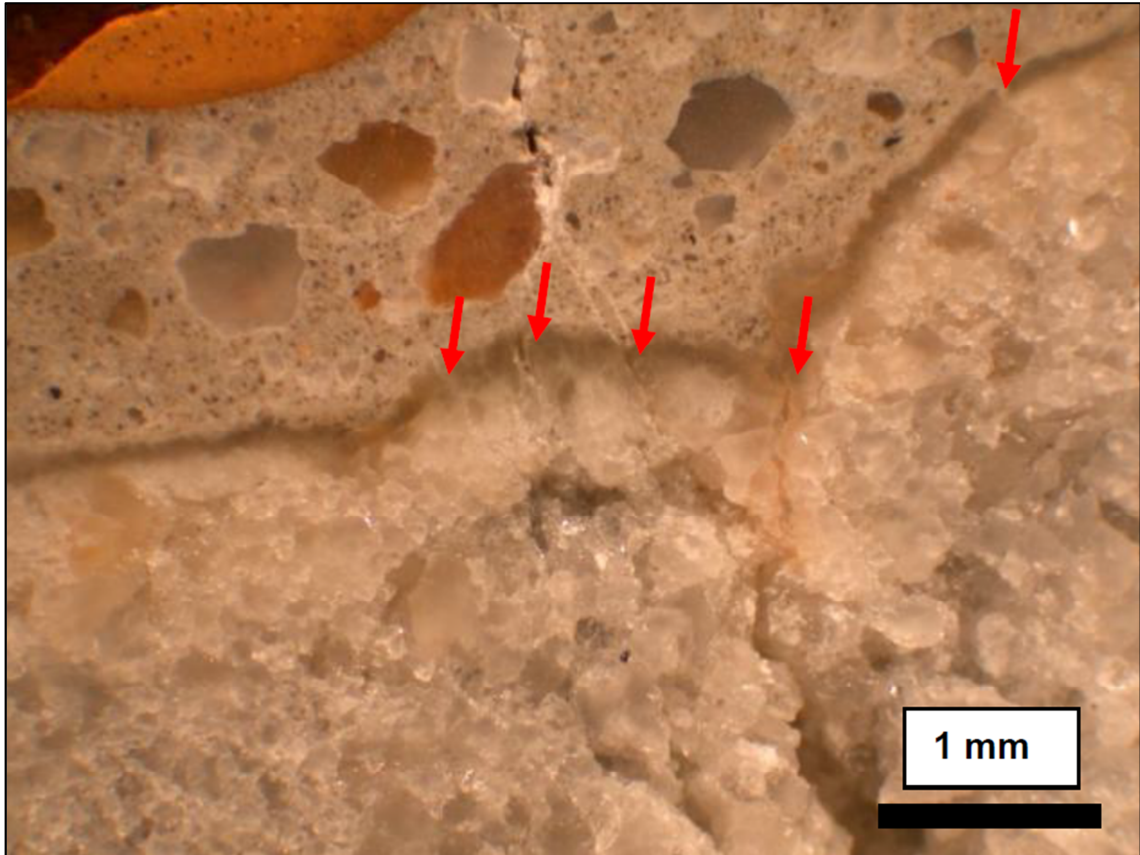


**Figure 3.12:** Core 1A – South: Typical dark glassy rim on white friable quartzite coarse aggregate particle. Arrows show ASR cracks in aggregate periphery (WJE 2010)

#### **3.3.1.2.2 Secondary Deposits**

Cores 1A – South and 1A – North contained major amounts of secondary deposits in voids and fractures. ASR gel was most commonly found in cracks within the outer portion of aggregate particles, as shown in Figure 3.13. ASR gel was found to be less prominent than ettringite. An example of ettringite formation in a microcrack is shown in Figure 3.14. No such deposits were found in cores 1B – South and 1B – North.



**Figure 3.13:** Crack at periphery of quartzite aggregate particle (top right) and multiple veinlets, indicated with arrows, filled with ASR gel (WJE 2010)



**Figure 3.14:** Core 1A – South: Microcracks filled with ettringite, shown with arrows. Small amount of gel at outside edge of crack in aggregate is circled.

Field width is 1.2 mm (WJE 2010)

### **3.3.1.2.3 Causes of Distress**

WJE (2010) states,

Cracking distress in the concrete represented by cores 1A-S and 1A-N is attributed to alkali-silica reaction involving quartzite and chert aggregate particles. ASR distress was possibly exacerbated by the formation of major amounts of ettringite. Cracks resulting from ASR allowed the ingress of water, which interacted with the cementitious paste locally removing calcium, aluminum, and sulfur. Ettringite was deposited in open spaces such as cracks and voids when conditions were suitable for its formation.

### **3.3.1.3 The Transtec Group's Petrographic Study Results**

All of the information in this section was adapted from The Transtec Group (2010). The Transtec Group was sent four concrete cores: 2A-South, 2A-North, 2B-South, and 2B-North. The evaluation performed mainly consisted of the Damage Rating Index (DRI). Recall from chapter two that the The Transtec Group (2010) stated,

There is currently no rating system for the DRI values that correspond to concrete affected to a low, moderate or severe degree by ASR. However, our experience is such that values below 200-250 are indicative of a low degree of reaction / deterioration, DRIs in excess of about 500-600 represent a high to very high (DRI > 1000) degree of ASR. It is important to mention, however, that since the DRI is not a standardized method, values can vary significantly from one petrographer to another.

A summary of the petrographic observations is shown in Table 3.2.

**Table 3.2:** Summary of the petrographic observations of the cores  
(The Transtec Group 2010)

| Sample   | DRI  | Typical crack width in the concrete (mm)  | Extent of ASR           | Reactive aggregates in the polished sections                |
|----------|------|---|-------------------------|---|
| 2A-South | 1430 | Extensive cracking in the cement paste and the aggregate particles; cracks were found to reach 1 mm in width (mainly 0.1 to 0.3 mm)   | Very high degree of ASR | Quartzite and chert   |
| 2A-North | 1081 | Extensive cracking in the cement paste and the aggregate particles; cracks were found to reach 1 mm in width (mainly 0.1 to 0.2 mm; several very fine cracks of < 0.05 mm in size are filled with compacted ettringite) | High degree of ASR      | Quartzite and chert   |
| 2B-South | 141  | No significant cracking in the cement paste (i.e. at the 16x magnification used for the DRI)  | No significant ASR      | Same type of aggregates as in 2A series but no signs of ASR |
| 2B-North | 205  | No significant cracking in the cement paste (i.e. at the 16x magnification used for the DRI)  | No significant ASR      |   |

Core 2A-South and 2A-North obtained a DRI of 1430 and 1081, respectively, which is, “indicative of a very high degree of damage in the concrete” (The Transtec Group 2010). Dark reaction rims around coarse aggregate particles were observed in both samples, as shown in Figure 3.15. No significant ASR was found in Core 2B-South and 2B-North.



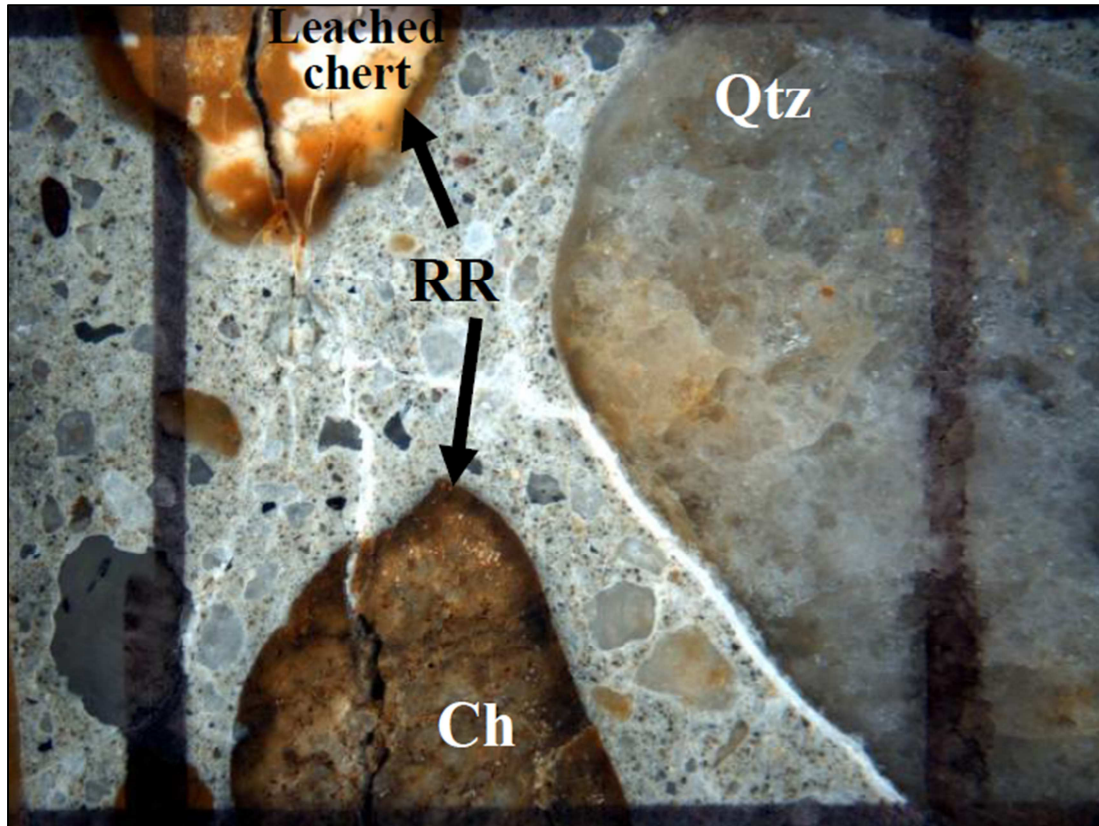


**Figure 3.15:** Reaction rims (RR) surrounding chert (CH) coarse aggregates  
(The Transtec Group 2010)

#### ***3.3.1.3.1 The Transtec Group's Conclusions and Recommendations***

Through petrographic analysis it was determined that the two cores removed from span 5 exhibited severe distress due to ASR, and that the two cores from span 4 did not. Consequently, Transtec Group (2010) recommended that,

The damaged portions of the arch be treated with a suitable hydrophobic sealer such as a silane. Before application of the silane it is recommended that the concrete surface be cleaned by sand blasting and that the larger cracks be filled with a suitable flexible sealant.

### **3.3.2 Crack mapping**

On November 4 and 5, 2010, a survey was taken of the cracks on the tops and bottoms of the northern and southern arch of span 5, and the southern arch of span 4. A system using a 100-foot tape measure, string, and small bungees was devised to create a grid across the top and bottom of the arch as it was surveyed. The following steps were taken to install the grid system:

1. The tape measure was run longitudinally along the length of the arch.
2. From the top of the arch, a 11-foot long string with loops on each end was placed perpendicular to the tape measure at approximately every 3 feet.
3. From underneath the arch, a worker secured the string to the arch by connecting the string's ends with a small bungee, shown in Figure 3.16.

The installed grid system is shown in Figure 3.17. Once the grid system was in place, the cracks were then hand-drawn to scale on grid paper, and the crack widths were recorded. The cracks were measured at the widest point along their length, between the two grid lines, using a crack width gauge, as shown in Figure 3.18. The results of the crack mapping are shown in Figures 3.19 to 3.24.



**Figure 3.16:** Installation of grid lines for crack survey

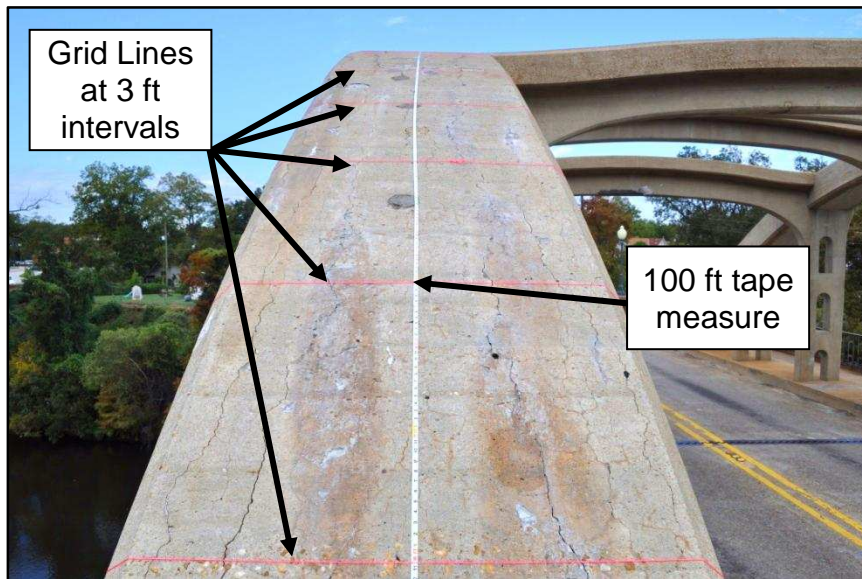


**Figure 3.17:** Crack mapping grid system after installation



**Figure 3.18:** Crack width gauge in use

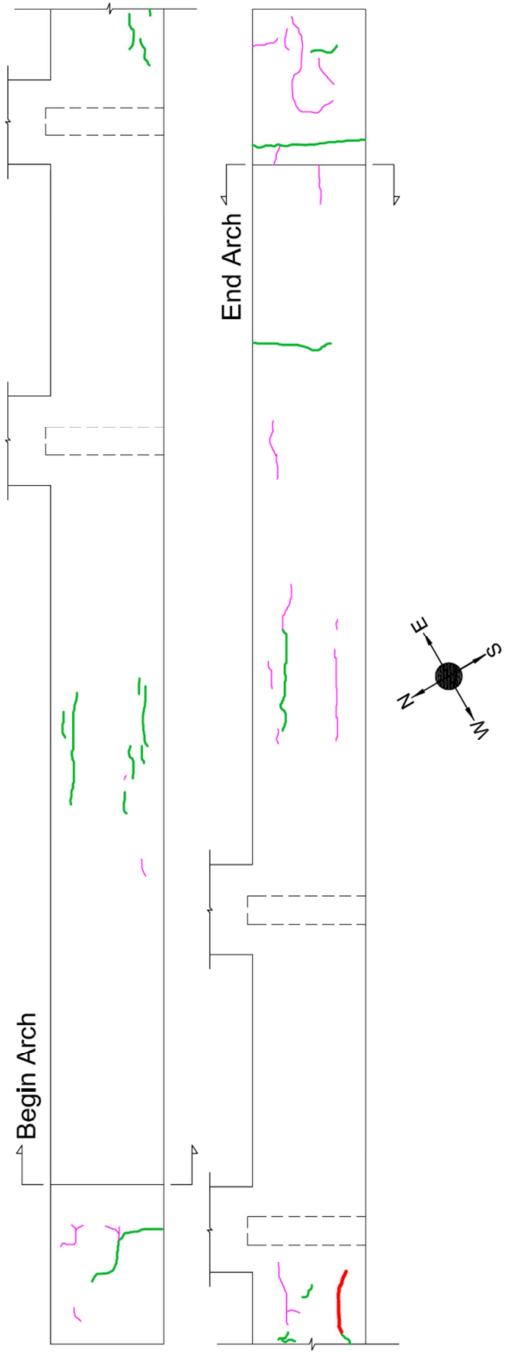
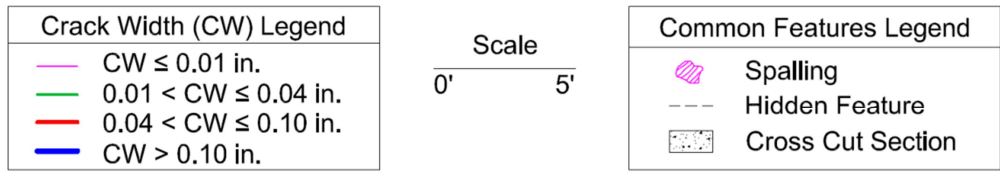


**Figure 3.19:** Crack-mapping survey. November 5, 2010.

Span 4 – South Arch – Plan View



| Crack Width (CW) Legend |                      |
|-------------------------|----------------------|
|                         | CW ≤ 0.01 in.        |
|                         | 0.01 < CW ≤ 0.04 in. |
|                         | 0.04 < CW ≤ 0.10 in. |
|                         | CW > 0.10 in.        |

Scale  
0' 5'

| Common Features Legend |                   |
|------------------------|-------------------|
|                        | Spalling          |
|                        | Hidden Feature    |
|                        | Cross Cut Section |

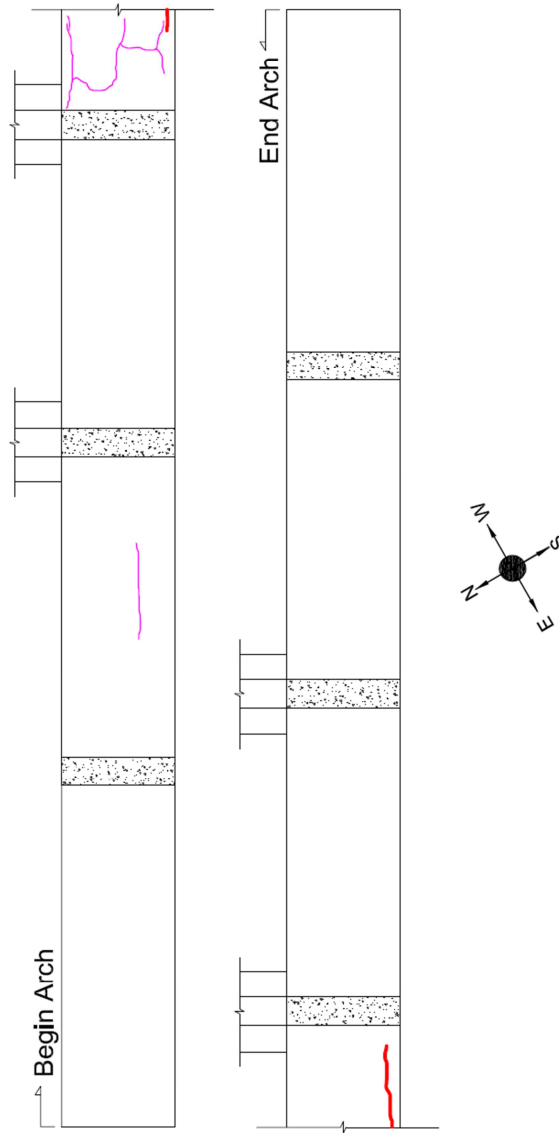


**Figure 3.20:** Crack-mapping survey. November 5, 2010.

Span 4 – South Arch – Bottom View

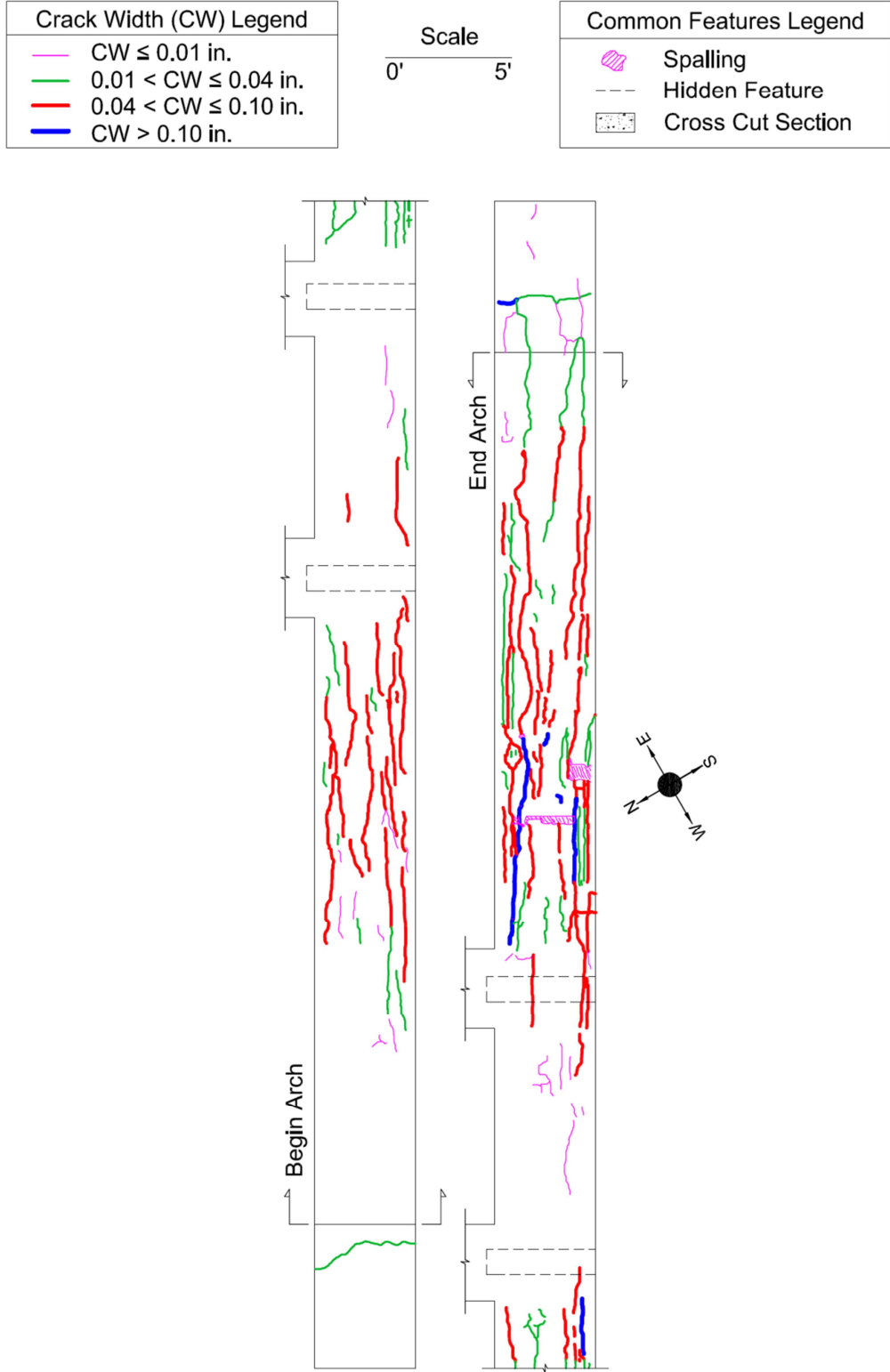


**Figure 3.21:** Crack-mapping survey. November 4, 2010.

Span 5 – South Arch – Plan View

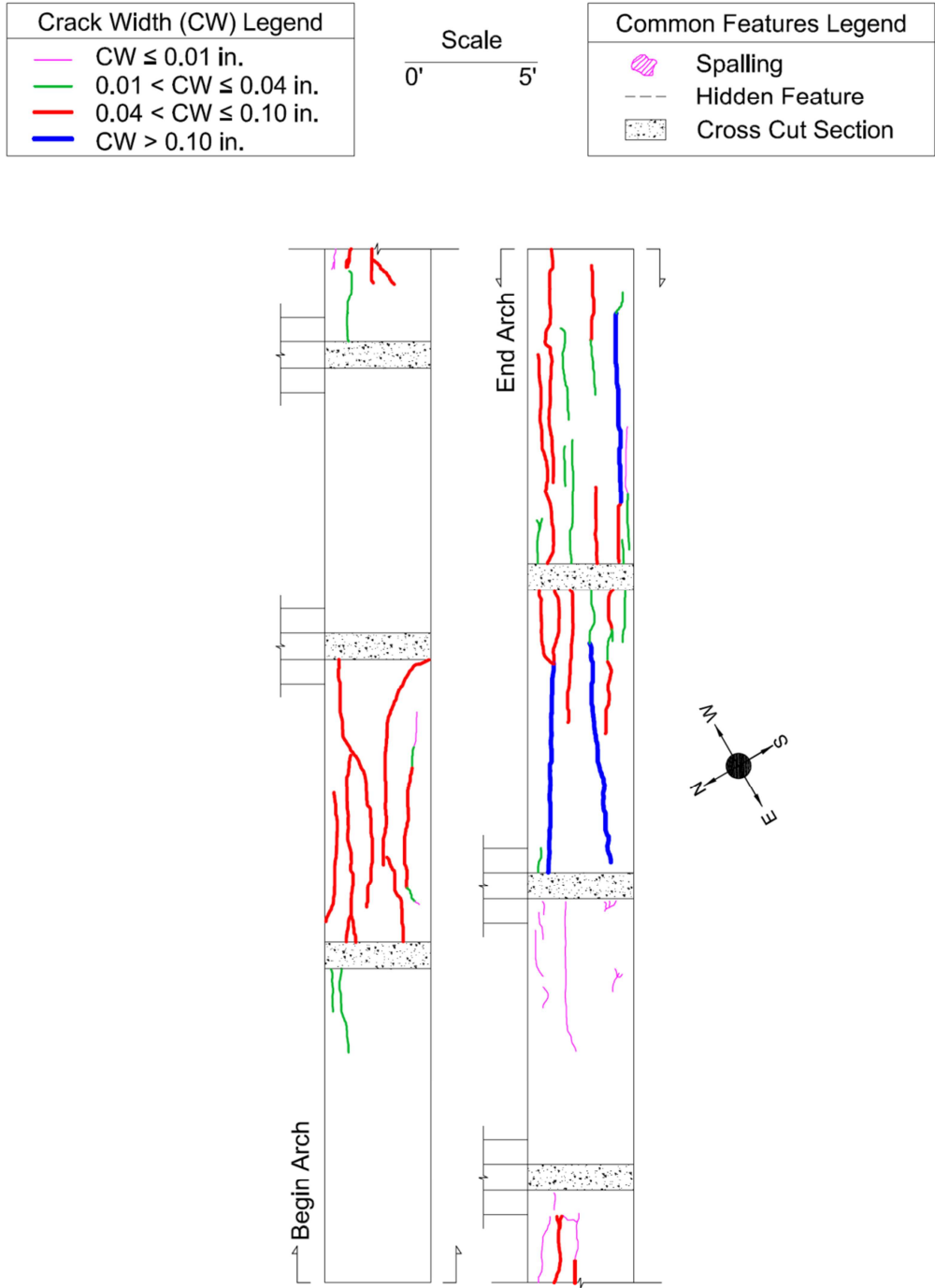


**Figure 3.22:** Crack-mapping survey. November 4, 2010.

Span 5 – South Arch – Bottom View

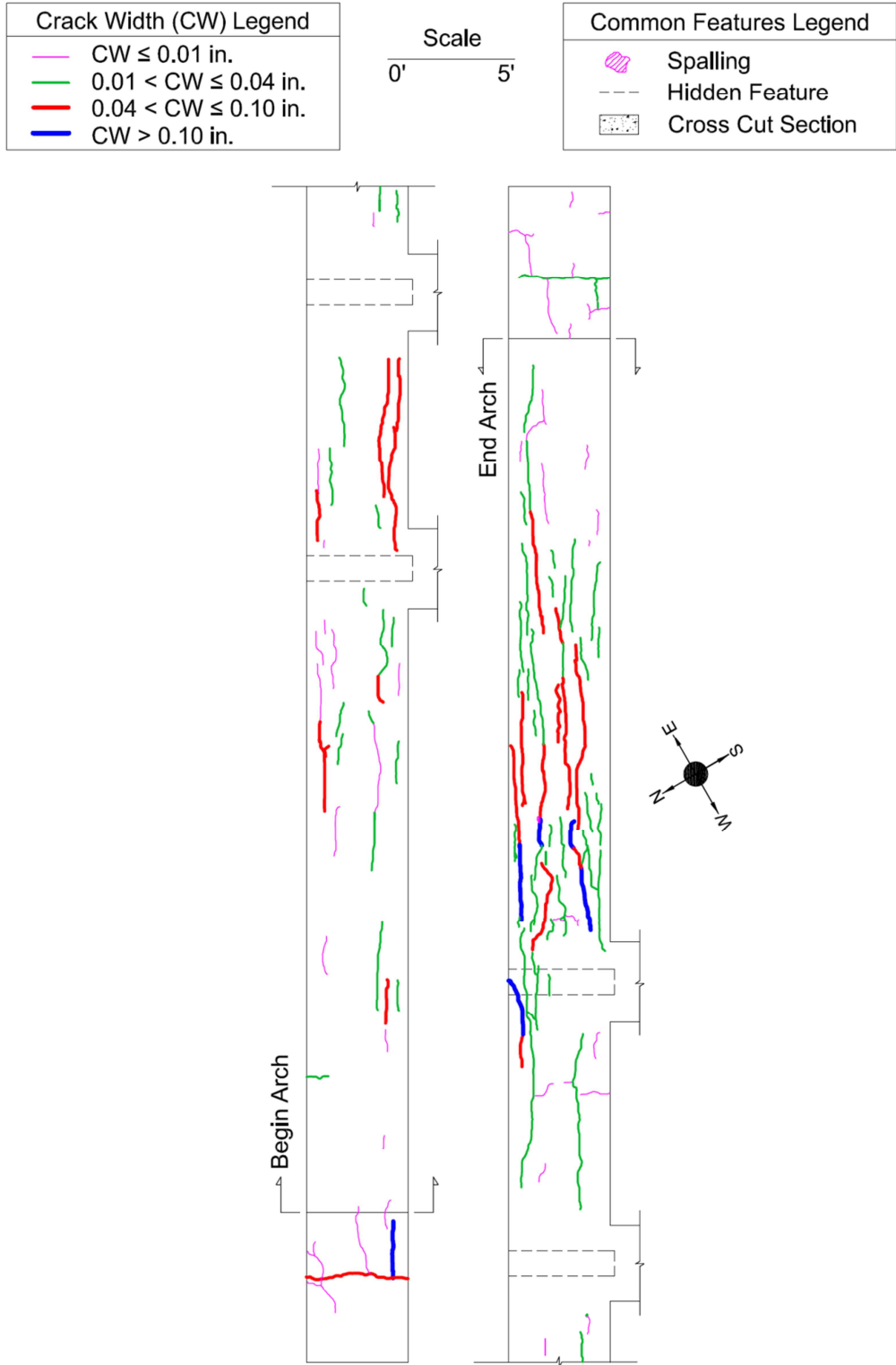
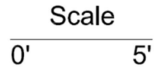


**Figure 3.23:** Crack-mapping survey. November 4, 2010.

Span 5 – North Arch – Top View

| Crack Width (CW) Legend |                      |
|-------------------------|----------------------|
|                         | CW ≤ 0.01 in.        |
|                         | 0.01 < CW ≤ 0.04 in. |
|                         | 0.04 < CW ≤ 0.10 in. |
|                         | CW > 0.10 in.        |



| Common Features Legend |                   |
|------------------------|-------------------|
|                        | Spalling          |
|                        | Hidden Feature    |
|                        | Cross Cut Section |

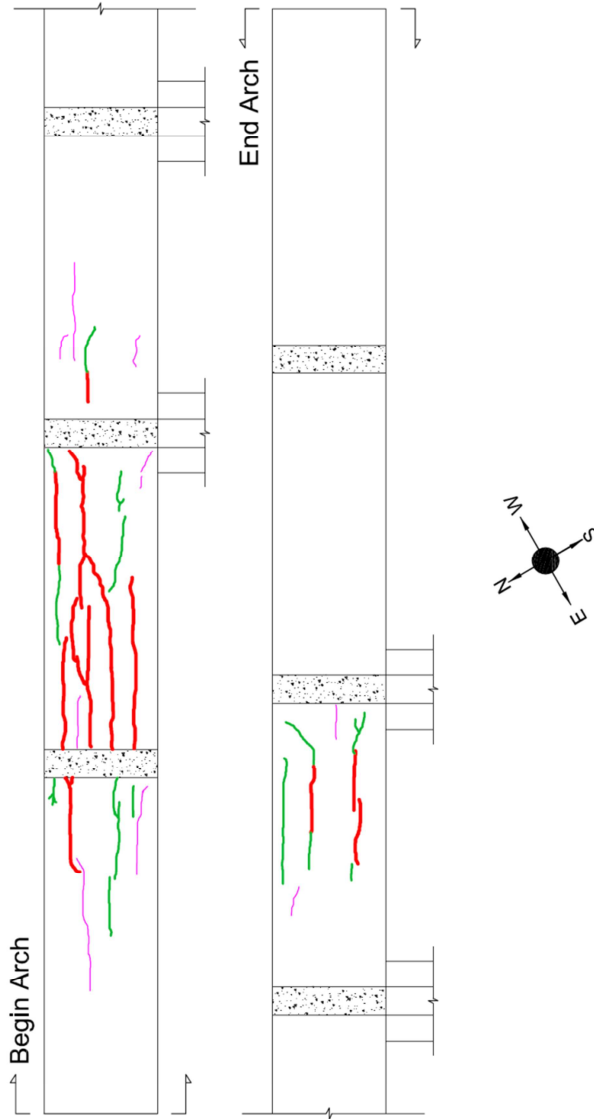


**Figure 3.24:** Crack-mapping survey. November 4, 2010.

Span 5 – North Arch – Bottom View

### 3.3.3 Examples of distress

This section contains examples of distress due to ASR in span 5. A view of the eastern side of the southern arch of span 5 is shown in Figure 3.25. Note the deposits of ASR gel and efflorescence.



**Figure 3.25:** Severe distress due to ASR on the eastern side of the southern arch of span 5 on 3-11-2008



A closer view of the distress on the eastern side of the southern arch of span 5 can be seen in Figure 3.26. Note the longitudinal cracks running parallel with the direction of the steel reinforcement.



**Figure 3.26:** A closer view of the severe distress due to ASR on the eastern side of the southern arch of span 5 on 3-11-2008

An example of spalling on the eastern side of the southern arch of span 5 is shown in Figure 3.27. Severe cracking on the bottom of the arch, with crack widths greater than 0.1 inches, is shown in Figure 3.28.



**Figure 3.27:** An example of spalling on span 5 on 12-14-2009



**Figure 3.28:** Severe cracks greater than 0.1 inches on 3-11-2008



An example of the severe distress on the underside of the arches can be seen in Figure 3.29. An example of map-cracking on the abutment of the arch is shown in Figure 3.30.



**Figure 3.29:** Severe cracks on the bottom of the arch on 3-11-2008



**Figure 3.30:** Map-cracking on the abutment of span 5

### **3.4 Summary**

The Bibb Graves Bridge, located in Wetumpka, AL, is a reinforced concrete bridge that is 700 feet long and has a 24 foot wide roadway. The bridge consists of seven arches that support the bridge deck, as shown in Figure 3.6. Other than span 1 and 7, the bridge deck is suspended from the arches at half-height.

After a petrographic analysis from two separate organizations, it was determined that ASR was present in the northern and southern arches of span 5. A crack mapping survey was performed by Auburn University to record the distress caused by ASR in these arches. These surveys are shown in Figures 3.19 through 3.24. Examples of the distress can be found in Figures 3.25 through 3.30.

## **Chapter 4**

### **ASR Mitigation Procedure**

#### **4.1 Introduction**

During the summer of 2010, ALDOT, FHWA, and Auburn University developed an ASR mitigation procedure to slow or stop the expansion due to ASR in the arches of span 5 of this bridge. The ASR mitigation procedure included the application of

- a water repelling silane sealer on all exposed concrete of the arches,
- a flexible silicone sealant in the wide cracks of the ASR affected arches, and
- an epoxy flood coat on the top surface of the arches to seal all intermediate to narrow cracks.

From October to November of 2010, Auburn University assisted in the implementation and documentation of the ASR mitigation procedure at the Bibb Graves Bridge.

#### **4.2 Selection of installation technique for the ASR mitigation method**

Typically, ASR mitigation procedures such as silane are applied per manufacturer's standards. However, due to the severely deteriorated nature of the concrete in the arches affected by ASR, typical application procedures could not be used. Preliminary discussions between the FHWA, Auburn University,

ALDOT's Materials and Test Bureau, and ALDOT's Maintenance Bureau led to four pertinent options to be considered for the ASR mitigation protocol. The options mainly differed in methods of application, order of application, and practicality of application. The following four options were considered:

#### **4.2.1 Protocol Option A**

1. Water-blast all concrete surfaces to clean concrete surfaces and remove loose impediments, efflorescence, ASR gel, algae, etc.
2. Seal all cracks 0.04 in. and wider with a UV-resistant, flexible sealant.
3. Apply silane to all surfaces.
4. Apply an epoxy flood coat to the top arch surface to seal the unsealed cracks on this surface.
5. Install instrumentation for monitoring.

Protocol option A was ALDOT's preferred mitigation procedure due to ease of installation and cleanup. ALDOT's Maintenance Bureau reported that a crack width of 0.04 inches and greater was the smallest crack they could practically apply a flexible sealant into, without the need for routing the crack. Although easy to apply, there was concern surrounding the effect of the epoxy flood coat to the ASR mitigation procedure's performance; an epoxy flood coat will prevent moisture migration and will not allow drying on the face where it is applied.

#### **4.2.2 Protocol Option B**

1. Water-blast all concrete surfaces to clean concrete surfaces and remove loose impediments, efflorescence, ASR gel, algae, etc.
2. Temporarily tape all cracks 0.04 in. and wider on the top arch surface.

3. Apply an epoxy flood coat to the top arch surface to seal the untaped cracks on this surface.
4. Water-blast the top arch surface to remove the excess epoxy from the concrete surface.
5. Remove tape from the arch.
6. Seal all cracks 0.04 in. and wider with a UV-resistant, flexible sealant
7. Apply silane to all surfaces.
8. Install instrumentation for monitoring.

Not considering practicality of implementation, protocol option B was the option of choice. It was uncertain how much the epoxy flood coat would penetrate and if the excess epoxy could effectively be removed from the surface. This protocol option leaves the maximum amount of the exterior concrete surface area covered with silane only. Therefore, the silane's effectiveness is minimally compromised. However, protocol option B is the most difficult to practically implement. Additionally, there were concerns about the potential environmental impacts of the water-blasted epoxy falling into the river.

#### **4.2.3 Protocol Option C**

1. Water-blast all concrete surfaces to clean concrete surfaces and remove loose impediments, efflorescence, ASR gel, algae, etc.
2. Apply silane to all surfaces.
3. Seal all cracks 0.01 in. and wider with a UV-resistant, flexible sealant.
4. Install instrumentation for monitoring.

This protocol option lowered the flexible-sealant crack-width threshold down to 0.01 inches, and excluded the use of an epoxy flood coat. The idea being that sealing smaller cracks with flexible sealant would possibly negate the need for an epoxy flood coat, and therefore the concerns of having a water-vapor-impermeable layer. However, the lack of an epoxy flood coat on the top surface of the arch leaves the possibility of water penetration into cracks smaller than 0.01 inches. Additionally, ALDOT's Maintenance Bureau would have to rout all of the cracks under 0.04 inches, therefore, this option would increase installation time and cost.

#### **4.2.4 Protocol Option D**

1. Water-blast all concrete surfaces to clean concrete surfaces and remove loose impediments, efflorescence, ASR gel, algae, etc.
2. Seal all cracks 0.01 in. and wider with a UV-resistant, flexible sealant.
3. Apply an epoxy flood coat to the top arch surface to seal the unsealed cracks on this surface.
4. Apply silane to all remaining surfaces.
5. Install instrumentation for monitoring.

This protocol option, while similar to C, included an epoxy flood coat, and moved the application of silane to the last step. This was deemed ineffective by all parties, as there were many concerns surrounding silane's ability to bond to the epoxy, and the previous concerns of sealing small cracks with flexible sealant.

### **4.3 Final ASR Mitigation Procedure**

Following a conference call between the FHWA, ALDOT, and Auburn University the following ASR mitigation procedure was chosen:

1. Water-blast all concrete surfaces to clean concrete surfaces and remove loose impediments, efflorescence, ASR gel, algae, etc.
2. Apply silane to all surfaces.
3. Seal all cracks 0.04 inch and wider with a UV-resistant, flexible sealant.
4. Apply an epoxy flood coat to the top arch surface to seal the cracks on this surface.
5. Install instrumentation for monitoring.

The mitigation procedure was applied to both ASR-affected arches on span 5, and the south arch of span 4 as a control, as shown in Figure 4.1. A schematic of the ASR mitigation method applied is shown in Figure 4.2. After water-blasting all of the concrete surfaces, the first step in the procedure involved coating all the concrete surfaces with silane. This created a hydrophobic layer on the uncracked concrete that allowed the evaporation of internal moisture, shown in Figure 4.2a. The silane sealant was applied first so that it would penetrate and seal as much concrete surface as possible before the flexible sealant and epoxy flood coat were applied.

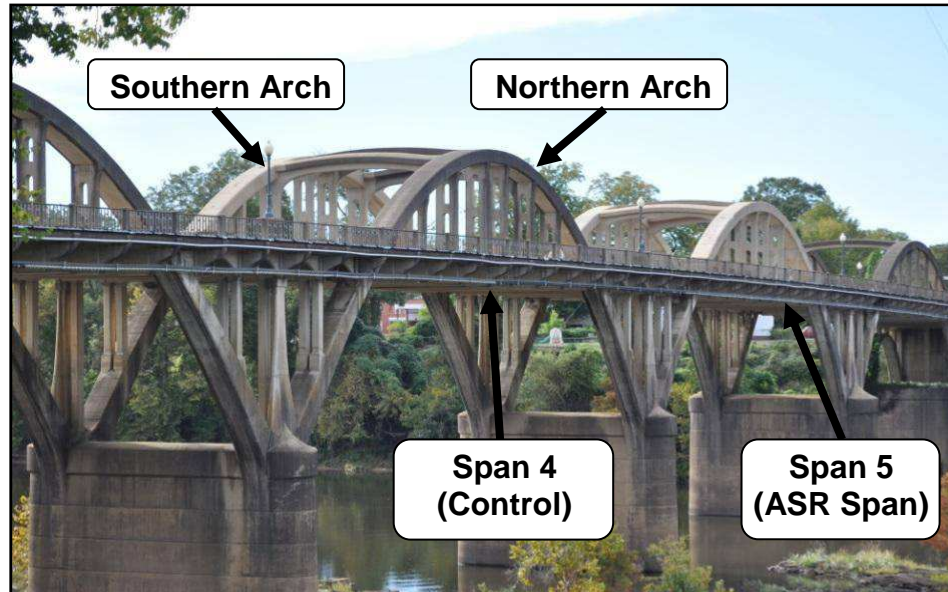


**Figure 4.1:** Span 4 and 5 of the Bibb Graves Bridge

Next, the cracks 0.04 in. and larger were then filled with a UV-resistant, flexible sealant, as shown in Figure 4.2b. To reiterate, the 0.04-inch crack width was chosen because it was the smallest crack width that could be filled with a flexible sealant using a caulk gun, without the need for routing. The flexibility of the sealant was vital in the large cracks to accommodate the movement that occurs from temperature and ASR-related expansions and contractions.

Finally, the epoxy flood coat was applied to the top arch surface to seal any unsealed cracks that were in direct exposure to liquid water, shown in Figure 4.2c. Although this created an impermeable layer for the diffusion of the internal RH, the assumption was that the moisture would diffuse from the other three surfaces. One potential problem with the final ASR mitigation procedure is that the scheme does leave the cracks smaller than 0.04 inches on the bottom and sides of the arches potentially unsealed, as shown in Figure 4.2d. This was considered, but deemed insignificant.



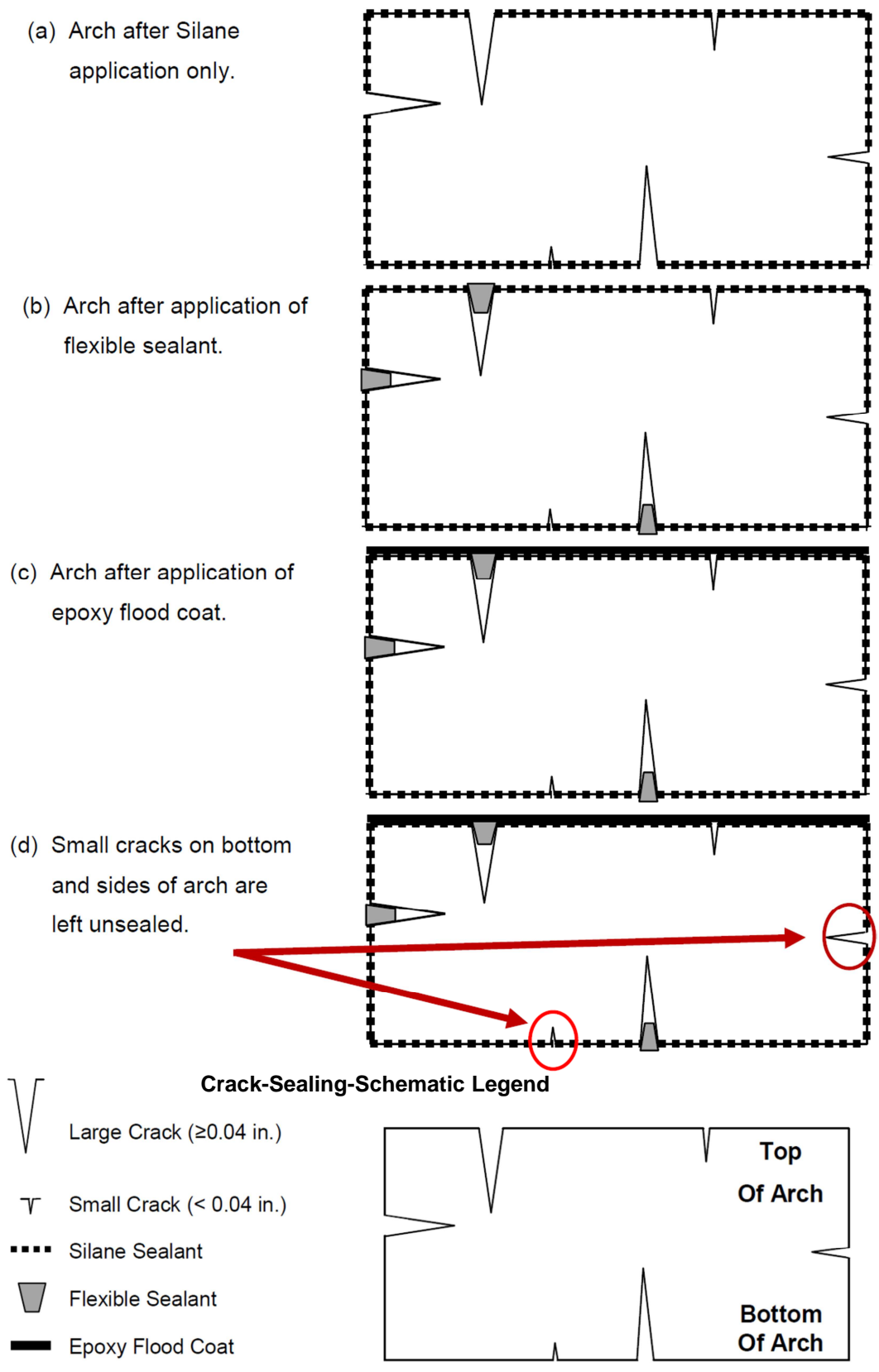


**Figure 4.2:** Schematic of the ASR mitigation procedure applied

#### 4.4 Installation of ASR mitigation method

From October to November 2010, the final ASR mitigation procedure was implemented. In this section, the ASR mitigation procedure is described chronologically as it was applied to the arches. The installation order of the ASR mitigation procedure is summarized in Figure 4.3.

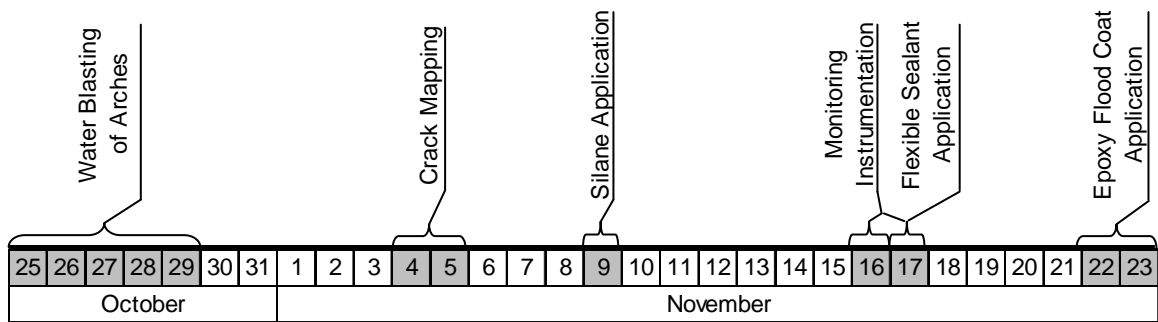


**Figure 4.3:** Timeline of the fall 2010 installation of the ASR mitigation procedure

These actions were performed on both the north and south ASR affected arches of span 5, and on the southern “control” arch of span 4, as shown in Figure 4.4. The northern arch of span 4 was fitted with instrumentation for monitoring, but was not treated with silane, epoxy, or flexible sealant.

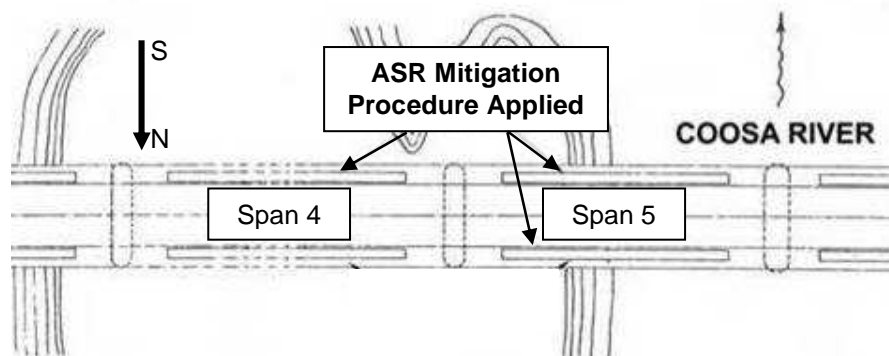


**Figure 4.4:** Overview of ASR mitigation procedure implementation

From October 25-29, these arches were water-blasted to clean the concrete surfaces and remove loose impediments, efflorescence, ASR gel,

algae, etc. Figure 4.5 shows the water-blasted arches of span 5 prepared for silane application. A 72-hour drying period was required before the silane membrane could be applied.



**Figure 4.5:** Water-blasted arches prepared for ASR mitigation procedure

On November 9, silane was applied to the arches. The silane used was Enviroseal 40, shown in Figure 4.6a. Enviroseal 40 is a water-based, 40 % silane penetrating sealer. The sealant was applied using a low-pressure garden sprayer, as shown in Figure 4.6b. The liquid silane is white when applied, but dries clear. The silane is applied with long deliberate strokes across the application surface using a fine mist.

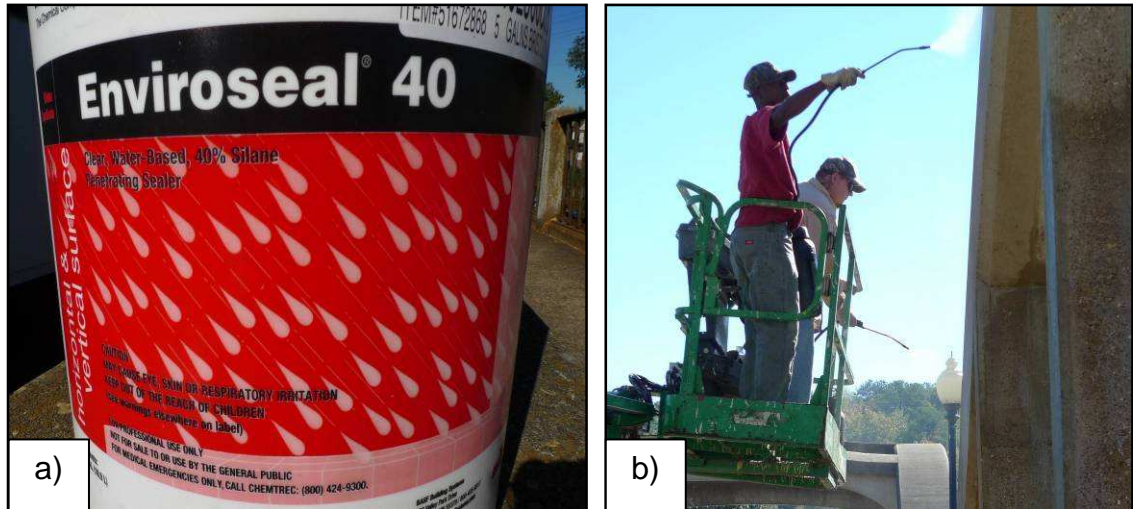


**Figure 4.6:** (a) Water-based silane sealant and (b) application of silane

The next step in the sealing procedure involved sealing all cracks larger than 0.04 inches from water penetration using a flexible sealant, described schematically in Figure 4.2b. The flexible sealant used was Pecora 895NST, Structural Silicone Glazing & Weatherproofing Sealant. This sealant was applied using a caulk gun, shown in Figure 4.7a. After application, the bead of sealant was forced into the crack and smoothed by hand as shown in Figure 4.8b.

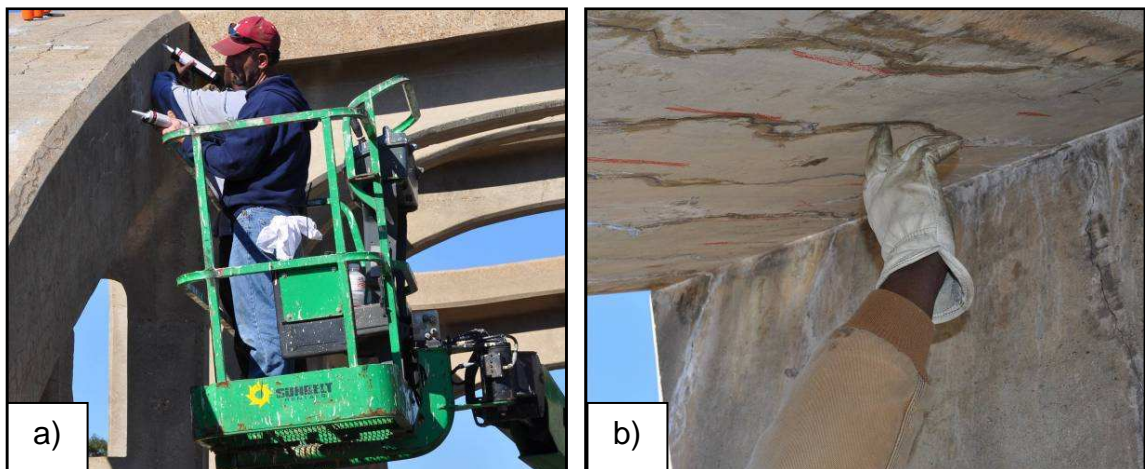


**Figure 4.7:** (a) Application of flexible sealant and (b) smoothing sealant by hand

The last step in the sealing process involved applying an epoxy flood coat over the top of the arch to seal the cracks smaller than 0.04 inches exposed to direct rainfall. The epoxy used was Dayton Superior Sure Seal™ LV/LM. The two-part epoxy used was combined using a 1:1 ratio. Before application, the mixture was blended for 3 minutes. The epoxy was then applied using a paint roller.

#### **4.5 Summary**

The final ASR mitigation procedure chosen by the FHWA, ALDOT, and Auburn University consisted of the following five steps:

1. Water-blast all concrete surfaces to clean concrete surfaces and remove loose impediments, efflorescence, ASR gel, algae, etc.
2. Apply silane to all surfaces.
3. Seal all cracks 0.04 inch and wider with a UV-resistant, flexible sealant.
4. Apply an epoxy flood coat to the top arch surface to seal the cracks on this surface.
5. Installation of instrumentation for monitoring.

From October to November 2010, the final ASR mitigation procedure was implemented. The installation order of the ASR mitigation procedure is summarized in Figure 4.3. These actions were performed on both the north and south ASR affected arches of span 5, and on the southern “control” arch of span 4, as shown in Figure 4.4. The northern arch of span 4 was fitted with

instrumentation for monitoring, but was not treated with silane, epoxy, or flexible sealant.

From October 25-29, these arches were water-blasted to clean the concrete surfaces and remove loose impediments, efflorescence, ASR gel, algae, etc. On November 9, silane was applied to the arches. The next step in the sealing procedure involved sealing all cracks larger than 0.04 inches from water penetration using a flexible sealant. The last step in the sealing process involved applying an epoxy flood coat over the top of the arch to seal the cracks smaller than 0.04 inches exposed to direct rainfall.

## **Chapter 5**

### **Monitoring Instrumentation**

#### **5.1 Introduction**

This chapter documents the installation of the instrumentation used to monitor the effectiveness of the ASR mitigation procedure, and summarizes the use of the equipment used with this instrumentation.

During November 16 and 17, 2010, instrumentation was added by personnel from the FHWA, Auburn University, and ALDOT's Materials and Test Bureau to monitor the effectiveness of the ASR mitigation procedure. The instrumentation was installed to collect data pertaining to internal RH and expansion in the north and south arches on spans 4 and 5.

#### **5.2 RH Measurements**

The RH measuring equipment used is Vaisala's HM44 Structural Humidity Measurement Kit. The kit includes:

- HMI41 indicator
- HMP44 RH & temperature probes
- Protective orange cups with lids
- Plastic tubes
- Rubber plugs



- Long rubber plunger

The plastic tubes are installed by drilling a 5/8-inch diameter hole into the concrete to the desired depth, cleaning the hole using compressed air, epoxying the end of the tube, and inserting it into the hole. Once the plastic tubes are inserted into the hole, and the seams are sealed with a flexible sealant, a long rubber plug can be inserted into the tube, sealing the inside of the tube from ambient conditions, as shown in Figure 5.1.



**Figure 5.1:** RH tube with plug installed and tube sealed with a flexible silicone sealant

To take a RH reading, the plugs are first removed from the tube, as shown in Figure 5.2, and a RH probe is inserted into the tube, as shown in Figure 5.3. The probe is pushed to the bottom of the tube, and a cord plug is placed around the cord of the probe, as shown in Figure 5.4. Next, a plastic cup is placed around the entire assembly, and the lid placed on top, as shown in Figure 5.5. Finally, probes must equilibrate for 1 hour before taking a RH reading. All of these steps allow the RH probe to reach equilibrium with the internal RH at the end of the tube.





**Figure 5.2:** Plug being removed from tube



**Figure 5.3:** RH probe being inserted into tube





**Figure 5.4:** Plug being placed around probe wire

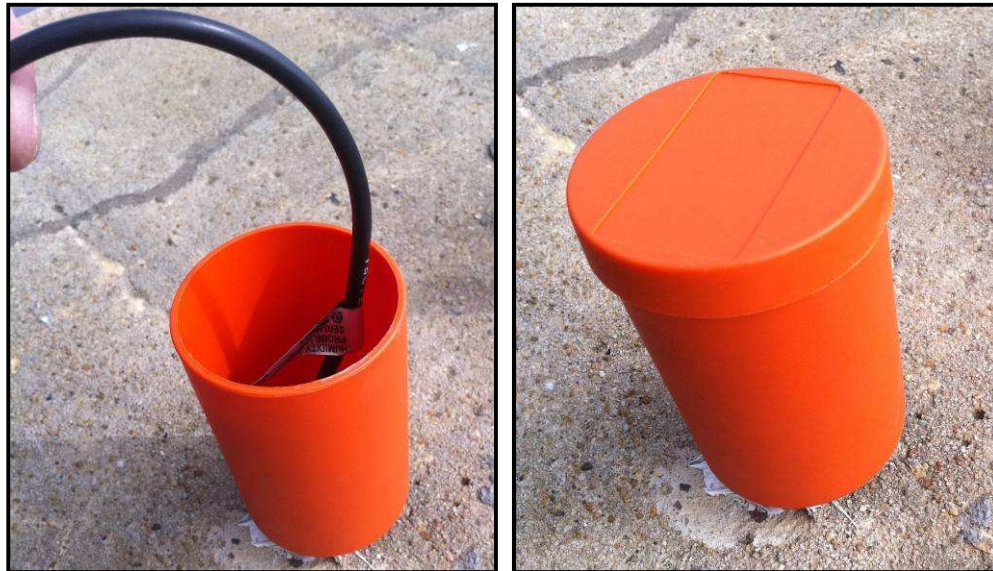


**Figure 5.5:** Plastic cup being placed around probe assembly

There are four RH locations per arch: west top, west bottom, east top, and east bottom. At each location, there are three RH tube depths: 1 inch, 2 inch, and 3-inch. The RH probe locations are graphically shown on Figure 5.6. With four RH locations per arch, and three tubes per location, 48 RH readings are taken during each survey.

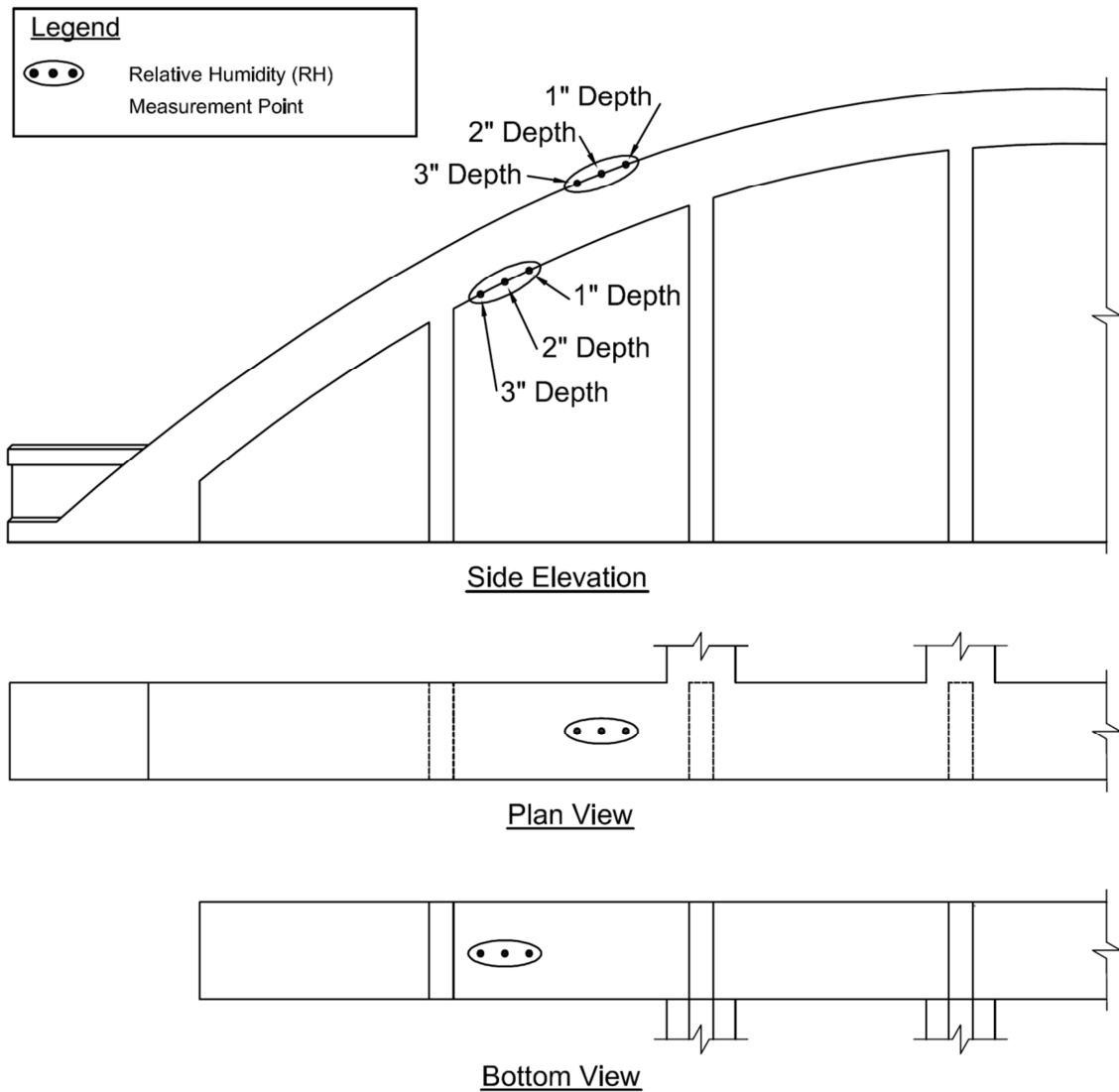


**Figure 5.6:** RH measurement locations for all arches

The Vaisala HMP44 RH probes used were calibrated to high relative humidities to account for the internal RH within the concrete. The lower-bound RH was calibrated to 75% RH, and the upper bound was calibrated to 97% RH. The probes were calibrated by using the Vaisala Humidity Calibrator, HMK15, shown in Figure 5.7, following the manufacturer’s instructions. The calibration salts used were NaCl for 75% RH ( $\pm 1.5$  % RH) and  $K_2SO_4$  for 97 % RH ( $\pm 2.0$  % RH).



**Figure 5.7:** Vaisala's Humidity Probe Calibrator, HMK15

### 5.3 Concrete strain measurements

Concrete strain is measured with a Mayes demountable mechanical (DEMEC) concrete strain gauge. The instrument uses a dial gauge and lever mechanism that is mounted on a 19.69-inch (500-mm) beam. The concrete strain gauge has one fixed location point, and one movable measuring point, attached to a lever and dial mechanism. Using two punched DEMEC studs, the concrete strain gauge measures to an accuracy of  $\pm 5 \times 10^{-6}$  in/in (Mayes Instruments Limited, n.d.).

Installation of the DEMEC studs involves using a template, and drilling two holes in the concrete approximately 500 mm apart. The two stainless steel DEMEC studs are then epoxied into the holes, with the ends of the studs flush



with the surface of the concrete, as shown in Figure 5.8. An example of the field use of the DEMEC concrete strain gauge is shown in Figure 5.9a, and the dial for the gauge is shown in Figure 5.9b.



**Figure 5.8:** Example of installed DEMEC stud in the Bibb Graves Bridge.

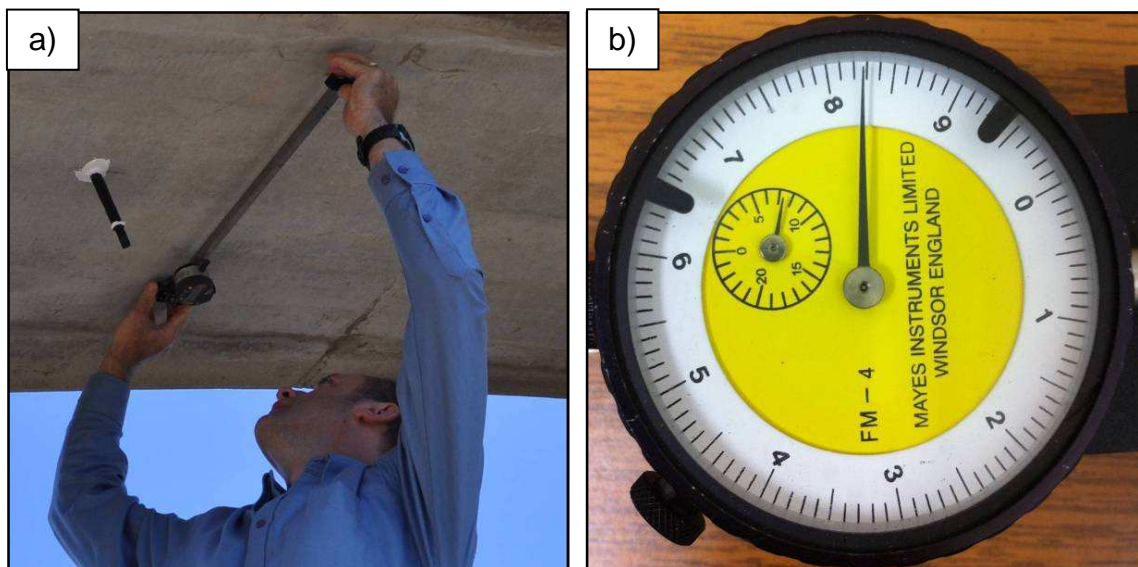


**Figure 5.9:** Mayes DEMEC Concrete strain Gauge a) field use and b) dial gauge

There are DEMEC studs installed in various locations on each of the four arches of spans four and five. These locations can be seen in Figures 5.10

through 5.13. The DEMEC measurement locations have codes to help indicate their location in the arches:

- AB - Abutment
- SH - Side Horizontal
- SP - Side Perpendicular
- BL - Bottom Low
- BH - Bottom High
- TL - Top Low
- TH - Top High

In 2005, 10 concrete strain measurement locations were installed by the FHWA. In 2010, 40 additional concrete strain measurement locations were installed by the FHWA, ALDOT's Maintenance Bureau, and Auburn University. These locations, along with their respective installation years, are summarized in Table 5.1. Five of the listed locations cannot be measured by Auburn University's DEMEC concrete strain gauge; these locations are indicated by a gray colored cell.

To take a concrete strain measurement, the following procedure is followed:


1. A reference bar reading is taken:
  - a. The movable measurement point of the concrete strain gauge is inserted into the punched point on the reference bar.
  - b. The fixed measurement point of the concrete strain gauge is inserted into the punched point on the reference bar.
  - c. While applying downward pressure to the gauge, the small dial is read first, and the large dial is read second. The small dial reading is the first one or two digits of the gauge reading, and the large dial

is last two digits of the gauge reading. For example, in Figure 5.9b the dial gauge is read as 783.

2. Using the same procedure as 1a – 1c, a measurement is taken using the installed DEMEC studs, as shown in Figure 5.9a.
3. The reference bar reading is then subtracted from the DEMEC stud measurement.
4. Using the included gauge factor (unique to each gauge), the difference of both readings is multiplied by the gauge factor to convert to a concrete strain measurement. The gauge factor for the DEMEC concrete strain gauge used in this project is  $3.235(10)^{-6}$  in./in./small division of dial gauge.

**Table 5.1:** Summary of concrete strain measurement locations on span 4 and 5

| Span 4        |                  |              |      |               | Span 5           |              |      |   |   |
|---------------|------------------|--------------|------|---------------|------------------|--------------|------|---|---|
| Arch Location | Location on Arch | Installed In |      | Arch Location | Location on Arch | Installed In |      |   |   |
|               |                  | 2005         | 2010 |               |                  | 2005         | 2010 |   |   |
| South         | West             | AB           |      | X             | South            | West         | AB   |   | X |
|               |                  | SH           |      | X             |                  |              | SP   | X |   |
|               |                  | SP           | X    |               |                  |              | BL   | X |   |
|               |                  | BL           | X    |               |                  |              | BH   |   | X |
|               |                  | BH           |      | X             |                  |              | TL   | X |   |
|               |                  | TL           | X    |               |                  |              | TH   |   | X |
|               |                  | TH           |      | X             |                  |              |      |   |   |
|               | East             | AB           |      | X             | East             | AB           | X    |   |   |
|               |                  | SH           |      | X             |                  | SH           |      | X |   |
|               |                  | BL           |      | X             |                  | SP           | X    |   |   |
|               |                  | BH           |      | X             |                  | BL           | X    |   |   |
|               |                  | TL           |      | X             |                  | BH           |      | X |   |
|               |                  | TH           |      | X             |                  | TL           | X    |   |   |
|               |                  |              |      |               |                  | TH           |      | X |   |
| North         | West             | AB           |      | X             | North            | West         | AB   |   | X |
|               |                  | SH           |      | X             |                  |              | SH   |   | X |
|               |                  | BL           |      | X             |                  |              | BL   |   | X |
|               |                  | BH           |      | X             |                  |              | BH   |   | X |
|               |                  | TL           |      | X             |                  |              | TL   |   | X |
|               |                  | TH           |      | X             |                  |              | TH   |   | X |
|               |                  |              |      |               |                  |              |      |   |   |
|               | East             | AB           |      | X             | East             | AB           |      | X |   |
|               |                  | SH           |      | X             |                  | SH           |      | X |   |
|               |                  | BL           |      | X             |                  | SP           |      | X |   |
|               |                  | BH           |      | X             |                  | BL           |      | X |   |
|               |                  | TL           |      | X             |                  | BH           |      | X |   |
|               |                  | TH           |      | X             |                  | TL           |      | X |   |
|               |                  |              |      |               |                  | TH           |      | X |   |

 = No longer measurable



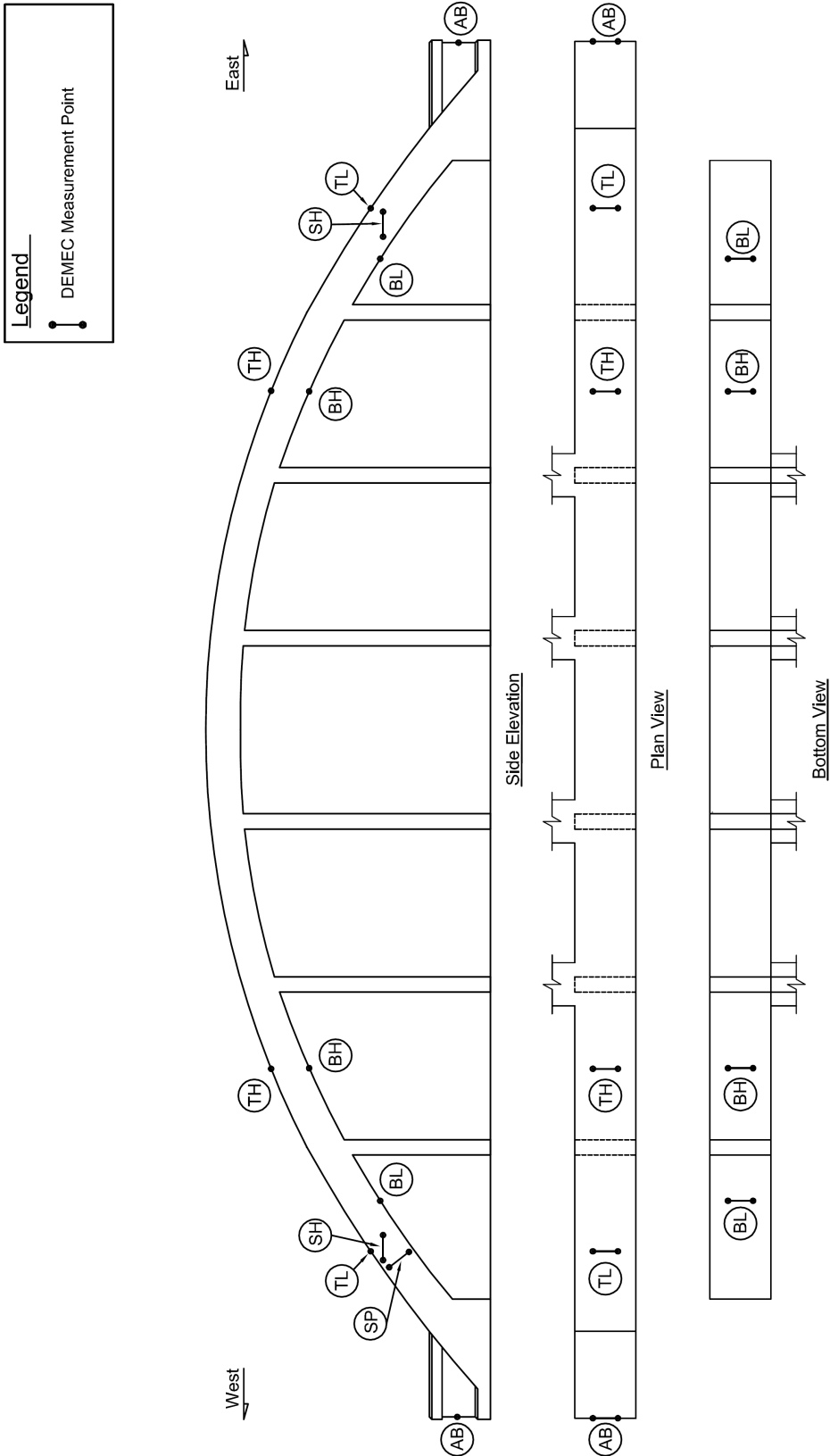


**Figure 5.10: DEMEC Locations - Span 4 - South Arch. Not to Scale**

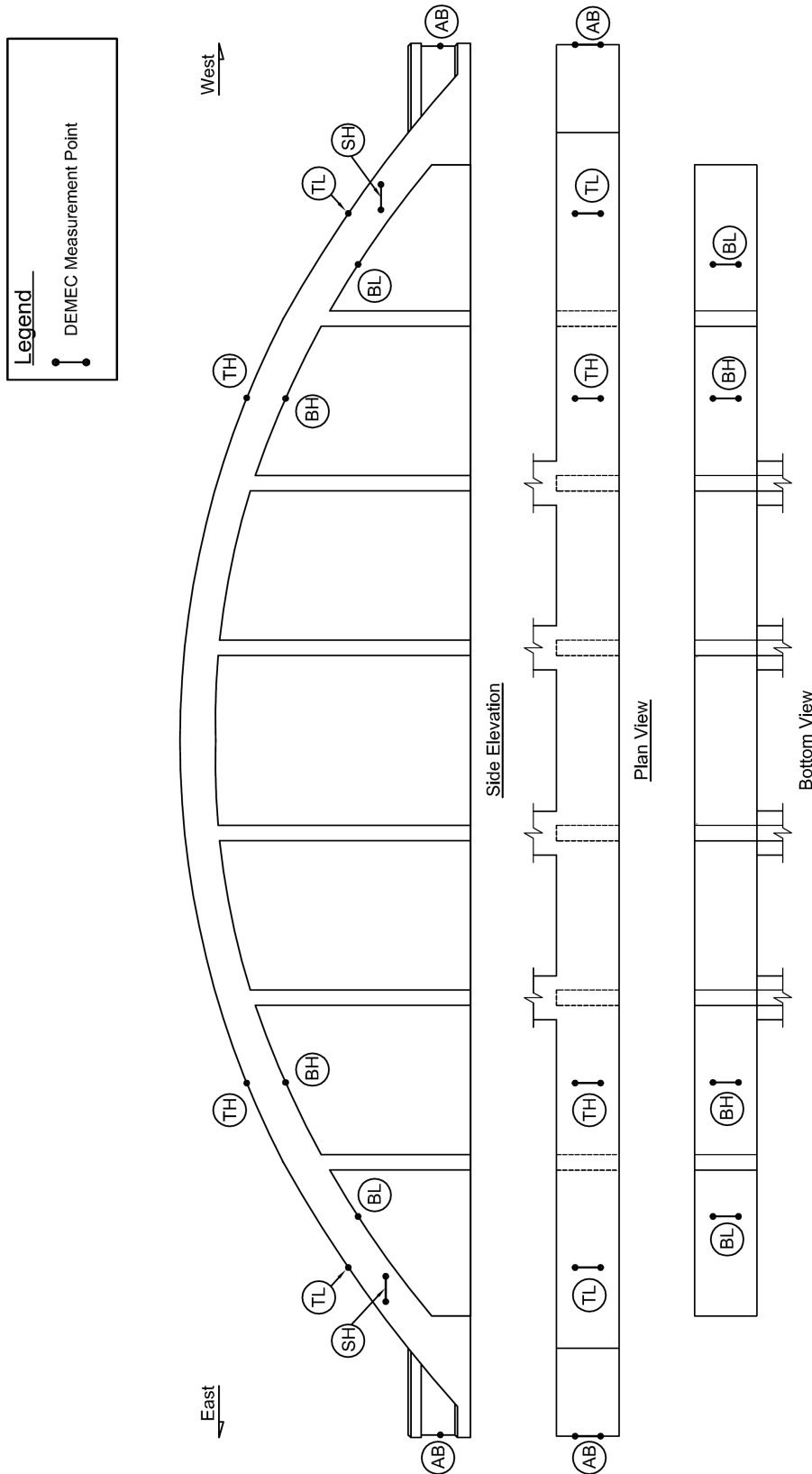


**Figure 5.11: DEMEC Locations - Span 4 - North Arch. Not to Scale**

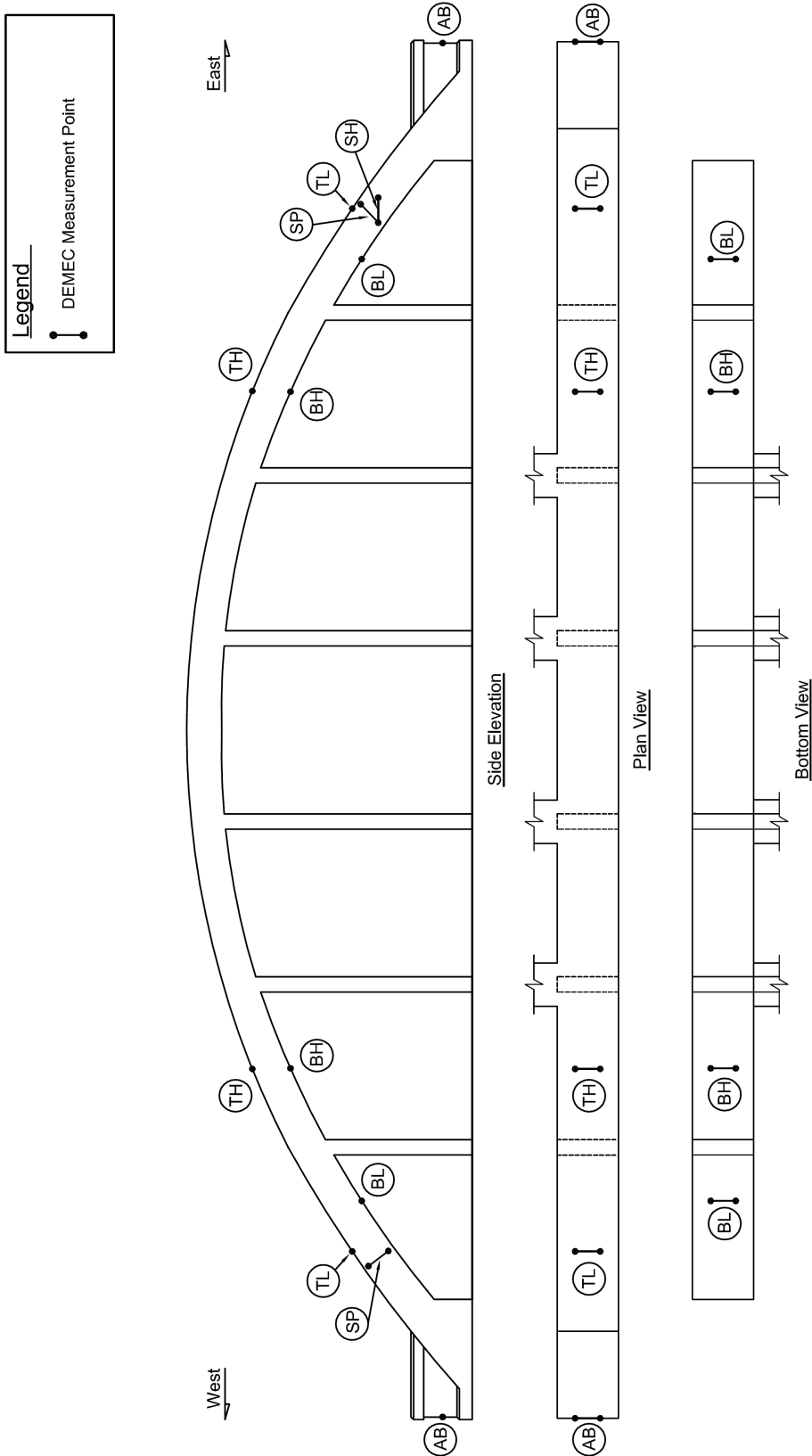


**Figure 5.12: DEMEC Locations - Span 5 - South Arch. Not to Scale**

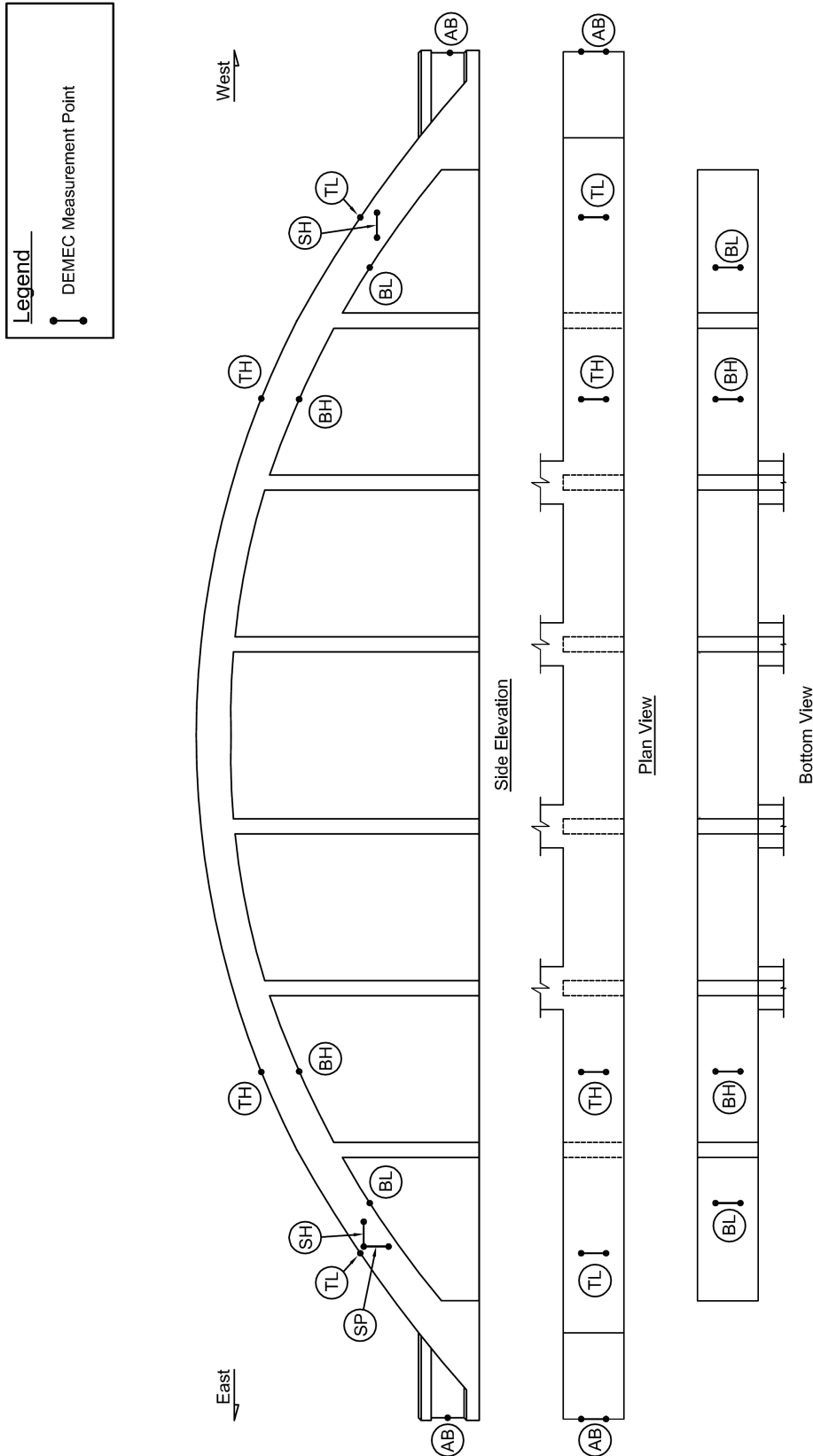


**Figure 5.13: DEMEC Locations - Span 5 - North Arch. Not to Scale**

## 5.4 Summary

During November 16 and 17, 2010, instrumentation was added by personnel from the FHWA, Auburn University, and ALDOT's Materials and Test Bureau to monitor the effectiveness of the ASR mitigation procedure. The instrumentation was installed to collect data pertaining to internal RH and concrete strain in the north and south arches on spans four and five.

The RH measuring equipment used is Vaisala's HM44 Structural Humidity Measurement Kit. There are four RH locations per arch: west top, west bottom, east top, and east bottom. At each location, there are three RH tube depths: 1 in., 2 in., and 3 in. The RH probe locations are graphically shown on Figure 5.6. With four RH locations per arch, and three tubes per location, forty-eight RH readings are taken during each survey.

Concrete strain is measured with a DEMEC concrete strain gauge. There are DEMEC studs installed in various locations on each of the four arches of spans four and five. These locations, along with their respective installation years, are summarized in Table 5.1, and are shown in Figures 5.10 through 5.13.

## Chapter 6

### Experimental Results and Discussion

#### 6.1 Introduction

The results from the data collection on the Bibb Graves Bridge until May 17, 2012 are presented in this chapter. RH and concrete strain data were collected from November 16, 2010, totaling 18-months of data collection. Additionally, concrete strain data from the ten concrete strain measurement locations installed by the FHWA were collected from December 16, 2005, totaling 77 months (6.4 years) of data collection.

In all analyses, span 4 serves as a control span that is not affected by ASR. The northern arch of span 4 received no ASR mitigation procedure, and the southern arch received the full ASR mitigation procedure. Span 5 is affected by ASR, and both arches received the ASR mitigation procedure.

Because any prominent downward trends in RH below 80 % should in turn affect the expansion due to ASR at the respective location of data collection, RH data are presented first. Within this section, raw humidity data are presented first, followed by linear regression analysis of the RH data and an examination designated as “RH difference” analysis.

Concrete strain measurement data are presented after the RH data. The raw data trends are shown alongside error bars that account for temperature

effects. Any apparent trends are then discussed and evaluated using linear regression analysis. Lastly, a concrete strain difference analysis was performed to account for temperature effects on the concrete strain data. Plots from these analyses were investigated and trends are discussed.

Finally, the relationships of the RH data and concrete strain data are explored, and conclusions are drawn to determine the effectiveness of the ASR mitigation procedure for the period between November 16, 2010 and May 17, 2012.

## **6.2 Internal Relative Humidity**

A summary of the internal RH survey dates, with the corresponding ages from ASR mitigation procedure application, are listed in Table 6.1.

All of the RH plots in this section have a bold line plotted horizontally along 80 % RH. This is representative of the threshold humidity at which ASR expansion is slowed or stopped (Stark 1991, Bérubé et al. 2002a). The internal RH readings are all presented along with the ambient RH collected from nearby Maxwell Air Force Base in Montgomery, AL, as shown in Figure 6.1. The plotted ambient RH is a 28-day running average. All of the raw data from the RH surveys can be found in Appendix B.

**Table 6.1:** RH survey dates, with corresponding ages from the first reading

| <b>Relative Humidity Survey Dates</b> |                             |
|---------------------------------------|-----------------------------|
| <i>Survey Date (MM/DD/YY)</i>         | <i>Months from 11/16/10</i> |
| 11 / 16 / 10                          | 0                           |
| 02 / 15 / 11                          | 3.0                         |
| 04 / 07 / 11                          | 4.7                         |
| 05 / 05 / 11                          | 5.6                         |
| 06 / 03 / 11                          | 6.5                         |
| 07 / 07 / 11                          | 7.7                         |
| 08 / 10 / 11                          | 8.8                         |
| 09 / 15 / 11                          | 10.0                        |
| 10 / 18 / 11                          | 11.0                        |
| 11 / 08 / 11                          | 11.7                        |
| 12 / 14 / 11                          | 12.9                        |
| 01 / 31 / 12                          | 14.5                        |
| 03 / 08 / 12                          | 15.7                        |
| 04 / 12 / 12                          | 16.8                        |
| 05 / 17 / 12                          | 18.0                        |

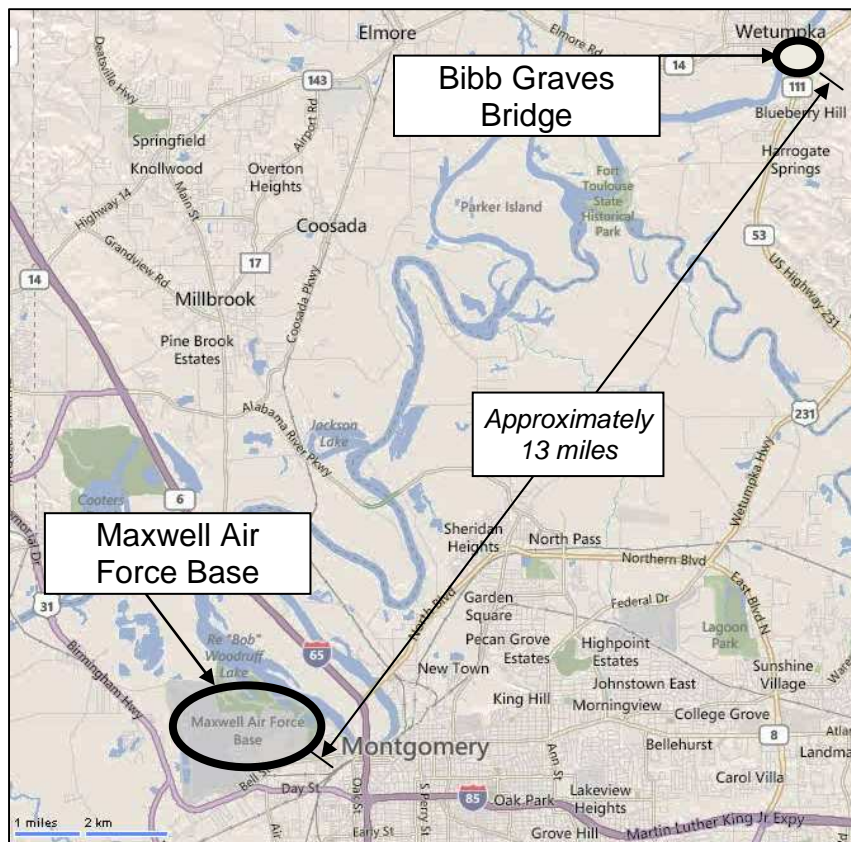


**Figure 6.1:** Maxwell Air Force Base near Montgomery, AL (Bing 2012b)



### 6.2.1 Relative humidity measurement identification system

The RH measurements were taken at 4 locations per arch, as defined in section 5.2. These locations are denoted as west top (WT), west bottom (WB), east top (ET), and east bottom (EB). At each location there are three measurement depths: 1 in., 2 in., and 3 in. Therefore, there are 48 total measurement locations on the bridge. To simplify the discussion of the RH measurements, the following identification system is used throughout this section:

| <u>Span number</u> | <u>Arch Location</u> | <u>Measurement Location</u> | <u>Measurement Depth</u> |
|--------------------|----------------------|-----------------------------|--------------------------|
| ↑                  | ↑                    | ↑                           | ↑                        |
| 4                  | South (S)            | WT                          | 1"                       |
| 5                  | North (N)            | WB                          | 2"                       |
|                    |                      | ET                          | 3"                       |
|                    |                      | EB                          | Average (AVG)            |

*Example: 4-S-ET-AVG*, represents the average of all three measurement depths, for the east top measurement location, on the southern arch of span 4.

### 6.2.2 RH data for the average of all measurement depths

The average of all three measurement depths at the west top, west bottom, east top, and east bottom measurement locations are shown in Figures 6.2 through 6.5 respectively. An 18-month average of all measurement depths at each location is shown in Table 6.2. Raw RH data for the average of all measurement depths is shown in Table B.1.

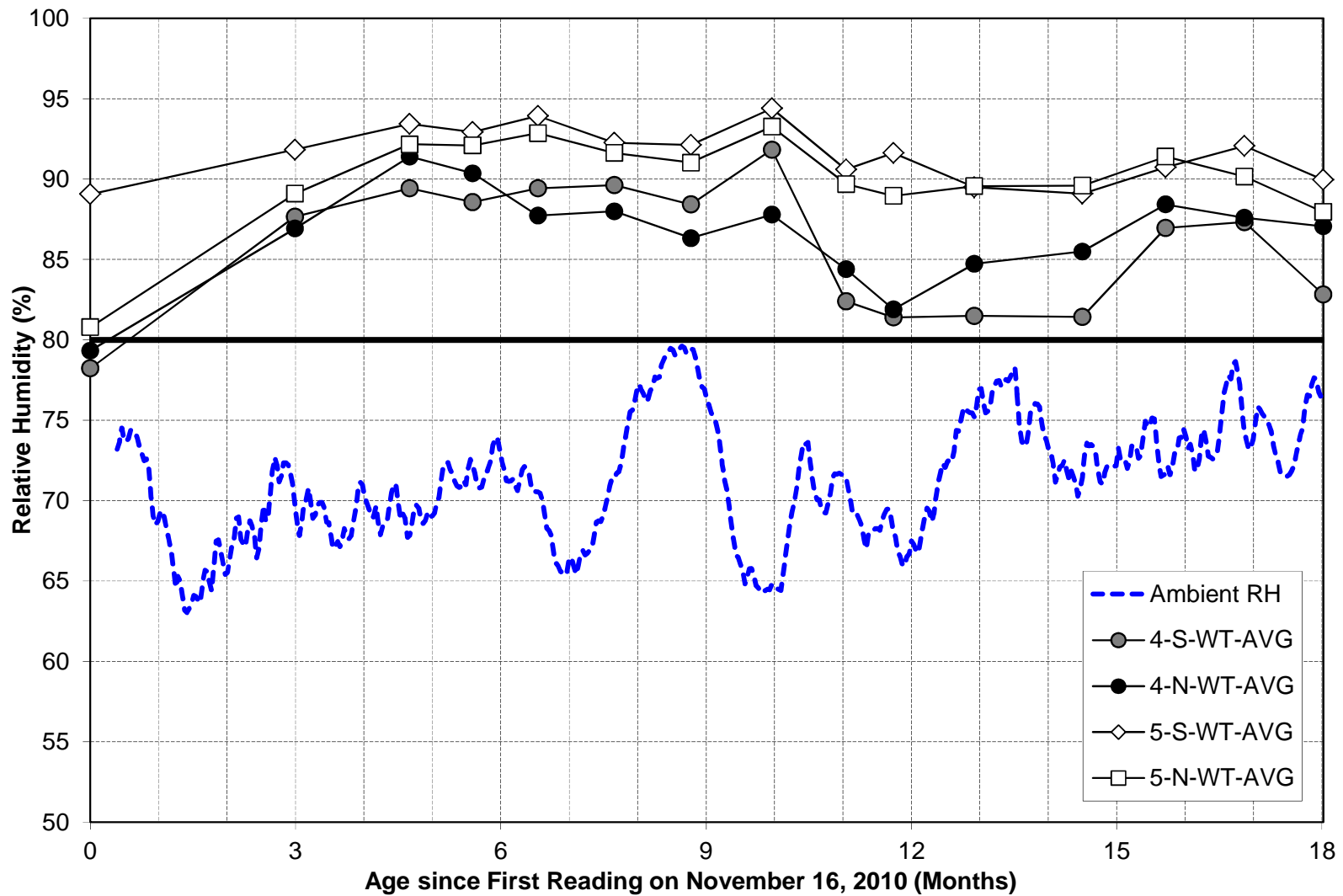


**Figure 6.2:** RH measurements, West Top, average of all measurement depths

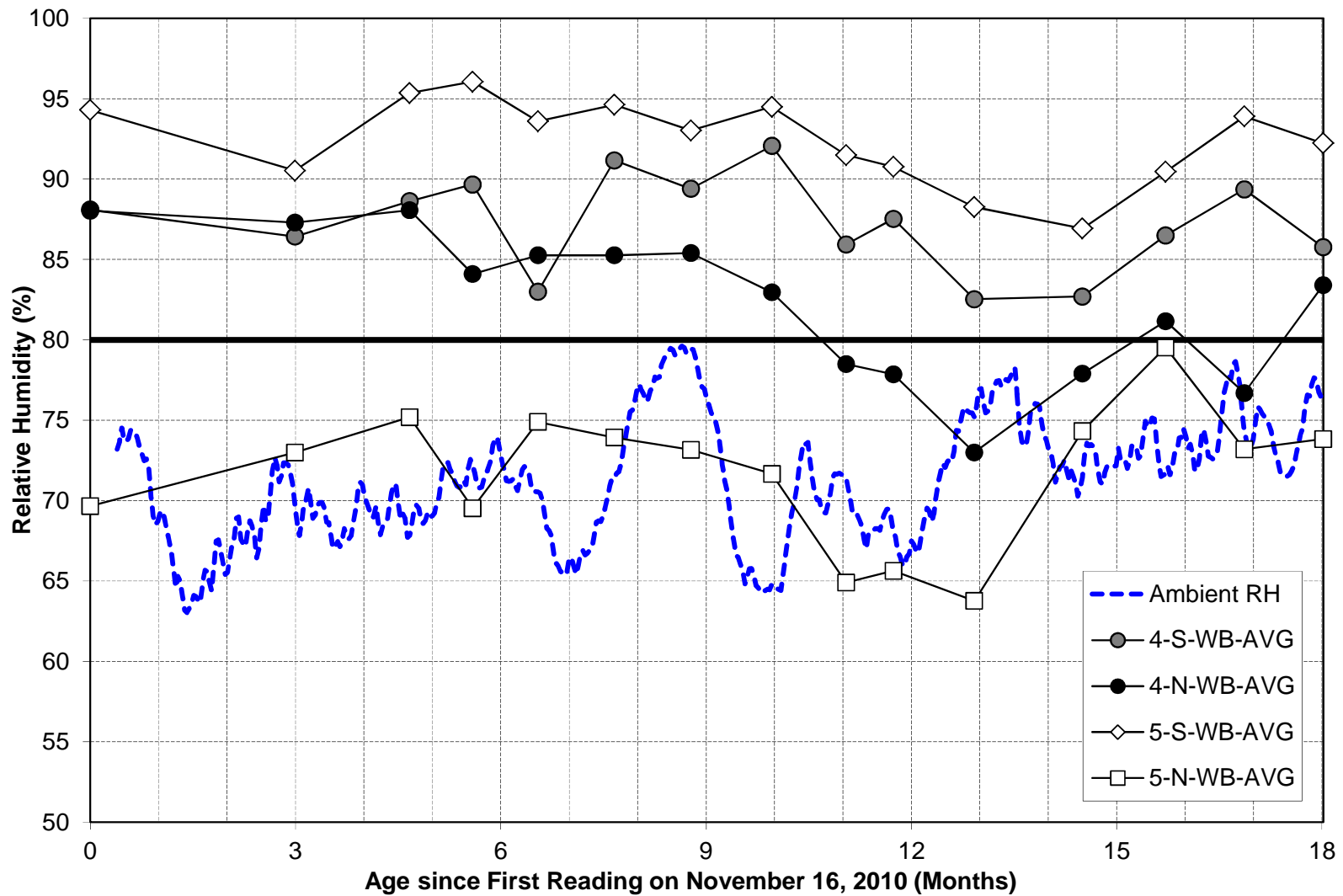


**Figure 6.3:** RH measurements, West Bottom, average of all measurement depths

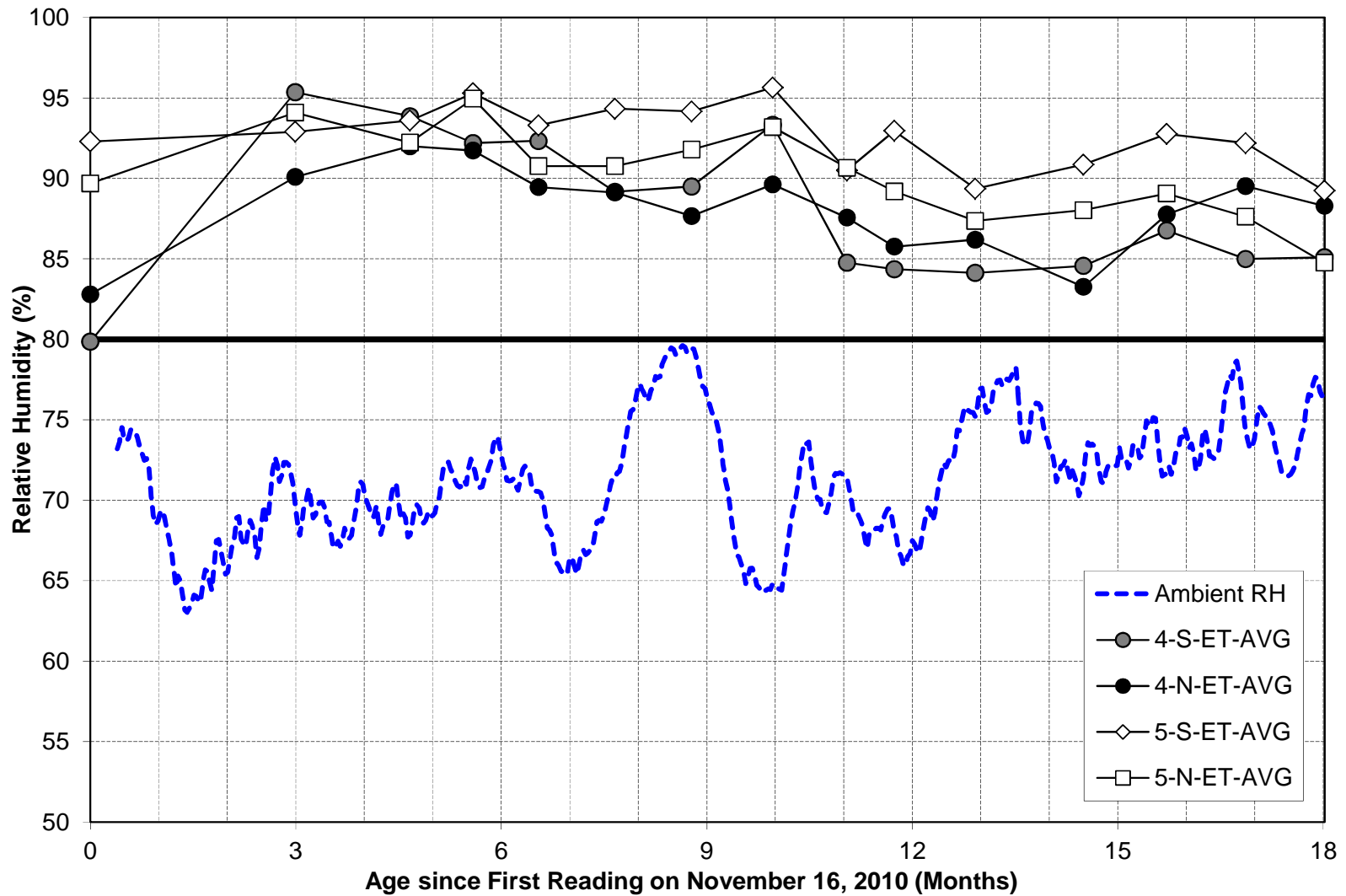


**Figure 6.4:** RH measurements, East Top, average of all measurement depths

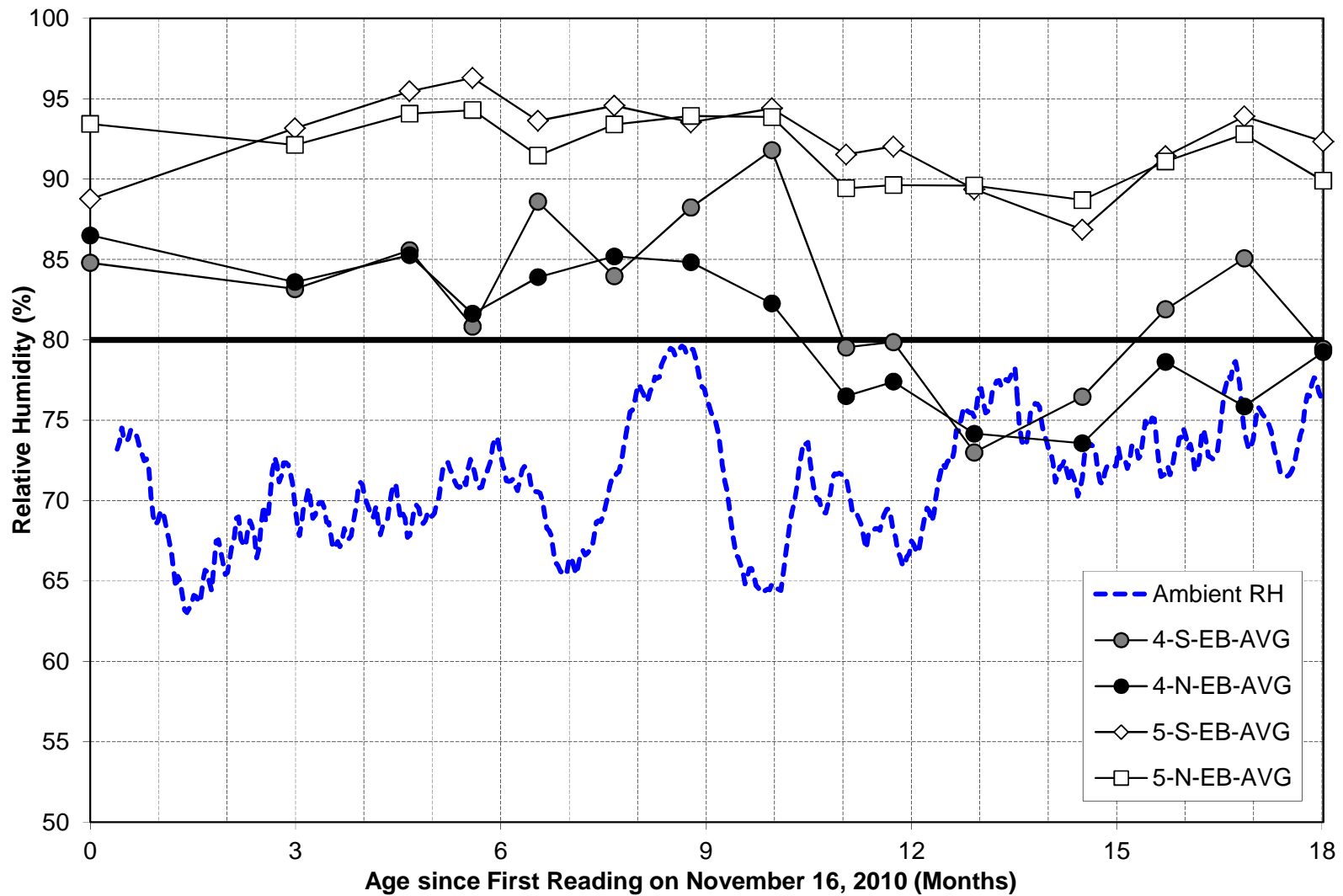


Figure 6.5: RH measurements, East Bottom, average of all measurement depths

**Table 6.2:** 18-month RH (%) averages for the average of all measurement depths

| <b>Eighteen Month RH Average (%)</b> |                             |                   |                   |           |
|--------------------------------------|-----------------------------|-------------------|-------------------|-----------|
| <i>Arch Location</i>                 | <i>Measurement Location</i> |                   |                   |           |
|                                      | <i>WT</i>                   | <i>WB</i>         | <i>ET</i>         | <i>EB</i> |
| <i>4-N</i>                           | 86.5                        | 82.3              | 88.1              | 80.6      |
| <i>4-S</i>                           | 85.8 <sup>a</sup>           | 87.3              | 88.0 <sup>a</sup> | 82.8      |
| <i>5-N</i>                           | 90.0                        | 71.8 <sup>a</sup> | 90.3              | 91.9      |
| <i>5-S</i>                           | 91.6                        | 92.4              | 92.6              | 92.5      |

Notes: Gray cells signify the control arch  
<sup>a</sup> = RH values below those from the control arch

From initial inspection of Figure 6.2, the majority of the readings for 5-N-WT-AVG, and 5-S-WT-AVG are greater than that of 4-N-WT-AVG and 4-S-WT-AVG. 5-N-WT-AVG and 5-S-WT-AVG average 90.0 % and 91.6 % RH over 18-months, respectively; whereas 4-N-WT-AVG and 4-S-WT-AVG average 86.5 % and 85.8 % RH, respectively. Overall, there is a lack of obvious trends in the data presented in Figure 6.2.

The most prominent feature of Figure 6.3 is that 5-N-WB-AVG ranges between approximately 63-80 % RH, and averaged 71.8 % RH for the 18-month data collection period. This is the only measurement location that was below the 80 % threshold for the entire 18-month data collection period. In fact, 5-N-WT-AVG, which is almost directly above the bottom measurement location, ranges between 85-95 % RH, as shown in Figure 6.2, and averaged 90.0 % RH. It should be noted that the concrete at 5-N-WB-AVG is of good quality and not affected by ASR. For the other two WB locations that received the ASR mitigation procedure, 5-S-WB-AVG and 4-S-WB-AVG, the RH measurements are greater than the control location 4-N-WB-AVG for the majority of the survey

dates. 5-S-WB-AVG and 4-S-WB-AVG averaged 92.4 % and 87.3 % RH, respectively, whereas 4-N-WB-AVG averaged 82.3 % RH.

The RH data in Figure 6.4 are closely grouped, but 5-N-ET-AVG shows a downward trend toward the 80 % RH threshold. 5-S-ET-AVG also shows a downward trend; however, it is less prominent. 4-S-ET-AVG begins at 80 % RH and then jumps to approximately 95 % RH after 3 months; the trend from the 3 month reading onward is downward. 5-N-ET-AVG and 5-S-ET-AVG average 90.3 % and 92.6 % RH, respectively; 4-N-ET-AVG and 4-S-ET-AVG average 88.1 % and 88.0 % RH, respectively.

The most noticeable feature of Figure 6.5 is the pairing of data for both locations of span 4 and both locations of span 5. 5-N-EB-AVG shows a slight downward trend. 4-S-EB-AVG also shows a downward trend; however, its data contain more fluctuations than that of the control, 4-N-EB-AVG. 5-N-EB-AVG and 5-S-EB-AVG average 91.9 % and 92.5 % RH, respectively; 4-N-EB-AVG and 4-S-EB-AVG average 80.6 % and 82.8 % RH, respectively.

For the measurement locations where the ASR mitigation procedure was applied, there were only three occurrences where the average for the 18-month data collection period fell below the 18-month average for the control span. Two of the occurrences are located on the top of the southern arch of span 4; which are 4-S-WT-AVG and 4-S-ET-AVG. The other location is located on the bottom of the northern arch of span 5, 5-N-WB-AVG. As previously discussed, 5-N-WB-AVG presented itself as an anomaly, as it was the only location that started below, and consistently stayed below the 80 % RH threshold. The two

locations on arch 4-S were on the top of the arch, whereas the two locations on the bottom of the arch had an 18-month average greater than arch 4-N.

### 6.2.2.1 Linear regression analysis of RH data for the average of all measurement depths

The primary feature of the raw data plots, shown in Figures 6.2 through 6.5, is the lack of definite trends that show that the ASR mitigation procedure is lowering the RH in the damaged and/or undamaged concrete toward the 80 % RH threshold. Therefore, a linear regression analysis was performed for all measurement locations. Coefficients of determination ( $r^2$ ) were then calculated; therefore, the presence of a trend is quantitatively defined. A summary of the  $r^2$  values of the linear regression trends for the average of all measurement depths is shown in Table 6.3.

**Table 6.3:** Coefficients of determination ( $r^2$ ) of the linear regression trends for the average of all measurement depths

| <b>Coefficients of determination of the linear regression trends</b> |                             |                    |                    |                    |
|--|-----------------------------|--------------------|--------------------|--------------------|
| <i>Arch Location</i>   | <i>Measurement Location</i> |                    |                    |                    |
|  | <i>WT</i>                   | <i>WB</i>          | <i>ET</i>          | <i>EB</i>          |
| 4 – N  | 0.009                       | 0.525 <sup>a</sup> | 0.018              | 0.610 <sup>a</sup> |
| 4 – S  | 0.021                       | 0.063              | 0.141              | 0.151              |
| 5 – N  | 0.051                       | 0.007              | 0.516 <sup>a</sup> | 0.339              |
| 5 – S  | 0.079                       | 0.216              | 0.251              | 0.053              |

Notes: Gray cells signify the control arch  
<sup>a</sup> = locations where  $r^2 \geq 0.5$



A lower-bound value of 0.5 for the coefficients of determination was used to determine if the linear regression trend was statistically significant. For measurement locations with the ASR mitigation procedure applied, the lower-bound  $r^2$ -value was only satisfied by the 5-N-ET-AVG measurement location, with an  $r^2$ -value of 0.516. The corresponding control measurement location, 4-N-ET-AVG, has an  $r^2$ -value of only 0.018, and therefore no conclusions can be drawn from the linear regression analysis.

#### **6.2.2.2 RH difference analysis for the average of all measurement depths**

To further determine the effectiveness of the ASR mitigation procedure, the difference in RH for arches 4-S, 5-N, and 5-S was taken with arch 4-N, per survey date, per measurement location. This was done to determine if the RH was decreasing relative to the control span which received no ASR mitigation procedure.

A schematic of a “RH difference” plot is shown in Figure 6.6. If the ASR mitigation was effective over the 18-month data collection period, one would expect to see a negative trend. This would indicate that the internal RH in the arch is lowering relative to the internal RH in arch 4-N, as shown in Case A of Figure 6.6. A trend with zero slope would indicate that the RH in the arch is unchanged relative to RH in arch 4-N, as shown in Case B of Figure 6.6. A trend with positive slope would indicate that the RH in the arch is worsening relative to the RH in arch 4-N, as shown in Case C of Figure 6.6.

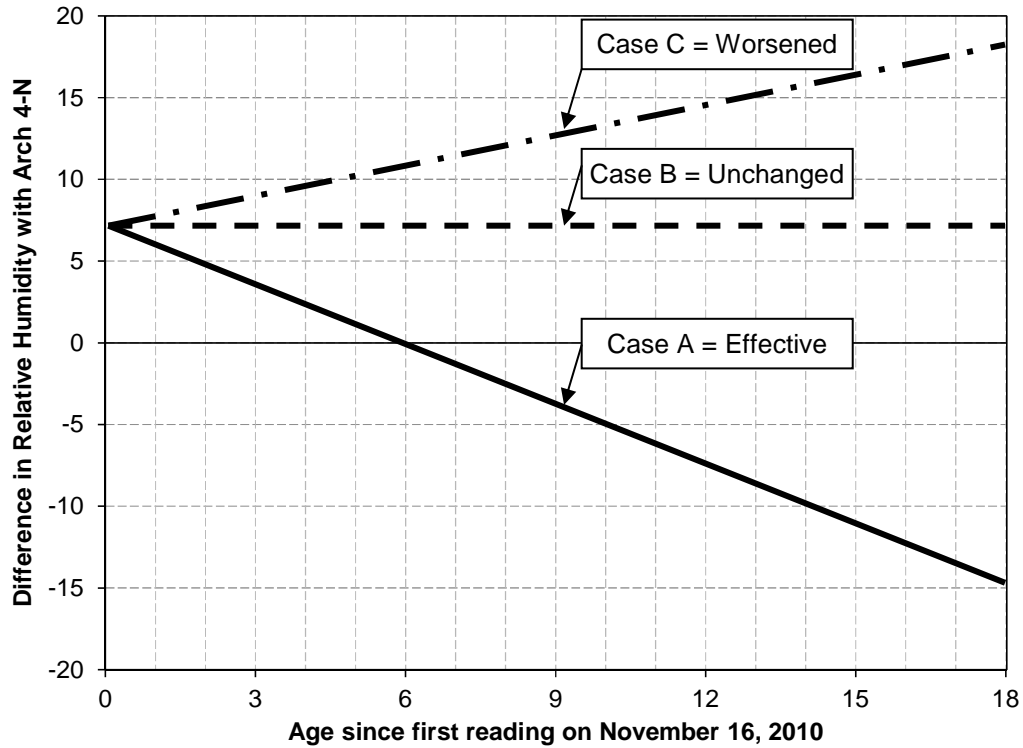


**Figure 6.6:** Schematic of “RH difference” plot for various scenarios

A summary of the coefficients of determination for the RH difference analyses, for arches 4-S, 5-N, and 5-S, is shown in Table 6.4.

**Table 6.4:** Coefficients of determination for RH difference analyses for the average of all measurement depths

| <b>Coefficients of Determination for RH Difference Analyses</b> |                             |                    |           |                    |
|---|-----------------------------|--------------------|-----------|--------------------|
| <i>Arch Location</i>  | <i>Measurement Location</i> |                    |           |                    |
|   | <i>WT</i>                   | <i>WB</i>          | <i>ET</i> | <i>EB</i>          |
| 4 – S   | 0.136                       | 0.355              | 0.227     | 0.181              |
| 5 – N   | 0.042                       | 0.653 <sup>a</sup> | 0.064     | 0.550 <sup>a</sup> |
| 5 – S   | 0.103                       | 0.342              | 0.372     | 0.532 <sup>a</sup> |

Notes: - a = locations where  $r^2 \geq 0.5$

For the RH difference analyses, the only measurement locations that exceeded the 0.5 minimum  $r^2$ -value were 5-N-WB-AVG, 5-N-EB-AVG, and

5-S-EB-AVG. These RH difference plots are shown in Figures 6.7 through 6.9, respectively. All of the RH difference plots with linear regression trends that have an  $r^2$  of 0.5 or greater are located on the bottom of the arches. Additionally, all of the linear regression lines with an  $r^2$  value greater than or equal to 0.5 have a positive slope. Once again, a positive slope means that the difference in the RH measurements is increasing over time; therefore, the ASR mitigation procedure may be ineffective at these bottom measurement locations.

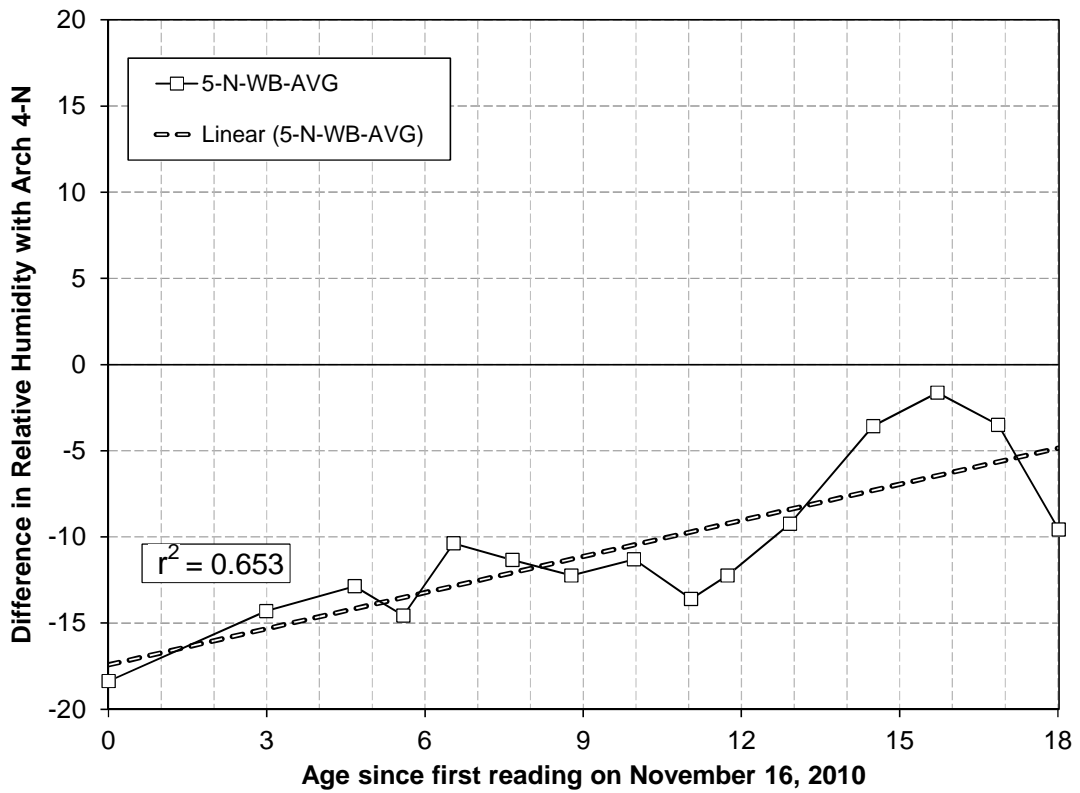


**Figure 6.7:** RH difference for 5-N-WB-AVG

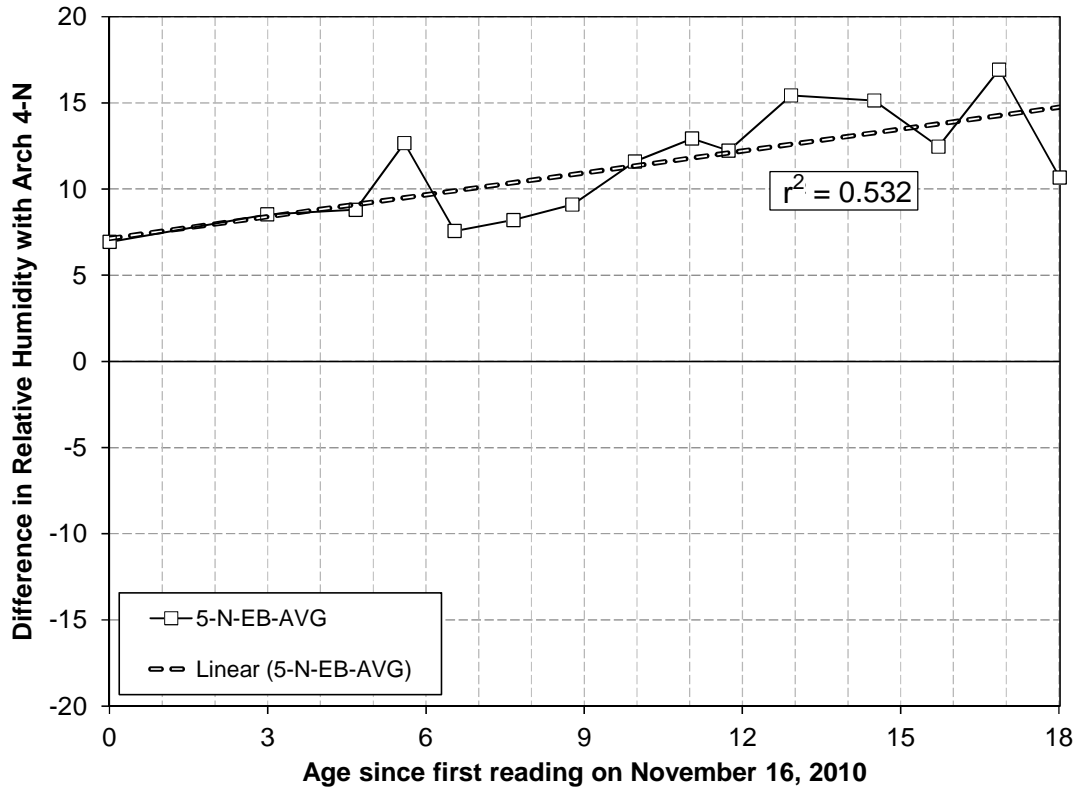


**Figure 6.8:** RH difference for 5-N-EB-AVG

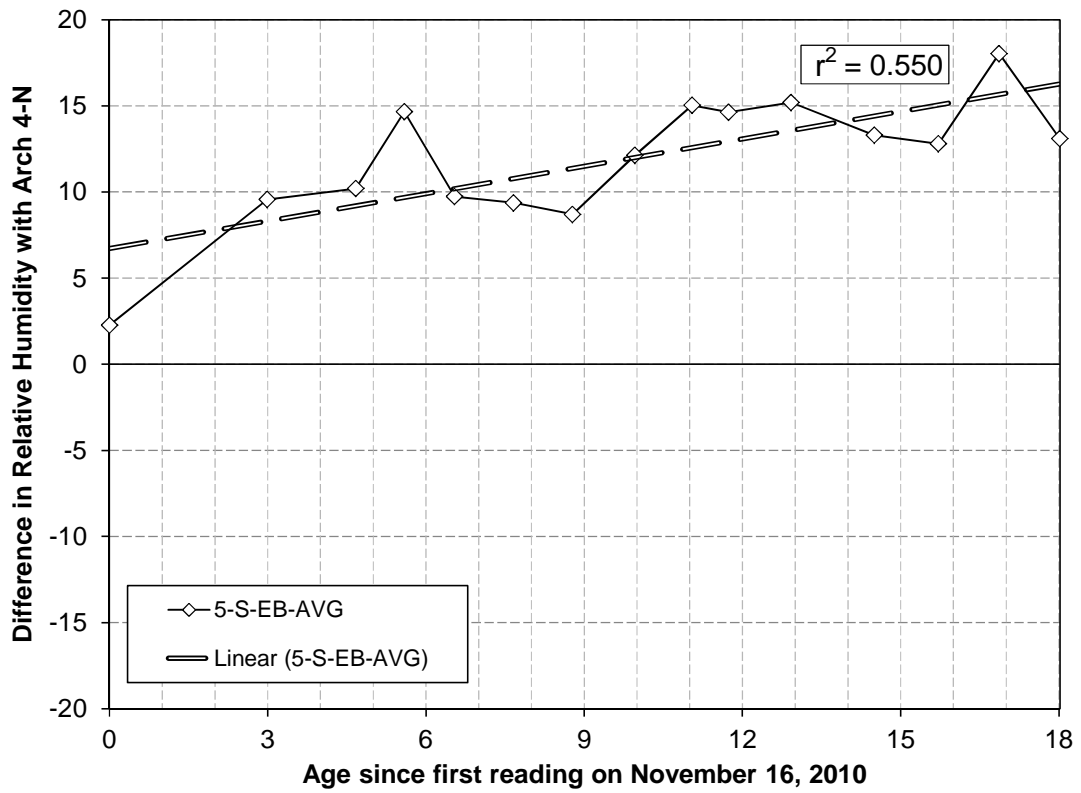


**Figure 6.9:** RH difference for 5-S-EB-AVG

### **6.2.3 RH data for the 3-inch measurement depth**

There is the possibility that the lack of trends in the analysis of the average of all three measurement depths is due to the fact that the 1 in. and 2 in. measurement depths are adding erroneous data into the average, due to ease of which ambient humidity can enter and leave the concrete's outer surfaces.

To evaluate this possibility, only the 3-in. measurement depth is evaluated in this section. The RH for the west top, west bottom, east top, and east bottom measurement locations are shown in Figures 6.10 through 6.13 respectively. A summary of all the 18-month averages, for the 3-in. measurement depth, is shown in Table 6.5.

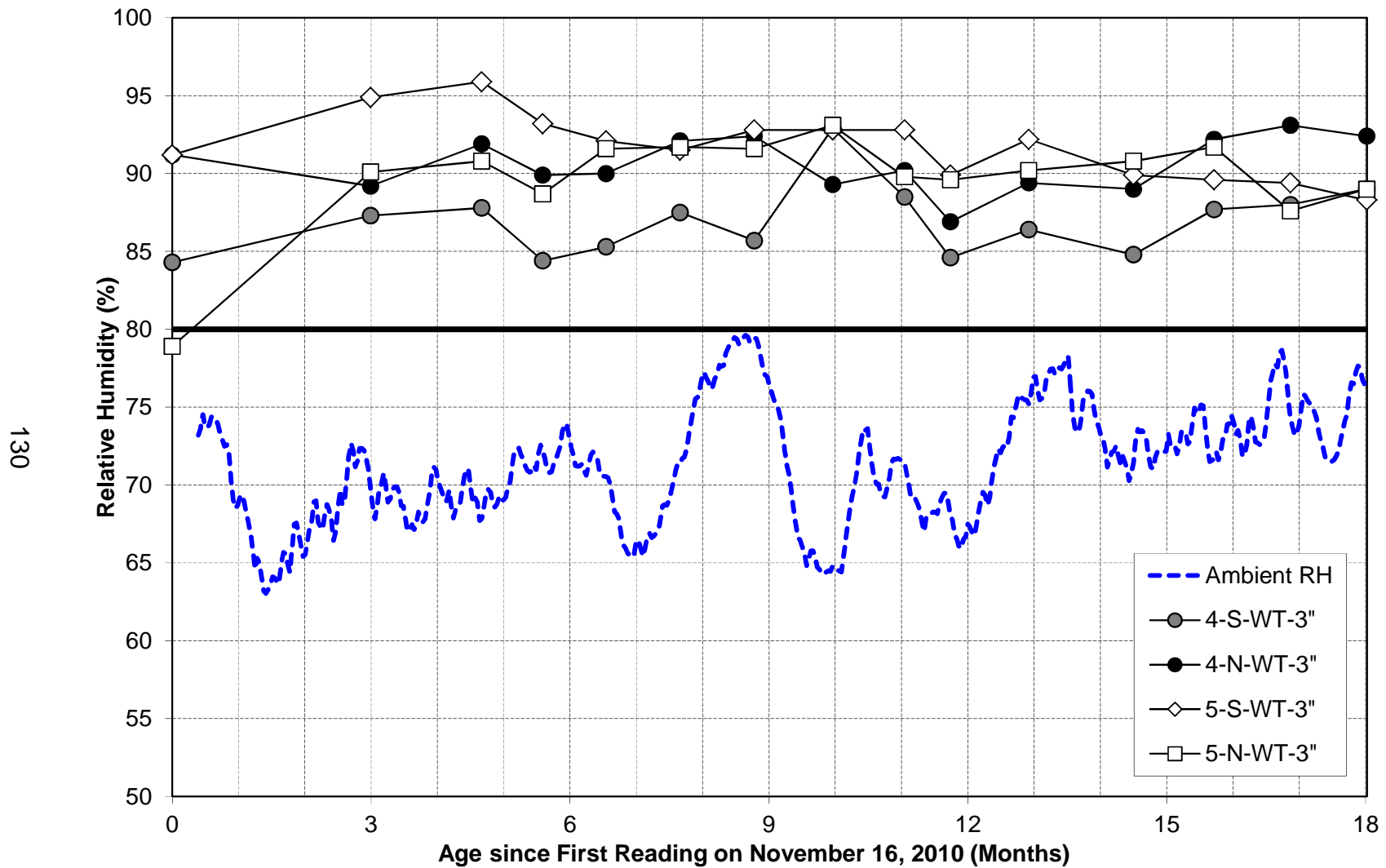


Figure 6.10: RH measurements, West Top, 3-inch depth

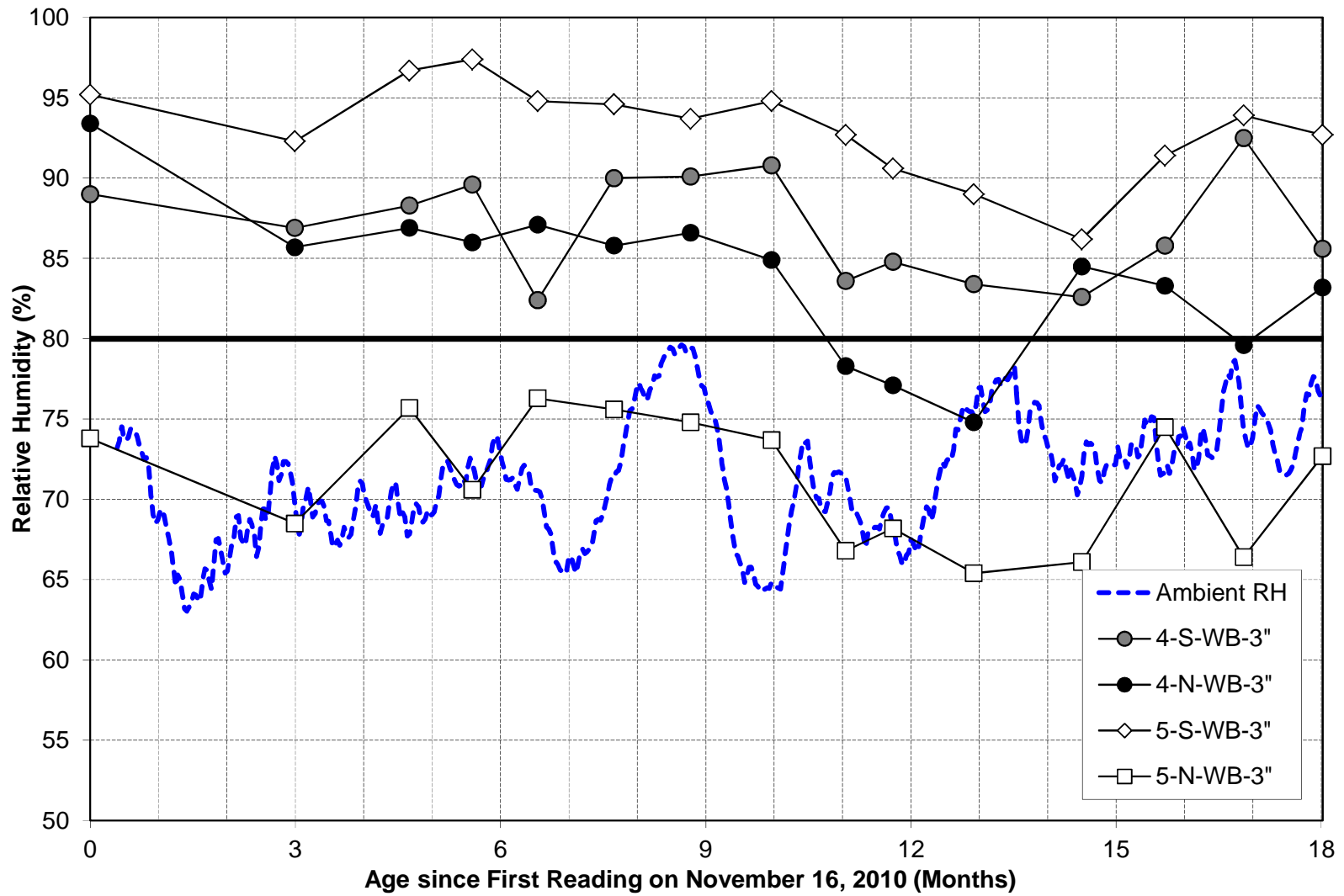


Figure 6.11: RH measurements, West Bottom, 3-inch depth

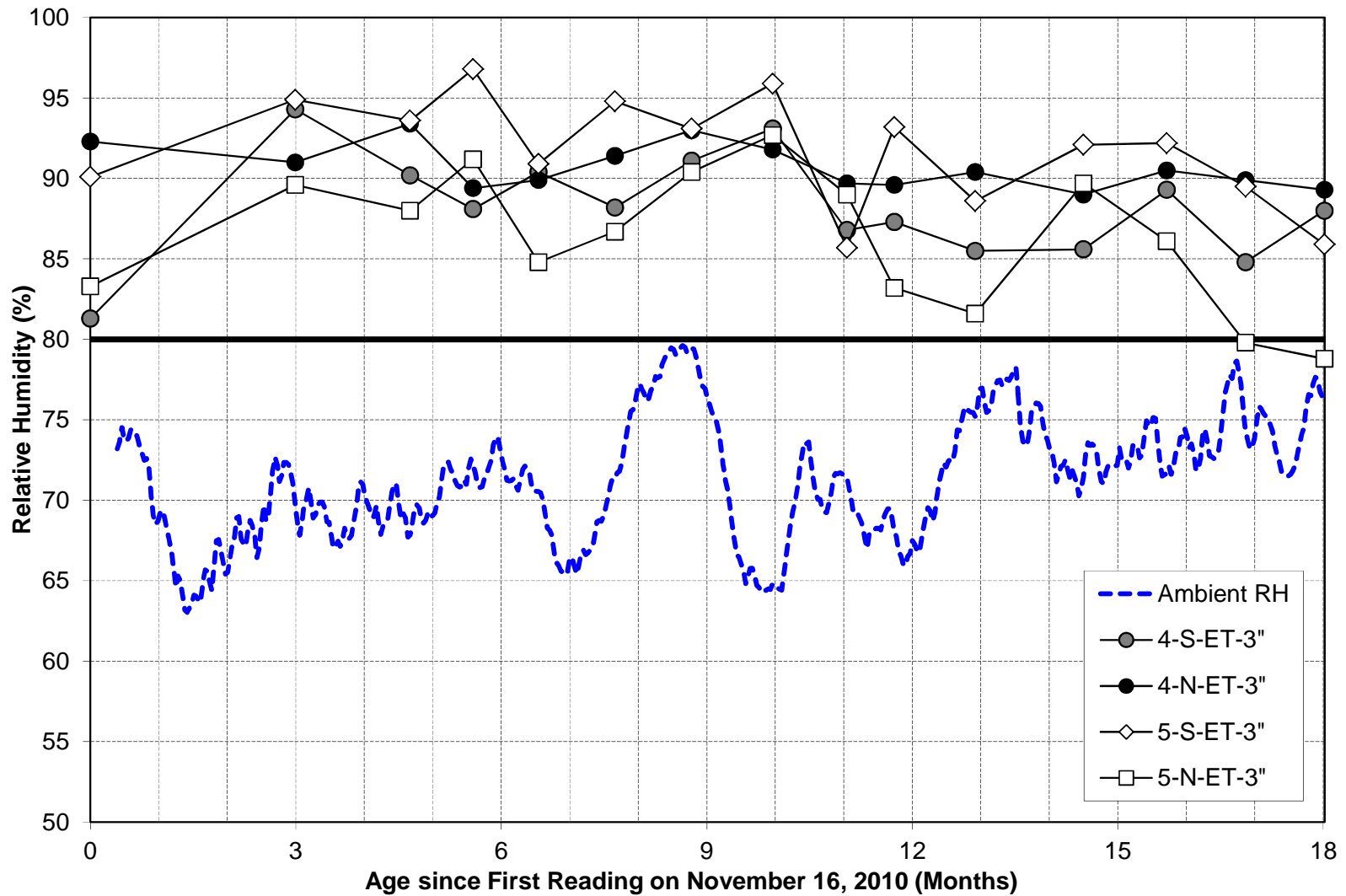


Figure 6.12: RH measurements, East Top, 3-inch depth



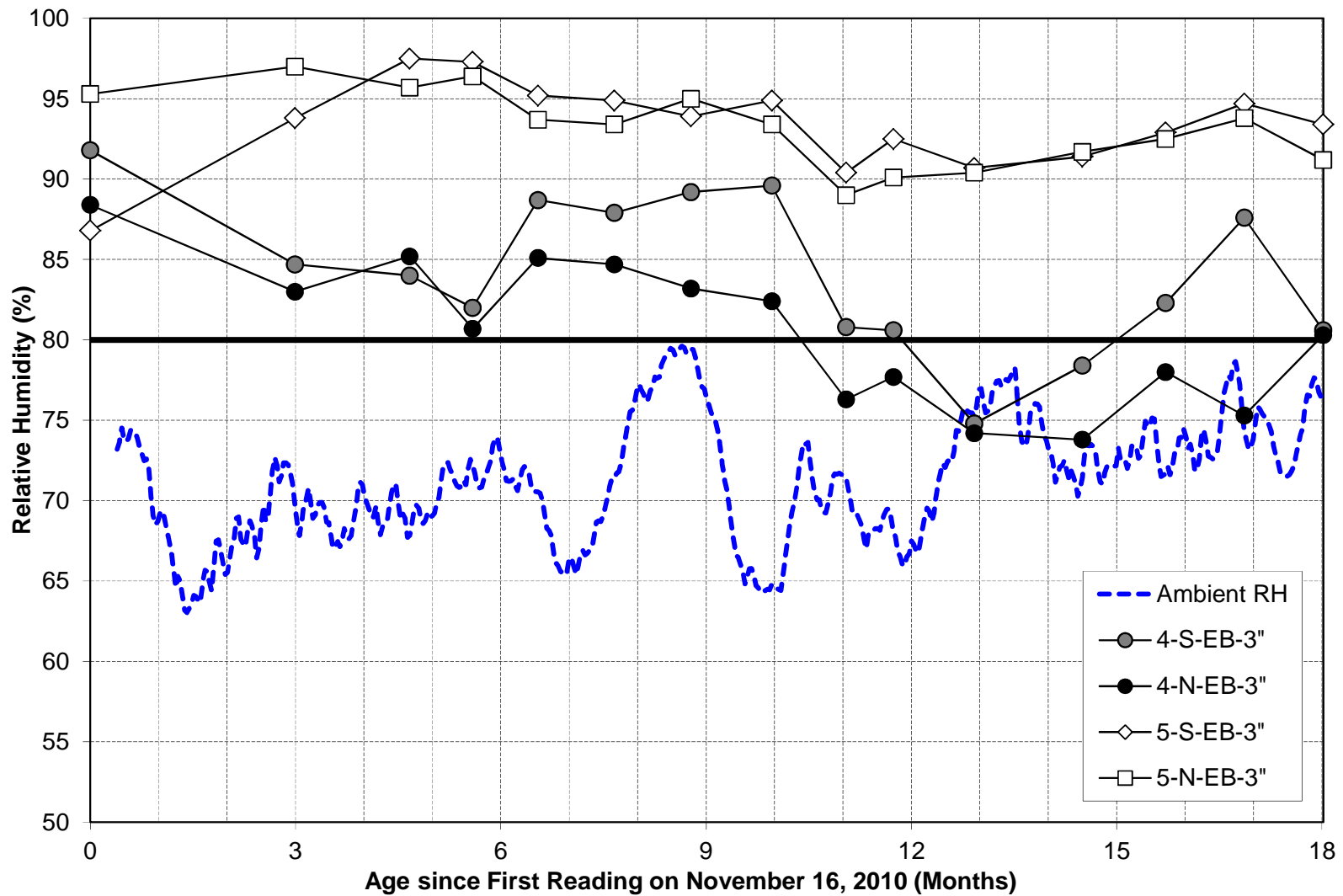


Figure 6.13: RH measurements, East Bottom, 3-inch depth

**Table 6.5:** 18-month averages for the 3-inch measurement depth

| <i>18-month RH Averages (%)</i> |                             |                   |                   |           |
|---------------------------------|-----------------------------|-------------------|-------------------|-----------|
| <i>Arch Location</i>            | <i>Measurement Location</i> |                   |                   |           |
|                                 | <i>WT</i>                   | <i>WB</i>         | <i>ET</i>         | <i>EB</i> |
| 4-N                             | 90.6                        | 83.8              | 90.7              | 80.6      |
| 4-S                             | 86.9 <sup>a</sup>           | 87.0              | 88.3 <sup>a</sup> | 84.2      |
| 5-N                             | 89.7 <sup>a</sup>           | 71.3 <sup>a</sup> | 86.3 <sup>a</sup> | 93.2      |
| 5-S                             | 91.8                        | 93.1              | 91.8              | 93.4      |

Notes: Gray cells signify the control arch  
<sup>a</sup> = RH values below those from the control arch

All of the plotted data lines in Figure 6.10 are closely grouped; however, there are a few noticeable characteristics. The first is the 18-month average for 4-S-WT moved up from 86.5 % RH for the average of all three depths, to 90.6 % RH for the 3 in. depth. Secondly, a slightly downward trend for 5-S-WT-3" is evident. Finally, the initial reading for 5-N-WT-3" was less than 80 % RH; however, every reading thereafter averaged around 90 % RH.

Once again, the most prominent feature of the west bottom measurement location plot, shown in Figure 6.11, is that 5-N-WB-3" averages 71.3 % RH for the 18-month data collection period. Just as before, this is the only measurement location that was below the 80 % threshold for the entire 18-month data collection period. Additionally, 5-N-WT-3", which is directly above the 5-N-WB-3", averages 89.7 % RH for the 18-month data collection period. Therefore, the 5-N-WB measurement location remains an anomaly. For 5-S-WB-3", a very slight downward trend is apparent. There were no major changes in the 18-month RH averages for all measurement locations.

The downward trend for 5-N-ET-AVG, shown in Figure 6.4, is not apparent for 5-N-ET-3", shown in Figure 6.12. Also when comparing the 3-inch depth to the average of all three measurement depths, the 18-month average for 4-N-ET increased from 88 % RH to 91 % RH, and 5-N-ET decreased from 90 % RH to 86 % RH, as shown in Figure 6.12.

The downward trend for 5-N-EB-AVG, shown in Figure 6.5, becomes increasingly prominent for 5-N-EB-3", shown in Figure 6.13. The respective pairing of the data between spans 4 and 5, shown in Figure 6.5, becomes less apparent in Figure 6.13; however, it is still noticeable. Additionally, a slight downward trend can be seen for 4-S-EB-3" in Figure 6.13.

For the 12 measurement locations with the ASR mitigation procedure applied, there were only five locations where the average for the 18-month data collection period fell below the 18-month average for the control span, as shown in Table 6.5. Just as with the average for all three measurement depths, two of these locations for the 3-in. measurement depth are located on the top of arch 4-S and one of the locations is 5-N-WB. Conversely, two new occurrences for the 3-inch measurement depth are located on the top of arch 5-N.

### **6.2.3.1 Linear regression analysis of RH data for the 3-inch measurement depth**

Once again, the primary feature of the raw data plots, shown in Figures 6.10 through 6.13, is the lack of definite trends that show the ASR mitigation procedure is lowering the damaged and/or undamaged concrete toward the 80 % RH threshold. Therefore, a linear regression analysis was performed for all

measurement locations for the 3-inch depth.  $R^2$ -values were then calculated; therefore, the presence of a trend is quantitatively defined. A summary of the  $r^2$  - values of the linear regression trends for the 3-inch measurement depth is shown in Table 6.6.

The only measurement location where the ASR mitigation procedure is applied that has an  $r^2$ -value greater than 0.5 is 5-S-WT-3", which has an  $r^2$  value of 0.517. The corresponding control measurement location, 4-N-WT-3", has an  $r^2$ -value of only 0.023; therefore, no conclusions can be drawn from the linear regression analysis.

**Table 6.6:** Coefficients of determination ( $r^2$ ) of the linear regression trends for the 3-inch measurement depth

| <b>Coefficients of Determination of the Linear Regression Trends</b> |                             |           |           |                    |
|--|-----------------------------|-----------|-----------|--------------------|
| <i>Arch Location</i>   | <i>Measurement Location</i> |           |           |                    |
|  | <i>WT</i>                   | <i>WB</i> | <i>ET</i> | <i>EB</i>          |
| 4 – N  | 0.023                       | 0.444     | 0.315     | 0.611 <sup>a</sup> |
| 4 – S  | 0.090                       | 0.044     | 0.022     | 0.251              |
| 5 – N  | 0.129                       | 0.144     | 0.173     | 0.453              |
| 5 – S  | 0.517 <sup>a</sup>          | 0.303     | 0.211     | 0.000              |

Notes: Gray cells signify the control arch  
<sup>a</sup> = locations where  $r^2 \geq 0.5$

### 6.2.3.2 RH difference analysis for the 3-inch measurement depth

To further determine the effectiveness of the ASR mitigation procedure, the difference in RH for arches 4-S, 5-N, and 5-S was taken with arch 4-N, per survey date, per measurement location. Other than the measurement depths used, this approach matches the approach used in section 6.2.2.2.

A summary of the coefficients of determination for the RH difference analyses, for arches 4-S, 5-N, and 5-S, is shown in Table 6.7. The only measurement location that exceeded the 0.5 minimum  $r^2$ -value was 5-S-EB. The RH difference plot for 5-S-EB-3" is shown in Figure 6.14. Just as with the RH difference plots for the average of all the measurement depths, the RH difference only plot that has an  $r^2$ -value of 0.5 or greater is located on the *bottom* of the arch. Additionally, the linear regression line for 5-S-EB has a positive slope. This positive slope means that the difference in the RH measurements is increasing over time; therefore, the ASR mitigation procedure at this location may be ineffective.

**Table 6.7:** Coefficients of determination for RH difference analyses for the 3-inch measurement depth

| <b>Coefficients of determination for RH difference analyses</b> |                             |           |           |                    |
|---|-----------------------------|-----------|-----------|--------------------|
| <i>Arch Location</i>  | <i>Measurement Location</i> |           |           |                    |
|   | <i>WT</i>                   | <i>WB</i> | <i>ET</i> | <i>EB</i>          |
| <i>4 – S</i>  | 0.027                       | 0.270     | 0.008     | 0.114              |
| <i>5 – N</i>  | 0.056                       | 0.216     | 0.059     | 0.306              |
| <i>5 – S</i>  | 0.375                       | 0.143     | 0.058     | 0.510 <sup>a</sup> |

Notes: <sup>a</sup> = locations where  $r^2 \geq 0.5$

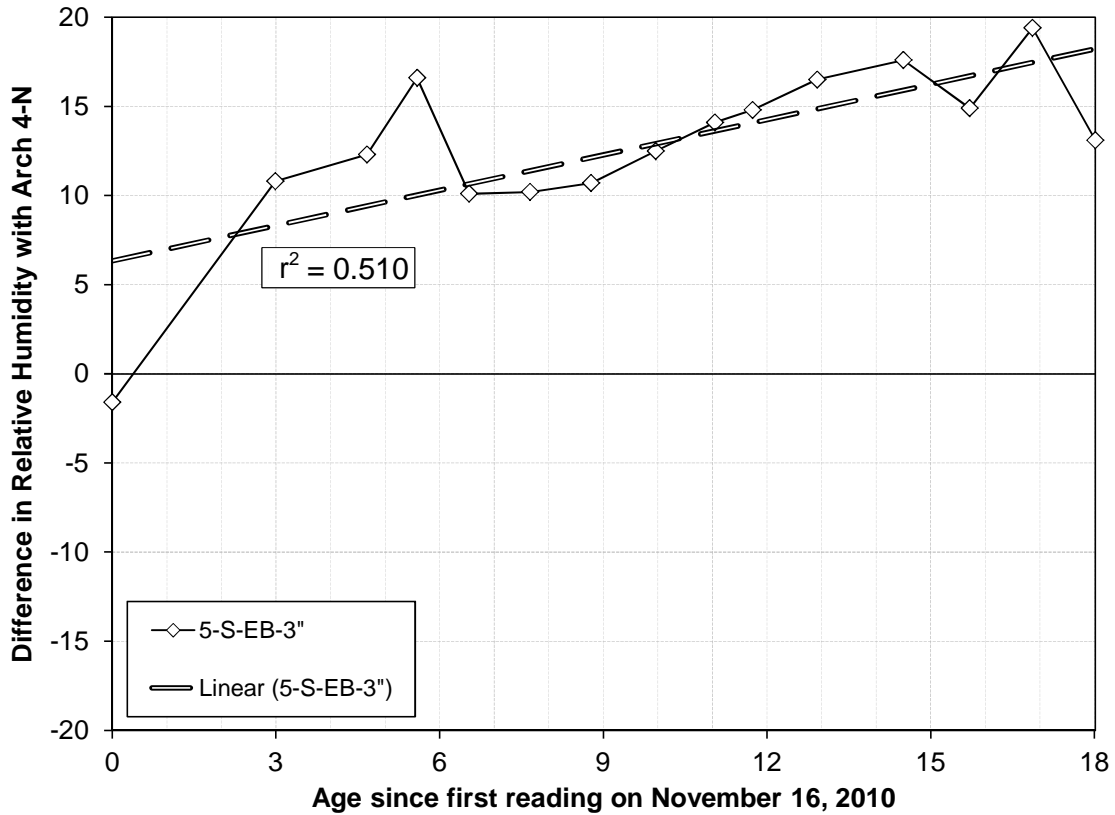


**Figure 6.14:** RH difference for 5-S-EB-3"

#### 6.2.4 RH data analysis summary

The main feature for all of the RH data plots is the lack of statistically significant trends, or evidence that the ASR mitigation procedure has been effective for the first 18 months after its application. However, the following conclusions can be made

- 1) According to the RH difference analysis for 5-N-WB-AVG, 5-N-EB-AVG, and 5-S-EB-AVG, the ASR mitigation procedure may be ineffective, meaning that the RH trend for these arches is diverging from arch 4-N RH trend. When this analysis was repeated for the 3-inch depth, 5-S-EB-3" was ineffective once again. Therefore, it can be

said with some certainty that the ASR mitigation procedure is ineffective at this location.

- 2) The RH data for the 3-inch depth was no more consistent than the average of all three measurement depths.

### 6.3 Concrete strain measurements

A summary of the concrete strain survey dates, with corresponding ages from 12/16/05 and 11/17/10, are listed in Table 6.8. Silane was applied on 11/09/10.

**Table 6.8:** Concrete strain measurement survey dates

| <i>Concrete strain measurement survey dates</i> |                                 |                                 |
|---|---------------------------------|---------------------------------|
| <i>Survey Date</i>                              | <i>Months from 12 / 16 / 05</i> | <i>Months from 11 / 17 / 10</i> |
| 12 / 16 / 05                                    | 0                               | -                               |
| 12 / 09 / 09                                    | 47.8                            | -                               |
| 11 / 17 / 10                                    | 59.1                            | 0                               |
| 02 / 02 / 11                                    | 61.6                            | 2.5                             |
| 04 / 07 / 11                                    | 63.7                            | 4.6                             |
| 05 / 05 / 11                                    | 64.6                            | 5.6                             |
| 06 / 03 / 11                                    | 65.6                            | 6.5                             |
| 07 / 07 / 11                                    | 66.7                            | 7.6                             |
| 08 / 10 / 11                                    | 67.8                            | 8.7                             |
| 09 / 15 / 11                                    | 69.0                            | 9.9                             |
| 10 / 18 / 11                                    | 70.0                            | 11.0                            |
| 11 / 08 / 11                                    | 70.8                            | 11.7                            |
| 12 / 14 / 11                                    | 72.0                            | 12.9                            |
| 01 / 31 / 12                                    | 73.5                            | 14.5                            |
| 03 / 08 / 12                                    | 74.8                            | 15.7                            |
| 04 / 12 / 12                                    | 75.9                            | 16.8                            |
| 05 / 17 / 12                                    | 77.1                            | 18.0                            |

### 6.3.1 Concrete strain measurement identification system

The concrete strain measurements were taken at 47 locations on spans 4 and 5. These locations are shown in Figures 5.10 through 5.13. To simplify the discussion of the concrete strain measurements, the following identification system is used throughout this section:

| <u>Span number</u> | <u>Arch Location</u> | <u>Arch Side</u> | <u>Measurement Location</u> |
|--------------------|----------------------|------------------|-----------------------------|
| ↑                  | ↑                    | ↑                | ↑                           |
| 4                  | South (S)            | West (W)         | Abutment (AB)               |
| 5                  | North (N)            | East (E)         | Side Horizontal (SH)        |
|                    |                      |                  | Side Perpendicular (SP)     |
|                    |                      |                  | Bottom Low (BL)             |
|                    |                      |                  | Bottom High (BH)            |
|                    |                      |                  | Top Low (TL)                |
|                    |                      |                  | Top High (TH)               |

*Example: 4-S-E-TH*, represents the Top High measurement location, for the east side of the southern arch of span 4.

### 6.3.2 Concrete strain measurement data

There are two types of concrete strain graphs presented in this section. The first shows the change in concrete strain from 12/16/05 until 05/17/12, including data taken by both the FHWA and Auburn University. These plots also include a vertical bold line at 58.8 months, indicating the date of silane application.



The other types of graphs in this section show the change in concrete strain plots from 11/17/10 until 05/17/12, after silane application. These data were recorded by Auburn University.

In both types of concrete strain graphs, the concrete strains associated with temperature effects are shown using error bars. In warm weather the concrete expands, and in cold weather the concrete contracts. The maximum expansion or contraction that could have occurred due to temperature is calculated by:

- Expansion:  $+\Delta\varepsilon_{T,\max} = (T_{\max} - T) \cdot \alpha_t$
- Contraction:  $-\Delta\varepsilon_{T,\max} = (T - T_{\min}) \cdot \alpha_t$

Where:

- $T$  = Average 3-inch RH probe temperature observed
- $T_{\max}$  = Maximum Internal Concrete Temperature
- $T_{\min}$  = Minimum Internal Concrete Temperature
- $\alpha_t$  = Coefficient of Thermal Expansion

The following assumptions were made for the formulation of the error bars

- $\alpha_t = 6.95 \times 10^{-6} / ^\circ\text{F}$   
for concretes made with river gravel (Schindler et al. 2010)
- $T_{\max} = 100.8^\circ\text{F}$ , maximum 3-inch RH probe temperature observed
- $T_{\min} = 58.6^\circ\text{F}$ , minimum 3-inch RH probe temperature observed
- $58.6^\circ\text{F} \leq T \leq 100.8^\circ\text{F}$

An example of an error bar for a 70 °F day is shown in Figure 6.15. The total range of strain that temperature could cause is approximately  $293 \times 10^{-6}$  in./in.

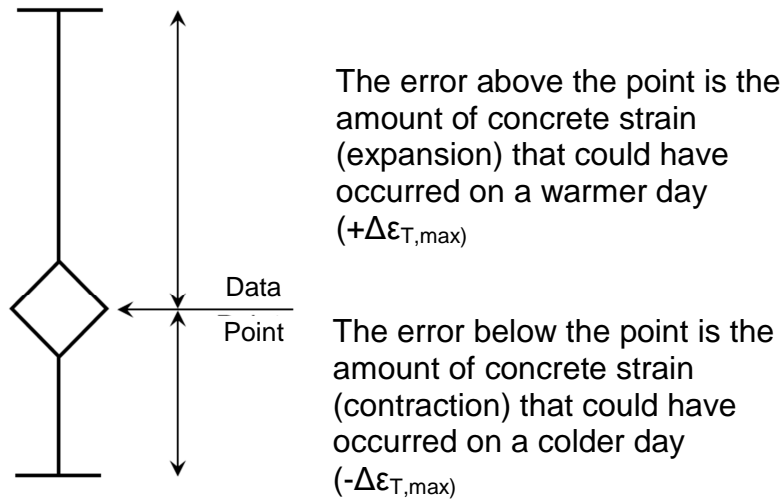


**Figure 6.15:** Temperature effect error bar for a 70 °F day

The expansion plots for spans 4 and 5, east and west are shown in Figures 6.16 through 6.25. For the concrete strain plots from 2005, the temperatures used for the error bars for the first two readings (collected by the FHWA) is the average ambient temperature from the Maxwell Air Force Base for the respective day. All collected data can be found in Appendix C.

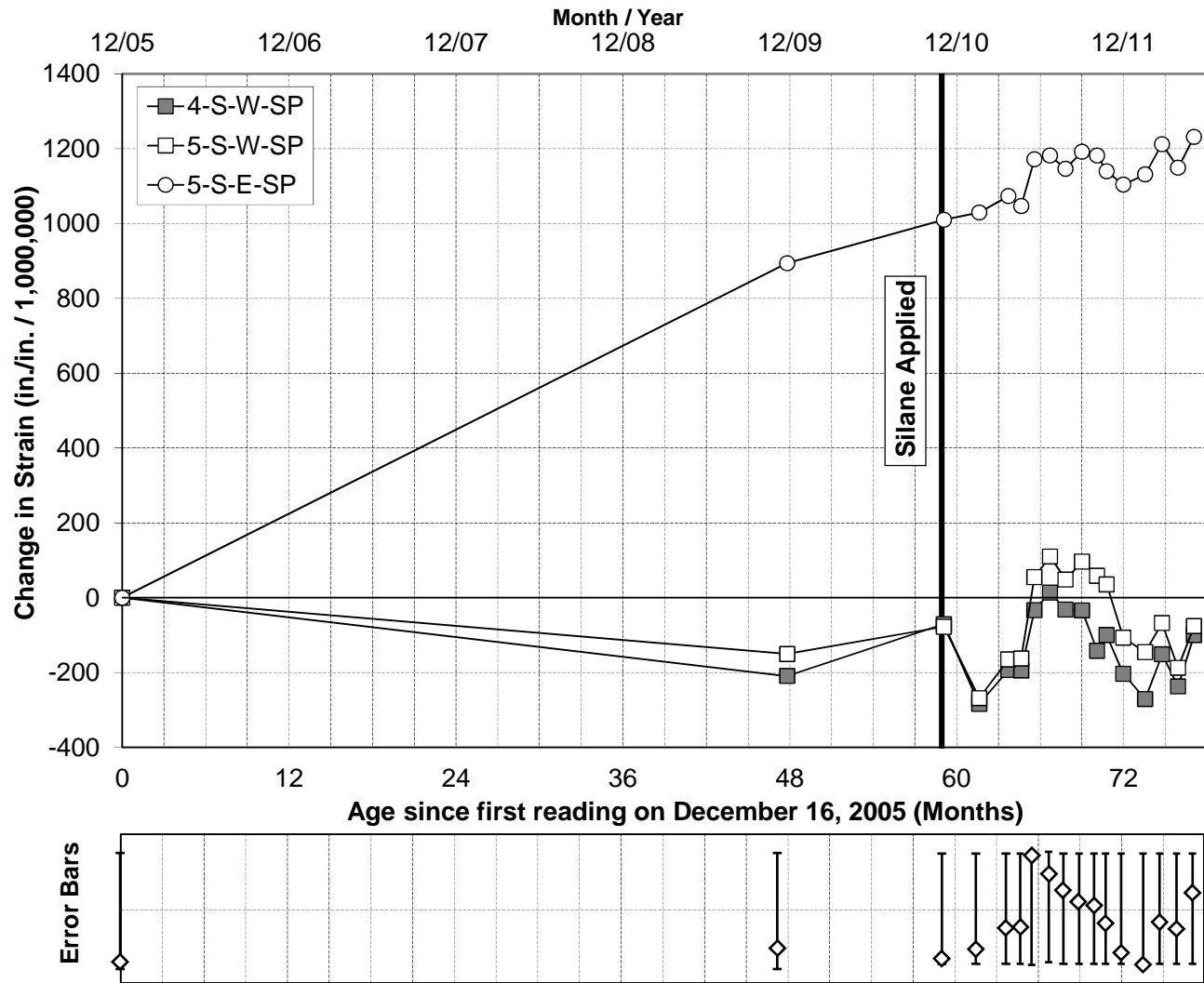


Figure 6.16: Change in concrete strain for Side Perpendicular since 2005

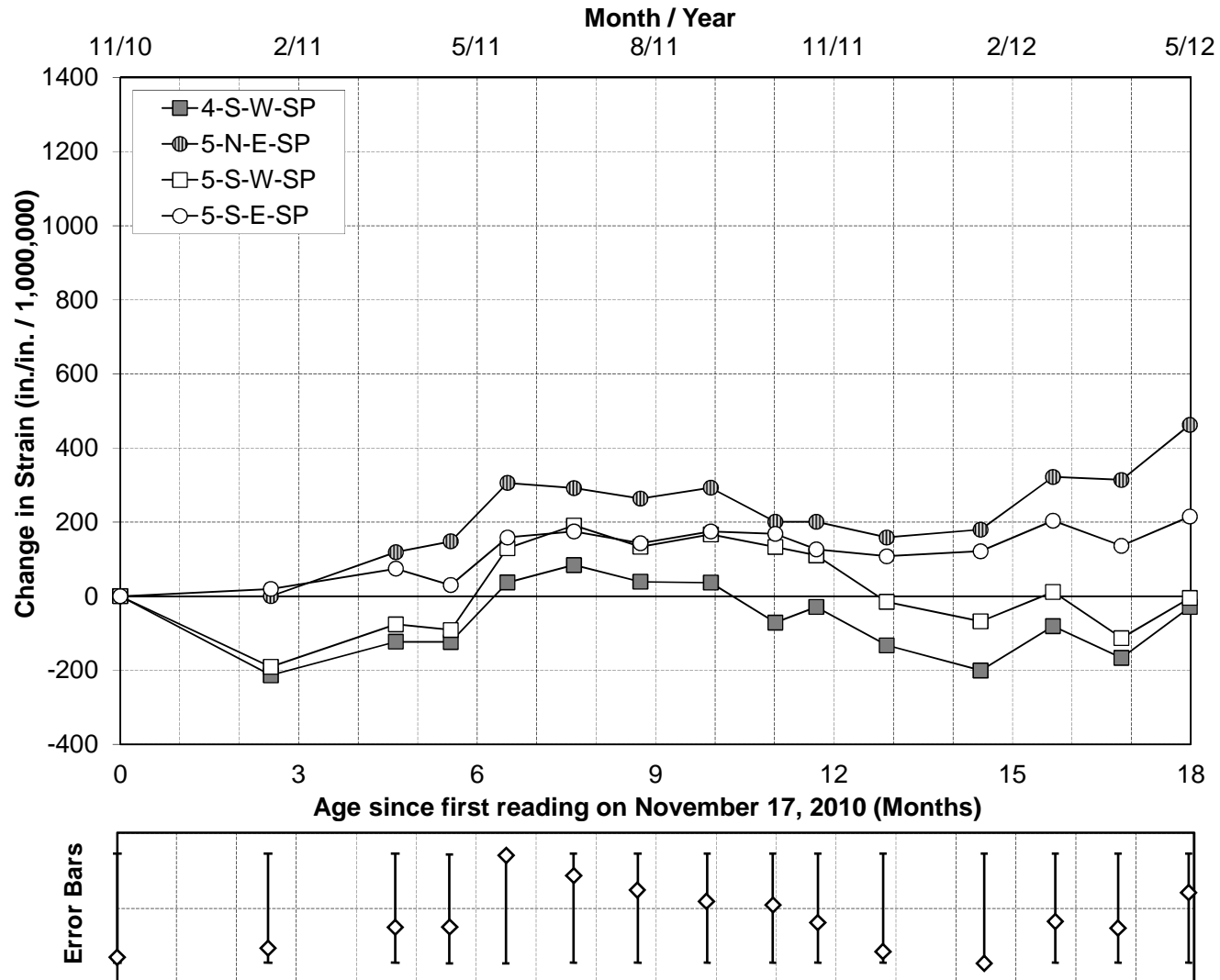


Figure 6.17: Change in concrete strain for Side Perpendicular since 11/2010

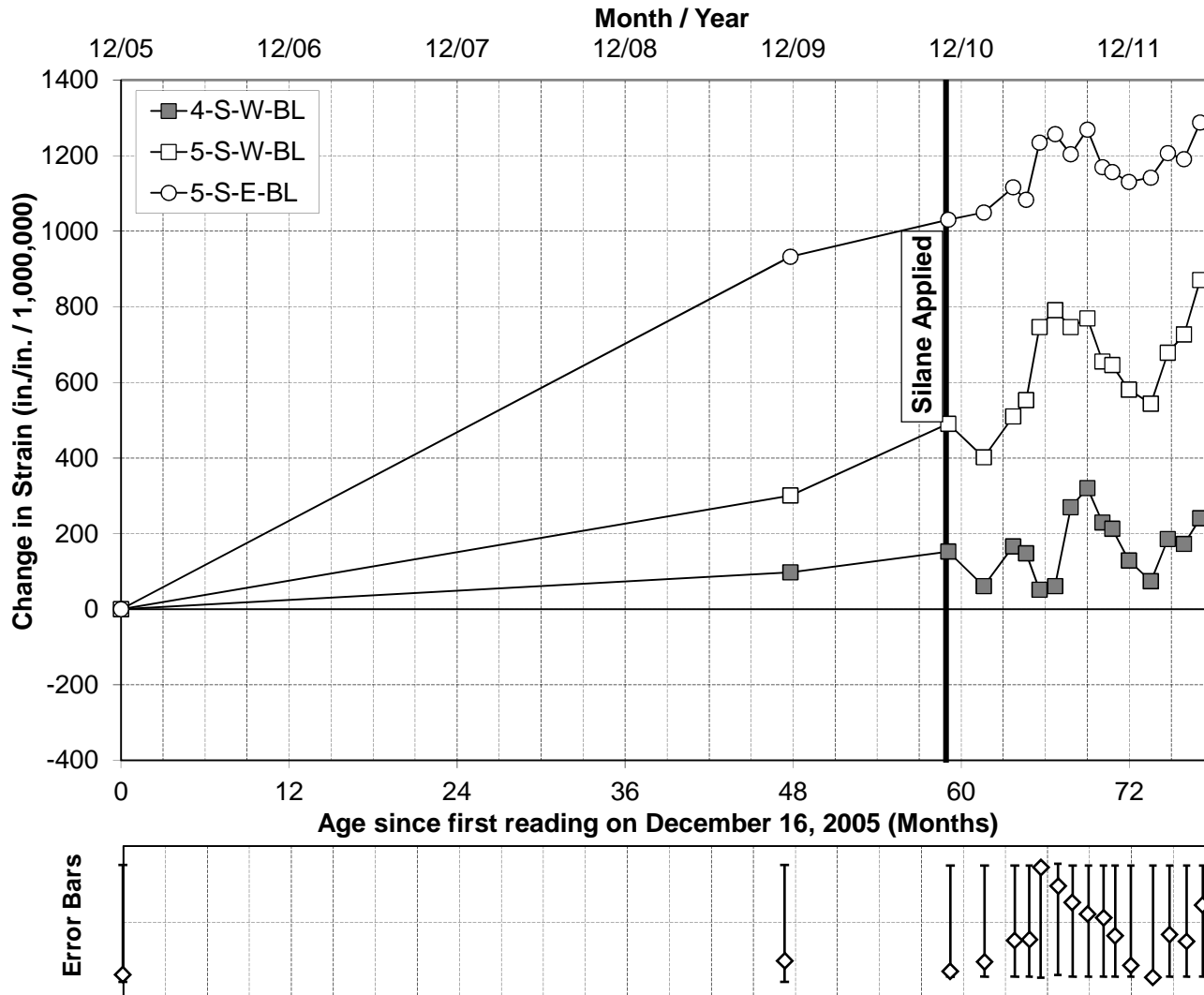


Figure 6.18: Change in concrete strain for Bottom Low since 2005

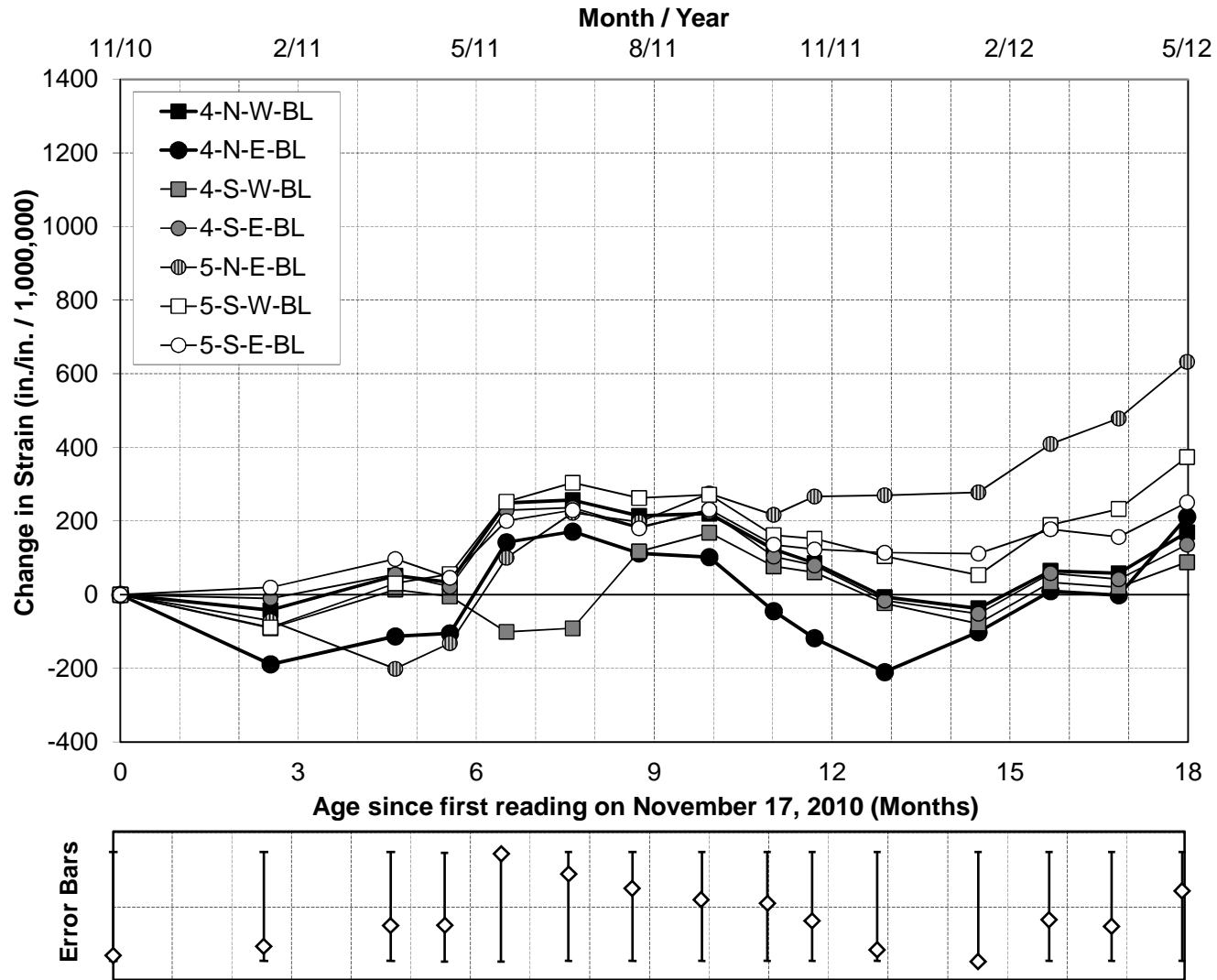


Figure 6.19: Change in concrete strain for Bottom Low since 11/2010

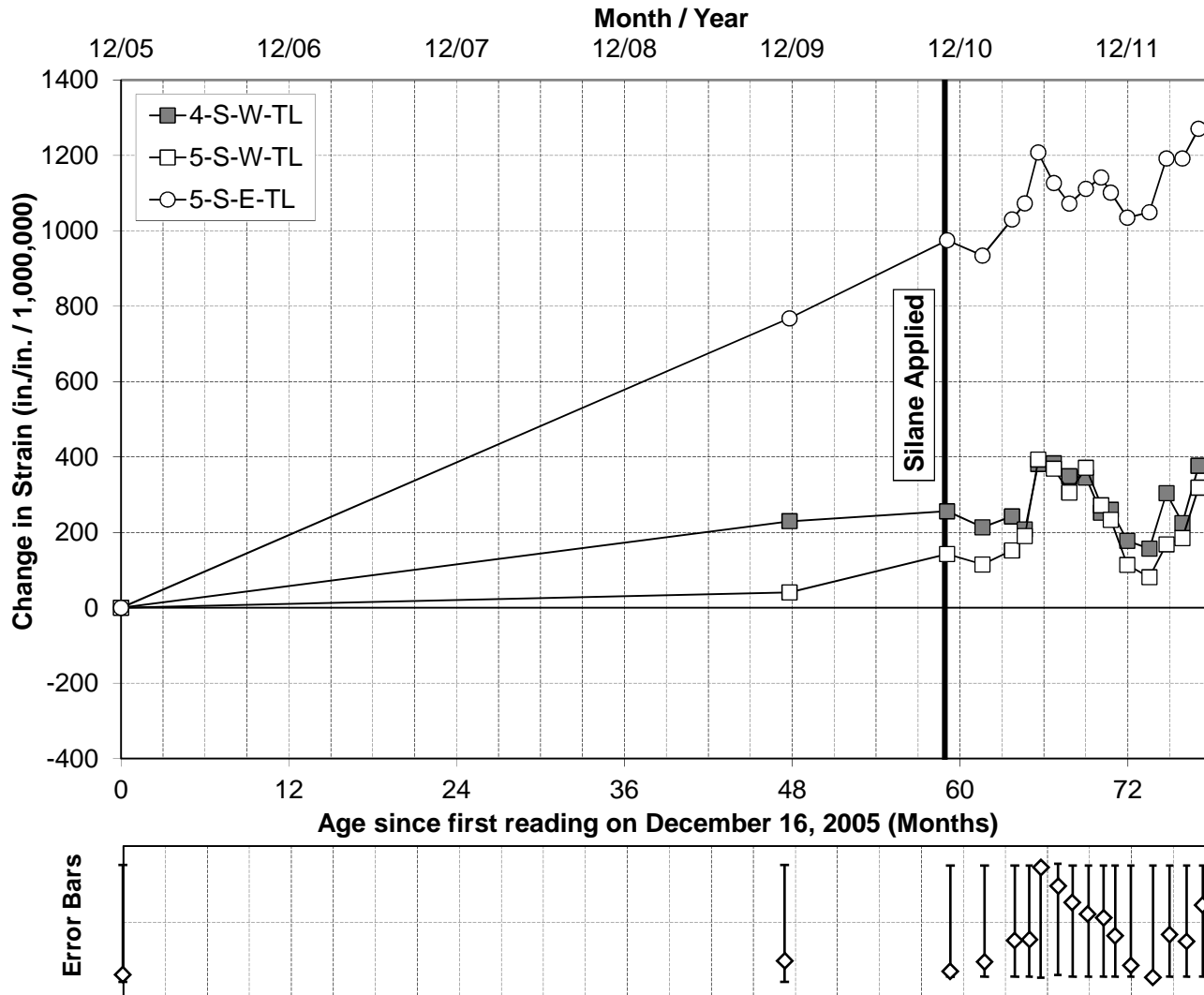


Figure 6.20: Change in concrete strain for Top Low since 2005

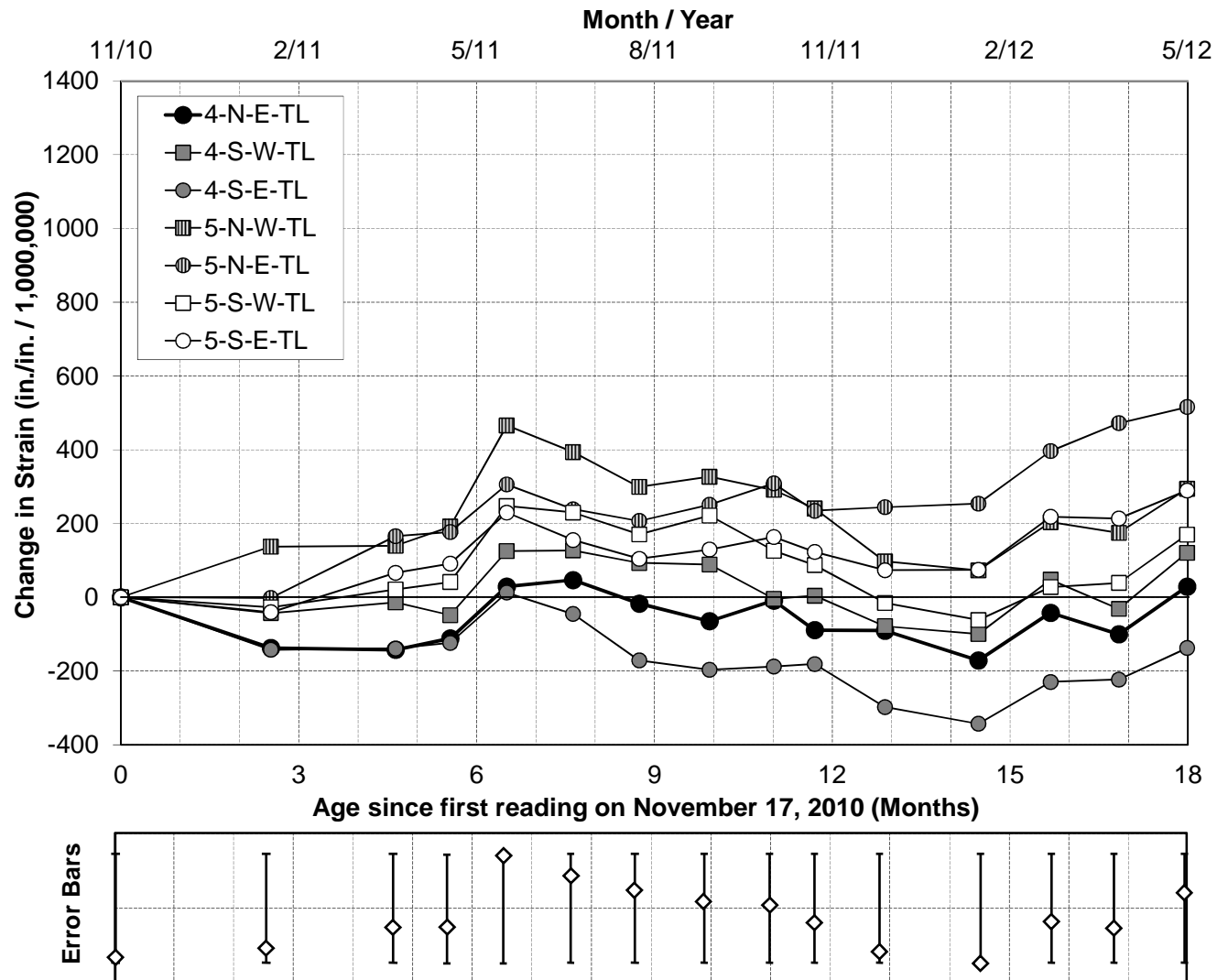


Figure 6.21: Change in concrete strain for Top Low since 11/2010



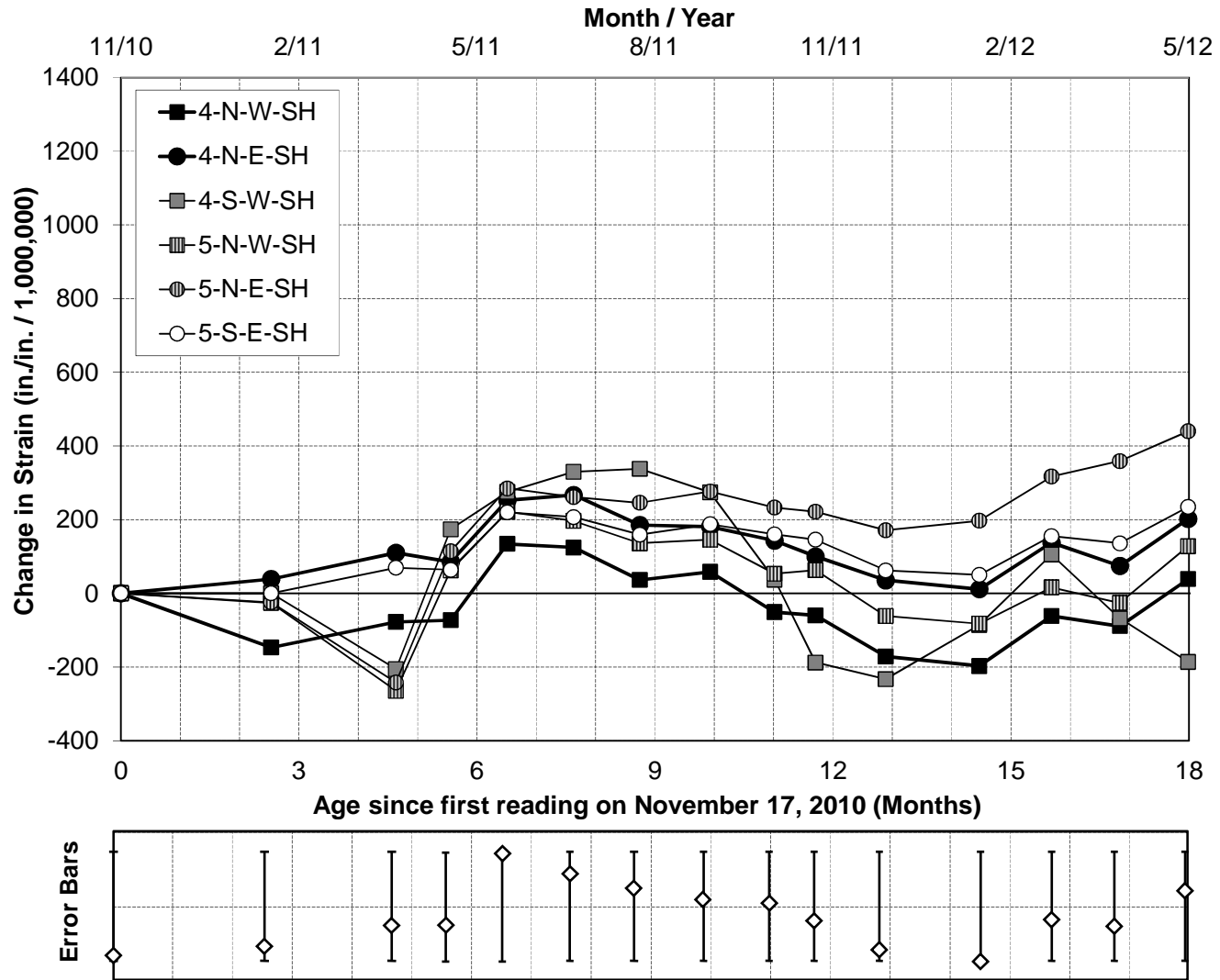


Figure 6.22: Change in concrete strain for Side Horizontal since 11/2010

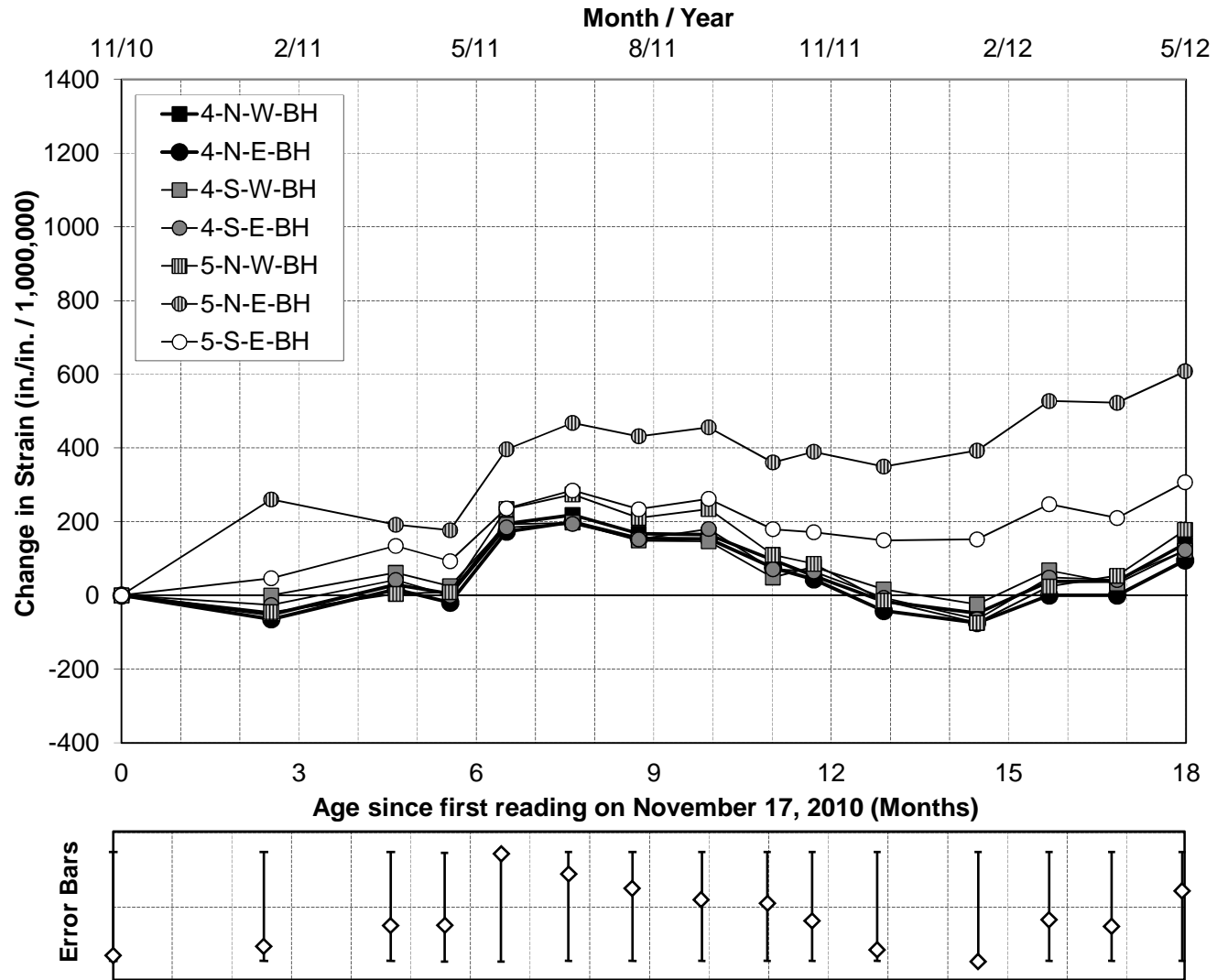


Figure 6.23: Change in concrete strain for Bottom High since 11/2010

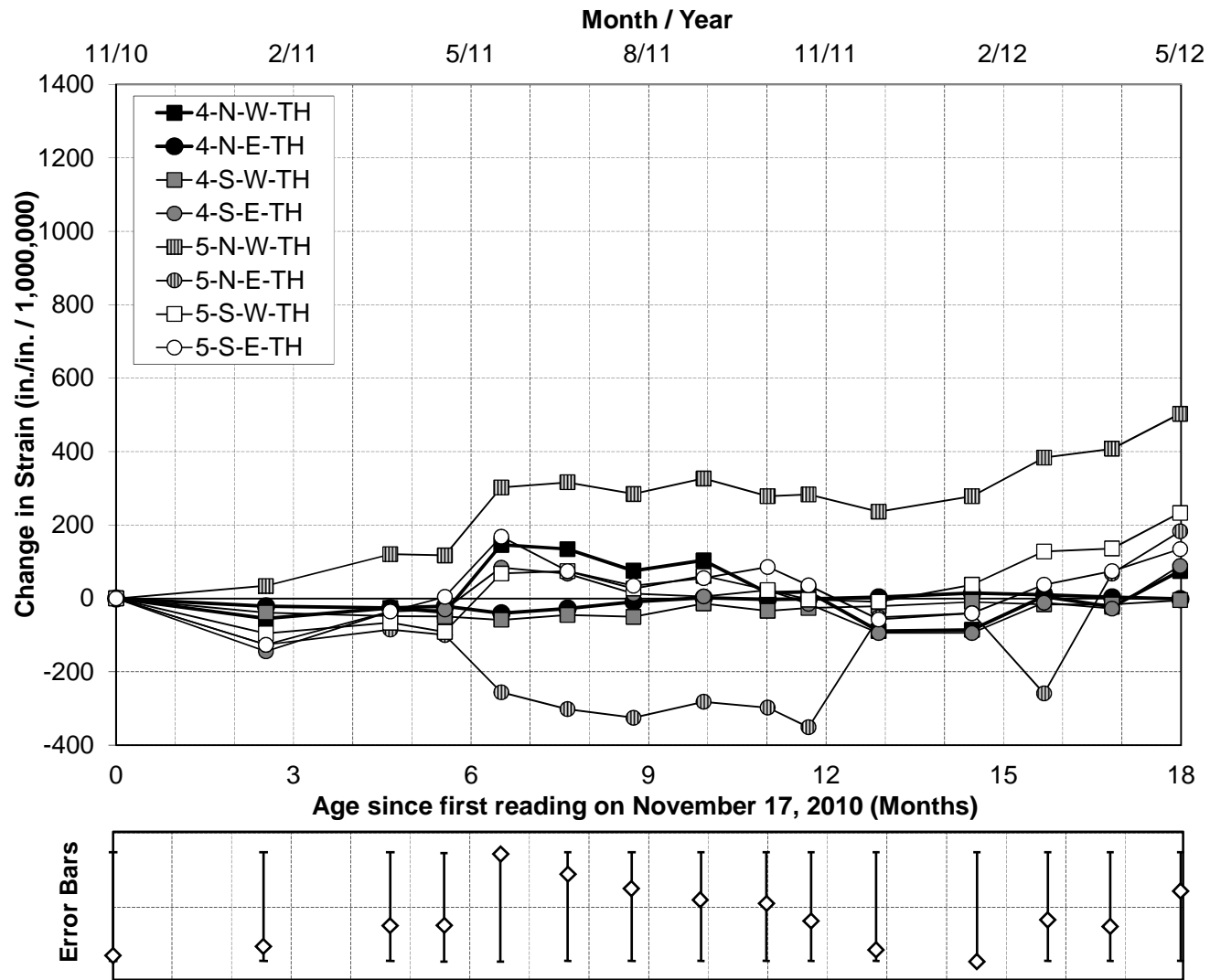
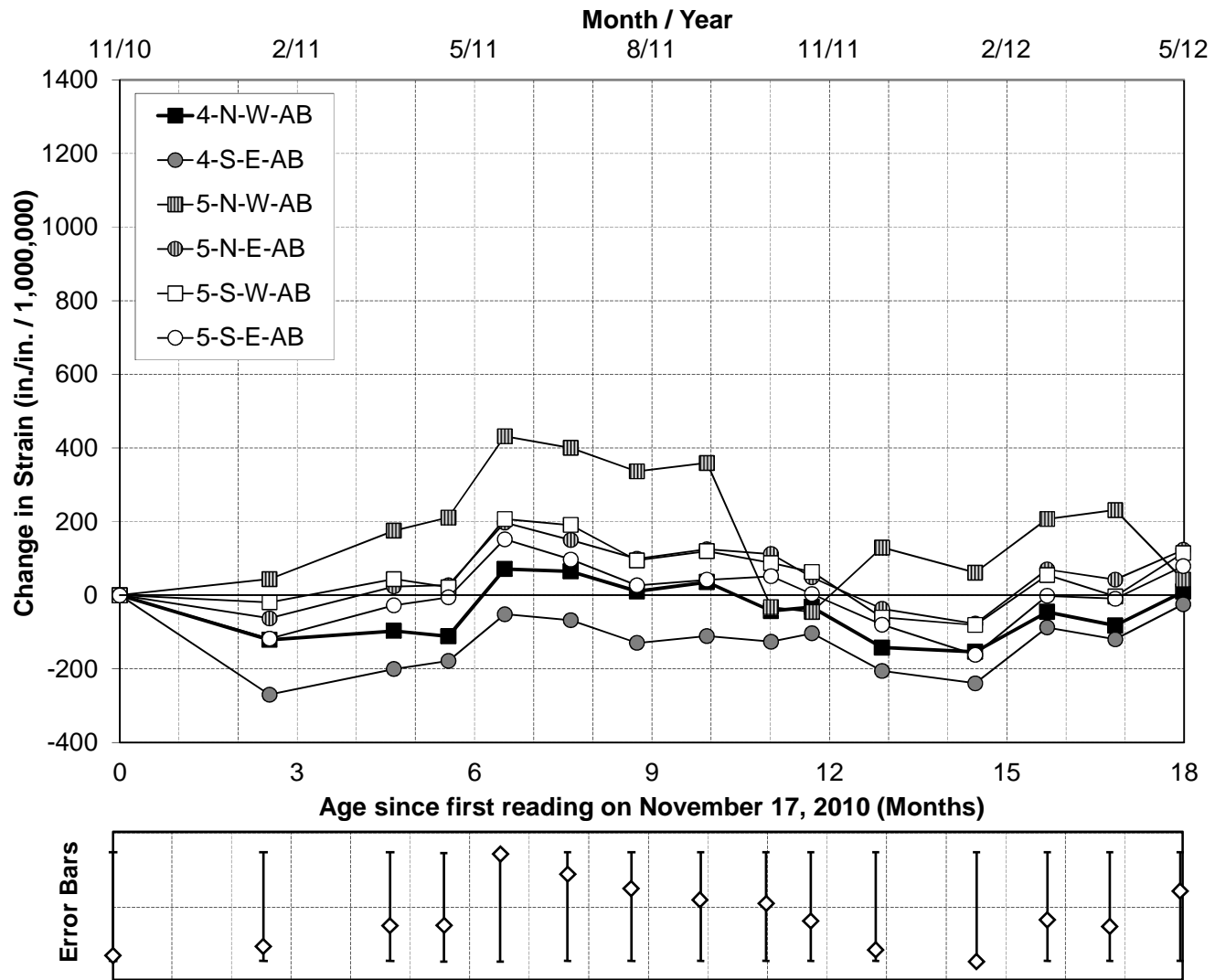


Figure 6.24: Change in concrete strain for Top High since 11/2010



**Figure 6.25:** Change in concrete strain for Abutment since 11/2010

The plot for SP since 2005 clearly shows that 5-S-E-SP has expanded over  $1,200 \times 10^{-6}$  in./in. since the first measurement in 2005, as shown in Figure 6.16. Since silane application, concrete strains have not exceeded the strains that temperature effects may have caused. 4-S-W-SP and 5-S-W-SP seem to only be experiencing strains that temperature effects may cause.

When the date of origin of the SP concrete strain plot is moved to 11/17/2010, the most prominent trend is that of 5-N-E-SP, which has expanded over  $400 \times 10^{-6}$  in./in., as shown in Figure 6.17. The change in concrete strains of 5-S-E-SP is less prominent in this plot, with an expansion of approximately  $200 \times 10^{-6}$  in./in., which could be mostly due to temperature effects. Locations 4-S-W-SP and 5-S-W-SP still only seem to be experiencing strains that temperature effects may cause.

The plot for BL since 2005 clearly shows that 5-S-E-BL has expanded over  $1,200 \times 10^{-6}$  in./in. since the first measurement in 2005, as shown in Figure 6.18. 5-S-W-BL also shows a large net expansion of over  $800 \times 10^{-6}$  in./in. since the first reading in 2005. Since silane application, 4-S-W-BL seems to be experiencing mainly strains that temperature effects may cause, with a slight net expansion of  $200 \times 10^{-6}$  in./in. over approximately 6.5 years. However, 5-S-W-BL shows an expansion of approximately  $400 \times 10^{-6}$  in./in., and therefore, could fall outside the boundaries of temperature effects.

When the date of origin of the BL expansion plot is moved to 11/17/2010, the most prominent trend is that of 5-N-E-BL, which has expanded over

$600 \times 10^{-6}$  in./in., as shown in Figure 6.19. 4-S-W-BL and 4-S-E-BL still only seem to be experiencing only strains that temperature effects may cause.

The plot for TL since 2005 clearly shows that 5-S-E-TL has expanded over  $1,200 \times 10^{-6}$  in./in. since the first measurement in 2005, as shown in Figure 6.20. However, since silane application, only 5-N-E-TL has concrete strains that exceed those that temperature effects may have caused. 4-S-W-TL and 4-S-W-TL seem to only be experiencing strains that temperature effects may cause, with a slight net expansion of approximately  $400 \times 10^{-6}$  in./in over 6.5 years.

When the date of origin of the TL concrete strain plot is moved to 11/17/2010, the most prominent trend is that of 5-N-E-TL, which has expanded over  $500 \times 10^{-6}$  in./in., as shown in Figure 6.21. 5-S-E-TL is less prominent in this plot with an expansion of approximately  $300 \times 10^{-6}$  in./in., which could be mostly due to temperature effects. 4-S-W-TL, 4-S-E-TL, 5-N-W-TL and 5-S-W-TL seem to be experiencing strains that temperature effects may cause.

The most prominent trend in the plot for SH is that of 5-N-E-SH, which has expanded over  $400 \times 10^{-6}$  in./in., as shown in Figure 6.22. The remaining measurement locations on this plot seem to be experiencing only strains that temperature effects may cause.

The most prominent trend in the plot for BH is that of 5-N-E-BH, which has expanded approximately  $600 \times 10^{-6}$  in./in., as shown in Figure 6.23. The remaining measurement locations on this plot seem to be experiencing only strains that temperature effects may cause.

The most prominent trend in the plot for TH is that of 5-N-W-TH, which has expanded over  $400 \times 10^{-6}$  in./in., as shown in Figure 6.24. 5-N-W-TH had a period between the 6<sup>th</sup> and 12<sup>th</sup> month where it experienced contractions of approximately  $300 \times 10^{-6}$  in./in., but then started expanding again. The remaining measurement locations on this plot seem to be experiencing only strains that temperature effects may cause.

The most prominent feature in the plot for AB is that of 5-N-W-AB, where in the period between the 6<sup>th</sup> and 10<sup>th</sup> month it experienced expansions of approximately  $400 \times 10^{-6}$  in./in., but then contracted as shown in Figure 6.25. The remaining measurement locations on this plot seem to be experiencing only strains that temperature effects may cause.

#### **6.3.2.1 Linear regression analysis of prominent trends**

For Figures 6.16 through 6.25, each of the prominent trends were fitted with a linear regression trend line with the y-intercepts set to zero, and the coefficients of determination ( $r^2$ ) were calculated. These prominent trends are summarized in Table 6.9 with their corresponding  $r^2$ -values, trend-line slopes, and figure numbers.

After examining the historical plots, shown in Figures 6.16, 6.18, and 6.20, one can determine a threshold slope above which continued expansion may be occurring. The average of the slope of the data collected since 2005 of 5-S-E-SP, 5-S-E-BL, 5-S-E-TL was found to be  $16.5 \times 10^{-6}$  in./in./month, this threshold will be used to identify areas exhibiting continued expansion.

Using this threshold slope, 6 measurement locations have slopes that would indicate continued expansions over the 18-month data collection period. They are 5-N-E-SP, 5-N-E-BL, 5-N-E-TL, 5-N-E-SH, 5-N-E-BH, 5-N-W-TH. All of these locations are located on arch 5-N, and only one is on the west side of the arch.

**Table 6.9:** Prominent trends in Figures 6.16 through 6.25, with corresponding  $r^2$  - values, trend line slopes, and figure numbers

| <b>Information for Prominent Trends within Concrete Strain Data</b> |                                     |  |                      |
|---|-------------------------------------|--|----------------------|
| <i>Measurement Location</i>   | <i>Coefficient of Determination</i> | <i>Trend Line Slope (<math>10^{-6}</math> in./in./month)</i> | <i>Figure Number</i> |
| 5-S-E-SP  | 0.9540                              | 16.5   | 6.16                 |
| 5-N-E-SP <sup>a</sup>   | 0.5200                              | 21.2   | 6.17                 |
| 5-S-E-SP  | 0.4979                              | 11.9   | 6.17                 |
| 5-S-E-BL  | 0.9316                              | 17.0   | 6.18                 |
| 5-S-W-BL  | 0.7339                              | 9.3  | 6.18                 |
| 5-N-E-BL <sup>a</sup>   | 0.6587                              | 24.1   | 6.19                 |
| 5-S-E-TL  | 0.9490                              | 16.0   | 6.20                 |
| 5-N-E-TL <sup>a</sup>   | 0.7922                              | 25.4   | 6.21                 |
| 5-S-E-TL  | 0.4897                              | 12.7   | 6.21                 |
| 5-N-E-SH <sup>a</sup>   | 0.5579                              | 24.0   | 6.22                 |
| 5-N-E-BH <sup>a</sup>   | 0.5465                              | 35.0   | 6.23                 |
| 5-N-W-TH <sup>a</sup>   | 0.7602                              | 25.7   | 6.24                 |

Notes: Gray cells indicate graphs with data from 2005  
<sup>a</sup> = locations with a trend line slope greater than  $16.5 \times 10^{-6}$  in./in./month



### 6.3.3 Concrete strain difference analysis

To further analyze the concrete strain data, a “concrete strain difference” analysis was performed. It can be assumed that, because arch 4-N did not receive the ASR mitigation procedure, and its concrete has shown very little sign of ASR-related distress, all of the concrete strains for arch 4-N, shown in Figures 6.16 through 6.26, were associated with temperature and moisture effects. Only dates since 11/2010 will be used, since arch 4-N was instrumented for the first time on this date. Therefore, for measurement locations on arches 4-S, 5-N, and 5-S that have similar locations on arch 4-N (ex. 5-N-W-TH and 4-N-W-TH), the difference of these two locations was taken to eliminate the concrete strains associated with temperature and moisture effects. This analysis assumes that the internal RH and concrete temperature of arch 4-S, 5-N, and 5-S is similar to that of arch 4-N. Thus far, the internal RH for all of the arches is similar; however, concrete temperature varies for each measurement location, even from the beginning of data collection to the end of data collection for a given survey date.

Linear regression trend lines were then fitted to these plots with their intercept set to zero. The coefficients of determination ( $r^2$ ) and slopes are presented in Tables 6.10 and 6.11, respectively.

Once again, a minimum  $r^2$  value of 0.5 was used to determine if the trend lines statistically significant. For all of the locations examined, 7 measurement locations showed statistical significance. These locations were 5-S-W-BL, 5-N-E-BL, 4-S-E-TL, 5-N-E-TL, 5-N-E-BH, 5-S-E-BH, and 5-N-W-TH, as shown

in Table 6.12. Of these locations, 4-S-E-TL was the only one with a negative slope, indicating potential contraction of the cross section.

**Table 6.10:** Coefficients of determination for linear regression trend lines for the concrete strain difference analyses

| <b>Coefficients of determination (<math>r^2</math>)</b> |                                      |                    |                    |
|---|--------------------------------------|--------------------|--------------------|
| <i>Measurement Location</i>                             | <i>Span Number and Arch Location</i> |                    |                    |
|   | <i>4-S</i>                           | <i>5-N</i>         | <i>5-S</i>         |
| <i>W-BL</i>   | -0.223                               | -                  | 0.695 <sup>a</sup> |
| <i>E-BL</i>   | -0.653                               | 0.674 <sup>a</sup> | -0.287             |
| <i>E-TL</i>   | 0.678 <sup>a</sup>                   | 0.754 <sup>a</sup> | 0.448              |
| <i>W-SH</i>   | -0.146                               | -                  | 0.078              |
| <i>E-SH</i>   | -                                    | 0.385              | 0.151              |
| <i>W-BH</i>   | -0.033                               | -0.062             | -                  |
| <i>E-BH</i>   | 0.103                                | 0.764 <sup>a</sup> | 0.705 <sup>a</sup> |
| <i>W-TH</i>   | -0.137                               | 0.983 <sup>a</sup> | 0.271              |
| <i>E-TH</i>   | 0.000                                | -0.294             | 0.047              |
| <i>W-AB</i>   | -                                    | -0.587             | -1.609             |

Notes: <sup>a</sup> =  $r^2 \geq 0.5$   
 A dash represents a measurement location that does not have a corresponding measurement location on 4-N, or a measurement location that does not exist

The statistically significant trends are shown in Figure 6.26 for the BL measurement location, in Figure 6.27 for the TL measurement location, in Figure 6.28 for the BH measurement location, and in Figure 6.29 for the TH measurement location. The remainder of the concrete strain difference plots can be found in Appendix C.

**Table 6.11:** Slopes of the trend lines for the concrete strain difference analyses

| Slope of trend lines ( $10^{-6}$ in./in./month) |                               |                   |                   |
|---|-------------------------------|-------------------|-------------------|
| Measurement Location                            | Span Number and Arch Location |                   |                   |
|   | 4-S                           | 5-N               | 5-S               |
| W-BL  | -6.1                          | -                 | 7.5 <sup>a</sup>  |
| E-BL  | 6.7                           | 23.8 <sup>a</sup> | 12.7              |
| E-TL  | -10.8 <sup>a</sup>            | 30.1 <sup>a</sup> | 17.3              |
| W-SH  | 4.2                           | -                 | 6.9               |
| E-SH  | -                             | 10.3              | 1.3               |
| W-BH  | 0.2                           | 1.4               | -                 |
| E-BH  | 1.8                           | 31.3 <sup>a</sup> | 13.1 <sup>a</sup> |
| W-TH  | -3.2                          | 24.5 <sup>a</sup> | 4.2               |
| E-TH  | 0.3                           | -10.3             | 3.7               |
| W-AB  | -                             | 16.9              | 8.0               |

Notes: <sup>a</sup> =  $r^2 \geq 0.5$   
 A dash represents a measurement location that does not have a corresponding measurement location on 4-N, or a measurement location that does not exist

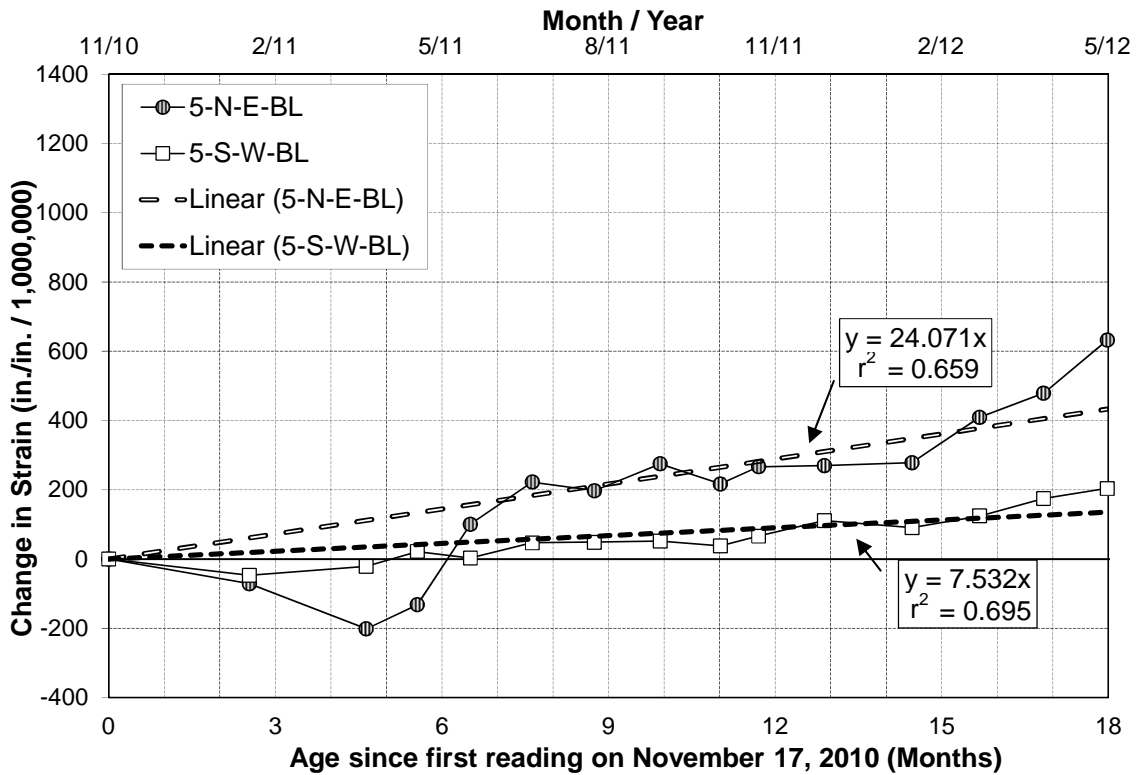


**Figure 6.26:** Concrete strain difference plot for BL measurement location

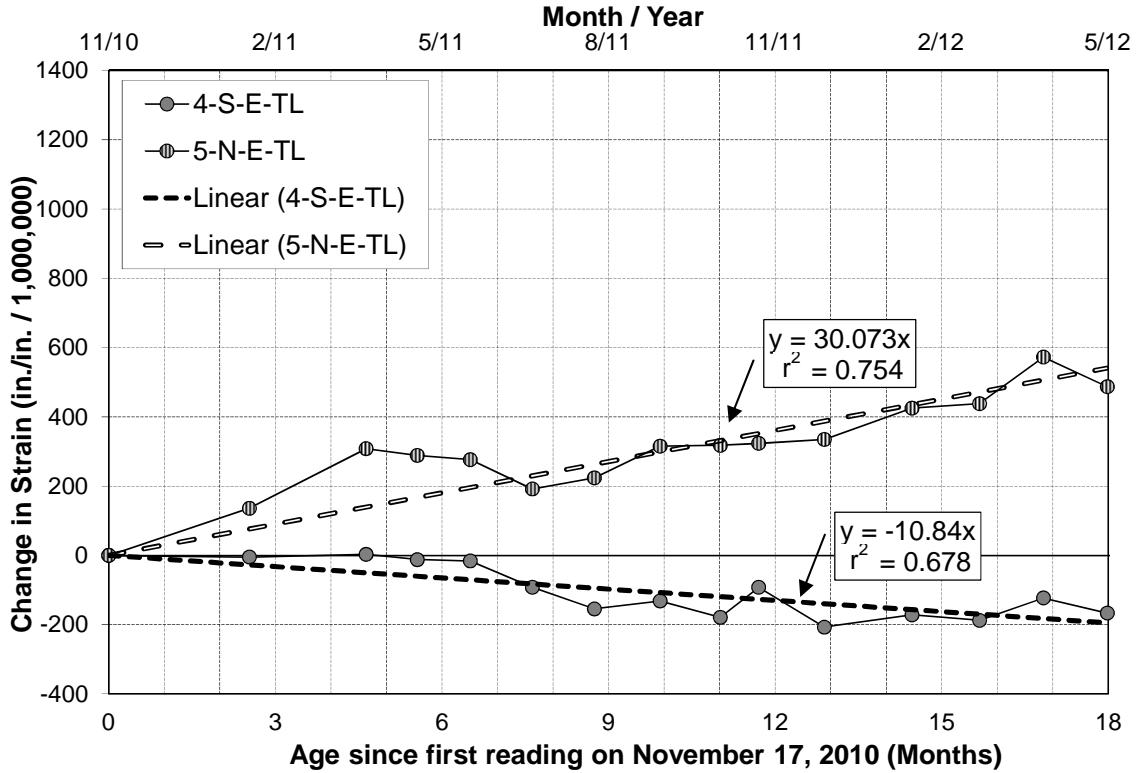


Figure 6.27: Concrete strain difference plot for TL measurement location

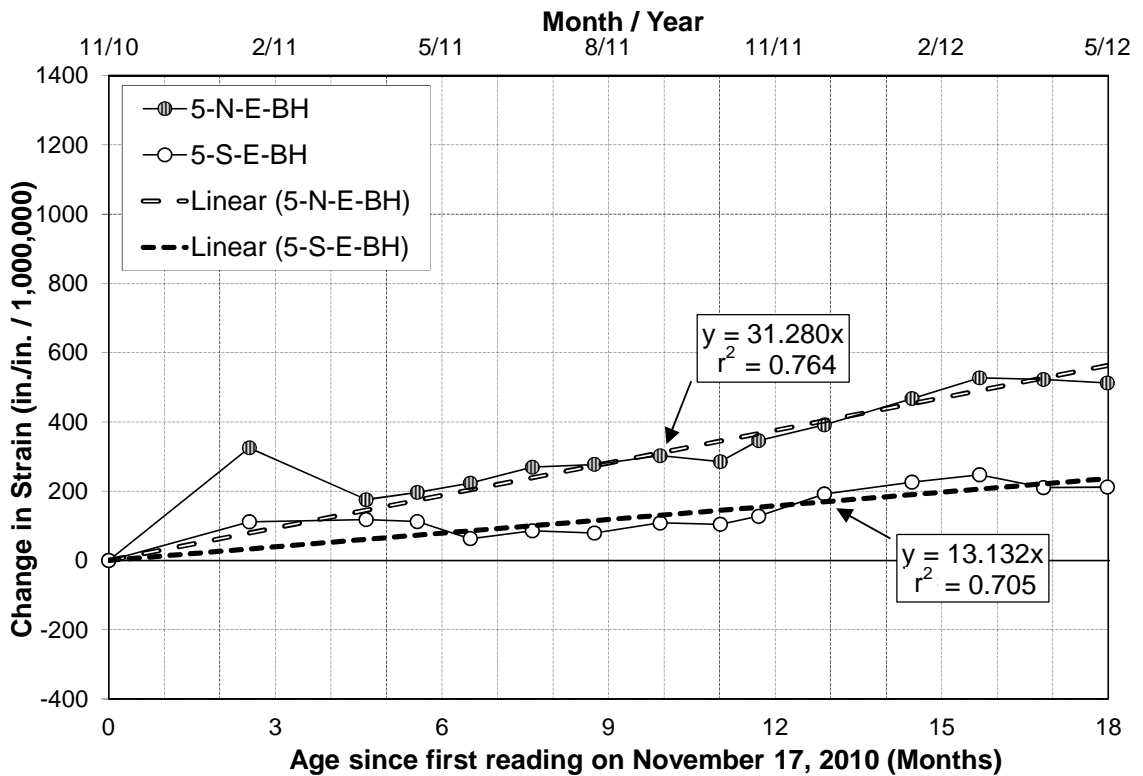
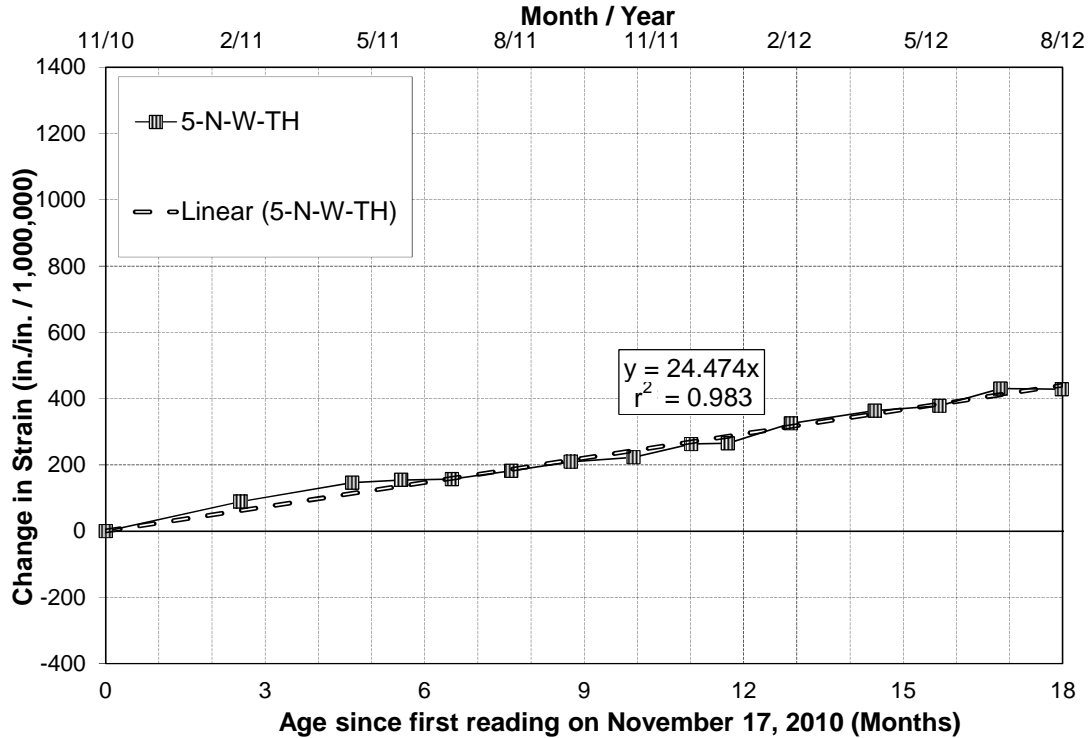


Figure 6.28: Concrete strain difference plot for BH measurement location



**Figure 6.29:** Concrete strain difference plot for TH measurement location

The prevailing trend in Figures 6.26 through 6.29 is that the change in concrete strain for 5-N-E-BL, 5-N-E-TL, 5-N-E-BH, and 5-N-W-TH all show expansions greater than  $400 \times 10^{-6}$  in./in. relative to the respective locations on span 4-N. From the crack mapping survey, the concrete at 5-N-E-BL, 5-N-E-BH, and 5-N-E-TH had crack widths ranging from less than 0.01 to 0.10 inches. The concrete at 5-N-E-TL has crack widths ranging from less than 0.01 to 0.04 inches. Therefore, all of the measurements that show expansion already have moderate to severe cracking due to ASR. The relative expansions indicate that the ASR mitigation procedure is currently not effective at these locations.

Both locations for span 5, 5-S-W-BL and 5-S-E-BH, showed moderate levels of expansion as they had changes in concrete strain of at least  $200 \times 10^{-6}$  in./in. greater than their respective locations on span 4-N, as shown in

Figures 6.26 and 6.28. The relative expansions indicate that the ASR mitigation procedure is currently not effective at these locations.

For 4-S-E-TL there was an decrease in concrete strain of approximately  $200 \times 10^{-6}$  in./in. when compared to the corresponding location on span 4-N, as shown in Figure 6.27. The reason for this apparent contraction is unknown.

#### **6.3.3.1 Concrete strain difference plots with $r^2 < 0.5$**

Also worthy of note are the trends for 4-S-W-BL, 5-S-E-TL, 5-N-E-SH, 5-S-E-SH, 4-S-W-BH, 5-N-W-BH, and 4-S-E-BH that have  $r^2$  values of less than 0.5, shown in Figures 6.30 through 6.33. Despite the low  $r^2$  values, these measurement locations have obvious visual trends.

The concrete strain difference plot for 4-S-W-BL is shown in Figure 6.30. For 4-S-W-BL it can be seen that, other than the 7.6 and 8.7 month surveys, this measurement location experiences little to no movement, which would be expected for arch 4-S.

For 5-S-E-TL, a slight upward trend resulting in a net expansion of approximately  $250 \times 10^{-6}$  in./in. relative to arch 4-N is shown in Figure 6.31.

The concrete strain difference plot for 5-N-E-SH and 5-S-E-SH is shown in Figure 6.32. For 5-N-E-SH, a slight upward trend resulting in a net expansion of approximately  $200 \times 10^{-6}$  in./in. relative to arch 4-N is seen. The measurement location 5-S-E-SH experienced little to no movement relative to arch 4-N.

The concrete strain difference plot for 4-S-W-BH, 5-N-W-BH, and 4-S-E-BH is shown in Figure 6.33. All of these measurement locations experienced little to no movement relative to arch 4-N. It should be noted that concrete at all of these locations is of good quality.

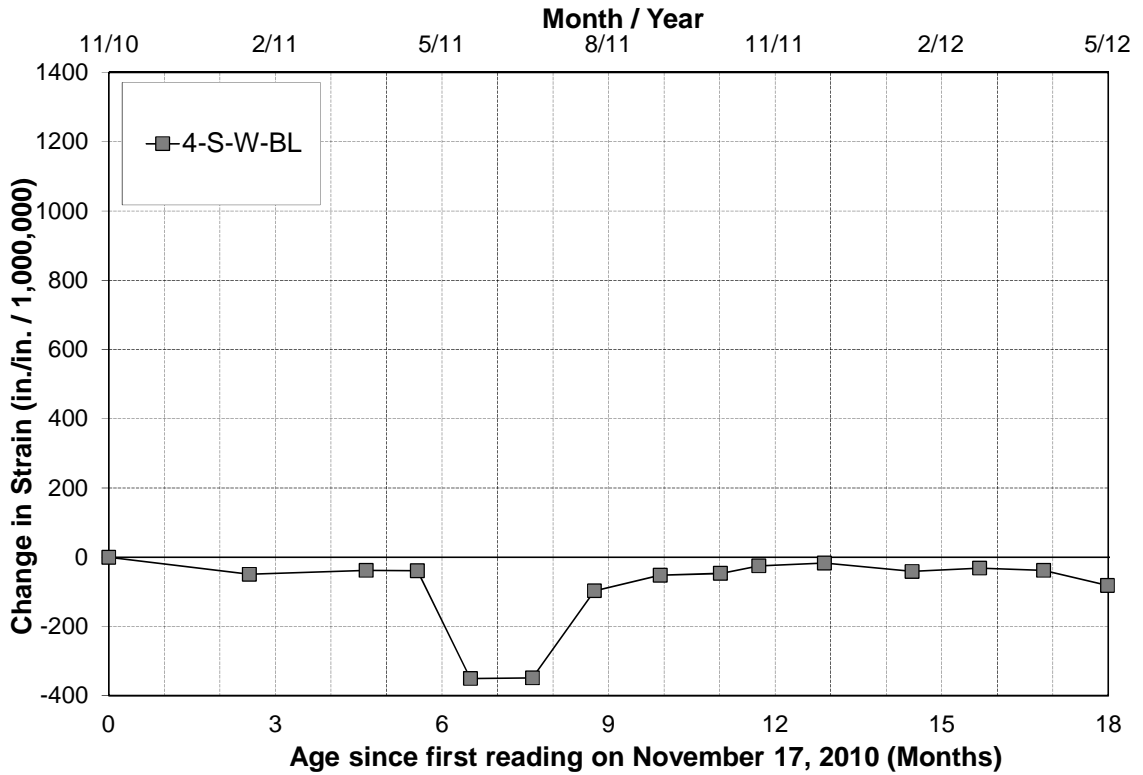


Figure 6.30: Concrete strain difference plot for BL, with  $r^2 < 0.5$

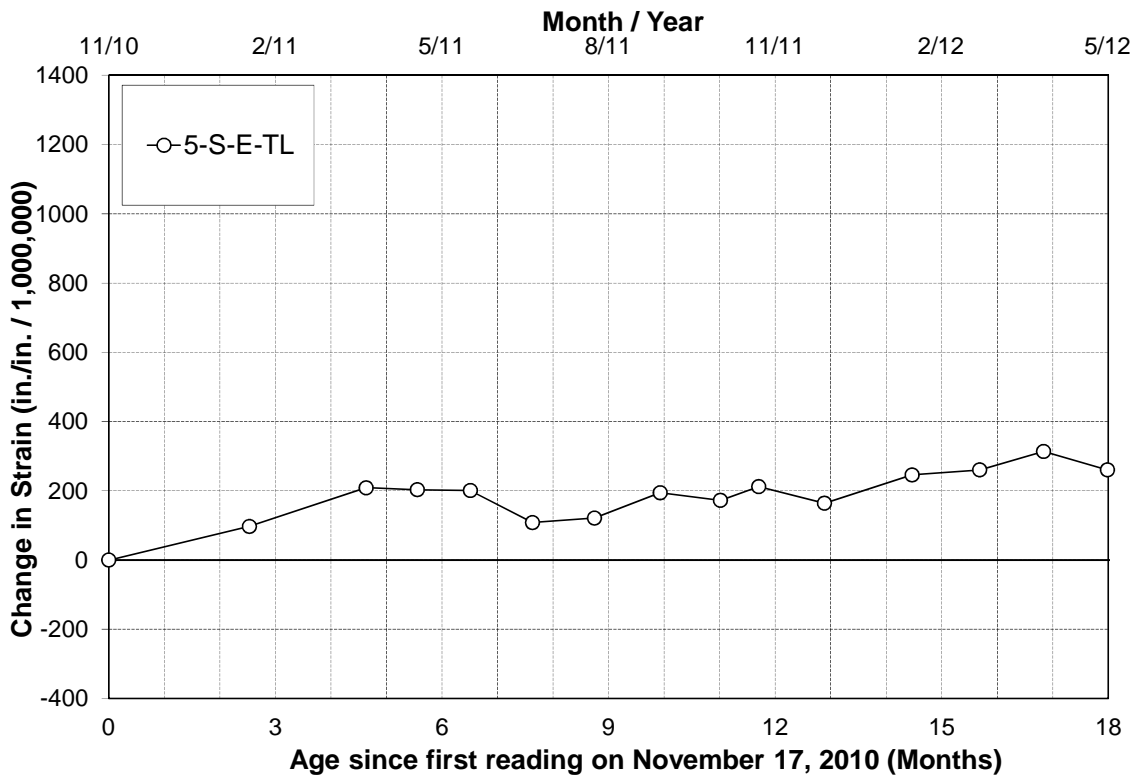


Figure 6.31: Concrete strain difference plot for TL, with  $r^2 < 0.5$

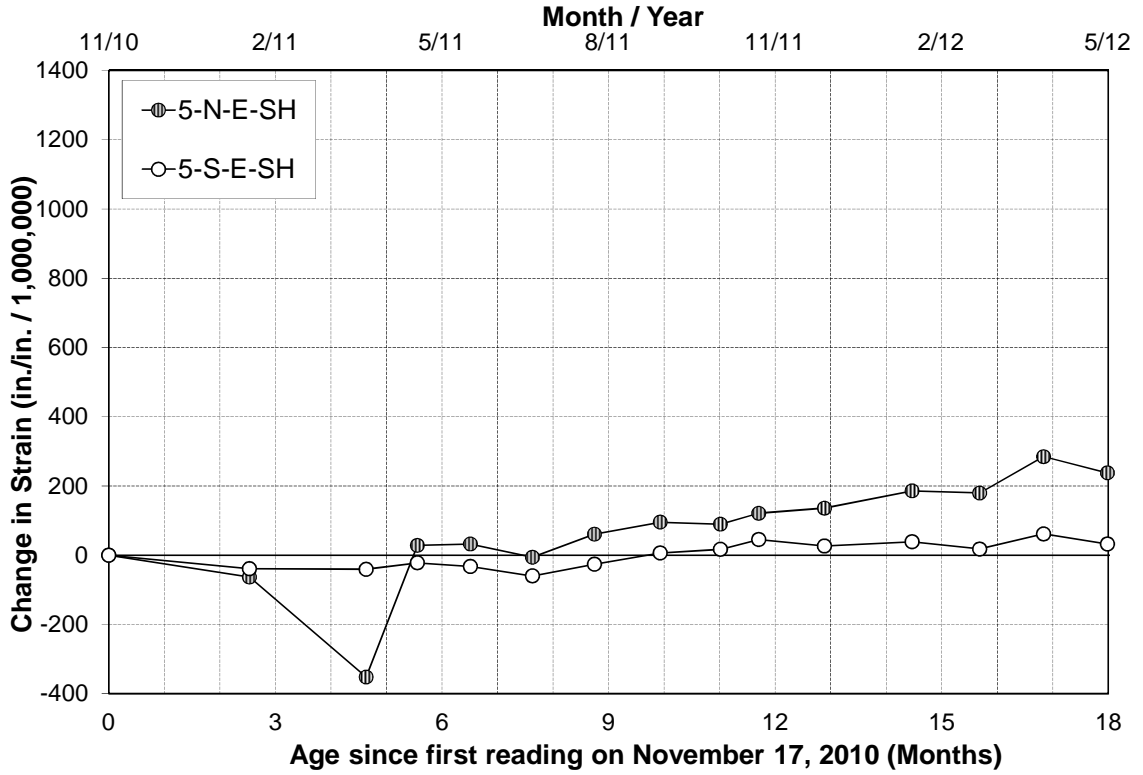


Figure 6.32: Concrete strain difference plot for SH, with  $r^2 < 0.5$

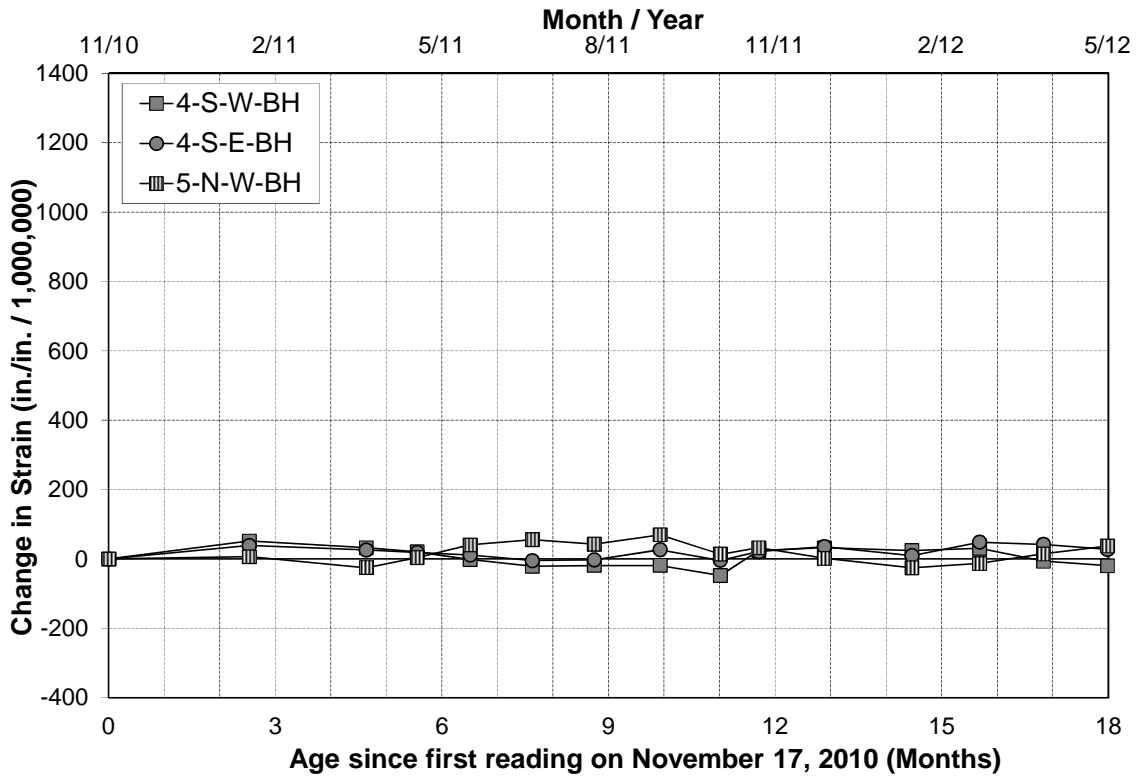


Figure 6.33: Concrete strain difference plot for BH, with  $r^2 < 0.5$



### 6.3.4 Concrete strain measurement summary

To summarize all of the concrete strain data, trends, and analyses, the slopes of the trend lines will be used as a measure of expansion. The threshold slope of  $16.5 \times 10^{-6}$  in./in./month, defined in section 6.3.2.1, will be used in this section. The slopes of the prominent trends in the concrete strain plots for the data only and difference analysis with  $r^2 \geq 0.5$ , for the 18-month survey period, are summarized in Table 6.12.

**Table 6.12:** Slopes ( $10^{-6}$  in./in./month) of the prominent trends for all concrete strain data and analyses

| <b>Slopes (<math>10^{-6}</math> in./in./month) of Trend Lines for Prominent Trends</b> |                                     |                            |
|--|-------------------------------------|----------------------------|
| <i>Measurement Location</i>  | <i>Type of Concrete Strain Plot</i> |                            |
|  | <i>Data Only</i>                    | <i>Difference Analysis</i> |
| <i>5-N-W-TH</i>  | 25.7 <sup>a</sup>                   | 24.5 <sup>a</sup>          |
| <i>5-N-E-SP</i>  | 21.2 <sup>a</sup>                   | *                          |
| <i>5-N-E-BL</i>  | 24.1 <sup>a</sup>                   | 23.8 <sup>a</sup>          |
| <i>5-N-E-TL</i>  | 25.4 <sup>a</sup>                   | 30.1 <sup>a</sup>          |
| <i>5-N-E-SH</i>  | 24.0 <sup>a</sup>                   | *                          |
| <i>5-N-E-BH</i>  | 35.0 <sup>a</sup>                   | 31.3 <sup>a</sup>          |
| <i>5-S-W-BL</i>  | *                                   | 7.5                        |
| <i>5-S-E-BH</i>  | *                                   | 13.1                       |
| <i>4-S-E-TL</i>  | *                                   | -10.8                      |

Notes:        - \* =  $r^2 < 0.5$   
                   - a = locations with a trend line slope greater than  $16.5 \times 10^{-6}$  in./in./month

From Table 6.12 it can be seen that arch 5-N experienced continued expansion over the 18-month survey period. Less significant expansion was measured in arch 5-S, and arch 4-S experienced little to no expansion. Since

arch 4-S is not affected by ASR, this was to be expected. Arch 5-S is severely distressed, so it is surprising that continued expansion is not measured at some of its locations. However, in terms of the ASR mitigation procedure, it can be said with some certainty that it is not effective for locations 5-N-W-TH, 5-N-E-SP, 5-N-E-BL, 5-N-E-TL, 5-N-E-SH, 5-N-E-BH, 5-S-W-BL, 5-S-E-BH, 5-S-E-TL. Therefore, locations that were already severely affected by ASR do not exhibit strains indicating slowing of expansion due to the implemented ASR mitigation procedure.

#### **6.4 Correlations between RH and concrete strain trends**

A summary of the RH trends versus the trends seen at the respective concrete strain measurement locations is shown in Table 6.13. To try and account for temperature effects, the slopes and  $r^2$  values used in Table 6.13 are from the concrete strain difference analysis.

RH measurement locations 5-N-ET and 5-S-WT indicate that the ASR mitigation procedure may be effective; however, both of these locations did not reach the 80 % RH threshold. These two RH measurement locations correspond with the concrete strain measurement locations 5-N-E-TH and 5-S-W-TH respectively. The  $r^2$  values of the concrete strain difference analysis for both of these concrete strain locations did not exceed 0.5.

**Table 6.13:** RH trends versus concrete strain trends at various locations

| <b>RH Trends versus Concrete Strain Trends</b> |  |   |  |  |
|--|--|---|--|--|
| <i>RH Location</i>                             | <i>RH Trend Seen</i>   | <i>Concrete strain Measurement Location</i> | <i>Slope of concrete strain difference trend</i> | <i>R<sup>2</sup> of concrete strain difference trend</i> |
| 5-N-ET-AVG                                     | Negative trend converging from arch 4-N, ASR mitigation procedure may be effective       | 5-N-E-TH                                    | -10.2  | -0.2940  |
| 5-S-WT-3"                                      |  | 5-S-W-TH                                    | 4.2  | 0.2711   |
| 5-N-WB-AVG                                     | RH difference plots with a positive slope, ASR mitigation procedure may not be effective | 5-N-W-BH                                    | 1.41   | -0.0620  |
| 5-N-EB-AVG                                     |  | 5-N-E-BH                                    | 31.3   | 0.7638   |
| 5-S-EB-AVG                                     |  | 5-S-E-BH                                    | 13.1   | 0.7049   |

Although the trend line for 5-N-E-TH had a slope of -10.2 when the y-intercept was set to zero, as shown in Table 6.13, the observation can be made that after the initial contraction, at 16.8 months 5-N-E-TH started to expand, as shown in Figure 6.34. More time is needed to determine if the expansion that has been shown over the last two months will continue.

5-S-W-TH showed no expansion for the first year after the ASR mitigation procedure was applied, but then started expanding slightly at 12.9 months, as shown in Figure 6.34. The trend line for 5-S-W-TH had a slope of 4.2 when the y-intercept was set to zero, as shown in Table 6.13. Therefore, the ASR mitigation procedure seemed to not be effective for the first 18 months after its application. More time is needed to determine if the expansion that has been shown over the last six months will continue.

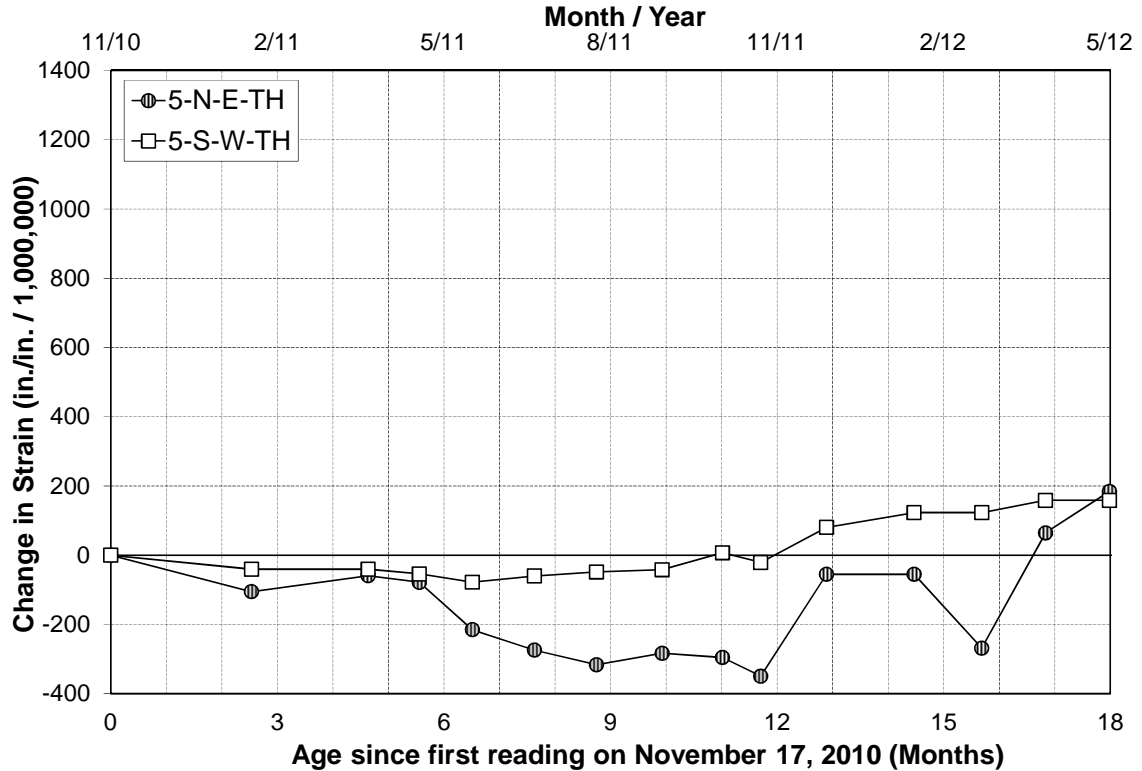


**Figure 6.34:** Concrete strain difference for TH measurement locations for span 5

Conversely, the RH difference analysis for measurement locations 5-N-WB-AVG, 5-N-EB-AVG, and 5-S-EB-AVG displayed a positive slope, indicating the ASR mitigation procedure may not be effective at these locations. These three RH measurement locations correspond with the concrete strain measurement locations 5-N-W-BH, 5-N-E-BH, and 5-S-E-BH respectively. The concrete strain difference plot for these concrete strain locations is shown in Figure 6.35.

For 5-N-W-BH, the slope of the concrete strain difference trend line was 1.41, and although its  $r^2$ -value was less than 0.1, it experienced little to no expansion over the 18-month data collection period, as shown in Figure 6.35.

Recall that the concrete at 5-N-W-BH is of very good quality, and the RH readings here were all below the 80 % threshold.

For 5-N-E-BH, the slope of the concrete strain difference trend line was 31.3, indicating continued expansion over the 18-month data collection period, as shown in Figure 6.35. This confirms that the ASR mitigation procedure is not yet effective at this location.

For 5-S-E-BH, the slope of the concrete strain difference trend line was 13.1, and its  $r^2$ -value was above 0.5, indicating some additional expansion over the 18-month data collection period, as shown in Figure 6.35. This confirms that the ASR mitigation procedure is not yet effective at this location.

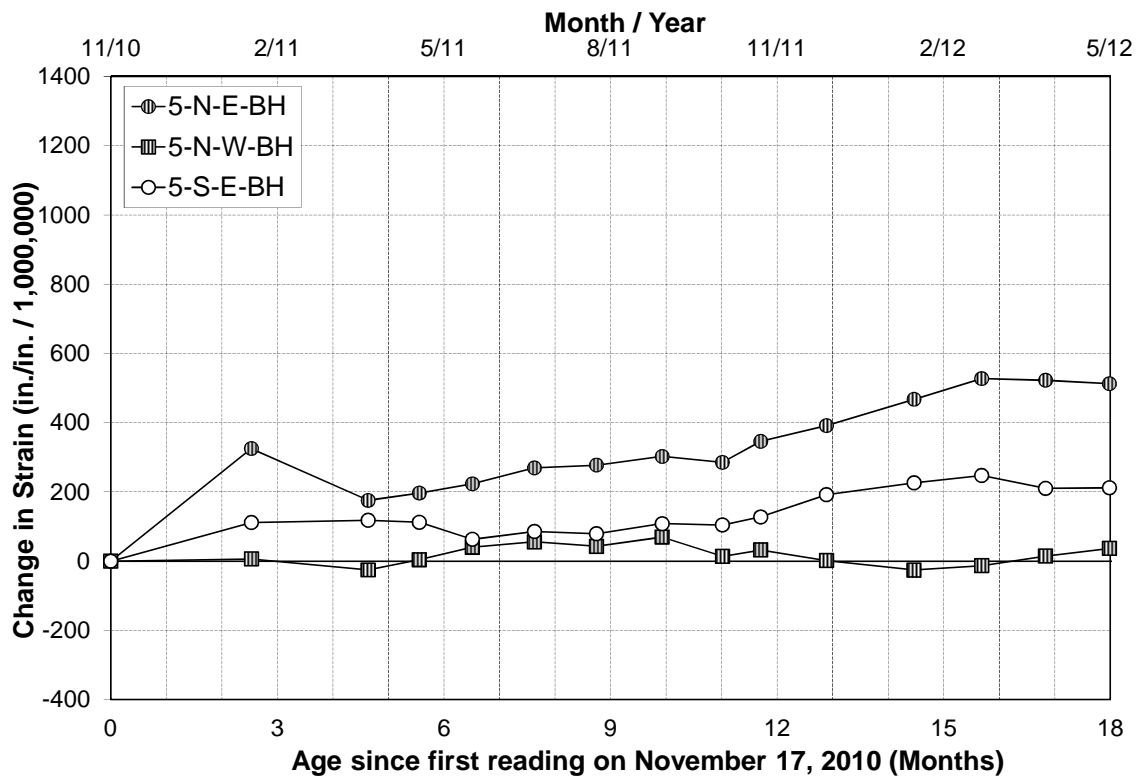


**Figure 6.35:** Concrete strain difference for BH measurement locations

## **Chapter 7**

### **Moisture Diffusion Modeling**

#### **7.1 Purpose of moisture diffusion modeling**

In Chapter 6 it was concluded that up to May 17, 2012, the ASR mitigation procedure has shown little effect on lowering the internal RH in spans 4 and 5. This may be due to the fact that the large cross section may need a longer time to diffuse moisture, and monitoring must simply continue. However, if an “effectiveness time frame” could be determined through analytical analysis it would help determine if the results, in the form of lowered internal humidities, should have already been seen at the instrumentation locations of the Bibb Graves Bridge.

Additionally, there is uncertainty surrounding the epoxy flood coat’s effect on the silane’s effectiveness and the ability of the arch to diffuse water close to the epoxy coating. Therefore, the effect of the epoxy layer on the diffusion of moisture from the cross section needs to be determined. Finally, if the moisture is evaporating from the treated arches, the period in which the ASR mitigation procedures effect might be seen is unknown.

## 7.2 Finite-element methods

To model the moisture diffusion of a concrete cross section similar to that of an arch of the Bibb Graves Bridge, the finite-element software ANSYS 12.0 was used. The moisture diffusion / heat transfer analogy (reviewed in Chapter 2) was used, and thermal elements were used to model moisture diffusion.

All input and output data in section 7.2 are referred to by their respective thermal terminology, unless otherwise noted, since the moisture diffusion / heat transfer analogy has been defined.

### 7.2.1 Element selection

Using ANSYS 12.0, a thermal graphical user interface (GUI) was used, and elements were selected. The elements used in the finite-element model are Plane55 thermal conduction elements. The elements have one degree of freedom, which is temperature, and can be used in steady-state or transient analysis. The geometry of the individual elements is shown in Figure 7.1. The four-node element option was used in this analysis.

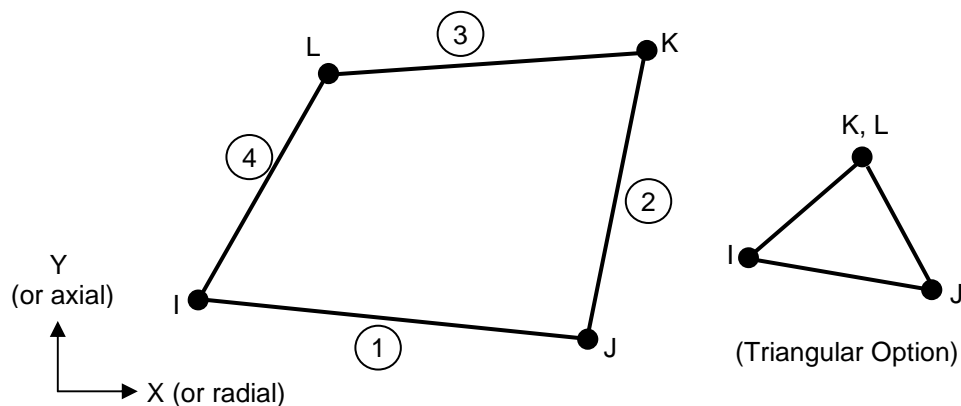


**Figure 7.1:** Plane55 Geometry (SAS IP 2009)

### 7.2.2 Defining the material model

After the element selection, a thermal material model was defined. The thermal material model included isotropic conductivity as the diffusion coefficient, density and the specific gravity of water, and specific heat as the saturated moisture content of the concrete.

Based on the in-situ concrete of the bridge arches, two compressive strengths were used to calculate the moisture diffusion coefficient. A lower-bound concrete compressive strength of 2,000 psi, and an upper-bound concrete compressive strength of 3,250 psi was used. These values were selected based on the specified strength values in the arches of span 4 and 5 shown in Figure 3.8.

The isotropic conductivity input was based on a multilinear approximation of the moisture diffusion coefficient developed by Ouyang and Wan (2008), in order to simplify computational efforts. The multilinear approximation of the moisture diffusion coefficient is shown in Figure 7.2.

To find the saturated moisture content,  $C_{sat}$ , of the modeled concrete, a concrete cylinder made with river gravel with a compressive strength of approximately 2,000 psi was weighted in a saturated surface-dry state, heated for 5 days at 350 °F, and then weighed again. The saturated moisture concentration was determined to be approximately 0.0068 lb/in<sup>3</sup> by subtracting the final weight from the initial weight, and then dividing by the volume of the cylinder. Using this information, the conductivity was calculated and input into the material model. The respective transformed thermal conductivities,  $k_{xx}$ , used



for the various material models are tabulated in Tables 3.1 and 3.2. The transformed thermal density and transformed specific heat were input into both models as 1 and 0.0068 lb/in<sup>3</sup>, respectively.

**Table 7.1:** Conductivity information for 2,000 psi concrete input into ANSYS

| $C_{sat}$              | Diffusion Coefficient |                          | Conductivity             |
|------------------------|-----------------------|--------------------------|--------------------------|
|                        | $RH$                  | $D$                      | $k_{xx}$                 |
| (lb/in. <sup>3</sup> ) | (%)                   | (in. <sup>2</sup> /hour) | (lb/in.-hour)            |
| 0.0068                 | 0                     | 0.000482                 | 3.270 x 10 <sup>-6</sup> |
| 0.0068                 | 50                    | 0.000482                 | 3.271 x 10 <sup>-6</sup> |
| 0.0068                 | 74                    | 0.000658                 | 4.461 x 10 <sup>-6</sup> |
| 0.0068                 | 78                    | 0.002253                 | 1.527 x 10 <sup>-5</sup> |
| 0.0068                 | 84                    | 0.009606                 | 6.512 x 10 <sup>-5</sup> |
| 0.0068                 | 100                   | 0.009649                 | 6.541 x 10 <sup>-5</sup> |

**Table 7.2:** Conductivity information for 3,250 psi concrete input into ANSYS

| $C_{sat}$              | Diffusion Coefficient |                          | Conductivity             |
|------------------------|-----------------------|--------------------------|--------------------------|
|                        | $RH$                  | $D$                      | $k_{xx}$                 |
| (lb/in. <sup>3</sup> ) | (%)                   | (in. <sup>2</sup> /hour) | (lb/in.-hour)            |
| 0.0068                 | 0                     | 0.000194                 | 1.314 x 10 <sup>-6</sup> |
| 0.0068                 | 50                    | 0.000194                 | 1.314 x 10 <sup>-6</sup> |
| 0.0068                 | 74                    | 0.000264                 | 1.792 x 10 <sup>-6</sup> |
| 0.0068                 | 78                    | 0.000905                 | 6.135 x 10 <sup>-6</sup> |
| 0.0068                 | 84                    | 0.003858                 | 2.615 x 10 <sup>-5</sup> |
| 0.0068                 | 100                   | 0.003876                 | 2.627 x 10 <sup>-5</sup> |

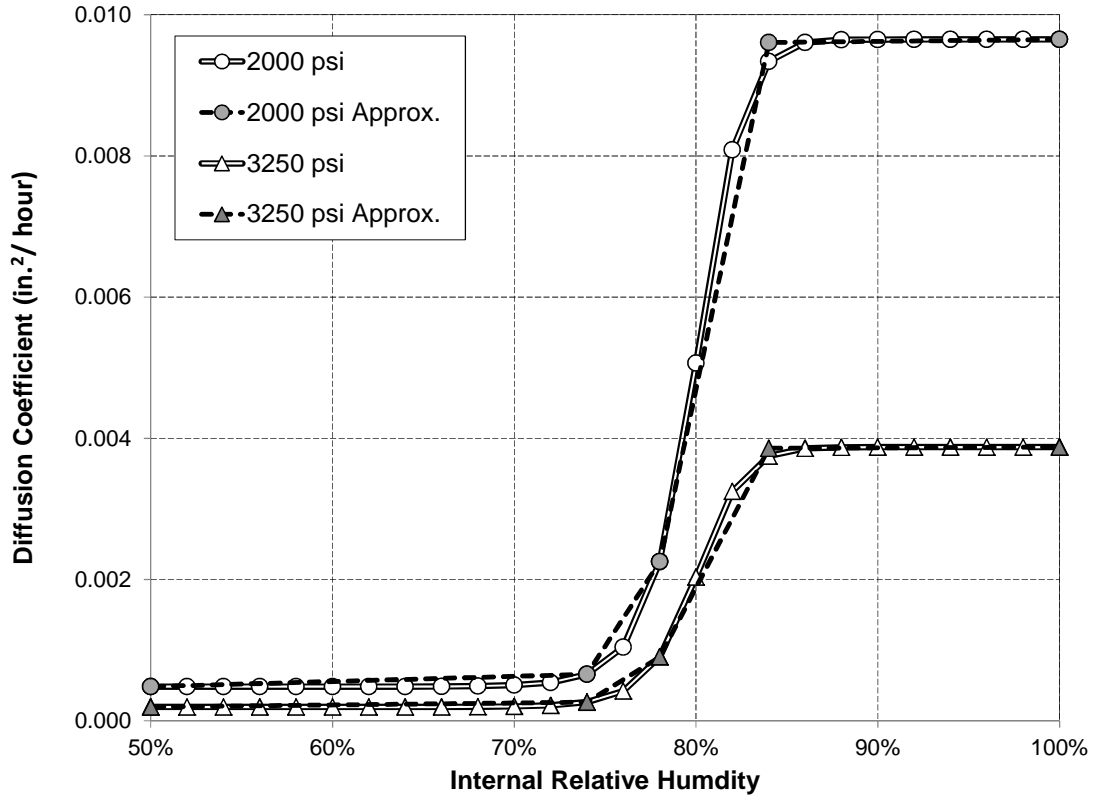


**Figure 7.2:** Multilinear approximation of the moisture diffusion coefficient

### 7.2.3 Cross sectional model and loads applied

The cross section of the bridge arch is 48 in. wide and 24 in. tall, and was meshed using 1152 1 in. x1 in. Plane55 square elements, as shown in Figure 7.3.

A 95 % internal RH (internal temperature) was defined as the initial condition for all models. This corresponds to the worst-case internal relative humidities in the damaged concrete of span 5 of the bridge. The ambient RH was modeled as a “temperature on line”, which applies a constant ambient RH to the exterior surface of the cross section. The ambient RH was changed per month, based on a 30-year average from Montgomery, AL, as shown in Table 7.3 (Horstmeyer 2008).

**Table 7.3:** 30-year average for monthly ambient RH for Montgomery, AL,  
(Horstmeyer 2008)

| <i>Month</i> | <i>RH (%)</i> |
|--------------|---------------|
| January      | 71.0          |
| February     | 67.5          |
| March        | 68.0          |
| April        | 68.5          |
| May          | 71.0          |
| June         | 71.5          |
| July         | 75.5          |
| August       | 75.5          |
| September    | 73.0          |
| October      | 70.5          |
| November     | 70.5          |
| December     | 71.0          |

The epoxy flood coat was assumed to be completely impermeable, and was therefore modeled by setting the heat flux to zero, and by not applying a “temperature on line” along the top surface of the cross section. Heat flux is defined as the energy per unit time per unit area (SAS IP 2009).

One set of analyses was conducted using an epoxy flood coat, and another was conducted without the epoxy present. Therefore, four analyses were conducted in total:

1. 2,000 psi, no epoxy flood coat,
2. 3,250 psi, no epoxy flood coat,
3. 2,000 psi, with an epoxy flood coat, and
4. 3,250 psi, with an epoxy flood coat.

1  
ELEMENTS  
MAT NUM

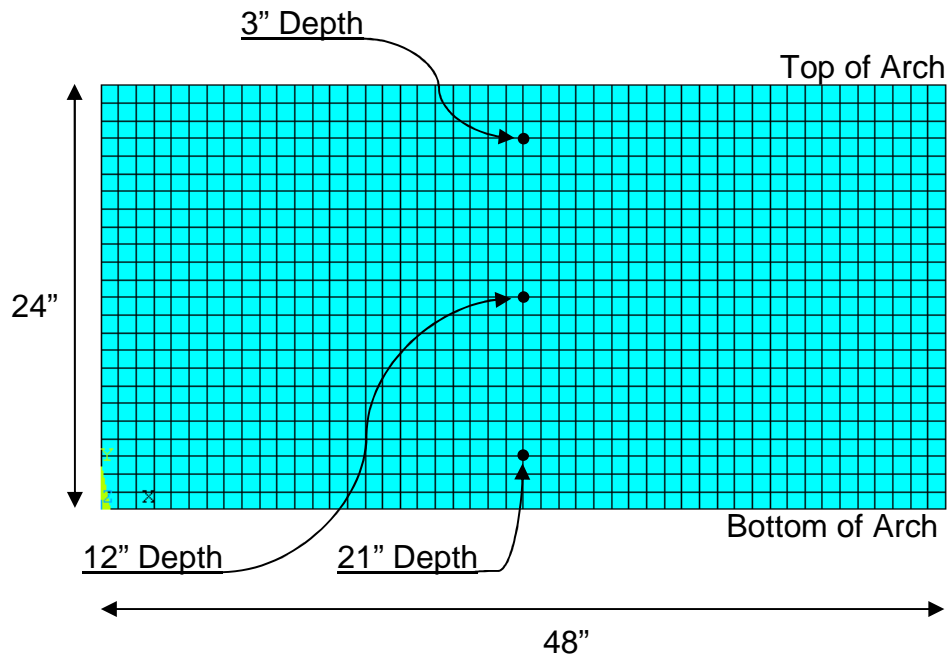


**Figure 7.3:** Arch cross section modeled in ANSYS

The analyses performed were all small displacement transient analyses. The time at the end of the last load step was set to 122,640 hours (14 years), automatic time stepping was turned on, and every substep was recorded. The time increments specified were as follows:

- Time Step Size = 24 hours
- Minimum Step Size = 24 hours
- Maximum Step Size = 168 hours (1 week)

### **7.3 Results from finite-element analysis**

After the four analyses were run, time-history post-processing and general post-processing were collected and organized. For all four analyses, internal RH calculations for each substep were collected. In addition, the moisture flux vector plot at 10 years was determined.

For the models with no epoxy flood coat, internal RH calculations were reported versus time. The internal RH data were taken from nodes in the center of the cross section at depths of 3 and 12 inches from the top surface, as shown in Figure 7.3. Due to symmetry of the cross section and loading conditions, the 3 and 21 inch depths are identical.

For the models with an epoxy flood coat, internal RH calculations were also reported versus time. The internal RH data were taken from nodes in the center of the cross section at depths of 3, 12, and 21 inches from the top surface, as shown in Figure 7.3.

For the models with no epoxy flood coat, the decrease in RH over time is plotted in Figure 7.4. Moisture diffuses out of the surface of the concrete relatively quickly, but moisture from the core of the cross section diffuses much slower. Snapshots of the moisture flux at 10 years for the 2,000 psi and 3,250 psi concrete models are illustrated in Figure 7.5 and 7.6 respectively. After 10 years, the moisture flux values are larger for the 3,250 psi concrete; this is due to the fact that there is more moisture available to diffuse for less permeable concrete. It should also be noted that the moisture diffuses out of all surfaces symmetrically, as shown in Figures 7.5 and 7.6.

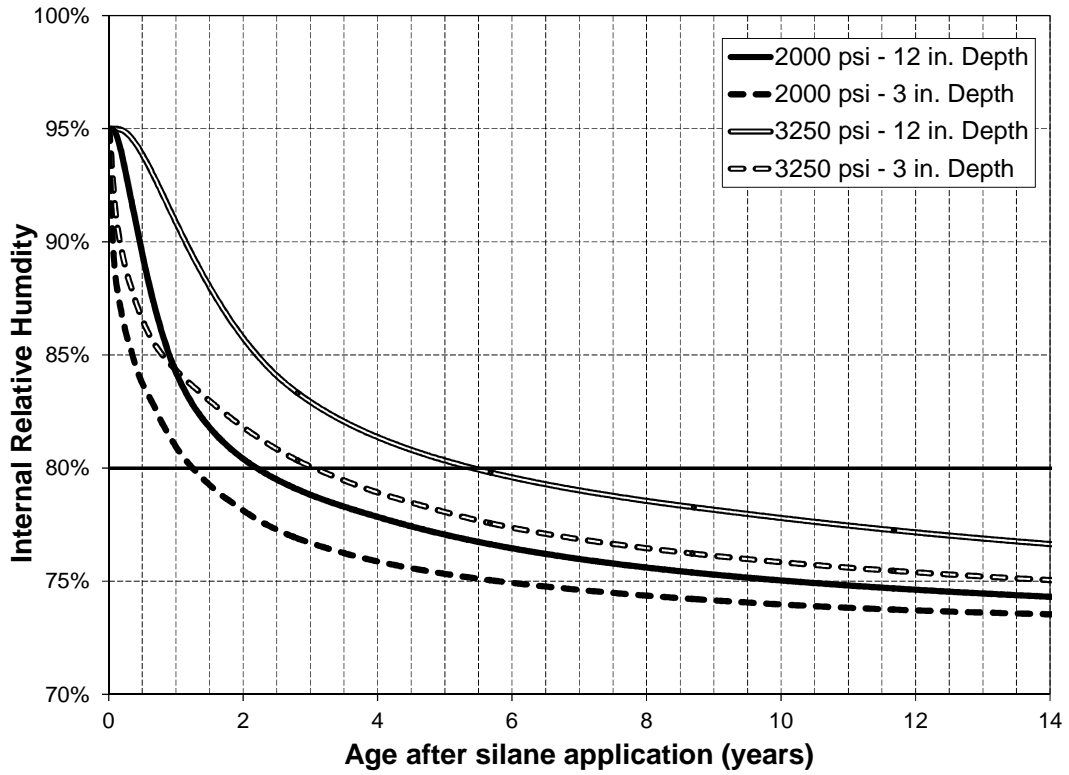


Figure 7.4: Moisture loss in concrete coated with silane only

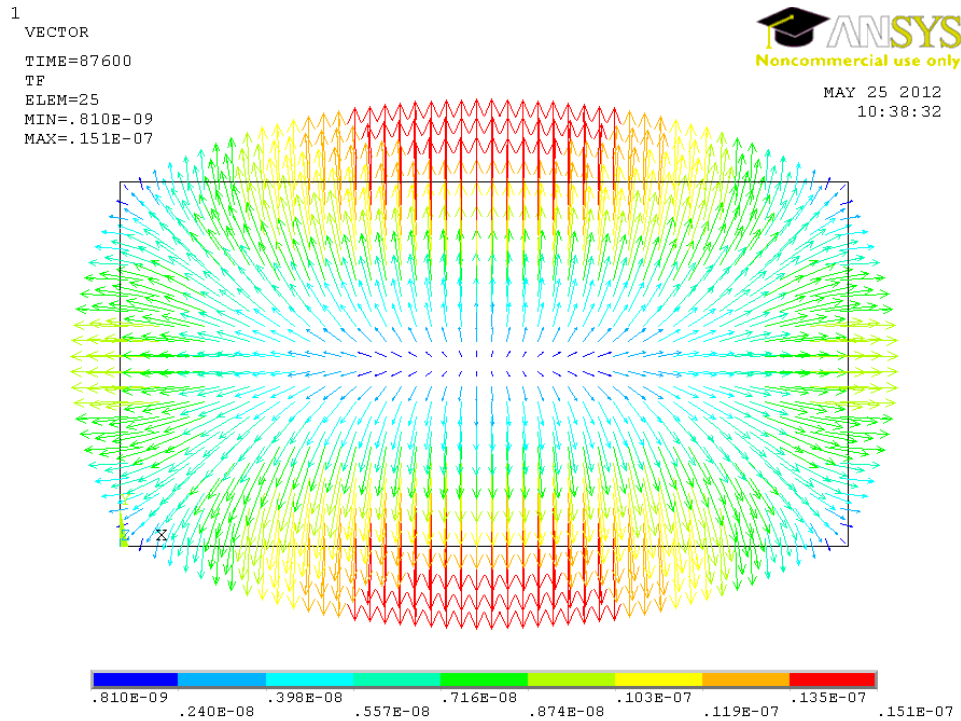
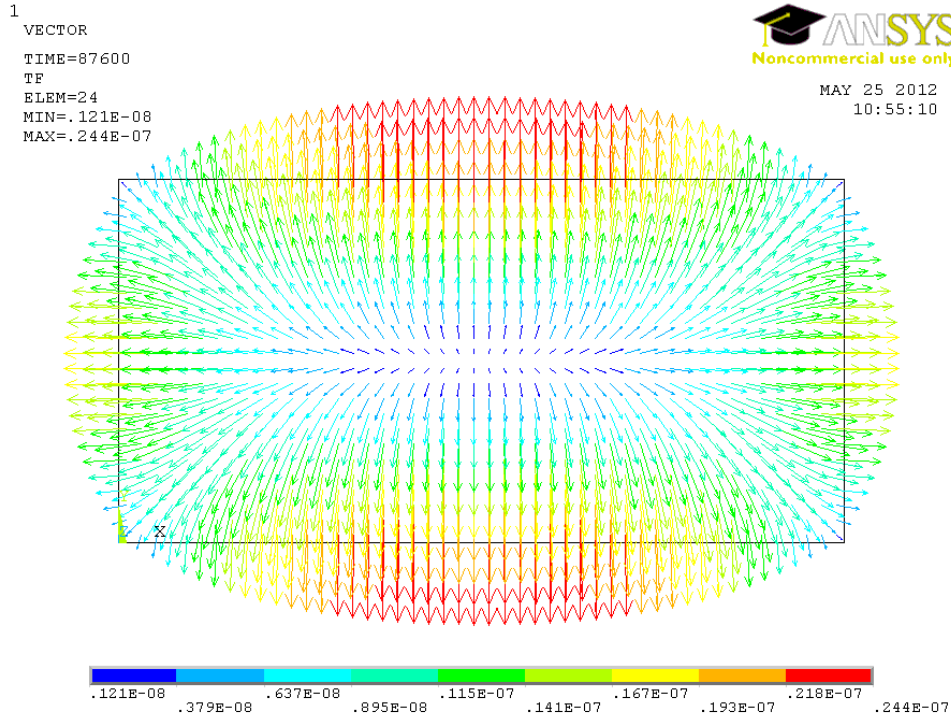


Figure 7.5: Moisture flux at 10 years for 2,000 psi concrete and no epoxy flood coat



**Figure 7.6:** Moisture flux at 10 years for 3,250 psi concrete and no epoxy flood coat

When the boundary conditions are changed to model the impermeable epoxy flood coat, the results change substantially. For these models, the RH change with time is plotted in Figure 7.7. It can be seen that due to the non-permeable epoxy flood coat, the moisture becomes “trapped” in the region directly below the top surface in the center of the cross section.

This “trapped moisture” phenomenon can be seen in results at the 3-inch depth shown in Figure 7.7, and in the snapshots of the moisture flux at 10 years for the 2,000 psi and 3,250 psi concrete models, shown in Figure 7.8 and 7.9, respectively. With the addition of an epoxy flood coat, the time needed for the entire cross section to reach 80 % RH increases from 5.4 years to 13.4 years for the 3,250 psi concrete, and from 2.2 to 5.4 years for the 2,000 psi concrete.

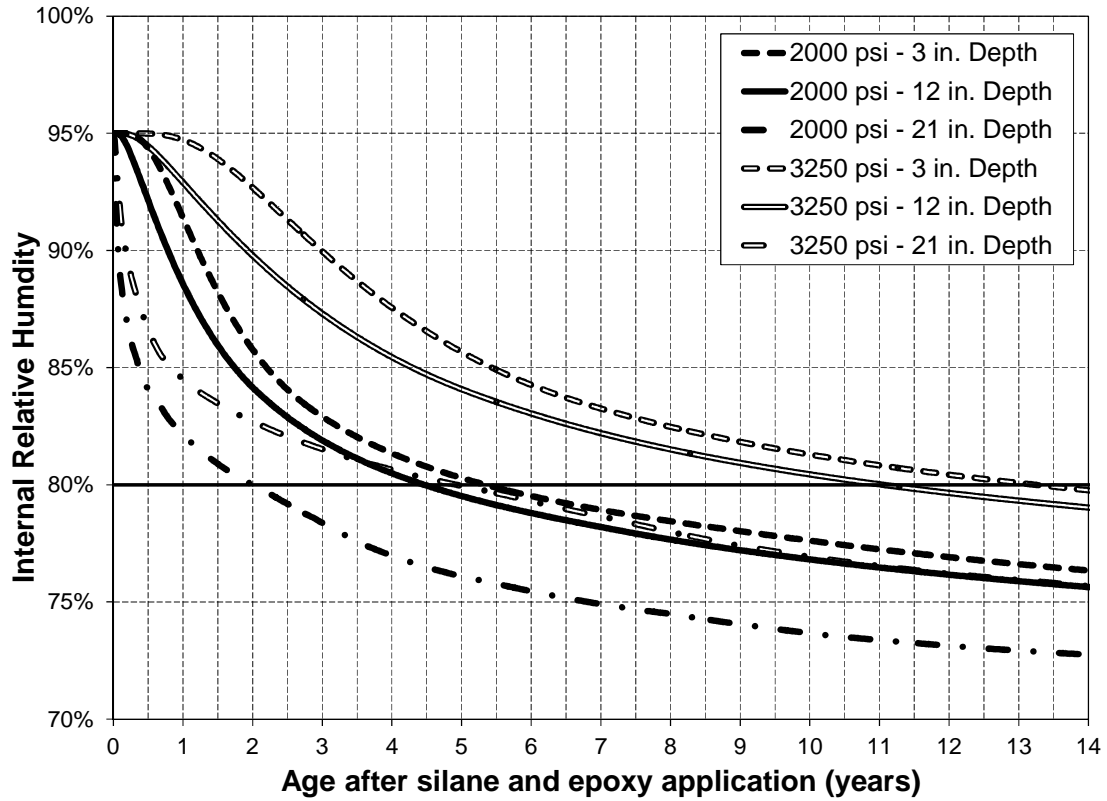


Figure 7.7: Concrete RH change when coated with an epoxy flood coat

1  
VECTOR  
TIME=87600  
TF  
ELEM=1105  
MIN=.107E-08  
MAX=.400E-07



MAY 25 2012  
10:00:25

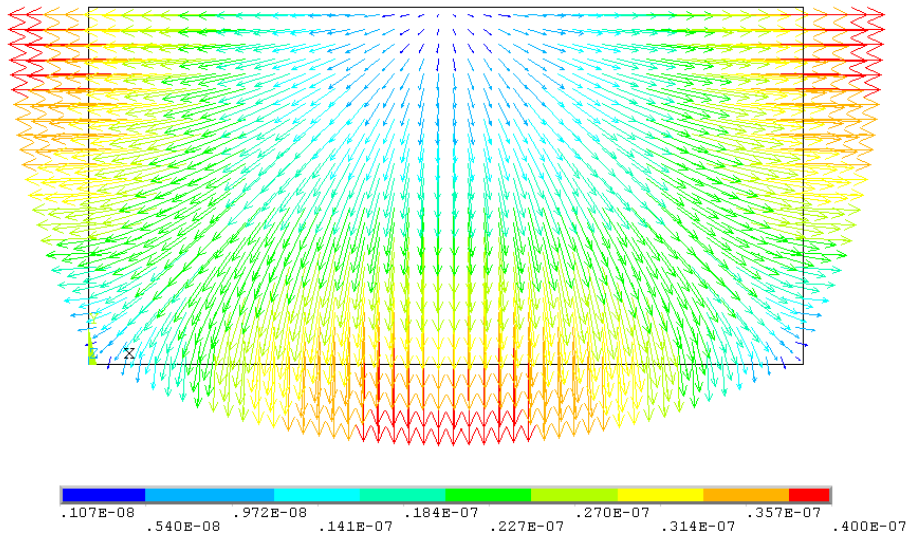
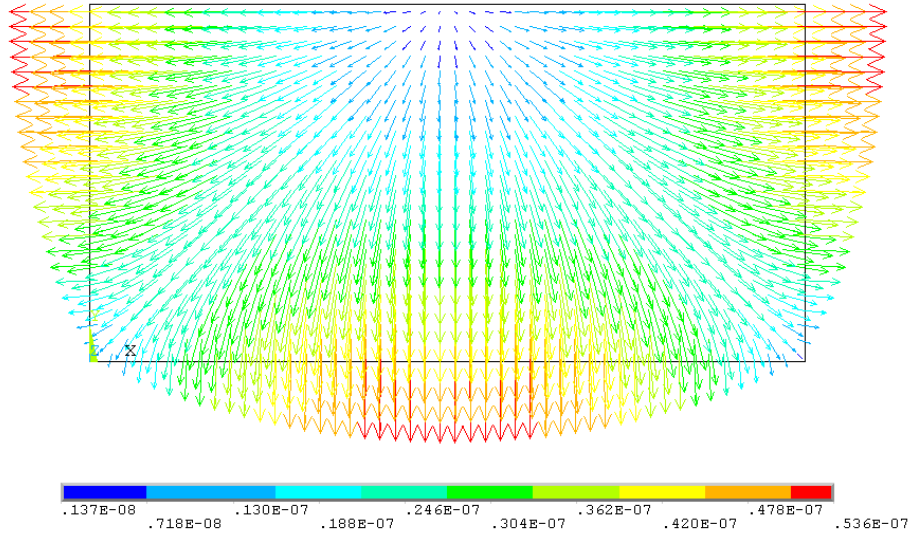


Figure 7.8: Moisture flux at 10 years for 2000 psi concrete with an epoxy flood coat



1  
 VECTOR  
 TIME=87600  
 TF  
 ELEM=25  
 MIN=.137E-08  
 MAX=.536E-07



**Figure 7.9:** Moisture flux at 10 years for 3250 psi concrete  
 with an epoxy flood coat

Based on the analysis results, the time needed to reach 80 % internal RH for the four models, for the various depths, is shown in Table 7.4. The addition of the epoxy flood coat increases the time needed to reach 80% RH by approximately 150 %.

**Table 7.4:** Years needed to reach 80 percent internal RH  
 for various depths within the concrete

| Time Needed to reach 80 % RH (years) |                   |                        |        |        |
|--------------------------------------|-------------------|------------------------|--------|--------|
| Model Type                           | Concrete Strength | Depth from top surface |        |        |
|                                      |                   | 3 in.                  | 12 in. | 21 in. |
| <i>Silane Only</i>                   | 2,000 psi         | 1.2                    | 2.2    | 1.2    |
|                                      | 3,250 psi         | 3.1                    | 5.4    | 3.1    |
| <i>Silane &amp; Epoxy</i>            | 2,000 psi         | 5.3                    | 4.5    | 2.0    |
|                                      | 3,250 psi         | 13.2                   | 11.1   | 4.9    |

### 7.3.1 Moisture diffusion time frames

For the cross sections with silane only, the 12-inch depth is the last location to reach 80 % RH, but with the application of the epoxy flood coat, the last location to reach 80 % RH is in the middle of the top of the cross section directly below the epoxy layer. Table 7.5 is a summary of the time needed for entire cross section to reach 80 % internal RH.

**Table 7.5:** Years needed for entire cross section to reach 80 percent internal RH

| <i>Time needed for the entire cross section to reach 80 % RH (years)</i> |                    |                  |                         |                  |
|--|--------------------|------------------|-------------------------|------------------|
|  | <i>Silane Only</i> |                  | <i>Silane and Epoxy</i> |                  |
|  | <i>2,000 psi</i>   | <i>3,250 psi</i> | <i>2,000 psi</i>        | <i>3,250 psi</i> |
| <i>Years needed to reach 80 % internal RH</i>                            | 2.2                | 5.4              | 5.4                     | 13.4             |

Using Table 7.5, Figure 7.4, and Figure 7.7, the moisture diffusion time frames were determined. The following periods can be used to compare with experimental values to insure that the various ASR mitigation procedures are in fact effective. The time frames for the top and bottom three measurement depths should correspond with data collected from the Bibb Graves Bridge.

1. Bridge arch with no epoxy flood coat
  - Approximately 1.2 – 3.1 years for the top and bottom three measurement depths
  - Approximately 2.2 – 5.4 years for the entire cross section

## 2. Bridge arch with an epoxy flood coat

- Approximately 5.3 – 13.2 years for the top 3 measurement depths
- Approximately 2.0 – 4.9 years for the bottom 3 measurement depths
- Approximately 5.4 – 13.4 for the entire cross section

*Therefore, the addition of the epoxy flood coat increases the time needed to reach 80 % RH by approximately 150 %.*

### **7.3.2 Steady-state humidity analysis**

Bažant and Najjar (1971) found that

It is curious to note that nonlinear diffusion exhibits some very peculiar and unexpected features. For instance, having two identical specimens drying in environments of different humidities, the time needed to reach certain humidity in the core may be greater for the specimen which is in the environment of the lower humidity.

To evaluate this phenomenon, a steady state RH analysis was performed on the same cross section, instead of a variable humidity for each month.

Using a similar procedure as before, a lower-bound analysis of 60 % ambient RH and an upper bound analysis of 75 % ambient RH was applied to both the 2,000 psi and 3,250 psi concrete cross sections, with and without an epoxy flood coat.

For all analyses, the time needed for the entire cross section to reach 80 % internal RH from an initial condition of 95 % RH is summarized in Table 7.6.

**Table 7.6:** Years needed for entire cross section to reach 80 % internal RH

| <i>Time needed for the entire cross section to reach 80 % RH (years)</i> |                    |                  |                         |                  |
|--|--------------------|------------------|-------------------------|------------------|
| <i>Ambient RH</i>  | <i>Silane Only</i> |                  | <i>Epoxy Flood Coat</i> |                  |
|  | <i>2,000 psi</i>   | <i>3,250 psi</i> | <i>2000 psi</i>         | <i>3,250 psi</i> |
| 60 %   | 2.1                | 5.2              | 5.0                     | 12.5             |
| 75 %   | 2.3                | 5.6              | 5.6                     | 14.0             |

Finally, in agreement with Bažant and Najjar (1971), the initial RH diffusion out of the cross section is greater for the 75 % ambient RH for both concrete strengths, with and without an epoxy flood coat, as shown in Figures 7.10 and 7.11. However, the initially steep slopes of the 75 % ambient RH analyses begin to level out, and the 60 % ambient RH analyses reach 80 % internal RH faster in all cases.

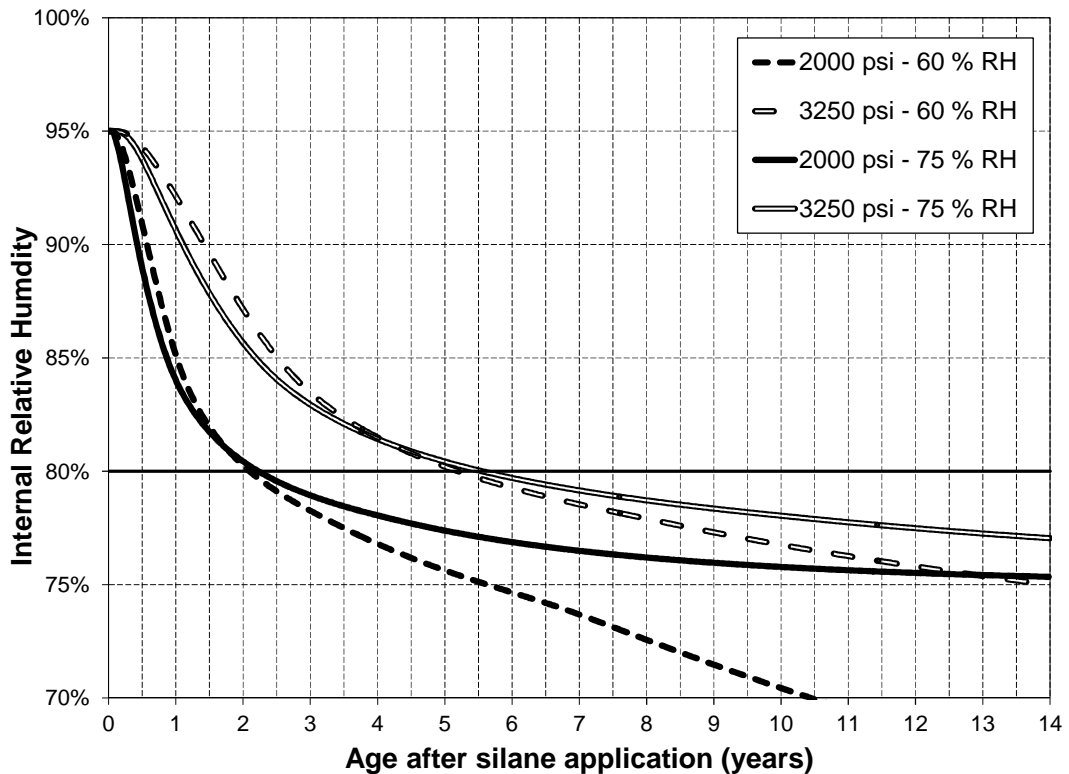


**Figure 7.10:** Moisture diffusion with steady state ambient RH, with silane only

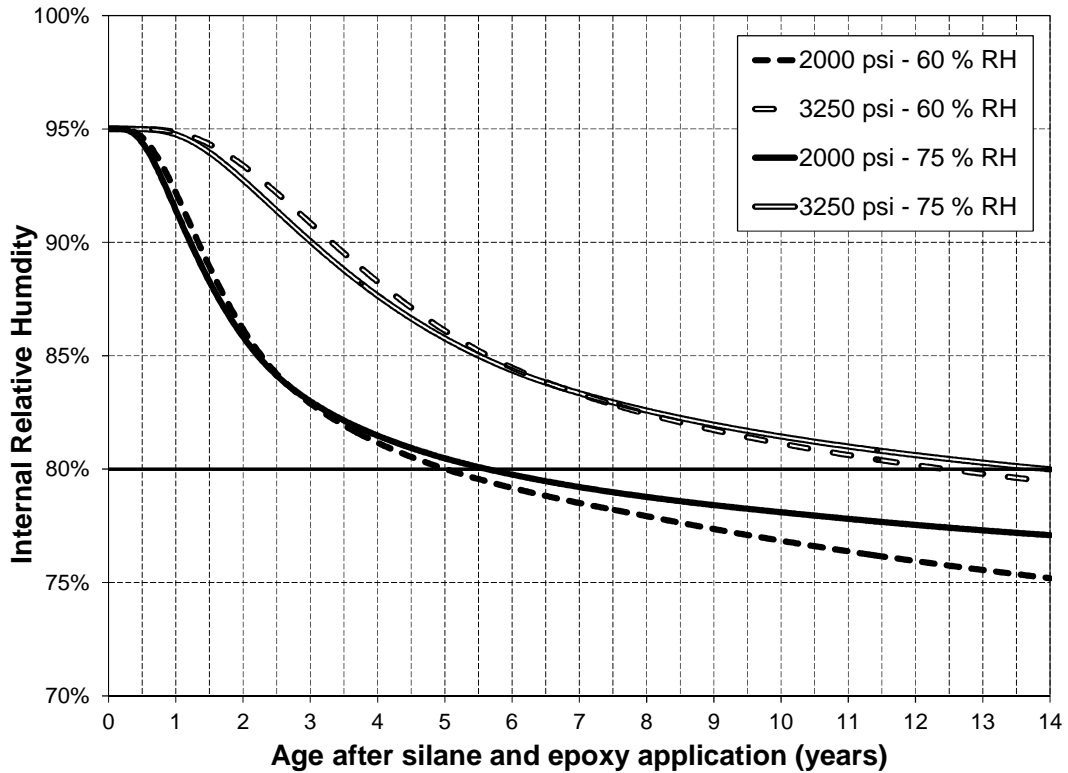


**Figure 7.11:** Moisture loss with steady state ambient RH, with silane and an epoxy flood coat

#### 7.4 Experimental work to calibrate the finite-element model results

As with all finite-element models, theoretical results need to be verified with experimental data. Due to the deteriorated nature of some of the concrete, and uncertainties of in-place properties, a separate experimental study was started to collect data pertaining to the diffusion of moisture out of a cross section similar to that of the Bibb Graves Bridge arches.

Three arch test sections were constructed during the summer of 2011. The arch test sections were designed to allow data collection similar to that being done on the Bibb Graves Bridge. The cross section properties of each test section are also similar to that of the Bibb Graves Bridge. The arch test sections are 4 ft wide, 2 ft tall, and due to length constraints, only 8 ft long; however, 8 ft

was deemed a sufficient length for the moisture to diffuse out of the smaller dimensions foremost. Because of the finite-element analysis performed, three arch sections were built to collect data for a cross section with a silane and an epoxy flood coat application, a silane application only, and a control arch with no treatment. The arch test sections were then fitted with RH measurement instrumentation similar to that on the Bibb Graves Bridge.

#### **7.4.1 Arch test section construction**

The foundation of the arch test sections consists of two strip footings, each supporting a line of columns, and a 6-inch thick slab-on-grade. The construction of the strip footings and slab on grade is shown in Figure 7.13, and the final strip footing and slab-on-grade is shown in Figure 7.14. The columns were placed using 12-inch diameter SonoTubes, as shown in Figure 7.15. The finished columns are shown in Figure 7.16.

Wooden formwork was built for the arch test sections, and minimum temperature and shrinkage reinforcement per ACI 318 (2001) was used, as shown in Figure 7.17. The concrete used in the arch test sections was tested at 28 days and has an in-place compressive strength of approximately 2,100 psi, which is similar to the lowest strength concrete used in the arches of the Bibb Graves Bridge. The finished arch test sections, without treatment, are shown in Figure 7.18.



**Figure 7.13:** Construction of strip footings and slab on grade



**Figure 7.14:** Finished strip footings and slab on grade





**Figure 7.15:** 12 inch SonoTubes column formwork



**Figure 7.16:** Finished columns





**Figure 7.17:** Arch test section formwork and reinforcement

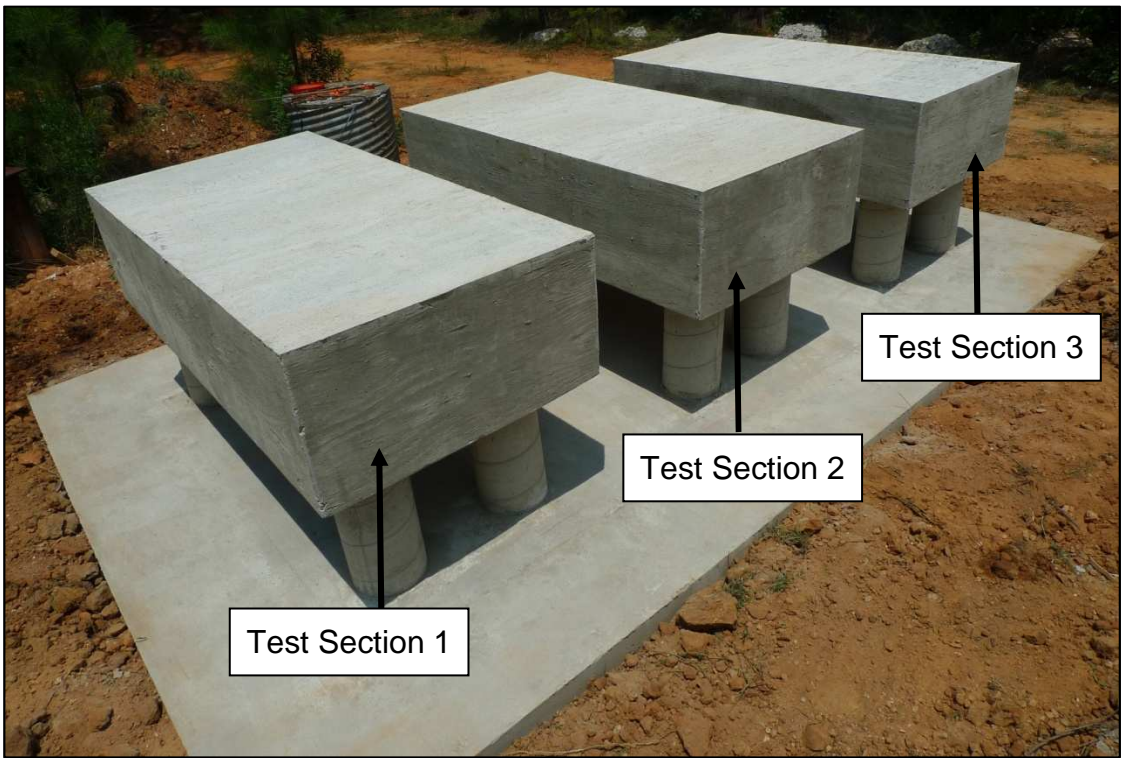


**Figure 7.18:** Finished arch test sections with no treatment

#### 7.4.2 Arch test section sealing treatments

Arch test section 1 received the exact ASR mitigation procedure treatment as the Bibb Graves Bridge. Silane was applied first, using a garden sprayer, per manufacturer's standards. Only arch test sections 1 and 2 received the silane treatment, as shown in Figure 7.19. Arch test section 1 then received an epoxy flood coat on the top surface, as shown in Figure 7.20. Arch test section 2 received only silane and is shown in Figure 7.19. Finally, arch test section 3 received no treatment, as shown in Figure 7.19.



**Figure 7.19:** Silane application on arch test section



**Figure 7.20:** Epoxy flood coat application on arch test section

### **7.4.3 RH instrumentation for arch test sections**

RH instrumentation identical to that used on the Bibb graves Bridge was installed in the concrete at depths of 1, 2, and 3-inches in the top and bottom of each model. In addition, instrumentation was installed at a depth of 12 inches through the top of each model. The RH values are being recorded at each location, and this effort will be continued by future research assistants working on this project. Once enough time has passed, these RH values will be used to calibrate the final finite-element model.

## **7.5 Summary**

Until May 17, 2012, the ASR mitigation procedure has shown little effect on lowering the internal RH in both spans four and five. Therefore, an “effectiveness time frame” was determined through analytical analysis to help determine if the results, in the form of lowered internal humidities, should have already been seen in the Bibb Graves Bridge.

To determine how the internal RH decreases after silane application, one must first understand the movement of moisture through concrete. Fick’s second law is the fundamental principle that governs moisture movement through concrete. Using Fick’s second law, Bažant and Najjar (1971) derived a model for the diffusion coefficient in relation to RH and concrete strength.

The CEB-FIP Model Code (2010) adopted Bažant and Najjar’s work and produced a standardization of the coefficients within the equation. Using the

CEB-FIP Model Code's diffusion coefficient, a moisture diffusion/ heat transfer analogy can be made to be used in modern finite-element software.

To model the moisture diffusion of a concrete cross section similar to that of an arch of the Bibb Graves Bridge, the finite-element software ANSYS 12.0 was used. The moisture diffusion/ heat transfer analogy was used, and a transient thermal analysis was performed on a cross section model 48-in. wide and 24-in. tall.

A 95 % internal RH was defined as the initial condition for all models. This corresponded to the worst-case internal relative humidities in the damaged concrete of span 5 of the bridge. The ambient RH was defined per month based on a 30-year average from Montgomery, AL. The epoxy flood coat was assumed to be completely impermeable.

Based on the in-situ concrete of the bridge arches, two compressive strengths were used to calculate the moisture diffusion coefficient. The lower-bound concrete compressive strength was 2,000 psi, and the upper-bound concrete compressive strength was 3,250 psi.

One set of analyses was conducted using an epoxy flood coat, and another was conducted without. Therefore, four analyses were conducted in total:

1. 2,000 psi, no epoxy flood coat
2. 3,250 psi, no epoxy flood coat
3. 2,000 psi, with an epoxy flood coat
4. 3,250 psi, with an epoxy flood coat

All finite-element results must be verified by experimental data before any of the following conclusions are considered valid. This being said, from the moisture diffusion analyses the following moisture diffusion time frames were determined:

1) Bridge arch with no epoxy flood coat

- Approximately 1.2 – 3.1 years for the top and bottom three measurement depths
- Approximately 2.2 – 5.4 years for the entire cross section

2) Bridge arch with an epoxy flood coat

- Approximately 5.3 – 13.2 years for the top three measurement depths
- Approximately 2.0 – 4.9 years for the bottom three measurement depths
- Approximately 5.4 – 13.4 years for the entire cross section

Finally, the addition of the epoxy flood coat increases the time needed to reach 80 % RH by approximately 150 %.

## Chapter 8

### Summary, Conclusions, Recommendations

#### 8.1 Project Summary

ASR is a deleterious reaction that occurs in concrete with the sufficient alkalinity in the cement, the presence of reactive silica in the aggregates, and sufficient moisture within the concrete (Forster et al. 1998). When these three ingredients are present, the reaction produces ASR gel. ASR gel swells in the presence of moisture, and can create significant distress leading to major deterioration. If the internal RH of the concrete can be lowered under 80 % internal RH, it has been shown that ASR expansion can be slowed or stopped (Bérubé et al. 2002a; Stark 1991). Previous studies have shown that silane sealants have been effective in lowering internal RH to less than 80 % in laboratory cylinders and thin field structures, provided the ambient RH is under 80 % (Bérubé et al. 2002a, 2002b).

##### 8.1.1 Presence of ASR in Bibb Graves Bridge

The Bibb Graves Bridge, located in Wetumpka, AL, is a reinforced concrete bridge that is 700-feet long and has a 24-foot wide roadway. The bridge consists of seven arches that support the bridge deck, as shown in Figure 3.6. Other than span 1 and 7, the bridge deck is suspended from the arches at half-height.

After a petrographic analysis from two separate organizations, it was determined that ASR was present in the northern and southern arches of span 5.

The arches in this span are exhibiting significant cracking due to ASR. A crack mapping survey was performed by Auburn University to record the distress caused by ASR in these arches. These surveys are shown in Figures 3.21 through 3.26. Examples of the distress can be found in Figures 3.27 through 3.32.

### **8.1.2 ASR mitigation procedure**

The ASR mitigation procedure chosen by the FHWA, ALDOT, and Auburn University consisted of the following five steps:

1. Water-blast all concrete surfaces to clean concrete surfaces and remove loose impediments, efflorescence, ASR gel, algae, etc.
2. Apply silane to all surfaces.
3. Seal all cracks 0.04 inch and wider with a UV-resistant, flexible sealant.
4. Apply an epoxy flood coat to the top arch surface to seal the cracks on this surface.
5. Install instrumentation for monitoring.

From October to November 2010, the ASR mitigation procedure was implemented. The installation order of the ASR mitigation procedure is summarized in Figure 4.3. These actions were performed on both the north and south ASR-affected arches of span 5, and on the southern arch of span 4, as shown in Figure 4.4. The northern arch of span 4 was fitted with instrumentation for monitoring, but was not treated with silane, epoxy, or flexible sealant.

### **8.1.3 Monitoring the effectiveness of the ASR mitigation procedure**

RH and concrete strain data analyzed in this research were collected once a month from November 16, 2010, until May 17, 2012, totaling 18 months of data collection. Additionally, concrete strain data from the ten concrete strain measurement locations installed by the FHWA were collected from December 16, 2005, totaling 77 months (6.4 years) of data collection. RH data were collected using the Vaisala relative humidity probes at forty-eight measurement locations. Concrete strain data were collected using a Mayes demountable mechanical (DEMEC) concrete strain gauge at forty-seven measurement locations.

In all data analyses, span 4 serves as a control span that is not affected by ASR. The northern arch of span 4 was used as a base measure for relative humidity and expansion measurements for an arch without the ASR mitigation procedure. Using this arch, data were compared to examine the effects of the ASR mitigation procedure.

### **8.1.4 Moisture diffusion modeling**

Effectiveness time frames were determined through analytical analysis to help determine if the results, in the form of lowered internal humidities, should have already been seen in the Bibb Graves Bridge.

Using the CEB-FIP Model Code's (2010) diffusion coefficient, and a moisture diffusion/ heat transfer analogy, the moisture diffusion of a concrete cross section similar to that of an arch of the Bibb Graves Bridge was modeled. The analysis was done using the finite-element software ANSYS 12.0.



A 95 % internal RH was defined as the initial condition for all models. This corresponded to the worst case internal relative humidities in the damaged concrete of span 5 of the bridge. The ambient RH was defined per month based on a 30-year average from Montgomery, Alabama. The epoxy flood coat was assumed to be completely impermeable.

Based on the in-situ concrete of the bridge arches, two compressive strengths were used to calculate the moisture diffusion coefficient. A lower-bound concrete compressive strength of 2,000 psi, and an upper-bound concrete compressive strength of 3,250 psi was used.

One set of analyses was conducted using an epoxy flood coat, and another was conducted without. Therefore, four analyses were conducted in total:

1. 2,000 psi, no epoxy flood coat
2. 3,250 psi, no epoxy flood coat
3. 2,000 psi, with an epoxy flood coat
4. 3,250 psi, with an epoxy flood coat

## 8.2 Conclusions

### 8.2.1 Effectiveness of the ASR Mitigation Procedure

From this research, the following conclusions can be drawn about the effectiveness of the ASR mitigation procedure:

- 1) The ASR mitigation procedure has not yet been effective at lowering the internal relative humidity of the concrete at any location on span 4 or span 5 below the 80 % RH threshold.
- 2) The internal relative humidity of three of the four *bottom* measurement locations for span 5 seems to be *increasing* compared to internal relative humidity of the bottom measurement locations for control arch 4-N.

### 8.2.2 Moisture Diffusion Modeling

*All finite-element results must be verified by experimental data before conclusions 1 through 3 are considered valid.* From this research, the following conclusions can be drawn about the moisture diffusion modeling:

- 1) For a bridge arch with a silane and epoxy flood coat application, the time needed to reach 80 % internal RH from 95 % internal RH, for the entire cross section, is approximately 5.4 – 13.4 years.
- 2) For a bridge arch with a silane application only, the time needed to reach 80 % internal RH from 95 % internal RH, for the entire cross section, is approximately 2.2 – 5.4 years for the entire cross section
- 3) The addition of the epoxy flood coat increases the time needed to reach 80 % RH by approximately 150 %.

- 4) Conclusion 2 of section 8.2.1 is in direct contradiction to what the finite-element model predicts; however, the finite-element analysis results still need to be calibrated to actual field measurements. Therefore, it can be assumed that the effectiveness time frames determined should not be used for prediction purposes until further revisions to the model are made.

### **8.3 Recommendations**

After completing the 18-month data collection period, data analysis, and modeling required for this research, the following recommendations can be made:

- 1) Monitoring of internal RH and concrete strains on the Bibb Graves Bridge should continue. If the ASR mitigation procedure continues to be ineffective at lowering the internal RH to the 80 % RH threshold, a second treatment of silane should be considered. Instead of using Enviroseal 40 — a water-based 40 % silane sealer — a silane sealer with the highest percentage of silane that is environmentally acceptable should be used. For example, Hydrozo 100 is a 100 % silane sealer; however, it is uncertain if this sealer is environmentally acceptable. There are also solvent-based silane sealers that are reported to be more effective than the 40 % water-based silane used on the Bibb Graves Bridge. Additionally, due to the moisture diffusion modeling results, if an epoxy flood coat is used to seal cracks smaller

than 0.04 in., the epoxy should be applied to seal these cracks without sealing the entire top surface, as described by Protocol Option B in section 4.2.2.

- 2) The diffusion coefficients used for the upper- and lower-bound finite-element models should be refined. If these values could be determined experimentally it could greatly increase the applicability of the finite-element model. Additionally, the temperature effects on the moisture diffusion of cross section could be investigated.
- 3) Additional arch test sections should be constructed to evaluate the ability of other types of silane sealers to lower the internal relative humidity of the concrete below the 80 % RH threshold.
- 4) Finally, the arch test sections should continue to be monitored in an effort to have data that more closely matches the conditions resembling the finite-element model.

## References

- ALDOT, 2010. "Presentation on the Coring of the Bibb Graves Bridge." Alabama Department of Transportation.
- ASTM. 2011. "Standard Practice for Petrographic Examination of Hardened Concrete." C856-11. West Conshohocken, PA: ASTM International.
- Barborak, R., K.J. Folliard, and M.D.A. Thomas. 2004. "Using Lithium Compounds to Treat Hardened Concrete Suffering from ASR: Preliminary Laboratory Results." Proceedings of the 12th International Conference on Alkali-Aggregate Reactivity (ICAAR). Beijing, China, 483-589.
- BASF Construction Chemicals, LLC. 2007. "Product Data." Enviroseal 40.
- Bažant, Z.P., and L.J. Najjar. 1971. "Drying of Concrete as a Nonlinear Diffusion Problem." Cement and Concrete Research: 461-473.
- Bérubé, Marc-Andre, Dominique Chouinard, Michel Pigeon, Frenette Jean, Rivest Michel, and Daniel Vézina, 2002a. "Effectiveness of sealers in counteracting alkali-silica reaction in plain and air-entrained laboratory concretes exposed to wetting and drying, freezing and thawing, and salt water." Canadian Journal of Civil Engineering: 289-300.
- Bérubé, M. A., Chouinard, D., Pigeon, M., Jean, F., Michel, R., and Vézina, D., 2002b. "Effectiveness of sealers in counteracting alkali-silica reaction in highway median barriers exposed to wetting and drying, freezing and thawing, and deicing salt." Canadian Journal of Civil Engineering (NRC ): 329-337.

Bing. Bing.com. 2012a.

<http://www.bing.com/maps/#JnE9LmJpYmIIMmJncmF2ZXMIMmJicmlkZ2UIN2Vzc3QuMCU3ZXBNLjEmYml9NjluNzY1NzI3MjQ0MzI2MSU3ZS01NS45MDY1NDc1NDU1JTdlLTEyLjEwMTc2NDEwNjA3NjMIN2UtMTE1LjA1NjkzODE3MDU=> (accessed May 17, 2012).

Bing. Bing.com. 2012b.

<http://www.bing.com/maps/?FORM=Z9LH4#Y3A9MzluNDI4MjQ1OTE0NjYzMzh+LTg2LjI4MTA2ODc5OTI2MDE0Jmx2bD0xMiZzdHk9cg==> (accessed May 29, 2012).

Blackburn, P.. *The River Region Online*. 1997.

[http://www.wetumpkaonline.com/pages/history/history\\_bridges.asp](http://www.wetumpkaonline.com/pages/history/history_bridges.asp) (accessed June 30, 2011).

Carter, P.D., 1994. "Evaluation of Dampproofing Performance and Effective Penetration Depth of Silane Sealers in Concrete." *ACI Materials Journal Special Publication*: 95-118.

Federation Internationale du Beton (fib), 2010. *CEB-FIB Model Code*. Lausanne, Switzerland.

CSA, 2000. *Guide to the Evaluation and Management of Concrete Structures Affected by Alkali-Aggregate Reaction*. Ontario, Canada: Canadian Standards Association (CSA).

Diamond, S., 1989. "ASR - Another look at mechanisms." *Proceedings of the 8th International Conference on Alkali-Aggregate Reaction*. Kyoto, Japan, 83-94.

Dunbar, P.A., and P.E. Grattan-Bellew, 1995. "Results of damage rating evaluation of condition of concrete from a number of structures affected by AAR." *Proceedings of CANMET/ACI International Workshop on AAR in Concrete*. Dartmouth, Nova Scotia: CANMET, Department of Natural Resources Canada. 257-265.

- East, B.L., 2007. *Laboratory and Field Investigations on the Use of Lithium Nitrate to Prevent or Mitigate Alkali-Silica Reaction*. Master's Thesis, University of Texas at Austin.
- Engstrom, G. M., 1994. *Field Performance of High Molecular Weight Methacrylate Monomers and Silanes on a D-Cracked, Jointed Reinforced Concrete Pavement*. MN/RD-94/07, Maplewood, MN: Minnesota Department of Transportation.
- Forster, S. W., et al., 1998. *State-of-the-Art Report on Alkali-Aggregate Reactivity*. ACI 221.1R-98, American Concrete Institute.
- Fournier, B., M.A. Bérubé, M.D.A. Thomas, N. Smaoui, and K.J. Folliard, 2004. *Evaluation and Management of Concrete Structures Affected by Alkali-Silica Reaction - A Review*. MTL 2004-11 (OP), Ottawa, Canada: Natural Resources Canada,
- Fournier, B., M.-A. Bérubé, K. J. Folliard, and M. Thomas, 2010. *Report on the Diagnosis, Prognosis, and Mitigation of Alkali-Silica Reaction (ASR) in Transportation Structures*. Final Report, Washington D.C.: Federal Highway Administration.
- gkpedia. n.d.  
<http://www.webstersdictionaryencyclopedia.com/Alabama/AlabamaPhysicalMap-HighResolution/AlabamaPhysicalMap-HighResolution.php> (accessed May 11, 2012).
- Grattan-Bellew, P.E., 1992. "Comparison of laboratory and field evaluation of alkali-silica reaction in large dams." Proceedings of the First International Conference on Concrete Alkali-Aggregate Reactions in Hydroelectric Plants and Dams. Fredericton, NB, Canada, 23.

- Grattan-Bellew, P.E., and L.D. Mitchell. 2006. "Quantitative petrographic analysis of concrete – the damage rating index (DRI) method, a review." Proceedings of Marc-André Bérubé Symposium on Alkali-Aggregate Reaction (AAR) in Concrete. Montréal, Canada: CANMET-MTL, 45-70.
- Hadley, D. W., 1968. "Field and Laboratory Studies on the Reactivity of Sand-Gravel Aggregates." Journal of the Portland Cement Association Research and Development Laboratories (Jou): 17-33.
- Hester, J. A., and Smith, O.F., 1956. *The alkali aggregate phase of chemical reactivity in concrete. Part II. Deleterious Reactions observed in Field Concrete Structures*. Montgomery, AL. Alabama Department of Transportation.
- Holth, N. Bridge Hunter. 2010. <http://bridgehunter.com/al/elmore/928/> (accessed June 30, 2011).
- Horstmeyer, S., 2008. *United States of America, State, Islands and Territories Average Relative Humidity (%) - Morning and Afternoon*. 2008. <http://www.shorstmeyer.com/wxfaq/humidity/rh.html> (accessed June 12, 2012).
- Kosmatka, S. H., B. Kerkhoff, and W. C. Panarese, 2002. *Design and Control of Concrete Mixtures*. Skokie, Illinois: Portland Cement Association.
- Lerch, W., 1959. "A Cement-Aggregate Reaction that Occurs with Certain Sand-Gravel Aggregates." Journal of the Portland Cement Association, 42-50.
- Ludwig, U., 1989. "Effects of environmental conditions on alkali–aggregate reaction and preventive measures." Proceedings of the 8th International Conference on Alkali–Aggregate Reaction in Concrete. Kyoto, Japan: Society of Materials Science. 589-596.
- Madenci, E., and I. Guven, 2006. *The Finite Element Method and Applications in Engineering Using Ansys*. New York: Springer Science + Business Media, LLC.



- Mayes Instruments Limited. n.d. "User's Guide to the Mayes DEMEC Demountable Mechanical Concrete strain Gauge." Berkshire, UK.
- Mehta, P. K., and P. J. M. Monteiro. 2006. *Concrete - Microstructure, Properties, and Materials*. New York, NY: McGraw-Hill Companies, Inc.
- Nishibayashi, S., K. Yamura, and K. Sakata, 1989. "Evaluation of cracking of concrete due to alkali–aggregate reaction." Proceedings of the 8th International Conference on Alkali–Aggregate Reaction in Concrete. Kyoto, Japan: Society of Materials Science. 759-764.
- Ouyang, Z., and B. Wan. 2008. "Modeling Moisture Diffusion in FRP Strengthened Concrete Specimens." *Journal of Composites for Construction*: 425-434.
- Ozul, M. A., and D. O. Dusenberry, 1992. *Deterioration of Precast Panels with Crushed Quartz Coarse Aggregate Due to Alkali-Silica Reaction*. SP-131, Farmington Hills, MI: American Concrete Institute.
- SAS IP, 2009. Inc. ANSYS Help, 12.0 Release.
- Schindler, A. K., Hughes, M.L., Barnes, R.W., and Byard, B.E., 2010. *Evaluation of cracking of the US 331 bridge deck*. FHWA/ALDOT 930-645. Alabama Department of Transportation. 87p.
- Selley, David B., 2010. "Making Low-VOC Silicon-based Water Repellents." *Coatings Tech*: 26-35.
- Stark, D.C., 1978. "Alkali-Silica Reactivity in the Rocky Mountain Region." Proceedings, Fourth International Conference of the Effects of Alkalies in Cement & Concrete. Purdue University. 235-243.
- Stark, D.C. , 1980 "Alkali-Silica Reactivity: Some Reconsideration." *Cement, Concrete, and Aggregates*: 92-94.

- Stark, D.C., 1991. *Handbook for the Identification of Alkali-Silica Reactivity in Highway Structures*. SHRP-C/FR-91-101, TRB National Research Council, 49p.
- Stark, D.C., B. Morgan, P. Okamoto, and S. Diamond, 1993. *Eliminating or Minimizing Alkali-Silica Reactivity*. SHRP-C-343, Washington, D.C.: National Research Council.
- Stokes, D.S., M.D.A. Thomas, and S.G. Shashiprakash, 2000. "Development of a Lithium-based Material for Decreasing ASR-induced Expansion in Hardened Concrete." Proceedings of the 11th International Conference on Alkali-Aggregate Reaction in Concrete. Quebec City: CRIB, 1079-1087.
- Taylor, V.L., 1930. "A New Type of Highway Bridge." *The Auburn Engineer*, November: 34-35.
- The Transtec Group, 2010. *Evaluation of Bibb Graves Bridge in Wetumpka, Alabama*. The Transtec Group.
- Thomas, M.I, and FHWA, 2008. "What does ASR look like?" *Reactive Solutions*, Summer 2008: 2.
- Tuthill, L. H., 1980. "Performance Failures of Concrete Materials and of Concrete as a Material." *ACI Concrete International*: 33-39.
- Tuthill, L. H., 1982. "Alkali-Silica Reaction - 40 Years Later." *ACI Concrete International*: 32-36.
- WJE, 2010. *Bibb Graves Bridge Petrographic Studies of Concrete Cores*. Northbrook, Illinois: Wiss, Janney, Elstner Associates, Inc.

## Appendix A

### Coring Procedure

This appendix contains figures from ALDOT's Presentation on the Coring of the Bibb Graves Bridge (2010). The figures graphically describe the coring process which involved locating rebar, drilling, extracting, labeling, wrapping, packing, and shipping to Illinois and Canada. This is shown in Figures A.1, A.2-A.5, A.6, A.7, A.8, A.9, and A.10, respectively.

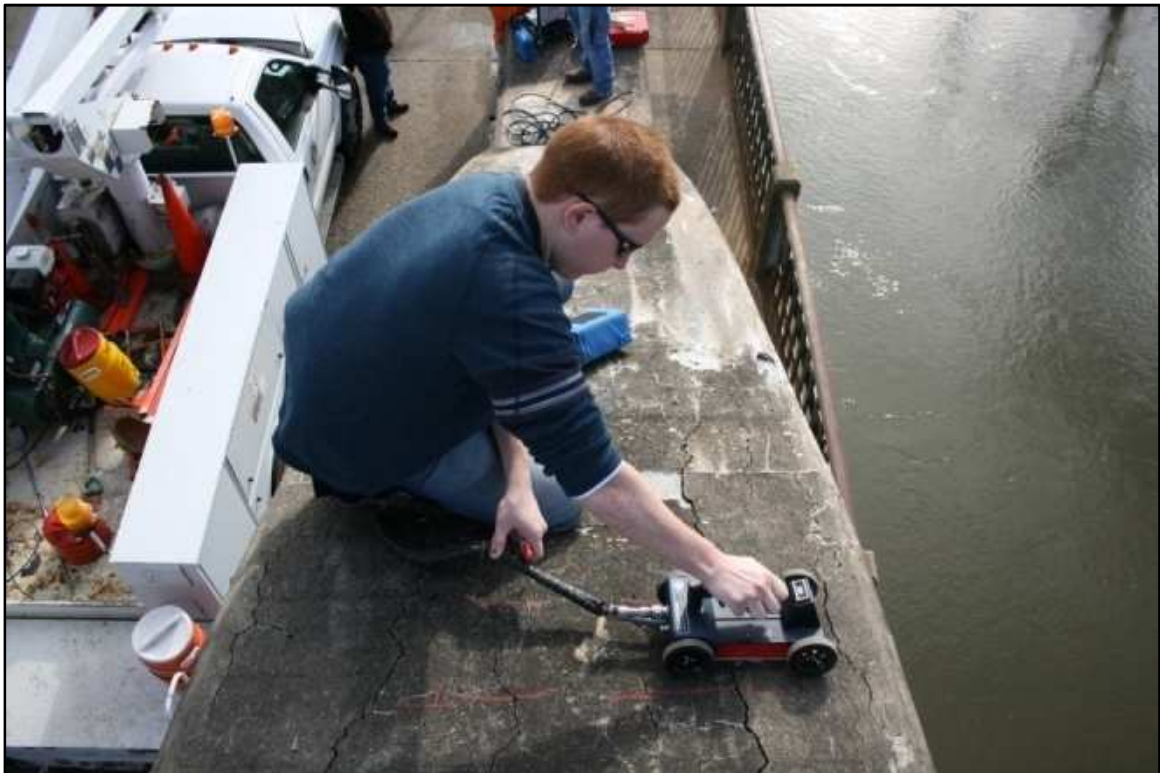


**Figure A.1:** Use of ground penetrating radar to locate rebar (ALDOT 2010)



**Figure A.2:** Close up of drilling interface (ALDOT 2010)



**Figure A.3:** Drilling for core specimen (ALDOT 2010)





**Figure A.4:** Close up of drilling process (ALDOT 2010)



**Figure A.5:** Core holes left after drilling (ALDOT 2010)



**Figure A.6:** Extraction of core samples (ALDOT 2010)



**Figure A.7:** Labeling of core samples (ALDOT 2010)





**Figure A.8:** Wrapping of core samples (ALDOT 2010)



**Figure A.9:** Packing of core sample for a) W.J.E. in Illinois and b) Laval University in Canada (ALDOT 2010)

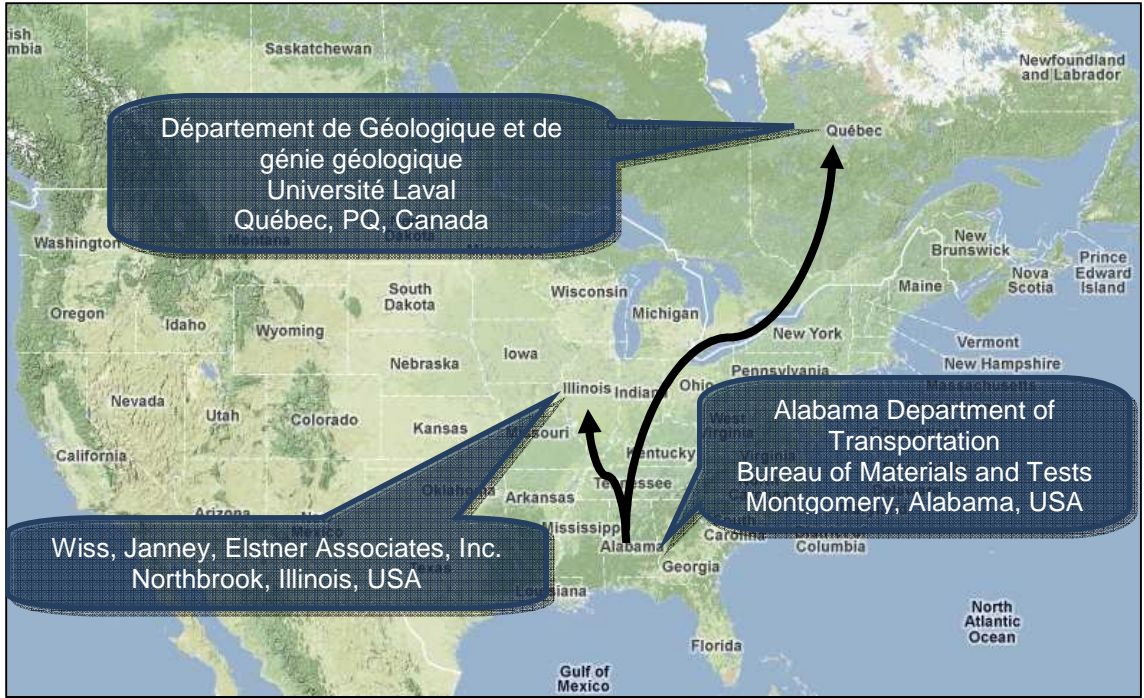


**Figure A.10:** Schematic of core shipping (ALDOT 2010)



Pictures of cores 1A-South and 2A-South are shown in Figure A.11 and A.12 respectively. Tables A.1 and A.2 summarize the core details for 1A-South and 2A-South.



**Figure A.11:** Core 1A – South (ALDOT 2010)

**Table A.1:** Information for 1A – South (ALDOT 2010)

| <b>Core Details</b> | <b>Core Information</b>  |
|---------------------|--|
| <b>ID</b>           | 1A - South   |
| <b>Location</b>     | South arch - Span 5. East side of arch. Approximately 17' 11" from top of pedestal.  |
| <b>Remarks</b>      | Full core extracted in two sections on 01/14/2010:<br>-Section 1: Approximately 4 ¼"<br>-Section 2: Approximately 4 ¾"<br>Red discoloration, if any, from labeling marker. |



**Figure A.12:** Core 2A – South (ALDOT 2010)

**Table A.2:** Information for Core 2A – South (ALDOT 2010)

| Core Details    | Core Information   |
|-----------------|--|
| <b>ID</b>       | 2A - South   |
| <b>Location</b> | South arch - Span 5. East side of arch. Approximately 17' 11" from top of pedestal.  |
| <b>Remarks</b>  | Full core extracted in three sections on 01/14/2010:<br>-Section 1: Approximately 3"<br>-Section 2: Approximately 6 ½"<br>-Section 3: Approximately 1"<br>Red discoloration, if any, from labeling marker. |

Pictures of cores 1B-South and 2B-South are shown in Figure A.13 and A.14 respectively. Tables A.3 and A.4 summarize the core details for 1B-South and 2B-South.



**Figure A.13:** Core 1B – South (ALDOT 2010)

**Table A.3:** Information for Core 1B – South (ALDOT 2010)

| <b>Core Details</b> | <b>Core Information</b>  |
|---------------------|--|
| <b>ID</b>           | 1B - South   |
| <b>Location</b>     | South arch - span 4. West side of arch.<br>Approximately 3' 6" from top of pedestal.   |
| <b>Remarks</b>      | Full core extracted in one section on 01/14/2010:<br>-Section 1: Approximately 10 ½"<br>Red discoloration, if any, from labeling marker. |



**Figure A.14:** Core 2B – South (ALDOT 2010)

**Table A.4:** Information for Core 2B – South (ALDOT 2010)

| <b>Core Details</b> | <b>Core Information</b>  |
|---------------------|--|
| <b>ID</b>           | 2B - South   |
| <b>Location</b>     | South arch - span 4. West side of arch.<br>Approximately 3' 6" from top of pedestal.   |
| <b>Remarks</b>      | Full core extracted in one section on 01/14/2010:<br>-Section 1: Approximately 10"<br>Red discoloration, if any, from labeling marker. |

Pictures of cores 1A-North and 2A-North are shown in Figure A.15 and A.16 respectively. Tables A.5 and A.6 summarize the core details for 1A-North and 2A-North.



**Figure A.15:** Core 1A – North (ALDOT 2010)

**Table A.5:** Information for 1A – North (ALDOT 2010)

| Core Details    | Core Information   |
|-----------------|--|
| <b>ID</b>       | 1A – North   |
| <b>Location</b> | North arch - Span 5. East side of arch.<br>Approximately 16' 3" from top of pedestal.  |
| <b>Remarks</b>  | Full core extracted in two sections on 01/14/2010:<br>-Section 1: Approximately 5 ¼"<br>-Section 2: Approximately 5 ½"<br>Red discoloration, if any, from labeling marker. |



**Figure A.16:** Core 2A – North (ALDOT 2010)

**Table A.6:** Information for 2A – North (ALDOT 2010)

| Core Details    | Core Information   |
|-----------------|--|
| <b>ID</b>       | 2A – North   |
| <b>Location</b> | North arch - Span 5. East side of arch.<br>Approximately 16' 3" from top of pedestal.  |
| <b>Remarks</b>  | Full core extracted in two sections on 01/14/2010:<br>-Section 1: Approximately 7"<br>-Section 2: Approximately 3 ¼"<br>Red discoloration, if any, from labeling marker. |



Pictures of cores 1B-North and 2B-North are shown in Figure A.17 and A.18 respectively. Tables A.7 and A.8 summarize the core details for 1B-North and 2B-North.



**Figure A.17:** Core 1B – North (ALDOT 2010)

**Table A.7:** Information for Core 1B – North (ALDOT 2010)

| Core Details    | Core Information   |
|-----------------|--|
| <b>ID</b>       | 1B – North   |
| <b>Location</b> | North arch - Span 4. West side of arch.<br>Approximately 3' 10" from top of pedestal.  |
| <b>Remarks</b>  | Full core extracted in one section on 01/14/2010:<br>-Section 1: Approximately 11 ¼"<br>Red discoloration, if any, from labeling marker. |



**Figure A.18:** Core 2B – North (ALDOT 2010)

**Table A.8:** Information for Core 2B – North (ALDOT 2010)

| Core Details    | Core Information   |
|-----------------|--|
| <b>ID</b>       | 2B – North   |
| <b>Location</b> | North arch - Span 4. West side of arch.<br>Approximately 3' 10" from top of pedestal.  |
| <b>Remarks</b>  | Full core extracted in one section on 01/14/2010:<br>-Section 1: Approximately 10"<br>Red discoloration, if any, from labeling marker. |



**Appendix B**  
**RH Survey Data**

This appendix contains the raw RH survey data that was taken on the Bibb Graves Bridge from November 16, 2010 to May 17, 2012.

The RH data per location for the average of all the depths, the 3-inch measurement depth, the 2 inch measurement depth, and the 1 inch measurement depth are summarized in Tables B.1 through B.4, respectively.

Collected RH data for all arches and measurement location that includes, temperature per reading, probes used for data collection, and time of day per reading are summarized in Tables B.5 through B.20.

**Table B.1:** RH data, average of all measurement depths

| Date           | Age<br>(Months) | West Bottom |       |       |       | West Top |       |       |       | East Bottom |       |       |       | East Top |       |       |       |
|----------------|-----------------|-------------|-------|-------|-------|----------|-------|-------|-------|-------------|-------|-------|-------|----------|-------|-------|-------|
|                |                 | 4 - S       | 4 - N | 5 - S | 5 - N | 4 - S    | 4 - N | 5 - S | 5 - N | 4 - S       | 4 - N | 5 - S | 5 - N | 4 - S    | 4 - N | 5 - S | 5 - N |
| 11/16/2010     | 0.0             | 88.1        | 88.0  | 94.3  | 69.7  | 78.2     | 79.3  | 89.1  | 80.8  | 84.8        | 86.5  | 88.8  | 93.4  | 79.9     | 82.8  | 92.3  | 89.7  |
| 2/15/2011      | 3.0             | 86.4        | 87.3  | 90.5  | 73.0  | 87.7     | 86.9  | 91.8  | 89.1  | 83.2        | 83.6  | 93.2  | 92.1  | 95.4     | 90.1  | 92.9  | 94.1  |
| 4/7/2011       | 4.7             | 88.6        | 88.1  | 95.4  | 75.2  | 89.4     | 91.4  | 93.4  | 92.2  | 85.6        | 85.3  | 95.5  | 94.1  | 93.9     | 92.0  | 93.6  | 92.2  |
| 5/5/2011       | 5.6             | 89.7        | 84.1  | 96.1  | 69.5  | 88.6     | 90.4  | 92.9  | 92.1  | 80.8        | 81.6  | 96.3  | 94.3  | 92.2     | 91.7  | 95.3  | 95.0  |
| 6/3/2011       | 6.5             | 83.0        | 85.3  | 93.6  | 74.9  | 89.4     | 87.7  | 93.9  | 92.9  | 88.6        | 83.9  | 93.6  | 91.5  | 92.3     | 89.5  | 93.3  | 90.8  |
| 7/7/2011       | 7.7             | 91.2        | 85.3  | 94.6  | 73.9  | 89.6     | 88.0  | 92.3  | 91.6  | 84.0        | 85.2  | 94.6  | 93.4  | 89.2     | 89.1  | 94.3  | 90.8  |
| 8/10/2011      | 8.8             | 89.4        | 85.4  | 93.0  | 73.2  | 88.4     | 86.3  | 92.1  | 91.0  | 88.2        | 84.8  | 93.5  | 93.9  | 89.5     | 87.7  | 94.2  | 91.8  |
| 9/15/2011      | 10.0            | 92.1        | 83.0  | 94.5  | 71.7  | 91.8     | 87.8  | 94.4  | 93.3  | 91.8        | 82.3  | 94.4  | 93.9  | 93.3     | 89.6  | 95.7  | 93.2  |
| 10/18/2011     | 11.0            | 85.9        | 78.5  | 91.5  | 64.9  | 82.4     | 84.4  | 90.6  | 89.7  | 79.5        | 76.5  | 91.5  | 89.4  | 84.8     | 87.6  | 90.5  | 90.7  |
| 11/8/2011      | 11.7            | 87.5        | 77.9  | 90.8  | 65.6  | 81.4     | 81.9  | 91.6  | 89.0  | 79.9        | 77.4  | 92.0  | 89.6  | 84.4     | 85.8  | 93.0  | 89.2  |
| 12/14/2011     | 12.9            | 82.5        | 73.0  | 88.3  | 63.8  | 81.5     | 84.7  | 89.5  | 89.6  | 73.0        | 74.2  | 89.4  | 89.6  | 84.1     | 86.2  | 89.4  | 87.4  |
| 1/31/2012      | 14.5            | 82.7        | 77.9  | 86.9  | 74.3  | 81.4     | 85.5  | 89.1  | 89.6  | 76.5        | 73.6  | 86.9  | 88.7  | 84.6     | 83.3  | 90.9  | 88.0  |
| 3/8/2012       | 15.7            | 86.5        | 81.2  | 90.5  | 79.5  | 87.0     | 88.4  | 90.7  | 91.4  | 81.9        | 78.6  | 91.4  | 91.1  | 86.8     | 87.8  | 92.8  | 89.1  |
| 4/12/2012      | 16.9            | 89.4        | 76.7  | 93.9  | 73.2  | 87.3     | 87.6  | 92.1  | 90.2  | 85.1        | 75.9  | 93.9  | 92.8  | 85.0     | 89.5  | 92.2  | 87.6  |
| 5/17/2012      | 18.0            | 85.8        | 83.4  | 92.2  | 73.8  | 82.8     | 87.1  | 90.0  | 88.0  | 79.4        | 79.2  | 92.3  | 89.9  | 85.1     | 88.3  | 89.2  | 84.8  |
| <i>Average</i> | -               | 87.3        | 82.3  | 92.4  | 71.8  | 85.8     | 86.5  | 91.6  | 90.0  | 82.8        | 80.6  | 92.5  | 91.9  | 88.0     | 88.1  | 92.6  | 90.3  |

**Table B.2:** RH data, 3-inch measurement depth

| Date       | Age<br>(Months) | West Bottom |       |       |       | West Top |       |       |       | East Bottom |       |       |       | East Top |       |       |       |
|------------|-----------------|-------------|-------|-------|-------|----------|-------|-------|-------|-------------|-------|-------|-------|----------|-------|-------|-------|
|            |                 | 4 - S       | 4 - N | 5 - S | 5 - N | 4 - S    | 4 - N | 5 - S | 5 - N | 4 - S       | 4 - N | 5 - S | 5 - N | 4 - S    | 4 - N | 5 - S | 5 - N |
| 11/16/2010 | 0.0             | 89.0        | 93.4  | 95.2  | 73.8  | 84.3     | 91.2  | 91.2  | 78.9  | 91.8        | 88.4  | 86.8  | 95.3  | 81.3     | 92.3  | 90.1  | 83.3  |
| 2/15/2011  | 3.0             | 86.9        | 85.7  | 92.3  | 68.5  | 87.3     | 89.2  | 94.9  | 90.1  | 84.7        | 83.0  | 93.8  | 97.0  | 94.3     | 91.0  | 94.9  | 89.6  |
| 4/7/2011   | 4.7             | 88.3        | 86.9  | 96.7  | 75.7  | 87.8     | 91.9  | 95.9  | 90.8  | 84.0        | 85.2  | 97.5  | 95.7  | 90.2     | 93.4  | 93.6  | 88.0  |
| 5/5/2011   | 5.6             | 89.6        | 86.0  | 97.4  | 70.6  | 84.4     | 89.9  | 93.2  | 88.7  | 82.0        | 80.7  | 97.3  | 96.4  | 88.1     | 89.4  | 96.8  | 91.2  |
| 6/3/2011   | 6.5             | 82.4        | 87.1  | 94.8  | 76.3  | 85.3     | 90.0  | 92.1  | 91.6  | 88.7        | 85.1  | 95.2  | 93.7  | 90.4     | 89.9  | 90.9  | 84.8  |
| 7/7/2011   | 7.7             | 90.0        | 85.8  | 94.6  | 75.6  | 87.5     | 92.1  | 91.5  | 91.7  | 87.9        | 84.7  | 94.9  | 93.4  | 88.2     | 91.4  | 94.8  | 86.7  |
| 8/10/2011  | 8.8             | 90.1        | 86.6  | 93.7  | 74.8  | 85.7     | 92.4  | 92.8  | 91.6  | 89.2        | 83.2  | 93.9  | 95.0  | 91.1     | 93.0  | 93.1  | 90.4  |
| 9/15/2011  | 10.0            | 90.8        | 84.9  | 94.8  | 73.7  | 92.9     | 89.3  | 92.8  | 93.1  | 89.6        | 82.4  | 94.9  | 93.4  | 93.1     | 91.8  | 95.9  | 92.7  |
| 10/18/2011 | 11.0            | 83.6        | 78.3  | 92.7  | 66.8  | 88.5     | 90.2  | 92.8  | 89.8  | 80.8        | 76.3  | 90.4  | 89.0  | 86.8     | 89.7  | 85.7  | 89.0  |
| 11/8/2011  | 11.7            | 84.8        | 77.1  | 90.6  | 68.2  | 84.6     | 86.9  | 89.9  | 89.6  | 80.6        | 77.7  | 92.5  | 90.1  | 87.3     | 89.6  | 93.2  | 83.2  |
| 12/14/2011 | 12.9            | 83.4        | 74.8  | 89.0  | 65.4  | 86.4     | 89.4  | 92.2  | 90.2  | 74.8        | 74.2  | 90.7  | 90.4  | 85.5     | 90.4  | 88.6  | 81.6  |
| 1/31/2012  | 14.5            | 82.6        | 84.5  | 86.2  | 66.1  | 84.8     | 89.0  | 89.9  | 90.8  | 78.4        | 73.8  | 91.4  | 91.7  | 85.6     | 89.0  | 92.1  | 89.7  |
| 3/8/2012   | 15.7            | 85.8        | 83.3  | 91.4  | 74.5  | 87.7     | 92.2  | 89.6  | 91.7  | 82.3        | 78.0  | 92.9  | 92.5  | 89.3     | 90.5  | 92.2  | 86.1  |
| 4/12/2012  | 16.9            | 92.5        | 79.6  | 93.9  | 66.4  | 88.0     | 93.1  | 89.4  | 87.6  | 87.6        | 75.3  | 94.7  | 93.8  | 84.8     | 89.9  | 89.5  | 79.8  |
| 5/17/2012  | 18.0            | 85.6        | 83.2  | 92.7  | 72.7  | 89.0     | 92.4  | 88.3  | 89.0  | 80.6        | 80.3  | 93.4  | 91.2  | 88.0     | 89.3  | 85.9  | 78.8  |
| Average    | -               | 87.0        | 83.8  | 93.1  | 71.3  | 86.9     | 90.6  | 91.8  | 89.7  | 84.2        | 80.6  | 93.4  | 93.2  | 88.3     | 90.7  | 91.8  | 86.3  |

**Table B.3:** RH data, 2 inch measurement depth

| Date           | Age<br>(Months) | West Bottom |       |       |       | West Top |       |       |       | East Bottom |       |       |       | East Top |       |       |       |
|----------------|-----------------|-------------|-------|-------|-------|----------|-------|-------|-------|-------------|-------|-------|-------|----------|-------|-------|-------|
|                |                 | 4 - S       | 4 - N | 5 - S | 5 - N | 4 - S    | 4 - N | 5 - S | 5 - N | 4 - S       | 4 - N | 5 - S | 5 - N | 4 - S    | 4 - N | 5 - S | 5 - N |
| 11/16/2010     | 0.0             | 88.5        | 89.4  | 94.7  | 70.2  | 75.8     | 81.0  | 91.8  | 82.5  | 85.2        | 85.3  | 89.9  | 94.0  | 85.5     | 81.0  | 93.6  | 90.4  |
| 2/15/2011      | 3.0             | 89.4        | 88.7  | 91.2  | 74.3  | 81.2     | 87.6  | 91.6  | 88.1  | 84.7        | 85.0  | 96.2  | 92.3  | 95.5     | 93.2  | 90.3  | 95.0  |
| 4/7/2011       | 4.7             | 92.2        | 88.2  | 96.2  | 76.7  | 85.4     | 90.2  | 91.7  | 94.0  | 86.5        | 83.9  | 96.6  | 95.0  | 95.0     | 96.0  | 93.1  | 92.9  |
| 5/5/2011       | 5.6             | 91.5        | 85.1  | 94.8  | 69.3  | 85.5     | 92.4  | 91.7  | 91.3  | 83.1        | 78.7  | 96.1  | 93.3  | 92.4     | 96.5  | 93.9  | 95.9  |
| 6/3/2011       | 6.5             | 84.9        | 86.4  | 92.2  | 75.3  | 88.1     | 89.2  | 92.7  | 91.9  | 91.0        | 82.2  | 94.9  | 92.4  | 93.7     | 91.5  | 92.0  | 91.7  |
| 7/7/2011       | 7.7             | 92.3        | 85.3  | 95.1  | 74.4  | 90.0     | 88.6  | 92.3  | 90.9  | 84.2        | 82.5  | 95.2  | 94.3  | 88.8     | 92.3  | 92.1  | 92.1  |
| 8/10/2011      | 8.8             | 90.3        | 85.5  | 94.1  | 74.0  | 85.9     | 86.3  | 90.8  | 90.4  | 90.8        | 83.2  | 93.3  | 93.6  | 85.2     | 93.2  | 94.1  | 91.7  |
| 9/15/2011      | 10.0            | 92.9        | 84.2  | 94.0  | 71.7  | 90.1     | 90.2  | 94.4  | 93.5  | 92.9        | 78.2  | 94.5  | 94.0  | 92.2     | 92.5  | 95.4  | 93.7  |
| 10/18/2011     | 11.0            | 89.9        | 81.0  | 94.0  | 66.5  | 82.0     | 85.8  | 87.7  | 91.2  | 83.5        | 74.7  | 93.4  | 91.6  | 87.3     | 92.5  | 92.3  | 92.0  |
| 11/8/2011      | 11.7            | 91.3        | 81.7  | 91.1  | 67.5  | 81.4     | 83.8  | 91.9  | 89.8  | 85.0        | 76.1  | 94.4  | 90.7  | 87.2     | 86.1  | 92.6  | 91.7  |
| 12/14/2011     | 12.9            | 84.7        | 75.4  | 89.1  | 65.7  | 79.7     | 87.4  | 90.8  | 89.8  | 75.4        | 75.0  | 89.3  | 90.5  | 83.8     | 86.7  | 89.9  | 91.1  |
| 1/31/2012      | 14.5            | 85.5        | 76.1  | 89.5  | 79.0  | 81.0     | 86.2  | 89.1  | 90.5  | 77.7        | 71.9  | 82.0  | 89.1  | 85.7     | 84.4  | 92.4  | 84.2  |
| 3/8/2012       | 15.7            | 88.1        | 81.7  | 90.6  | 82.5  | 84.1     | 88.3  | 91.1  | 90.7  | 83.1        | 77.6  | 90.9  | 92.0  | 88.6     | 87.6  | 92.8  | 88.4  |
| 4/12/2012      | 16.9            | 91.9        | 76.0  | 94.4  | 80.3  | 86.0     | 90.4  | 92.5  | 89.2  | 90.4        | 68.0  | 94.2  | 93.1  | 83.5     | 90.1  | 92.1  | 88.4  |
| 5/17/2012      | 18.0            | 87.1        | 82.6  | 93.1  | 78.4  | 79.4     | 89.9  | 90.4  | 88.0  | 80.8        | 75.1  | 92.1  | 90.7  | 83.8     | 88.3  | 88.2  | 85.6  |
| <i>Average</i> | -               | 89.4        | 83.2  | 92.9  | 73.7  | 83.7     | 87.8  | 91.4  | 90.1  | 85.0        | 78.5  | 92.9  | 92.4  | 88.5     | 90.1  | 92.3  | 91.0  |

**Table B.4:** RH data, 1 inch measurement depth

| Date           | Age<br>(Months) | West Bottom |             |             |             | West Top    |             |             |             | East Bottom |             |             |             | East Top    |             |             |             |
|----------------|-----------------|-------------|-------------|-------------|-------------|-------------|-------------|-------------|-------------|-------------|-------------|-------------|-------------|-------------|-------------|-------------|-------------|
|                |                 | 4 - S       | 4 - N       | 5 - S       | 5 - N       | 4 - S       | 4 - N       | 5 - S       | 5 - N       | 4 - S       | 4 - N       | 5 - S       | 5 - N       | 4 - S       | 4 - N       | 5 - S       | 5 - N       |
| 11/16/2010     | 0.0             | 86.8        | 81.3        | 93.0        | 65.0        | 74.6        | 65.8        | 84.2        | 81.0        | 77.4        | 85.8        | 89.6        | 91.0        | 72.8        | 75.1        | 93.2        | 95.4        |
| 2/15/2011      | 3.0             | 83.0        | 87.5        | 88.1        | 76.2        | 94.5        | 84.0        | 89.0        | 89.1        | 80.1        | 82.8        | 89.5        | 87.1        | 96.3        | 86.1        | 93.5        | 97.7        |
| 4/7/2011       | 4.7             | 85.4        | 89.1        | 93.2        | 73.2        | 95.1        | 92.1        | 92.7        | 91.7        | 86.2        | 86.7        | 92.3        | 91.5        | 96.4        | 86.6        | 94.1        | 95.8        |
| 5/5/2011       | 5.6             | 87.9        | 81.2        | 96.0        | 68.7        | 95.8        | 88.8        | 93.9        | 96.3        | 77.4        | 85.5        | 95.5        | 93.2        | 96.1        | 89.3        | 95.2        | 97.8        |
| 6/3/2011       | 6.5             | 81.7        | 82.3        | 93.8        | 73.1        | 94.9        | 84.0        | 97.0        | 95.1        | 86.1        | 84.4        | 90.8        | 88.3        | 92.9        | 87.0        | 97.0        | 95.8        |
| 7/7/2011       | 7.7             | 91.2        | 84.7        | 94.2        | 71.8        | 91.4        | 83.3        | 93.0        | 92.3        | 79.8        | 88.4        | 93.6        | 92.5        | 90.5        | 83.7        | 96.1        | 93.5        |
| 8/10/2011      | 8.8             | 87.8        | 84.1        | 91.3        | 70.7        | 93.7        | 80.3        | 92.8        | 91.1        | 84.7        | 88.1        | 93.4        | 93.2        | 92.2        | 76.8        | 95.3        | 93.3        |
| 9/15/2011      | 10.0            | 92.5        | 79.8        | 94.7        | 69.6        | 92.5        | 83.9        | 96.0        | 93.2        | 92.9        | 86.2        | 93.8        | 94.2        | 94.7        | 84.6        | 0.0         | 0.0         |
| 10/18/2011     | 11.0            | 84.3        | 76.2        | 87.8        | 61.4        | 76.7        | 77.2        | 91.3        | 88.1        | 74.3        | 78.5        | 90.8        | 87.7        | 80.2        | 80.5        | 93.5        | 91.0        |
| 11/8/2011      | 11.7            | 86.5        | 74.8        | 90.6        | 61.2        | 78.2        | 75.0        | 93.1        | 87.5        | 74.0        | 78.4        | 89.2        | 88.1        | 78.6        | 81.6        | 93.1        | 92.7        |
| 12/14/2011     | 12.9            | 79.5        | 68.8        | 86.7        | 60.2        | 78.4        | 77.4        | 85.5        | 88.7        | 68.8        | 73.3        | 88.1        | 87.9        | 83.1        | 81.5        | 89.6        | 89.4        |
| 1/31/2012      | 14.5            | 80.0        | 73.1        | 85.1        | 77.9        | 78.5        | 81.3        | 88.3        | 87.5        | 73.3        | 75.0        | 87.2        | 85.3        | 82.4        | 76.4        | 88.1        | 90.2        |
| 3/8/2012       | 15.7            | 85.6        | 78.5        | 89.4        | 81.6        | 89.1        | 84.8        | 91.5        | 91.8        | 80.3        | 80.3        | 90.5        | 88.8        | 82.4        | 85.2        | 93.3        | 92.7        |
| 4/12/2012      | 16.9            | 83.7        | 74.5        | 93.4        | 72.9        | 88.0        | 79.3        | 94.3        | 93.7        | 77.2        | 84.3        | 92.8        | 91.5        | 86.7        | 88.6        | 95.0        | 94.7        |
| 5/17/2012      | 18.0            | 84.6        | 84.4        | 90.9        | 70.4        | 80.1        | 78.9        | 91.2        | 86.9        | 76.9        | 82.3        | 91.5        | 87.8        | 83.5        | 87.3        | 93.6        | 89.9        |
| <i>Average</i> | -               | <i>85.4</i> | <i>80.0</i> | <i>91.2</i> | <i>70.3</i> | <i>86.8</i> | <i>81.1</i> | <i>91.6</i> | <i>90.3</i> | <i>79.3</i> | <i>82.7</i> | <i>91.2</i> | <i>89.9</i> | <i>87.3</i> | <i>83.4</i> | <i>87.4</i> | <i>87.3</i> |

**Table B.5:** 4-S-WT raw RH data

| Date       | Time In | Time Out | Depth: 1" |      |      | Depth: 2" |      |      | Depth: 3" |      |      |
|------------|---------|----------|-----------|------|------|-----------|------|------|-----------|------|------|
|            |         |          | Probe     | °C   | RH%  | Probe     | °C   | RH%  | Probe     | °C   | RH%  |
| 11/16/2010 | 10:15   | 11:15    | UT 1.7    | 18   | 74.6 | UT 1.8    | 15.7 | 75.8 | UT 1.4    | 14.2 | 84.3 |
| 2/15/2011  | 1:55    | 3:00     | 1         | 24.2 | 94.5 | 2         | 23   | 81.2 | 6         | 21.6 | 87.3 |
| 4/7/2011   | 12:50   | 1:45     | 3         | 29.8 | 95.1 | 9         | 28.2 | 85.4 | 5         | 27   | 87.8 |
| 5/5/2011   | 2:00    | 3:00     | 2         | 31.7 | 95.8 | 9         | 31.9 | 85.5 | 10        | 30.6 | 84.4 |
| 6/3/2011   | 1:45    | 2:35     | 3         | 47.6 | 94.9 | 8         | 46.7 | 88.1 | 4         | 46.3 | 85.3 |
| 7/7/2011   | 11:40   | 12:40    | 7         | 40.9 | 91.4 | 5         | 39.9 | 90   | 3         | 38.8 | 87.5 |
| 8/10/2011  | 11:50   | 12:40    | 8         | 39.1 | 93.7 | 1         | 38.2 | 85.9 | 9         | 36.9 | 85.7 |
| 9/15/2011  | 1:30    | 2:30     | 9         | 25.7 | 92.5 | 2         | 27.7 | 90.1 | 10        | 28.8 | 92.9 |
| 10/18/2011 | 1:20    | 2:10     | 3         | 33   | 76.7 | 9         | 30.6 | 82   | 10        | 29   | 88.5 |
| 11/8/2011  | 1:20    | 2:10     | 5         | 28.2 | 78.2 | 6         | 27.3 | 81.4 | 3         | 26.4 | 84.6 |
| 12/14/2011 | 3:00    | 4:00     | 3         | 20.7 | 78.4 | 9         | 19   | 79.7 | 1         | 17.7 | 86.4 |
| 1/31/2012  | 2:20    | 3:20     | 1         | 22.3 | 78.5 | 6         | 20.3 | 81   | 4         | 19.8 | 84.8 |
| 3/8/2012   | 2:10    | 3:10     | 7         | 28.8 | 89.1 | 1         | 27.8 | 84.1 | 4         | 27.4 | 87.7 |
| 4/12/2012  | 2:40    | 3:30     | 10        | 28.2 | 88   | 4         | 29.1 | 86   | 6         | 28   | 88   |
| 5/17/2012  | 9:45    | 10:40    | 3         | 31.4 | 80.1 | 5         | 29.8 | 79.4 | 1         | 28.6 | 89   |

UT – University of Texas Probe

**Table B.6:** 4-S-WB raw RH data

| Date       | Time In | Time Out | Depth: 1" |      |      | Depth: 2" |      |      | Depth: 3" |      |      |
|------------|---------|----------|-----------|------|------|-----------|------|------|-----------|------|------|
|            |         |          | Probe     | °C   | RH%  | Probe     | °C   | RH%  | Probe     | °C   | RH%  |
| 11/16/2010 | 11:30   | 12:30    | UT 1.7    | 15.8 | 86.8 | UT 1.4    | 15.7 | 88.5 | UT 1.8    | 15   | 89   |
| 2/15/2011  | 3:10    | 4:10     | 4         | 18.5 | 83   | 2         | 16.8 | 89.4 | 7         | 16.4 | 86.9 |
| 4/7/2011   | 1:50    | 2:50     | 9         | 22.2 | 85.4 | 5         | 20.6 | 92.2 | 10        | 20.5 | 88.3 |
| 5/5/2011   | 12:55   | 1:55     | 9         | 19.7 | 87.9 | 2         | 18.7 | 91.5 | 6         | 18.7 | 89.6 |
| 6/3/2011   | 1:40    | 2:30     | 7         | 35.4 | 81.7 | 5         | 34.7 | 84.9 | 6         | 34.5 | 82.4 |
| 7/7/2011   | 10:30   | 11:35    | 5         | 31.7 | 91.2 | 7         | 31.3 | 92.3 | 3         | 31.4 | 90   |
| 8/10/2011  | 10:40   | 11:40    | 9         | 29.2 | 87.8 | 1         | 28.2 | 90.3 | 8         | 28   | 90.1 |
| 9/15/2011  | 12:30   | 1:20     | 10        | 25.2 | 92.5 | 9         | 26.2 | 92.9 | 2         | 26.4 | 90.8 |
| 10/18/2011 | 2:15    | 3:15     | 1         | 26.2 | 84.3 | 6         | 24.9 | 89.9 | 7         | 24.7 | 83.6 |
| 11/8/2011  | 12:20   | 1:15     | 9         | 23   | 86.5 | 8         | 21.9 | 91.3 | 4         | 21.8 | 84.8 |
| 12/14/2011 | 10:30   | 11:30    | 3         | 16.8 | 79.5 | 7         | 15.1 | 84.7 | 7         | 16.1 | 83.4 |
| 1/31/2012  | 1:30    | 2:30     | 3         | 17.7 | 80   | 1         | 15.5 | 85.5 | 8         | 15.1 | 82.6 |
| 3/8/2012   | 2:10    | 3:10     | 3         | 24.6 | 85.6 | 5         | 23.1 | 88.1 | 9         | 23.1 | 85.8 |
| 4/12/2012  | 2:40    | 3:30     | 1         | 19.7 | 83.7 | 2         | 18.6 | 91.9 | 7         | 18.3 | 92.5 |
| 5/17/2012  | 12:10   | 1:25     | 9         | 28.8 | 84.6 | 7         | 27.8 | 87.1 | 2         | 27.7 | 85.6 |

UT – University of Texas Probe

**Table B.7:** 4-S-ET raw RH data

| Date       | Time In    | Time Out  | Depth: 1" |      |      | Depth: 2" |      |      | Depth: 3" |      |      |
|------------|------------|-----------|-----------|------|------|-----------|------|------|-----------|------|------|
|            |            |           | Probe     | °C   | RH%  | Probe     | °C   | RH%  | Probe     | °C   | RH%  |
| 11/16/2010 | 8:35       | 9:50      | UT 1.5    | 18.5 | 72.8 | UT 1.3    | 18.2 | 85.5 | UT 1.1    | 17.9 | 81.3 |
| 2/15/2011  | 2:00/3:05  | 3:05/4:05 | 9         | 25.1 | 96.3 | 9         | 22.8 | 95.5 | 1         | 22.7 | 94.3 |
| 4/7/2011   | 12:50/1:50 | 1:45/2:45 | 1         | 31.5 | 96.4 | 3         | 32.6 | 95   | 1         | 31.6 | 90.2 |
| 5/5/2011   | 2:00       | 3:00      | 4         | 32.4 | 96.1 | 1         | 32.2 | 92.4 | 6         | 32   | 88.1 |
| 6/3/2011   | 1:45       | 2:40      | 10        | 45.8 | 92.9 | 2         | 47.1 | 93.7 | 1         | 47.3 | 90.4 |
| 7/7/2011   | 11:40      | 12:40     | 8         | 43.6 | 90.5 | 4         | 43.8 | 88.8 | 10        | 42.7 | 88.2 |
| 8/10/2011  | 11:50      | 12:40     | 7         | 41.8 | 92.2 | 3         | 43.1 | 85.2 | 6         | 41.5 | 91.1 |
| 9/15/2011  | 1:30       | 2:30      | 7         | 27.2 | 94.7 | 8         | 28.8 | 92.2 | 1         | 29.6 | 93.1 |
| 10/18/2011 | 1:20/2:10  | 2:10/3:15 | 2         | 34.5 | 80.2 | 2         | 34.4 | 87.3 | 3         | 34.1 | 86.8 |
| 11/8/2011  | 1:20       | 2:10      | 5         | 29.2 | 78.6 | 9         | 28.5 | 87.2 | 2         | 28.2 | 87.3 |
| 12/14/2011 | 11:30      | 12:40     | 9         | 25   | 83.1 | 5         | 23.8 | 83.8 | 3         | 22.7 | 85.5 |
| 1/31/2012  | 2:30       | 3:30      | 9         | 21.7 | 82.4 | 5         | 20.3 | 85.7 | 3         | 19.4 | 85.6 |
| 3/8/2012   | 2:10       | 3:10      | 10        | 29.5 | 82.4 | 6         | 27.6 | 88.6 | 2         | 27.4 | 89.3 |
| 4/12/2012  | 2:40       | 3:30      | 3         | 30.3 | 86.7 | 9         | 30.2 | 83.5 | 5         | 29.7 | 84.8 |
| 5/17/2012  | 9:45       | 10:40     | 6         | 34.8 | 83.5 | 10        | 35.1 | 83.8 | 4         | 34.5 | 88   |

UT – University of Texas Probe



**Table B.8:** 4-S-EB raw RH data

| Date       | Time In | Time Out | Depth: 1" |      |      | Depth: 2" |      |      | Depth: 3" |      |      |
|------------|---------|----------|-----------|------|------|-----------|------|------|-----------|------|------|
|            |         |          | Probe     | °C   | RH%  | Probe     | °C   | RH%  | Probe     | °C   | RH%  |
| 11/16/2010 | 1:35    | 2:35     | 6         | 16.7 | 77.4 | 3         | 16.1 | 85.2 | 4         | 15.8 | 91.8 |
| 2/15/2011  | 3:15    | 4:15     | 6         | 19.8 | 80.1 | 3         | 17.8 | 84.7 | 5         | 17   | 84.7 |
| 4/7/2011   | 1:50    | 2:50     | 2         | 22.3 | 86.2 | 6         | 21.2 | 86.5 | 4         | 20.6 | 84   |
| 5/5/2011   | 12:05   | 1:55     | 8         | 20.1 | 77.4 | 5         | 19.3 | 83.1 | 10        | 18.9 | 82   |
| 6/3/2011   | 12:30   | 1:30     | 4         | 35   | 86.1 | 8         | 334  | 91   | 3         | 34   | 88.7 |
| 7/7/2011   | 10:30   | 11:35    | 10        | 32.2 | 79.8 | 4         | 31.7 | 84.2 | 8         | 31.5 | 87.9 |
| 8/10/2011  | 10:45   | 11:45    | 4         | 29.8 | 84.7 | 2         | 28.9 | 90.8 | 3         | 28.5 | 89.2 |
| 9/15/2011  | 12:30   | 1:25     | 8         | 25.1 | 92.9 | 7         | 26.3 | 92.9 | 1         | 26.8 | 89.6 |
| 10/18/2011 | 2:15    | 3:15     | 5         | 26.3 | 74.3 | 8*        | 25.8 | 83.5 | 4         | 25.3 | 80.8 |
| 11/8/2011  | 12:20   | 1:15     | 3         | 23   | 74   | 5         | 22.1 | 85   | 10        | 21.8 | 80.6 |
| 12/14/2011 | 11:30   | 12:40    | 2         | 18.5 | 68.8 | 6         | 16.7 | 75.4 | 4         | 16.3 | 74.8 |
| 1/31/2012  | 1:30    | 2:30     | 9         | 18.1 | 73.3 | 5         | 15.6 | 77.7 | 10        | 14.7 | 78.4 |
| 3/8/2012   | 3:20    | 4:20     | 3         | 25   | 80.3 | 5         | 23.9 | 83.1 | 9         | 23.6 | 82.3 |
| 4/12/2012  | 3:40    | 4:30     | 1         | 20.5 | 77.2 | 7         | 19.8 | 90.4 | 2         | 19.6 | 87.6 |
| 5/17/2012  | 12:15   | 1:25     | 5         | 28.8 | 76.9 | 1         | 28.2 | 80.8 | 4         | 27.9 | 80.6 |

\* Damaged Probe

**Table B.9:** 4-N-WT raw RH data

| Date       | Time In     | Time Out    | Depth: 1" |      |      | Depth: 2" |      |      | Depth: 3" |      |      |
|------------|-------------|-------------|-----------|------|------|-----------|------|------|-----------|------|------|
|            |             |             | Probe     | °C   | RH%  | Probe     | °C   | RH%  | Probe     | °C   | RH%  |
| 11/16/2010 | 8:30        | 9:30        | UT 1.4    | 15.1 | 65.8 | UT 1.7    | 12.7 | 81   | UT 1.8    | 11.3 | 91.2 |
| 2/15/2011  | 10:25/11:25 | 11:25/12:25 | 6         | 21.7 | 84   | 1         | 17.5 | 87.6 | 6         | 14.1 | 89.2 |
| 4/7/2011   | 9:30        | 10:30       | 3         | 21.1 | 92.1 | 2         | 19.7 | 90.2 | 10        | 18.7 | 91.9 |
| 5/5/2011   | 9:45/10:45  | 10:45/11:40 | 4         | 21.7 | 88.8 | 4         | 22.3 | 92.4 | 1         | 21   | 89.9 |
| 6/3/2011   | 9:30        | 10:30       | 8         | 36.4 | 84   | 5         | 35.2 | 89.2 | 1         | 34.7 | 90   |
| 7/7/2011   | 7:15/8:25   | 8:15/9:25   | 1         | 31.2 | 83.3 | 2         | 32.6 | 88.6 | 1         | 31.2 | 92.1 |
| 8/10/2011  | 7:30/8:30   | 8:30/9:30   | 9         | 27.1 | 80.3 | 9         | 28.4 | 86.3 | 8         | 26.8 | 92.4 |
| 9/15/2011  | 9:30/10:25  | 10:25/11:20 | 3         | 27.7 | 83.9 | 3         | 28.6 | 90.2 | 5         | 28.8 | 89.3 |
| 10/18/2011 | 9:50/10:50  | 10:50/11:40 | 2         | 26.1 | 77.2 | 2         | 25.2 | 85.8 | 9         | 23.9 | 90.2 |
| 11/8/2011  | 9:20/10:30  | 10:10/11:10 | 6         | 24.8 | 75   | 6         | 23.1 | 83.8 | 2         | 22.3 | 86.9 |
| 12/14/2011 | 3:00        | 4:00        | 10        | 21.1 | 77.4 | 7         | 19.1 | 87.4 | 6         | 18   | 89.4 |
| 1/31/2012  | 10:00/11:00 | 11:00/12:00 | 3         | 16.5 | 81.3 | 9         | 14.2 | 86.2 | 9         | 10.9 | 89   |
| 3/8/2012   | 11:00       | 12:00       | 3         | 25.6 | 84.8 | 5         | 24.4 | 88.3 | 6         | 23.2 | 92.2 |
| 4/12/2012  | 10:00       | 10:50       | 9         | 20.9 | 79.3 | 5         | 18   | 90.4 | 4         | 17   | 93.1 |
| 5/17/2012  | 8:40        | 9:35        | 3         | 30.8 | 78.9 | 4         | 28   | 89.9 | 1         | 26.8 | 92.4 |

UT – University of Texas Probe

**Table B.10:** 4-N-WB raw RH data

| Date       | Time In | Time Out | Depth: 1" |      |      | Depth: 2" |      |      | Depth: 3" |      |      |
|------------|---------|----------|-----------|------|------|-----------|------|------|-----------|------|------|
|            |         |          | Probe     | °C   | RH%  | Probe     | °C   | RH%  | Probe     | °C   | RH%  |
| 11/16/2010 | 12:30   | 1:30     | 4         | 15.6 | 81.3 | 3         | 14.9 | 89.4 | 6         | 14.8 | 93.4 |
| 2/15/2011  | 10:10   | 1:10     | 4         | 13.7 | 87.5 | 8         | 12.4 | 88.7 | 9         | 12.2 | 85.7 |
| 4/7/2011   | 9:30    | 10:30    | 1         | 17.5 | 89.1 | 6         | 17.1 | 88.2 | 8         | 17   | 86.9 |
| 5/5/2011   | 9:45    | 10:50    | 6         | 16.6 | 81.2 | 2         | 16.4 | 85.1 | 3         | 16.5 | 86   |
| 6/3/2011   | 9:30    | 10:25    | 7         | 31.8 | 82.3 | 3         | 32   | 86.4 | 2         | 31.9 | 87.1 |
| 7/7/2011   | 7:15    | 8:15     | 9         | 29.8 | 84.7 | 7         | 30.1 | 85.3 | 6         | 30.2 | 85.8 |
| 8/10/2011  | 7:30    | 8:30     | 5         | 25.3 | 84.1 | 1         | 25.7 | 85.5 | 7         | 25.7 | 86.6 |
| 9/15/2011  | 9:30    | 10:25    | 2         | 26.5 | 79.8 | 9         | 26.9 | 84.2 | 8         | 27   | 84.9 |
| 10/18/2011 | 9:40    | 10:30    | 6         | 22.6 | 76.2 | 4         | 22   | 81   | 5         | 21.8 | 78.3 |
| 11/8/2011  | 9:20    | 10:10    | 9         | 20.6 | 74.8 | 8         | 20   | 81.7 | 3         | 20   | 77.1 |
| 12/14/2011 | 12:55   | 1:45     | 5         | 18.5 | 68.8 | 6         | 16.7 | 75.4 | 4         | 16.3 | 74.8 |
| 1/31/2012  | 10:00   | 11:00    | 10        | 11.8 | 73.1 | 2         | 10.5 | 76.1 | 1         | 10.1 | 84.5 |
| 3/8/2012   | 9:45    | 10:45    | 3         | 20.6 | 78.5 | 4         | 19.8 | 81.7 | 5         | 19.5 | 83.3 |
| 4/12/2012  | 10:00   | 10:50    | 3         | 15.5 | 74.5 | 2         | 15.5 | 76   | 7         | 15.6 | 79.6 |
| 5/17/2012  | 2:40    | 3:35     | 5         | 29.1 | 84.4 | 1         | 28.8 | 82.6 | 4         | 28.8 | 83.2 |

**Table B.11: 4-N-ET raw RH data**

| Date       | Time In    | Time Out    | Depth: 1" |      |      | Depth: 2" |      |      | Depth: 3" |      |      |
|------------|------------|-------------|-----------|------|------|-----------|------|------|-----------|------|------|
|            |            |             | Probe     | °C   | RH%  | Probe     | °C   | RH%  | Probe     | °C   | RH%  |
| 11/16/2010 | 8:35       | 9:35        | 1         | 18.5 | 75.1 | 2         | 19.4 | 81   | 5         | 18.9 | 92.3 |
| 2/15/2011  | 10:20      | 11:20       | 2         | 23.5 | 86.1 | 7         | 22.9 | 93.2 | 10        | 22.5 | 91   |
| 4/7/2011   | 9:30/10:35 | 10:35/11:30 | 7         | 23   | 86.6 | 7         | 26   | 96   | 3         | 25.4 | 93.4 |
| 5/5/2011   | 9:40       | 10:45       | 1         | 24.3 | 89.3 | 8         | 25.6 | 96.5 | 7         | 25.5 | 89.4 |
| 6/3/2011   | 9:30/10:30 | 10:30/12:40 | 9         | 40.4 | 87   | 9         | 47   | 91.5 | 1         | 46.4 | 89.9 |
| 7/7/2011   | 7:15       | 8:15        | 10        | 33.9 | 83.7 | 3         | 32.9 | 92.3 | 2         | 32.5 | 91.4 |
| 8/10/2011  | 7:30       | 8:30        | 6         | 27.7 | 76.8 | 8         | 27.2 | 93.2 | 10        | 27   | 93   |
| 9/15/2011  | 9:30       | 10:25       | 5         | 29.7 | 84.6 | 4         | 29.5 | 92.5 | 6         | 29.5 | 91.8 |
| 10/18/2011 | 9:50       | 10:40       | 3         | 31.9 | 80.5 | 10        | 31.1 | 92.5 | 9         | 30.6 | 89.7 |
| 11/8/2011  | 9:20       | 10:10       | 7         | 27.3 | 81.6 | 2         | 26.7 | 86.1 | 1         | 26.3 | 89.6 |
| 12/14/2011 | 11:30      | 12:40       | 6         | 24.9 | 81.5 | 10        | 24.3 | 86.7 | 1         | 23.6 | 90.4 |
| 1/31/2012  | 10:00      | 11:00       | 3         | 16.5 | 76.4 | 8         | 16.4 | 84.4 | 7         | 15.8 | 89   |
| 3/8/2012   | 11:00      | 12:00       | 1         | 27.2 | 85.2 | 2         | 27.3 | 87.6 | 7         | 26.7 | 90.5 |
| 4/12/2012  | 11:00      | 12:00       | 4         | 26.2 | 88.6 | 5         | 28.6 | 90.1 | 9         | 29   | 89.9 |
| 5/17/2012  | 8:40       | 9:35        | 5         | 32.8 | 87.3 | 10        | 33   | 88.3 | 6         | 32.7 | 89.3 |

**Table B.12: 4-N-EB raw RH data**

| Date       | Time In | Time Out | Depth: 1" |      |      | Depth: 2" |      |      | Depth: 3" |      |      |
|------------|---------|----------|-----------|------|------|-----------|------|------|-----------|------|------|
|            |         |          | Probe     | °C   | RH%  | Probe     | °C   | RH%  | Probe     | °C   | RH%  |
| 11/16/2010 | 12:45   | 1:40     | 2         | 16.5 | 85.8 | 5         | 15.8 | 85.3 | 1         | 15.5 | 88.4 |
| 2/15/2011  | 10:15   | 11:15    | 3         | 15   | 82.8 | 1         | 13.3 | 85   | 5         | 12.7 | 83   |
| 4/7/2011   | 9:30    | 10:25    | 9         | 17.6 | 86.7 | 5         | 17   | 83.9 | 4         | 16.9 | 85.2 |
| 5/5/2011   | 9:40    | 10:40    | 10        | 17   | 85.5 | 5         | 16.5 | 78.7 | 9         | 16.3 | 80.7 |
| 6/3/2011   | 9:30    | 10:25    | 6         | 31.6 | 84.4 | 4         | 31.6 | 82.2 | 10        | 31.5 | 85.1 |
| 7/7/2011   | 7:15    | 8:15     | 5         | 29.2 | 88.4 | 4         | 29.7 | 82.5 | 8         | 29.7 | 84.7 |
| 8/10/2011  | 7:30    | 8:30     | 3         | 25.3 | 88.1 | 4         | 26   | 83.2 | 2         | 26.1 | 83.2 |
| 9/15/2011  | 9:30    | 10:25    | 7         | 25.9 | 86.2 | 1         | 26.8 | 78.2 | 10        | 27   | 82.4 |
| 10/18/2011 | 9:40    | 10:30    | 7         | 23.5 | 78.5 | 8         | 22.7 | 74.7 | 1         | 22.5 | 76.3 |
| 11/8/2011  | 9:20    | 10:12    | 10        | 21.3 | 78.4 | 4         | 20.6 | 76.1 | 5         | 20.1 | 77.7 |
| 12/14/2011 | 12:55   | 1:45     | 7         | 19.6 | 73.3 | 8         | 17.6 | 75   | 2         | 16.7 | 74.2 |
| 1/31/2012  | 10:00   | 11:00    | 4         | 12.6 | 75   | 5         | 11.2 | 71.9 | 6         | 10.7 | 73.8 |
| 3/8/2012   | 9:40    | 10:40    | 1         | 21   | 80.3 | 7         | 20.1 | 77.6 | 2         | 19.7 | 78   |
| 4/12/2012  | 10:00   | 10:50    | 6         | 16   | 84.3 | 10        | 16.1 | 68   | 1         | 16   | 75.3 |
| 5/17/2012  | 1:30    | 2:45     | 9         | 29   | 82.3 | 10        | 28.6 | 75.1 | 3         | 28.5 | 80.3 |

**Table B.13: 5-S-WT raw RH data**

| Date       | Time In     | Time Out    | Depth: 1" |      |      | Depth: 2" |      |      | Depth: 3" |      |      |
|------------|-------------|-------------|-----------|------|------|-----------|------|------|-----------|------|------|
|            |             |             | Probe     | °C   | RH%  | Probe     | °C   | RH%  | Probe     | °C   | RH%  |
| 11/16/2010 | 10          | 11          | UT 2.6    | 17.6 | 84.2 | UT 2.1    | 15.8 | 91.8 | UT 2.5    | 15   | 91.2 |
| 2/15/2011  | 12:45       | 1:40        | 10        | 23   | 89   | 7         | 21.1 | 91.6 | 9         | 20.6 | 94.9 |
| 4/7/2011   | 11:40       | 12:40       | 1         | 27.7 | 92.7 | 9         | 26   | 91.7 | 6         | 25.4 | 95.9 |
| 5/5/2011   | 11:45       | 12:46       | 6         | 27.6 | 93.9 | 2         | 27   | 91.7 | 3         | 26.9 | 93.2 |
| 6/3/2011   | 11:30/12:45 | 12:45/1:40  | 2         | 46   | 97   | 10        | 45.4 | 92.7 | 10        | 43.1 | 92.1 |
| 7/7/2011   | 10:30/11:40 | 11:40/12:30 | 9         | 39.7 | 93   | 9         | 39.9 | 92.3 | 2         | 40   | 91.5 |
| 8/10/2011  | 10:35       | 11:30       | 6         | 35.5 | 92.8 | 10        | 33.6 | 90.8 | 7         | 33.3 | 92.8 |
| 9/15/2011  | 12:30       | 1:30        | 6         | 27.9 | 96   | 3         | 28.9 | 94.4 | 5         | 29.4 | 92.8 |
| 10/18/2011 | 12:05       | 12:55       | 1         | 29.5 | 91.3 | 7         | 28.4 | 87.7 | 8         | 27.4 | 92.8 |
| 11/8/2011  | 12:20       | 11:15       | 1         | 20.9 | 93.1 | 6         | 26.2 | 91.9 | 2         | 26.4 | 89.9 |
| 12/14/2011 | 9:00        | 10:00       | 9         | 16.8 | 85.5 | 2         | 13.9 | 90.8 | 6         | 13.4 | 92.2 |
| 1/31/2012  | 1:20        | 2:20        | 4         | 21.4 | 88.3 | 6         | 19.9 | 89.1 | 7         | 18.6 | 89.9 |
| 3/8/2012   | 12:05       | 1:05        | 6         | 26.9 | 91.5 | 3         | 25.7 | 91.1 | 2         | 25.6 | 89.6 |
| 4/12/2012  | 1:30        | 2:30        | 3         | 27.8 | 94.3 | 10        | 27.3 | 92.5 | 9         | 27.4 | 89.4 |
| 5/17/2012  | 10:50       | 11:55       | 5         | 34.4 | 91.2 | 10        | 32.7 | 90.4 | 6         | 32.4 | 88.3 |

UT – University of Texas Probe

**Table B.14: 5-S-WB raw RH data**

| Date       | Time In | Time Out | Depth: 1" |      |      | Depth: 2" |      |      | Depth: 3" |      |      |
|------------|---------|----------|-----------|------|------|-----------|------|------|-----------|------|------|
|            |         |          | Probe     | °C   | RH%  | Probe     | °C   | RH%  | Probe     | °C   | RH%  |
| 11/16/2010 | 11:20   | 12:25    | 4         | 16   | 93   | 6         | 15.6 | 94.7 | 3         | 15.2 | 95.2 |
| 2/15/2011  | 1:50    | 2:50     | 5         | 17.8 | 88.1 | 4         | 16.1 | 91.2 | 7         | 14.8 | 92.3 |
| 4/7/2011   | 12:45   | 1:40     | 10        | 21.1 | 93.2 | 6         | 19.9 | 96.2 | 7         | 19   | 96.7 |
| 5/5/2011   | 11:45   | 12:46    | 1         | 18.6 | 96   | 4         | 18.1 | 94.8 | 7         | 17.6 | 97.4 |
| 6/3/2011   | 11:30   | 12:35    | 7         | 33.3 | 93.8 | 6         | 32.9 | 92.2 | 5         | 32.5 | 94.8 |
| 7/7/2011   | 9:30    | 10:20    | 7         | 30.6 | 94.2 | 5         | 30.4 | 95.1 | 3         | 30.5 | 94.6 |
| 8/10/2011  | 9:40    | 10:30    | 1         | 28   | 91.3 | 8         | 27.4 | 94.1 | 9         | 27.1 | 93.7 |
| 9/15/2011  | 11:20   | 12:30    | 9         | 26.1 | 94.7 | 10        | 26.6 | 94   | 7         | 26.8 | 94.8 |
| 10/18/2011 | 1:15    | 2:05     | 7         | 25.2 | 87.8 | 8*        | 24.4 | 94   | 4         | 23.8 | 92.7 |
| 11/8/2011  | 11:20   | 12:20    | 9         | 22.4 | 90.6 | 5         | 21.5 | 91.1 | 3         | 21   | 90.6 |
| 12/14/2011 | 10:15   | 11:15    | 10        | 16.8 | 86.7 | 4         | 15.5 | 89.1 | 1         | 14.3 | 89   |
| 1/31/2012  | 12:00   | 1:00     | 6         | 16.7 | 85.1 | 10        | 14.5 | 89.5 | 4         | 13.5 | 86.2 |
| 3/8/2012   | 1:10    | 2:10     | 9         | 23.6 | 89.4 | 3         | 22.5 | 90.6 | 5         | 21.5 | 91.4 |
| 4/12/2012  | 12:00   | 1:20     | 6         | 17.6 | 93.4 | 10        | 17.3 | 94.4 | 3         | 17.8 | 93.9 |
| 5/17/2012  | 12:05   | 1:20     | 10        | 28.5 | 90.9 | 6         | 27.7 | 93.1 | 3         | 27.3 | 92.7 |

**Table B.15: 5-S-ET raw RH data**

| Date       | Time In     | Time Out    | Depth: 1" |      |      | Depth: 2" |      |      | Depth: 3" |      |      |
|------------|-------------|-------------|-----------|------|------|-----------|------|------|-----------|------|------|
|            |             |             | Probe     | °C   | RH%  | Probe     | °C   | RH%  | Probe     | °C   | RH%  |
| 11/16/2010 | 8:40        | 10          | UT 2.5    | 18.4 | 93.2 | UT 2.6    | 18.8 | 93.6 | UT 2.1    | 19.3 | 90.1 |
| 2/15/2011  | 12:50       | 1:45        | 6         | 26.3 | 93.5 | 8         | 26.2 | 90.3 | 1         | 26.1 | 94.9 |
| 4/7/2011   | 11:40       | 12:40       | 7         | 31.1 | 94.1 | 2         | 30.6 | 93.1 | 8         | 31.1 | 93.6 |
| 5/5/2011   | 12:50/2:00  | 2:00/3:00   | 3         | 32.7 | 95.2 | 7         | 32.9 | 93.9 | 3         | 33.3 | 96.8 |
| 6/3/2011   | 12:50/1:45  | 1:45/2:35   | 1         | 47.9 | 97   | 9         | 48.3 | 92   | 9         | 48.8 | 90.9 |
| 7/7/2011   | 10:30       | 11:45       | 6         | 41.5 | 96.1 | 2         | 43   | 92.1 | 1         | 42.6 | 94.8 |
| 8/10/2011  | 10:40/11:35 | 11:30/12:40 | 5         | 39.2 | 95.3 | 5         | 42.2 | 94.1 | 10        | 42.1 | 93.1 |
| 9/15/2011  | 12:30/1:30  | 1:30/2:30   | 1         | 30.1 | *    | 3         | 30   | 95.4 | 6         | 30   | 95.9 |
| 10/18/2011 | 12:05       | 12:55       | 6         | 33.4 | 93.5 | 4         | 33.2 | 92.3 | 5         | 33.4 | 85.7 |
| 11/8/2011  | 12:20/1:20  | 11:10/12:10 | 7         | 27.9 | 93.1 | 7         | 28   | 92.6 | 1         | 28.2 | 93.2 |
| 12/14/2011 | 9:00        | 10:00       | 1         | 20   | 89.6 | 5         | 18.6 | 89.9 | 4         | 19.3 | 88.6 |
| 1/31/2012  | 1:20/2:20   | 2:20/3:20   | 2         | 22.2 | 88.1 | 2         | 20.1 | 92.4 | 7         | 20.1 | 92.1 |
| 3/8/2012   | 1:10        | 2:10        | 6         | 27.7 | 93.3 | 2         | 26.9 | 92.8 | 4         | 27.3 | 92.2 |
| 4/12/2012  | 1:30        | 2:30        | 6         | 29.2 | 95   | 5         | 30.4 | 92.1 | 4         | 30.7 | 89.5 |
| 5/17/2012  | 10:50       | 11:50       | 1         | 36.2 | 93.6 | 3         | 36.9 | 88.2 | 4         | 37   | 85.9 |

UT – University of Texas Probe

\*Data Reading Error



**Table B.16: 5-S-EB raw RH data**

| Date       | Time In | Time Out | Depth: 1" |      |      | Depth: 2" |      |      | Depth: 3" |      |      |
|------------|---------|----------|-----------|------|------|-----------|------|------|-----------|------|------|
|            |         |          | Probe     | °C   | RH%  | Probe     | °C   | RH%  | Probe     | °C   | RH%  |
| 11/16/2010 | 11:30   | 12:30    | UT 1.5    | 16.4 | 89.6 | UT 1.3    | 15.8 | 89.9 | UT 1.1    | 15.4 | 86.8 |
| 2/15/2011  | 1:55    | 2:55     | 8         | 18.4 | 89.5 | 3         | 16.6 | 96.2 | 10        | 15.9 | 93.8 |
| 4/7/2011   | 12:45   | 1:40     | 8         | 21.5 | 92.3 | 4         | 20.4 | 96.6 | 2         | 19.9 | 97.5 |
| 5/5/2011   | 12:50   | 1:50     | 7         | 20.1 | 95.5 | 1         | 19.5 | 96.1 | 4         | 19.2 | 97.3 |
| 6/3/2011   | 12:35   | 1:30     | 6         | 34.9 | 90.8 | 7         | 34   | 94.9 | 5         | 33.7 | 95.2 |
| 7/7/2011   | 9:30    | 10:20    | 4         | 31   | 93.6 | 8         | 30.8 | 95.2 | 10        | 30.8 | 94.9 |
| 8/10/2011  | 9:45    | 10:40    | 4         | 28.7 | 93.4 | 3         | 28.2 | 93.3 | 2         | 27.9 | 93.9 |
| 9/15/2011  | 11:20   | 12:30    | 2         | 26.2 | 93.8 | 1         | 27.1 | 94.5 | 8         | 27.3 | 94.9 |
| 10/18/2011 | 1:15    | 2:05     | 1         | 26.1 | 90.8 | 6         | 25.4 | 93.4 | 5         | 24.9 | 90.4 |
| 11/8/2011  | 11:20   | 12:20    | 4         | 22.6 | 89.2 | 8         | 21.8 | 94.4 | 10        | 21.3 | 92.5 |
| 12/14/2011 | 10:15   | 11:15    | 8         | 17.2 | 88.1 | 6         | 16.4 | 89.3 | 2         | 15   | 90.7 |
| 1/31/2012  | 12:00   | 1:10     | 1         | 16.9 | 87.2 | 8         | 17   | 82   | 2         | 13.9 | 91.4 |
| 3/8/2012   | 1:10    | 2:10     | 10        | 23.7 | 90.5 | 1         | 23.3 | 90.9 | 7         | 22   | 92.9 |
| 4/12/2012  | 1:30    | 2:30     | 1         | 19.3 | 92.8 | 7         | 18.8 | 94.2 | 2         | 18.7 | 94.7 |
| 5/17/2012  | 11:05   | 12:00    | 9         | 28   | 91.5 | 7         | 27.3 | 92.1 | 2         | 27.1 | 93.4 |

UT – University of Texas Probe

**Table B.17: 5-N-WT raw RH data**

| Date       | Time In     | Time Out    | Depth: 1" |      |      | Depth: 2" |      |      | Depth: 3" |      |      |
|------------|-------------|-------------|-----------|------|------|-----------|------|------|-----------|------|------|
|            |             |             | Probe     | °C   | RH%  | Probe     | °C   | RH%  | Probe     | °C   | RH%  |
| 11/16/2010 | 10:00       | 11:00       | UT 1.3    | 17   | 81   | UT 1.1    | 14.6 | 82.5 | UT 1.5    | 14.5 | 78.9 |
| 2/15/2011  | 11:40/12:35 | 12:35/1:35  | 3         | 21.8 | 89.1 | 3         | 18.7 | 88.1 | 2         | 16.9 | 90.1 |
| 4/7/2011   | 10:40/11:40 | 11:40/12:40 | 8         | 24.5 | 91.7 | 10        | 21.3 | 94   | 10        | 23.4 | 90.8 |
| 5/5/2011   | 11:45       | 12:46       | 5         | 26.3 | 96.3 | 10        | 25.8 | 91.3 | 9         | 25.1 | 88.7 |
| 6/3/2011   | 10:40/11:30 | 11:30/12:25 | 4         | 42.1 | 95.1 | 4         | 38.7 | 91.9 | 2         | 37.8 | 91.6 |
| 7/7/2011   | 8:30/9:30   | 9:30/10:20  | 9         | 33.3 | 92.3 | 6         | 31.9 | 90.9 | 6         | 33.2 | 91.7 |
| 8/10/2011  | 8:40/9:35   | 9:35/10:30  | 10        | 30   | 91.1 | 6         | 28.4 | 90.4 | 6         | 29.4 | 91.6 |
| 9/15/2011  | 11:20       | 12:30       | 5         | 28   | 93.2 | 3         | 28.9 | 93.5 | 4         | 29.1 | 93.1 |
| 10/18/2011 | 11:10/12:00 | 12:00/12:50 | 2         | 29.1 | 88.1 | 10        | 25.6 | 91.2 | 3         | 34.2 | 89.8 |
| 11/8/2011  | 10:20/11:20 | 11:10/12:10 | 6         | 27.6 | 87.5 | 7         | 23   | 89.8 | 1         | 22.3 | 89.6 |
| 12/14/2011 | 1:50        | 2:50        | 9         | 20.2 | 88.7 | 3         | 17.8 | 89.8 | 8         | 17.1 | 90.2 |
| 1/31/2012  | 12:00       | 1:00        | 3         | 18.4 | 87.5 | 9         | 15.8 | 90.5 | 7         | 14.6 | 90.8 |
| 3/8/2012   | 12:05       | 1:05        | 1         | 25.5 | 91.8 | 4         | 24.6 | 90.7 | 10        | 24.1 | 91.7 |
| 4/12/2012  | 12:00       | 1:15        | 2         | 23.8 | 93.7 | 7         | 23.7 | 89.2 | 1         | 23   | 87.6 |
| 5/17/2012  | 9:55        | 11:00       | 2         | 31.8 | 86.9 | 7         | 29.6 | 88   | 9         | 29   | 89   |

UT – University of Texas Probe

**Table B.18: 5-N-WB raw RH data**

| Date       | Time In | Time Out | Depth: 1" |      |      | Depth: 2" |      |      | Depth: 3" |      |      |
|------------|---------|----------|-----------|------|------|-----------|------|------|-----------|------|------|
|            |         |          | Probe     | °C   | RH%  | Probe     | °C   | RH%  | Probe     | °C   | RH%  |
| 11/16/2010 | 11:15   | 12:15    | 1         | 15.2 | 65   | 2         | 14.5 | 70.2 | 5         | 14.2 | 73.8 |
| 2/15/2011  | 11:35   | 12:30    | 4         | 15.1 | 76.2 | 5         | 13.2 | 74.3 | 9         | 12.6 | 68.5 |
| 4/7/2011   | 11:40   | 12:40    | 4         | 20   | 73.2 | 5         | 18.5 | 76.7 | 3         | 18.2 | 75.7 |
| 5/5/2011   | 10:50   | 11:45    | 9         | 17.8 | 68.7 | 5         | 17.2 | 69.3 | 10        | 17   | 70.6 |
| 6/3/2011   | 10:45   | 11:20    | 5         | 32.7 | 73.1 | 3         | 32.5 | 75.3 | 8         | 32.2 | 76.3 |
| 7/7/2011   | 8:25    | 9:25     | 8         | 30.5 | 71.8 | 4         | 30.4 | 74.4 | 5         | 30.3 | 75.6 |
| 8/10/2011  | 8:35    | 9:30     | 2         | 26.9 | 70.7 | 3         | 26.6 | 74   | 4         | 26.5 | 74.8 |
| 9/15/2011  | 10:30   | 11:20    | 1         | 26.3 | 69.6 | 2         | 26.8 | 71.7 | 8         | 26.9 | 73.7 |
| 10/18/2011 | 11:00   | 11:50    | 1         | 24.1 | 61.4 | 8         | 22.7 | 66.5 | 7         | 22.2 | 66.8 |
| 11/8/2011  | 10:20   | 11:10    | 3         | 21.5 | 61.2 | 9         | 20.4 | 67.5 | 8         | 20.1 | 68.2 |
| 12/14/2011 | 9:00    | 10:00    | 3         | 14.8 | 60.2 | 8         | 13.2 | 65.7 | 7         | 12.3 | 65.4 |
| 1/31/2012  | 11:00   | 11:50    | 8         | 14.2 | 77.9 | 4         | 11.6 | 79   | 6         | 10.6 | 66.1 |
| 3/8/2012   | 11:00   | 12:00    | 9         | 22.1 | 81.6 | 4         | 20.7 | 82.5 | 10        | 20   | 74.5 |
| 4/12/2012  | 11:00   | 12:00    | 3         | 16.2 | 72.9 | 6         | 16.1 | 80.3 | 10        | 16   | 66.4 |
| 5/17/2012  | 1:30    | 2:30     | 4         | 29.2 | 70.4 | 5         | 28.2 | 78.4 | 1         | 27.9 | 72.7 |

**Table B.19: 5-N-ET raw RH data**

| Date       | Time In     | Time Out    | Depth: 1" |      |      | Depth: 2" |      |      | Depth: 3" |      |      |
|------------|-------------|-------------|-----------|------|------|-----------|------|------|-----------|------|------|
|            |             |             | Probe     | °C   | RH%  | Probe     | °C   | RH%  | Probe     | °C   | RH%  |
| 11/16/2010 | 10:10       | 11:10       | 5         | 20.3 | 95.4 | 1         | 21.1 | 90.4 | 2         | 20.8 | 83.3 |
| 2/15/2011  | 12:40       | 1:35        | 5         | 25   | 97.7 | 2         | 25.4 | 95   | 4         | 24   | 89.6 |
| 4/7/2011   | 10:35       | 11:35       | 6         | 25.9 | 95.8 | 1         | 25.8 | 92.9 | 2         | 24.1 | 88   |
| 5/5/2011   | 10:50/11:45 | 11:45/12:46 | 8         | 28.1 | 97.8 | 8         | 27.9 | 95.9 | 7         | 27.3 | 91.2 |
| 6/3/2011   | 11:30       | 12:30       | 8         | 43.9 | 95.8 | 3         | 45.4 | 91.7 | 2         | 44.9 | 84.8 |
| 7/7/2011   | 9:30        | 10:30       | 9         | 37.1 | 93.5 | 2         | 38.4 | 92.1 | 1         | 37.4 | 86.7 |
| 8/10/2011  | 9:40        | 10:30       | 7         | 34.7 | 93.3 | 10        | 34.5 | 91.7 | 5         | 33.5 | 90.4 |
| 9/15/2011  | 10:30/11:30 | 11:20/12:30 | 6         | 29.4 |      | 6         | 29.8 | 93.7 | 4         | 29.7 | 92.7 |
| 10/18/2011 | 12:00       | 12:50       | 3         | 33.1 | 91   | 9         | 32.5 | 92   | 10        | 32.8 | 89   |
| 11/8/2011  | 11:20       | 12:30       | 2         | 28   | 92.7 | 1         | 27.9 | 91.7 | 7         | 27.7 | 83.2 |
| 12/14/2011 | 1:50        | 2:50        | 6         | 22.2 | 89.4 | 7         | 21   | 91.1 | 10        | 21.3 | 81.6 |
| 1/31/2012  | 11:00/12:00 | 12:00/1:00  | 5         | 17.2 | 90.2 | 7         | 16.4 | 84.2 | 5         | 17.5 | 89.7 |
| 3/8/2012   | 12:05       | 1:05        | 5         | 26.5 | 92.7 | 9         | 26.5 | 88.4 | 7         | 26.3 | 86.1 |
| 4/12/2012  | 12:00       | 1:15        | 5         | 26.5 | 94.7 | 4         | 28.6 | 88.4 | 9         | 29.1 | 79.8 |
| 5/17/2012  | 8:50        | 9:50        | 9         | 31.8 | 89.9 | 7         | 32.1 | 85.6 | 2         | 31.8 | 78.8 |

**Table B.20:** 5-N-EB raw RH data

| Date       | Time In | Time Out | Depth: 1" |      |      | Depth: 2" |      |      | Depth: 3" |      |      |
|------------|---------|----------|-----------|------|------|-----------|------|------|-----------|------|------|
|            |         |          | Probe     | °C   | RH%  | Probe     | °C   | RH%  | Probe     | °C   | RH%  |
| 11/16/2010 | 11:30   | 12:30    | UT 2.6    | 16.7 | 91   | UT 2.5    | 16   | 94   | UT 2.1    | 15.5 | 95.3 |
| 2/15/2011  | 11:30   | 12:25    | 7         | 16   | 87.1 | 8         | 14.4 | 92.3 | 10        | 13.7 | 97   |
| 4/7/2011   | 10:35   | 11:30    | 5         | 19.1 | 91.5 | 9         | 18.2 | 95   | 4         | 17.8 | 95.7 |
| 5/5/2011   | 10:50   | 11:40    | 2         | 18   | 93.2 | 6         | 17.6 | 93.3 | 3         | 17.3 | 96.4 |
| 6/3/2011   | 10:40   | 11:25    | 6         | 32.8 | 88.3 | 7         | 32.4 | 92.4 | 10        | 32.2 | 93.7 |
| 7/7/2011   | 8:25    | 9:25     | 10        | 30.1 | 92.5 | 3         | 30.3 | 94.3 | 7         | 30.1 | 93.4 |
| 8/10/2011  | 8:35    | 9:30     | 5         | 27.1 | 93.2 | 1         | 27   | 93.6 | 7         | 26.9 | 95   |
| 9/15/2011  | 10:30   | 11:20    | 10        | 26.1 | 94.2 | 9         | 26.9 | 94   | 7         | 27.1 | 93.4 |
| 10/18/2011 | 11:00   | 11:50    | 4         | 24.9 | 87.7 | 6         | 24   | 91.6 | 5         | 23.4 | 89   |
| 11/8/2011  | 10:20   | 11:10    | 10        | 21.7 | 88.1 | 4         | 20.9 | 90.7 | 5         | 20.5 | 90.1 |
| 12/14/2011 | 9:00    | 10:00    | 10        | 15.5 | 87.9 | 9         | 16   | 90.5 | 5         | 15.2 | 90.4 |
| 1/31/2012  | 11:00   | 11:50    | 10        | 14.4 | 85.3 | 2         | 12.5 | 89.1 | 1         | 11.5 | 91.7 |
| 3/8/2012   | 9:50    | 10:50    | 9         | 21   | 88.8 | 10        | 20   | 92   | 6         | 19.6 | 92.5 |
| 4/12/2012  | 11:00   | 12:00    | 2         | 16.4 | 91.5 | 7         | 16.9 | 93.1 | 1         | 17   | 93.8 |
| 5/17/2012  | 1:30    | 2:35     | 2         | 29.1 | 87.8 | 7         | 28.4 | 90.7 | 6         | 28.1 | 91.2 |

## **Appendix C**

### **Concrete Strain Measurement Survey Data and Plots**

This appendix contains the raw concrete strain survey data that was taken on the Bibb Graves Bridge from November 16, 2010 to May 17, 2012. Additionally, the data taken by the FHWA from 2005 is presented in this appendix.

Concrete strain gauge readings for arch 4-N, 4-S, 5-N, and 5-S are shown in Tables C.1 through C.4 respectively. Gauge readings from the FHWA and Auburn University since 2005 are shown in Table C.5.

Changes in concrete strain for arch 4-N, 4-S, 5-N, and 5-S are shown in Tables C.6 through C.9 respectively. Changes in concrete strain for the locations with data from 2005 are shown in Table C.10.

Finally, the concrete strain difference plots with  $r^2$  values less than 0.5 for BL, SH, E-TH, W-TH, and AB are shown in Figures C.1 through C.5 respectively.

**Table C.1: Arch 4-S concrete strain data gauge readings**

| Date       | Ambient Temp. | Ref. Bar | West |       |      |       |       |     |      | East |      |       |       |      |     |     |
|------------|---------------|----------|------|-------|------|-------|-------|-----|------|------|------|-------|-------|------|-----|-----|
|            |               |          | AB   | SH    | SP   | BL    | BH    | TL  | TH   | AB   | SH   | SP    | BL    | BH   | TL  | TH  |
| 11/17/2010 | 60.5          | 837      | CNM* | -2250 | 1696 | -2423 | -2103 | 877 | 2676 | 1890 | CNM* | DNE** | -2271 | 1250 | 270 | 300 |
| 2/2/2011   | 63.9          | 849      |      | -2262 | 1642 | -2407 | -2115 | 876 | 2676 | 1819 |      |       | -2280 | 1254 | 238 | 268 |
| 4/7/2011   | 72.1          | 852      |      | -2202 | 1673 | -2443 | -2137 | 888 | 2676 | 1843 |      |       | -2303 | 1278 | 242 | 304 |
| 5/5/2011   | 72.9          | 859.3    |      | -2326 | 1680 | -2444 | -2133 | 884 | 2683 | 1857 |      |       | -2300 | 1272 | 254 | 313 |
| 6/3/2011   | 100.8         | 857      |      | -2355 | 1728 | -2412 | -2183 | 936 | 2678 | 1894 |      |       | -2362 | 1327 | 294 | 346 |
| 7/7/2011   | 93.1          | 857      |      | -2372 | 1742 | -2415 | -2184 | 936 | 2682 | 1889 |      |       | -2364 | 1330 | 276 | 341 |
| 8/10/2011  | 86.8          | 858      |      | -2376 | 1729 | -2481 | -2170 | 927 | 2682 | 1871 |      |       | -2349 | 1318 | 238 | 325 |
| 9/15/2011  | 82.6          | 850.8    |      | -2349 | 1721 | -2489 | -2162 | 918 | 2686 | 1870 |      |       | -2355 | 1320 | 223 | 316 |
| 10/18/2011 | 80.8          | 853      |      | -2278 | 1690 | -2463 | -2134 | 892 | 2682 | 1867 |      |       | -2319 | 1288 | 228 | 323 |
| 11/8/2011  | 74.1          | 850      |      | -2205 | 1700 | -2455 | -2140 | 891 | 2681 | 1871 |      |       | -2309 | 1283 | 227 | 309 |
| 12/14/2011 | 63.0          | 849      |      | -2190 | 1667 | -2428 | -2120 | 865 | 2682 | 1839 |      |       | -2278 | 1260 | 190 | 283 |
| 1/31/2012  | 58.6          | 846      |      | -2233 | 1643 | -2408 | -2105 | 855 | 2682 | 1825 |      |       | -2264 | 1239 | 173 | 280 |
| 3/8/2012   | 74.4          | 848      |      | -2294 | 1682 | -2445 | -2135 | 903 | 2682 | 1874 |      |       | -2300 | 1276 | 210 | 308 |
| 4/12/2012  | 71.7          | 846      |      | -2238 | 1654 | -2439 | -2122 | 876 | 2680 | 1862 |      |       | -2293 | 1272 | 210 | 301 |
| 5/17/2012  | 85.6          | 844.5    |      | -2200 | 1695 | -2458 | -2148 | 922 | 2682 | 1890 |      |       | -2321 | 1296 | 235 | 335 |

\*CNM = Can Not Measure

\*\*DNE = Does Not Exist

**Table C.2: Arch 4-N concrete strain gauge readings**

| Date       | Ambient Temp. | Ref. Bar | West |       |       |     |      |      |      | East |     |       |      |     |       |      |
|------------|---------------|----------|------|-------|-------|-----|------|------|------|------|-----|-------|------|-----|-------|------|
|            |               |          | AB   | SH    | SP    | BL  | BH   | TL   | TH   | AB   | SH  | SP    | BL   | BH  | TL    | TH   |
| 11/17/2010 | 60.5          | 837      | 115  | -2143 | DNE** | 103 | 1170 | CNM* | 1171 | CNM* | 219 | DNE** | 1462 | 868 | -2368 | 2671 |
| 2/2/2011   | 63.9          | 849      | 89   | -2109 |       | 102 | 1166 |      | 1166 |      | 243 |       | 1415 | 860 | -2337 | 2676 |
| 4/7/2011   | 72.1          | 850      | 98   | -2132 |       | 132 | 1192 |      | 1176 |      | 266 |       | 1440 | 886 | -2337 | 2676 |
| 5/5/2011   | 72.9          | 859      | 102  | -2142 |       | 135 | 1193 |      | 1181 |      | 267 |       | 1451 | 884 | -2355 | 2686 |
| 6/3/2011   | 100.8         | 856      | 156  | -2204 |       | 199 | 1249 |      | 1235 |      | 316 |       | 1525 | 941 | -2396 | 2678 |
| 7/7/2011   | 93.1          | 857      | 155  | -2201 |       | 202 | 1257 |      | 1232 |      | 321 |       | 1535 | 949 | -2402 | 2682 |
| 8/10/2011  | 86.8          | 853      | 134  | -2170 |       | 185 | 1238 |      | 1210 |      | 292 |       | 1513 | 932 | -2379 | 2684 |
| 9/15/2011  | 82.6          | 851      | 140  | -2175 |       | 185 | 1235 |      | 1217 |      | 289 |       | 1508 | 930 | -2362 | 2686 |
| 10/18/2011 | 80.8          | 850      | 115  | -2140 |       | 154 | 1213 |      | 1189 |      | 276 |       | 1461 | 904 | -2378 | 2683 |
| 11/8/2011  | 74.1          | 851      | 119  | -2138 |       | 143 | 1200 |      | 1190 |      | 264 |       | 1439 | 895 | -2354 | 2684 |
| 12/14/2011 | 63.0          | 847      | 81   | -2100 |       | 111 | 1175 |      | 1154 |      | 240 |       | 1407 | 865 | -2350 | 2682 |
| 1/31/2012  | 58.6          | 845      | 76   | -2090 |       | 100 | 1163 |      | 1153 |      | 231 |       | 1439 | 853 | -2323 | 2684 |
| 3/8/2012   | 74.4          | 850      | 114  | -2137 |       | 136 | 1195 |      | 1186 |      | 275 |       | 1478 | 881 | -2368 | 2687 |
| 4/12/2012  | 71.7          | 845      | 98   | -2124 |       | 129 | 1190 |      | 1172 |      | 250 |       | 1470 | 876 | -2345 | 2680 |
| 5/17/2012  | 85.6          | 846      | 127  | -2164 |       | 165 | 1223 |      | 1203 |      | 291 |       | 1537 | 907 | -2386 | 2680 |

\*CNM = Can Not Measure

\*\*DNE = Does Not Exist



**Table C.3: Arch 5-S concrete strain gauge readings**

| Date       | Ambient Temp. | Ref. Bar | West |       |       |     |       |       |     | East |     |      |      |      |      |     |
|------------|---------------|----------|------|-------|-------|-----|-------|-------|-----|------|-----|------|------|------|------|-----|
|            |               |          | AB   | SH    | SP    | BL  | BH    | TL    | TH  | AB   | SH  | SP   | BL   | BH   | TL   | TH  |
| 11/17/2010 | 60.5          | 837      | 1447 | DNE** | -2322 | 372 | -1924 | -2385 | 430 | 1215 | 850 | 1270 | 1052 | 1347 | 2440 | 502 |
| 2/2/2011   | 63.9          | 849      | 1453 |       | -2275 | 357 | -1943 | -2389 | 413 | 1191 | 862 | 1288 | 1070 | 1374 | 2440 | 475 |
| 4/7/2011   | 72.1          | 849      | 1472 |       | -2310 | 393 | -1990 | -2403 | 421 | 1218 | 883 | 1305 | 1094 | 1400 | 2472 | 503 |
| 5/5/2011   | 72.9          | 861      | 1478 |       | -2318 | 414 | -2002 | -2422 | 426 | 1238 | 894 | 1304 | 1091 | 1400 | 2493 | 528 |
| 6/3/2011   | 100.8         | 858      | 1532 |       | -2383 | 471 | -2061 | -2483 | 472 | 1283 | 939 | 1340 | 1135 | 1441 | 2532 | 575 |
| 7/7/2011   | 93.1          | 856      | 1525 |       | -2400 | 485 | -2078 | -2475 | 472 | 1264 | 933 | 1343 | 1142 | 1454 | 2507 | 544 |
| 8/10/2011  | 86.8          | 856      | 1495 |       | -2382 | 472 | -2055 | -2457 | 457 | 1242 | 918 | 1333 | 1127 | 1438 | 2491 | 532 |
| 9/15/2011  | 82.6          | 853      | 1500 |       | -2390 | 472 | -2068 | -2470 | 465 | 1244 | 924 | 1340 | 1140 | 1444 | 2496 | 535 |
| 10/18/2011 | 80.8          | 854      | 1491 |       | -2380 | 439 | -2040 | -2441 | 454 | 1248 | 917 | 1339 | 1111 | 1420 | 2508 | 546 |
| 11/8/2011  | 74.1          | 851      | 1481 |       | -2370 | 433 | -2145 | -2426 | 443 | 1230 | 909 | 1323 | 1104 | 1414 | 2492 | 527 |
| 12/14/2011 | 63.0          | 845      | 1436 |       | -2325 | 412 | -2140 | -2388 | 435 | 1198 | 877 | 1311 | 1095 | 1401 | 2471 | 492 |
| 1/31/2012  | 58.6          | 846      | 1431 |       | -2310 | 398 | -2149 | -2375 | 451 | 1174 | 875 | 1317 | 1096 | 1403 | 2472 | 499 |
| 3/8/2012   | 74.4          | 848      | 1475 |       | -2336 | 441 | -2196 | -2404 | 480 | 1225 | 909 | 1344 | 1118 | 1434 | 2518 | 524 |
| 4/12/2012  | 71.7          | 847      | 1456 |       | -2297 | 454 | -2204 | -2407 | 482 | 1222 | 902 | 1322 | 1111 | 1422 | 2516 | 535 |
| 5/17/2012  | 85.6          | 847      | 1492 |       | -2330 | 497 | -2242 | -2447 | 512 | 1249 | 932 | 1346 | 1139 | 1452 | 2539 | 553 |

\*CNM = Can Not Measure

\*\*DNE = Does Not Exist

**Table C.4:** Arch 5-N concrete strain gauge readings

| Date       | Ambient Temp. | Ref. Bar | West |     |       |      |      |     |     | East |     |      |      |      |     |      |
|------------|---------------|----------|------|-----|-------|------|------|-----|-----|------|-----|------|------|------|-----|------|
|            |               |          | AB   | SH  | SP    | BL   | BH   | TL  | TH  | AB   | SH  | SP   | BL   | BH   | TL  | TH   |
| 11/17/2010 | 60.5          | 837      | 2500 | 171 | DNE** | CNM* | 959  | 0   | 392 | 387  | 60  | 2327 | 1751 | 1105 | 557 | 2177 |
| 2/2/2011   | 63.9          | 849      | 2526 | 175 |       |      | 957  | 55  | 415 | 380  | 65  | 2339 | 1741 | 1198 | 569 | 2150 |
| 4/7/2011   | 72.1          | 852      | 2569 | 104 |       |      | 975  | 58  | 444 | 410  | 0   | 2378 | 1704 | 1179 | 623 | 2166 |
| 5/5/2011   | 72.9          | 860      | 2588 | 213 |       |      | 985  | 82  | 451 | 419  | 118 | 2395 | 1733 | 1183 | 635 | 2169 |
| 6/3/2011   | 100.8         | 859      | 2655 | 261 |       |      | 1053 | 166 | 507 | 470  | 170 | 2443 | 1804 | 1249 | 673 | 2120 |
| 7/7/2011   | 93.1          | 856      | 2643 | 251 |       |      | 1063 | 141 | 509 | 453  | 160 | 2436 | 1839 | 1269 | 650 | 2103 |
| 8/10/2011  | 86.8          | 853      | 2620 | 229 |       |      | 1040 | 109 | 496 | 434  | 152 | 2424 | 1828 | 1255 | 637 | 2093 |
| 9/15/2011  | 82.6          | 851      | 2625 | 230 |       |      | 1046 | 115 | 507 | 440  | 160 | 2431 | 1850 | 1260 | 649 | 2104 |
| 10/18/2011 | 80.8          | 851      | 2504 | 201 |       |      | 1007 | 104 | 492 | 436  | 146 | 2402 | 1832 | 1230 | 666 | 2099 |
| 11/8/2011  | 74.1          | 854      | 2503 | 207 |       |      | 1002 | 91  | 496 | 419  | 145 | 2405 | 1850 | 1242 | 646 | 2085 |
| 12/14/2011 | 63.0          | 847      | 2550 | 162 |       |      | 965  | 40  | 475 | 386  | 123 | 2386 | 1845 | 1223 | 643 | 2171 |
| 1/31/2012  | 58.6          | 845      | 2527 | 154 |       |      | 944  | 31  | 486 | 372  | 129 | 2390 | 1845 | 1235 | 644 | 2173 |
| 3/8/2012   | 74.4          | 849      | 2576 | 188 |       |      | 979  | 75  | 523 | 421  | 170 | 2438 | 1890 | 1280 | 692 | 2109 |
| 4/12/2012  | 71.7          | 846      | 2581 | 172 |       |      | 985  | 63  | 527 | 410  | 180 | 2433 | 1908 | 1276 | 712 | 2207 |
| 5/17/2012  | 85.6          | 845      | 2521 | 219 |       |      | 1022 | 99  | 556 | 434  | 204 | 2478 | 1955 | 1301 | 725 | 2242 |

\*CNM = Can Not Measure

\*\*DNE = Does Not Exist

**Table C.5:** Concrete strain gauge readings from 2005 with new concrete strain gauge readings

| Date       | Ambient Temp. | Ref. Bar | Span 4 South |       |     | Span 5 South |     |       |      |      |      |      |
|------------|---------------|----------|--------------|-------|-----|--------------|-----|-------|------|------|------|------|
|            |               |          | West         |       |     | West         |     |       | East |      |      |      |
|            |               |          | SP           | BL    | TL  | SP           | BL  | TL    | AB   | SP   | BL   | TL   |
| 12/16/2005 | 59            | 850      | 1731         | -2389 | 811 | -2359        | 233 | -2354 | 1179 | 971  | 747  | 2152 |
| 12/9/2009  | 66            | 850      | 1666         | -2419 | 882 | -2312        | 326 | -2367 | 1179 | 1247 | 1035 | 2389 |
| 11/17/2010 | 60.5          | 837      | 1696         | -2423 | 877 | -2322        | 372 | -2385 | 1215 | 1270 | 1052 | 2440 |
| 2/2/2011   | 63.9          | 849      | 1642         | -2407 | 876 | -2275        | 357 | -2389 | 1191 | 1288 | 1070 | 2440 |
| 4/7/2011   | 72.1          | 852      | 1673         | -2443 | 888 | -2310        | 393 | -2403 | 1218 | 1305 | 1094 | 2472 |
| 5/5/2011   | 72.9          | 859      | 1680         | -2444 | 884 | -2318        | 414 | -2422 | 1238 | 1304 | 1091 | 2493 |
| 6/3/2011   | 100.8         | 857      | 1728         | -2412 | 936 | -2383        | 471 | -2483 | 1283 | 1340 | 1135 | 2532 |
| 7/7/2011   | 93.1          | 857      | 1742         | -2415 | 936 | -2400        | 485 | -2475 | 1264 | 1343 | 1142 | 2507 |
| 8/10/2011  | 86.8          | 858      | 1729         | -2481 | 927 | -2382        | 472 | -2457 | 1242 | 1333 | 1127 | 2491 |
| 9/15/2011  | 82.6          | 851      | 1721         | -2489 | 918 | -2390        | 472 | -2470 | 1244 | 1340 | 1140 | 2496 |
| 10/18/2011 | 80.8          | 853      | 1690         | -2463 | 892 | -2380        | 439 | -2441 | 1248 | 1339 | 1111 | 2508 |
| 11/8/2011  | 74.1          | 850      | 1700         | -2455 | 891 | -2370        | 433 | -2426 | 1230 | 1323 | 1104 | 2492 |
| 12/14/2011 | 63.0          | 849      | 1667         | -2428 | 865 | -2325        | 412 | -2388 | 1198 | 1311 | 1095 | 2471 |
| 1/31/2012  | 58.6          | 846      | 1643         | -2408 | 855 | -2310        | 398 | -2375 | 1174 | 1317 | 1096 | 2472 |
| 3/8/2012   | 74.4          | 848      | 1682         | -2445 | 903 | -2336        | 441 | -2404 | 1225 | 1344 | 1118 | 2518 |
| 4/12/2012  | 71.7          | 846      | 1654         | -2439 | 876 | -2297        | 454 | -2407 | 1222 | 1322 | 1111 | 2516 |
| 5/17/2012  | 86            | 845      | 1695         | -2458 | 922 | -2330        | 497 | -2447 | 1249 | 1346 | 1139 | 2539 |

**Table C.6:** Changes in concrete strain ( $10^{-6}$  in./in.) for arch 4-S

| Date       | West |      |      |      |     |     |     | East |    |    |     |     |      |      |
|------------|------|------|------|------|-----|-----|-----|------|----|----|-----|-----|------|------|
|            | AB   | SH   | SP   | BL   | BH  | TL  | TH  | AB   | SH | SP | BL  | BH  | TL   | TH   |
| 11/17/2010 |      | 0    | 0    | 0    | 0   | 0   | 0   | 0    |    |    | 0   | 0   | 0    | 0    |
| 2/2/2011   |      | 0    | -214 | -91  | 0   | -43 | -39 | -270 |    |    | -10 | -26 | -142 | -144 |
| 4/7/2011   |      | -205 | -123 | 14   | 61  | -14 | -49 | -201 |    |    | 55  | 42  | -139 | -36  |
| 5/5/2011   |      | 174  | -124 | -5   | 25  | -48 | -49 | -179 |    |    | 22  | -1  | -124 | -30  |
| 6/3/2011   |      | 275  | 37   | -101 | 192 | 125 | -58 | -52  |    |    | 230 | 184 | 13   | 84   |
| 7/7/2011   |      | 330  | 84   | -91  | 197 | 127 | -45 | -68  |    |    | 236 | 194 | -45  | 68   |
| 8/10/2011  |      | 338  | 39   | 117  | 149 | 93  | -50 | -129 |    |    | 184 | 152 | -171 | 13   |
| 9/15/2011  |      | 274  | 36   | 168  | 146 | 89  | -14 | -111 |    |    | 226 | 180 | -197 | 5    |
| 10/18/2011 |      | 37   | -71  | 77   | 49  | -4  | -34 | -126 |    |    | 104 | 71  | -188 | 22   |
| 11/8/2011  |      | -188 | -29  | 61   | 78  | 4   | -26 | -104 |    |    | 79  | 65  | -181 | -15  |
| 12/14/2011 |      | -233 | -133 | -23  | 16  | -78 | -21 | -205 |    |    | -16 | -6  | -298 | -94  |
| 1/31/2012  |      | -86  | -201 | -78  | -24 | -99 | -10 | -239 |    |    | -52 | -65 | -343 | -94  |
| 3/8/2012   |      | 105  | -81  | 33   | 68  | 48  | -16 | -87  |    |    | 58  | 49  | -230 | -12  |
| 4/12/2012  |      | -68  | -167 | 20   | 32  | -32 | -16 | -120 |    |    | 42  | 42  | -223 | -28  |
| 5/17/2012  |      | -186 | -29  | 88   | 121 | 121 | -5  | -24  |    |    | 136 | 123 | -137 | 89   |

**Table C.7:** Changes in concrete strain ( $10^{-6}$  in./in.) for arch 4-N

| Date       | West |      |    |     |     |    |     | East |     |    |      |     |      |     |
|------------|------|------|----|-----|-----|----|-----|------|-----|----|------|-----|------|-----|
|            | AB   | SH   | SP | BL  | BH  | TL | TH  | AB   | SH  | SP | BL   | BH  | TL   | TH  |
| 11/17/2010 | 0    | 0    |    | 0   | 0   |    | 0   |      | 0   |    | 0    | 0   | 0    | 0   |
| 2/2/2011   | -121 | -147 |    | -42 | -52 |    | -55 |      | 39  |    | -189 | -65 | -137 | -21 |
| 4/7/2011   | -97  | -78  |    | 52  | 29  |    | -26 |      | 110 |    | -113 | 16  | -142 | -26 |
| 5/5/2011   | -112 | -73  |    | 34  | 5   |    | -37 |      | 86  |    | -105 | -19 | -112 | -21 |
| 6/3/2011   | 71   | 134  |    | 249 | 194 |    | 146 |      | 252 |    | 142  | 173 | 29   | -40 |
| 7/7/2011   | 65   | 125  |    | 257 | 218 |    | 134 |      | 267 |    | 171  | 199 | 47   | -27 |
| 8/10/2011  | 11   | 36   |    | 214 | 167 |    | 75  |      | 185 |    | 112  | 154 | -17  | -9  |
| 9/15/2011  | 36   | 58   |    | 220 | 165 |    | 104 |      | 181 |    | 102  | 154 | -65  | 2   |
| 10/18/2011 | -43  | -51  |    | 124 | 96  |    | 15  |      | 143 |    | -44  | 75  | -9   | -2  |
| 11/8/2011  | -32  | -60  |    | 86  | 53  |    | 18  |      | 100 |    | -118 | 44  | -89  | -2  |
| 12/14/2011 | -142 | -171 |    | -6  | -16 |    | -89 |      | 36  |    | -210 | -42 | -91  | 3   |
| 1/31/2012  | -154 | -197 |    | -37 | -49 |    | -86 |      | 11  |    | -102 | -74 | -171 | 15  |
| 3/8/2012   | -45  | -61  |    | 65  | 37  |    | 5   |      | 137 |    | 10   | 0   | -42  | 10  |
| 4/12/2012  | -82  | -89  |    | 58  | 39  |    | -23 |      | 74  |    | -2   | 0   | -100 | 3   |
| 5/17/2012  | 10   | 39   |    | 170 | 141 |    | 74  |      | 202 |    | 212  | 95  | 29   | -2  |

**Table C.8:** Changes in concrete strain ( $10^{-6}$  in./in.) for arch 5-S

| Date       | West |    |      |     |     |     |     | East |     |     |     |     |     |      |
|------------|------|----|------|-----|-----|-----|-----|------|-----|-----|-----|-----|-----|------|
|            | AB   | SH | SP   | BL  | BH  | TL  | TH  | AB   | SH  | SP  | BL  | BH  | TL  | TH   |
| 11/17/2010 | 0    |    | 0    | 0   | 0   | 0   | 0   | 0    | 0   | 0   | 0   | 0   | 0   | 0    |
| 2/2/2011   | -19  |    | -191 | -89 | 21  | -27 | -95 | -118 | 0   | 19  | 19  | 47  | -40 | -126 |
| 4/7/2011   | 44   |    | -76  | 31  | 176 | 21  | -66 | -27  | 70  | 74  | 97  | 134 | 66  | -36  |
| 5/5/2011   | 22   |    | -91  | 56  | 174 | 41  | -91 | -6   | 64  | 30  | 46  | 93  | 91  | 4    |
| 6/3/2011   | 207  |    | 129  | 252 | 375 | 247 | 68  | 152  | 220 | 159 | 201 | 236 | 230 | 168  |
| 7/7/2011   | 191  |    | 191  | 304 | 437 | 230 | 74  | 97   | 207 | 175 | 230 | 285 | 155 | 74   |
| 8/10/2011  | 95   |    | 133  | 263 | 363 | 171 | 27  | 27   | 159 | 143 | 180 | 234 | 104 | 35   |
| 9/15/2011  | 120  |    | 167  | 272 | 414 | 222 | 61  | 42   | 188 | 175 | 231 | 262 | 129 | 55   |
| 10/18/2011 | 87   |    | 133  | 162 | 320 | 126 | 23  | 52   | 160 | 168 | 136 | 180 | 163 | 86   |
| 11/8/2011  | 63   |    | 110  | 152 | 670 | 87  | -3  | 3    | 146 | 126 | 123 | 171 | 123 | 36   |
| 12/14/2011 | -61  |    | -15  | 104 | 674 | -15 | -9  | -80  | 62  | 108 | 114 | 150 | 74  | -57  |
| 1/31/2012  | -81  |    | -68  | 53  | 697 | -61 | 37  | -162 | 50  | 121 | 112 | 152 | 74  | -40  |
| 3/8/2012   | 55   |    | 11   | 189 | 844 | 27  | 128 | -2   | 155 | 204 | 178 | 247 | 218 | 37   |
| 4/12/2012  | -3   |    | -113 | 233 | 873 | 39  | 136 | -10  | 136 | 136 | 157 | 210 | 214 | 74   |
| 5/17/2012  | 115  |    | -5   | 374 | 998 | 170 | 233 | 79   | 235 | 215 | 251 | 307 | 290 | 134  |

**Table C.9:** Changes in concrete strain ( $10^{-6}$  in./in.) for arch 5-N

| Date       | West |      |    |    |     |     |     | East |      |     |      |     |     |      |
|------------|------|------|----|----|-----|-----|-----|------|------|-----|------|-----|-----|------|
|            | AB   | SH   | SP | BL | BH  | TL  | TH  | AB   | SH   | SP  | BL   | BH  | TL  | TH   |
| 11/17/2010 | 0    | 0    |    |    | 0   | 0   | 0   | 0    | 0    | 0   | 0    | 0   | 0   | 0    |
| 2/2/2011   | 44   | -26  |    |    | -45 | 137 | 34  | -63  | -24  | 0   | -71  | 260 | -2  | -126 |
| 4/7/2011   | 175  | -264 |    |    | 4   | 140 | 121 | 24   | -242 | 119 | -201 | 192 | 166 | -85  |
| 5/5/2011   | 211  | 62   |    |    | 9   | 192 | 117 | 27   | 114  | 148 | -132 | 177 | 177 | -99  |
| 6/3/2011   | 432  | 222  |    |    | 235 | 466 | 302 | 198  | 285  | 306 | 100  | 396 | 306 | -256 |
| 7/7/2011   | 400  | 197  |    |    | 274 | 394 | 316 | 150  | 261  | 292 | 222  | 468 | 239 | -302 |
| 8/10/2011  | 336  | 136  |    |    | 210 | 299 | 285 | 99   | 246  | 264 | 197  | 432 | 207 | -325 |
| 9/15/2011  | 359  | 146  |    |    | 235 | 327 | 327 | 125  | 277  | 293 | 275  | 456 | 251 | -281 |
| 10/18/2011 | -32  | 53   |    |    | 110 | 291 | 278 | 112  | 233  | 201 | 217  | 361 | 309 | -298 |
| 11/8/2011  | -45  | 63   |    |    | 86  | 241 | 283 | 49   | 222  | 201 | 267  | 390 | 235 | -351 |
| 12/14/2011 | 129  | -61  |    |    | -15 | 97  | 236 | -37  | 171  | 159 | 270  | 349 | 244 | -52  |
| 1/31/2012  | 61   | -82  |    |    | -74 | 73  | 278 | -77  | 197  | 180 | 278  | 393 | 254 | -40  |
| 3/8/2012   | 207  | 16   |    |    | 24  | 204 | 383 | 70   | 317  | 322 | 409  | 527 | 396 | -259 |
| 4/12/2012  | 231  | -26  |    |    | 53  | 175 | 408 | 42   | 359  | 314 | 479  | 522 | 472 | 68   |
| 5/17/2012  | 42   | 128  |    |    | 178 | 294 | 503 | 123  | 440  | 463 | 632  | 608 | 516 | 183  |

**Table C.10:** Changes in concrete strain ( $10^{-6}$  in./in.) for plots with data from 2005

| Date       | Span 4 South |     |     | Span 5 South |     |     |      |      |      |      |
|------------|--------------|-----|-----|--------------|-----|-----|------|------|------|------|
|            | West         |     |     | West         |     |     | East |      |      |      |
|            | SP           | BL  | TL  | SP           | BL  | TL  | AB   | SP   | BL   | TL   |
| 12/16/2005 | 0            | 0   | 0   | 0            | 0   | 0   | 0    | 0    | 0    | 0    |
| 12/9/2009  | -209         | 98  | 230 | -150         | 301 | 41  | 2    | 894  | 933  | 768  |
| 1/0/1900   | -71          | 152 | 256 | -78          | 491 | 143 | 160  | 1010 | 1030 | 975  |
| 1/0/1900   | -284         | 61  | 213 | -268         | 402 | 115 | 41   | 1029 | 1050 | 934  |
| 1/0/1900   | -193         | 166 | 242 | -165         | 510 | 152 | 121  | 1073 | 1116 | 1030 |
| 1/0/1900   | -194         | 148 | 208 | -162         | 553 | 190 | 160  | 1046 | 1083 | 1073 |
| 1/0/1900   | -33          | 51  | 381 | 55           | 746 | 393 | 315  | 1172 | 1234 | 1208 |
| 7/7/2011   | 14           | 61  | 383 | 110          | 791 | 369 | 253  | 1182 | 1257 | 1127 |
| 8/10/2011  | -32          | 270 | 349 | 49           | 746 | 306 | 179  | 1146 | 1203 | 1072 |
| 9/15/2011  | -34          | 321 | 345 | 96           | 770 | 371 | 209  | 1192 | 1269 | 1112 |
| 10/18/2011 | -142         | 229 | 252 | 58           | 656 | 272 | 215  | 1182 | 1169 | 1141 |
| 11/8/2011  | -100         | 213 | 260 | 36           | 646 | 233 | 166  | 1139 | 1156 | 1101 |
| 12/14/2011 | -203         | 129 | 178 | -107         | 581 | 113 | 66   | 1104 | 1131 | 1035 |
| 1/31/2012  | -271         | 74  | 157 | -145         | 544 | 81  | -2   | 1131 | 1142 | 1049 |
| 3/8/2012   | -151         | 186 | 304 | -68          | 678 | 168 | 156  | 1212 | 1207 | 1192 |
| 4/12/2012  | -237         | 173 | 225 | -188         | 727 | 185 | 153  | 1149 | 1190 | 1192 |
| 5/17/2012  | -100         | 241 | 377 | -76          | 871 | 319 | 245  | 1232 | 1287 | 1271 |



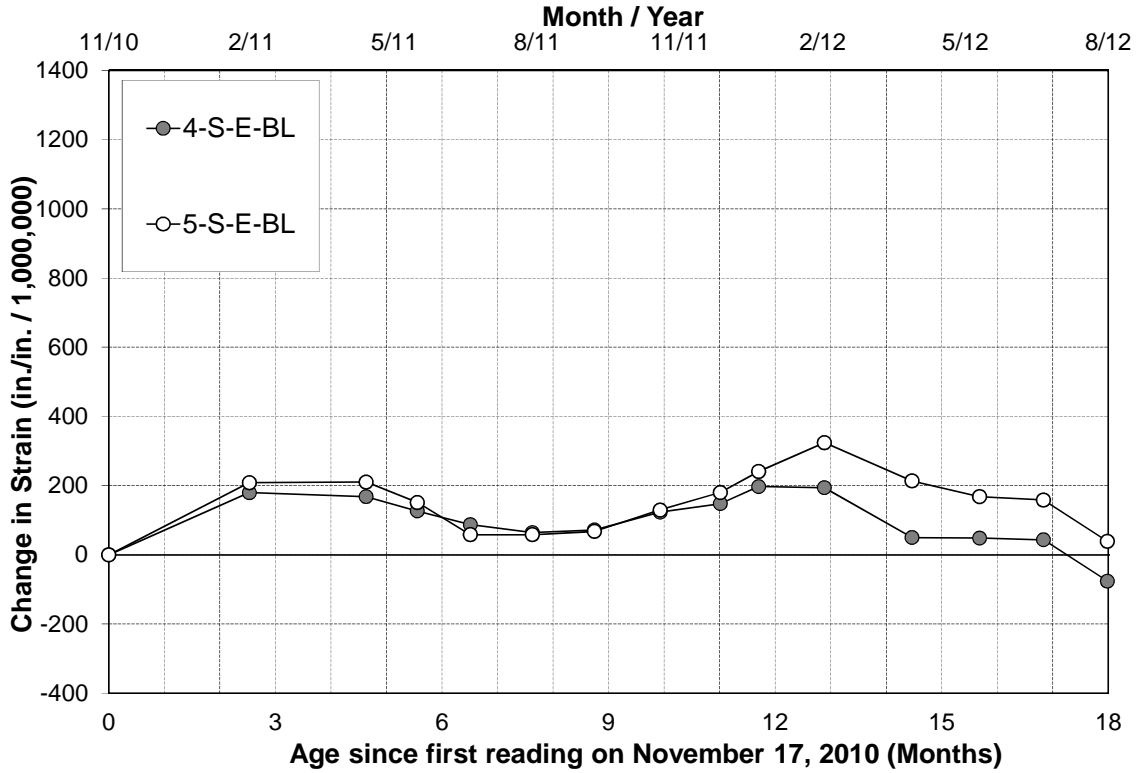


Figure C.1: Concrete strain difference plot for BL,  $r^2 < 0.5$

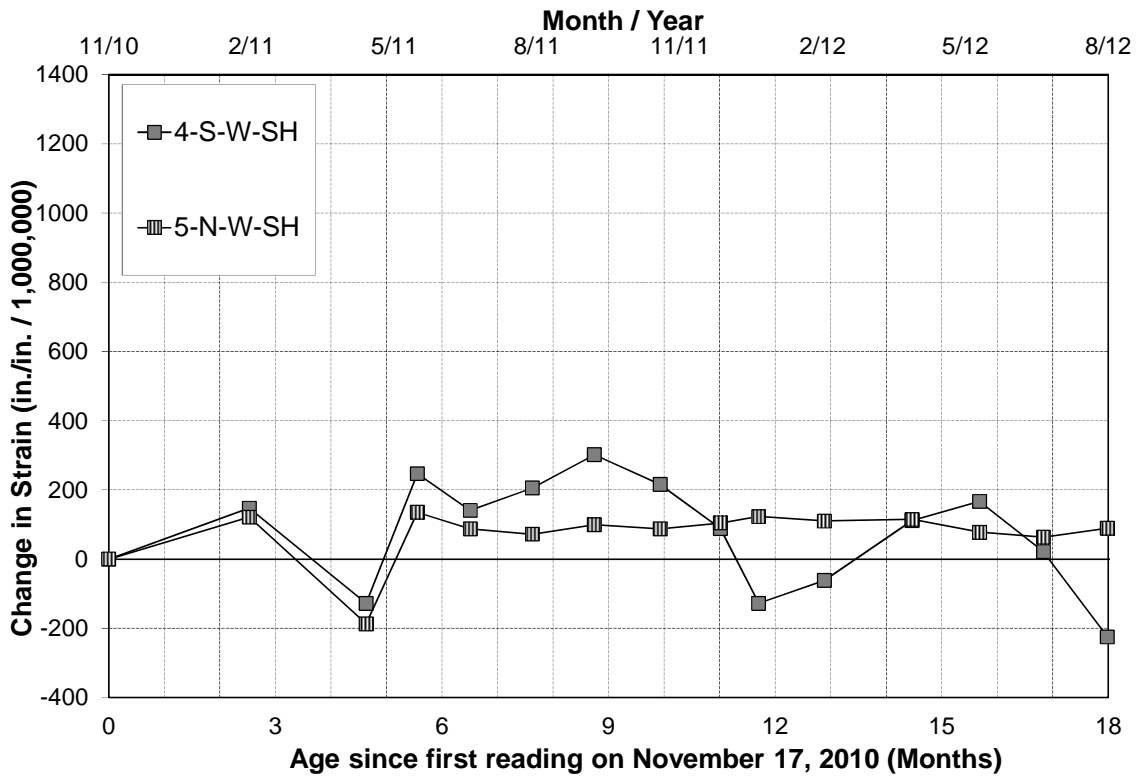
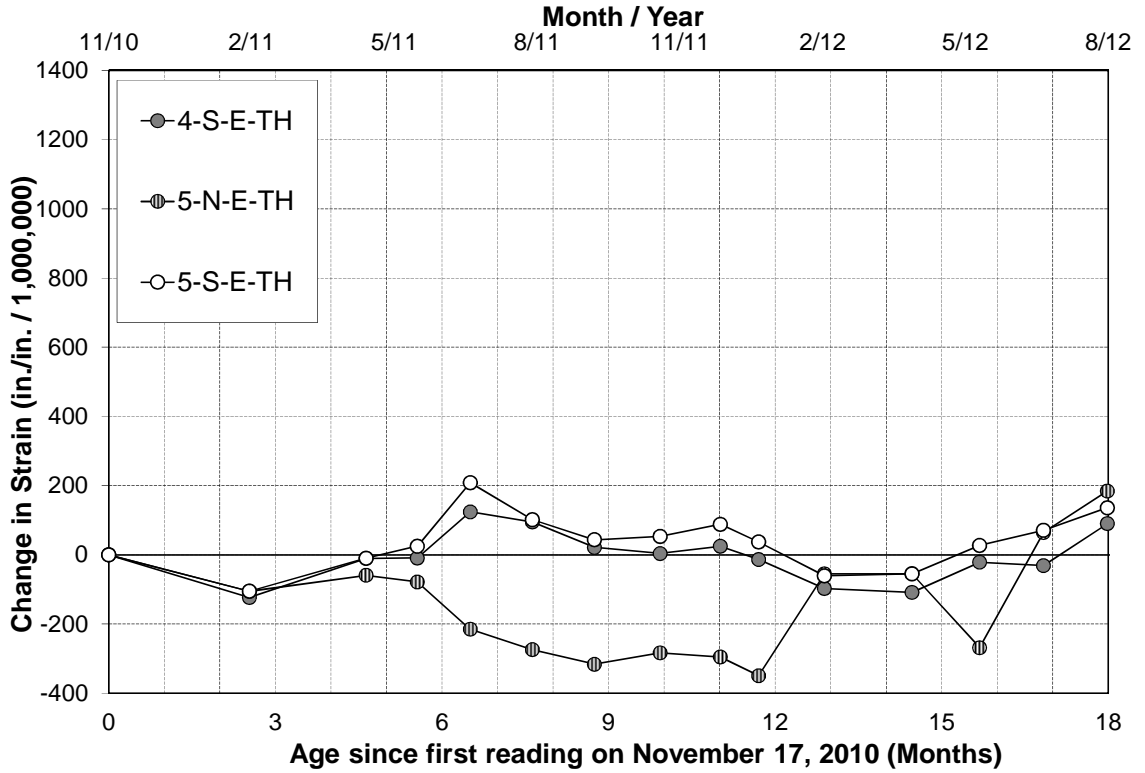
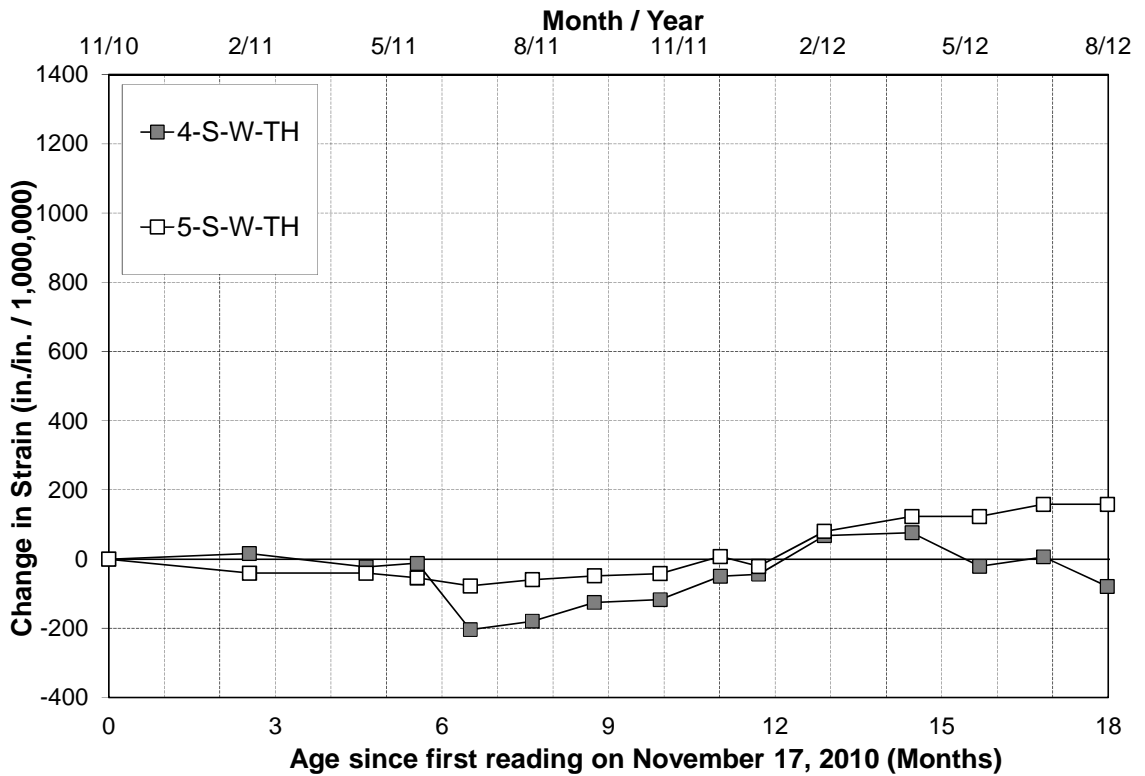


Figure C.2: Concrete strain difference plot for SH,  $r^2 < 0.5$



**Figure C.3:** Concrete strain difference plot for E-TH,  $r^2 < 0.5$



**Figure C.4:** Concrete strain difference plot for W-TH,  $r^2 < 0.5$

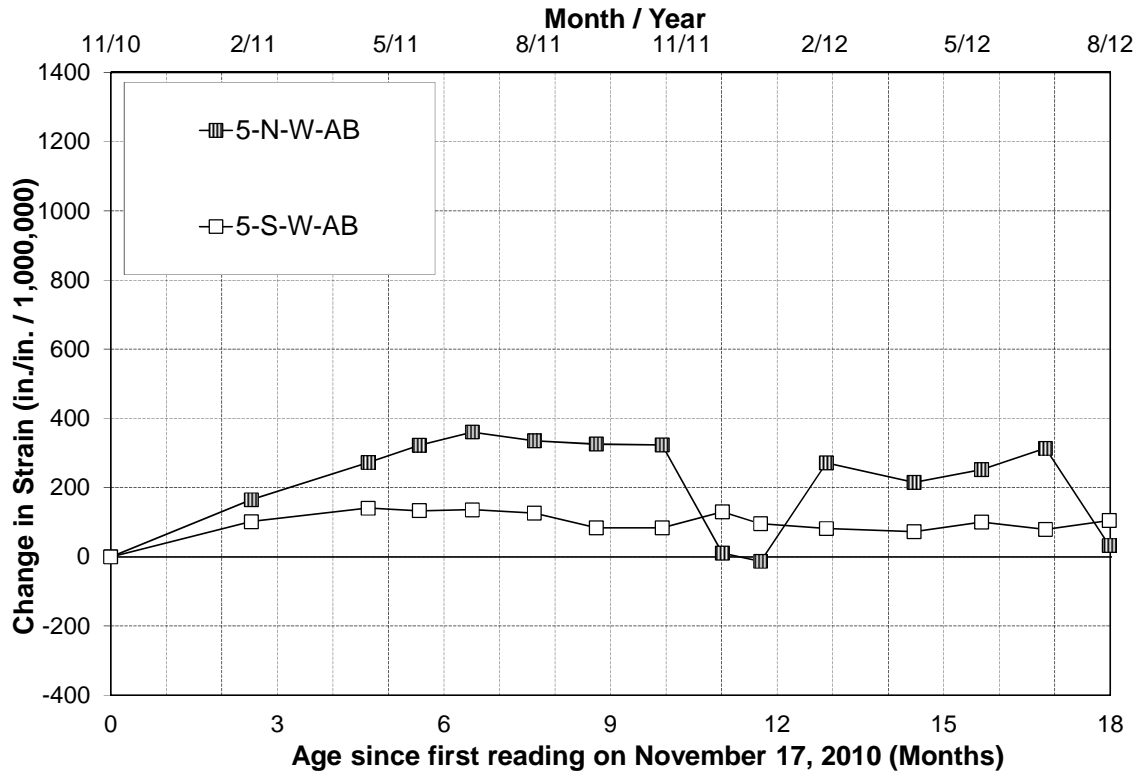


**Figure C.5:** Concrete strain difference plot for AB,  $r^2 < 0.5$